The Ganglionated Plexus: The Upstream Triggers of Atrial Fibrillation

A thesis submitted to Imperial College London for the

Degree of Doctor of Philosophy

by

Dr Min-young Kim, MBChB, MRCP

Myocardial Function Section,
National Heart and Lung Institute,
Imperial College London

Supervisors

Prof Prapa Kanagaratnam

Dr Nicholas Linton

Dr Fu Siong Ng

Dr Phang Boon Lim

STATEMENT OF ORIGINALITY

I confirm that the work presented herein is my own and was carried out under the supervision of Prof Prapa Kanagaratnam, Dr Nicholas Linton, Dr Fu Siong Ng and Dr Phang Boon Lim at Imperial College Healthcare NHS Trust and Imperial College London. Any contributions from others are clearly stated under "Acknowledgements".

Dr Min-young Kim

30th August 2019

COPYRIGHT DECLARATION

To my husband James,

My daughter Isabelle,

and our loving family.

ACKNOWLEDGEMENTS

Firstly, I am indebted to my wonderful supervisor and mentor, Professor Prapa Kanagaratnam. This has been one of the most enjoyable and rewarding journeys of my life. I thank him for this incredible opportunity. He has been a constant pillar of support, and a reassuring guide through every challenge I faced. He is a true inspirational figure, as a clinician, academic, leader, and person. I look forward to continuing to work with him for many years to come.

I am grateful to my co-supervisor, Dr Nick Linton for his invaluable expertise in bioengineering and electrophysiology, making it possible for the Tau-20 to come to fruition. I also thank my co-supervisor Dr Phang Boon Lim for his autonomic expertise throughout all my projects.

It has been a real pleasure to work with the bioengineers on the Tau-20 project, namely Simos Koutsoftidis. His work was key to building and translating the Tau-20 from bench to clinical setting successfully. I am also very grateful for his immeasurable patience working into the early hours of the morning with my porcine heart experiments. I must also thank Professor Emm Drakakis for his engineering expertise and supervising us on this project.

It would not have been possible to perform any of the research cases without the incredible efforts of the clinical electrophysiology fellows at Hammersmith Hospital: Vishal Luther, Kevin Leong, Louisa Malcolme-Lawes, Markus Sikkel and Afzal Sohaib. I thank them for their tireless energy and the shared enthusiasm discovering something new and exciting during GP ablation cases. I thank Dr Belinda Sandler for teaching me how to operate the Grass S88 stimulator and how to perform HFS. Her guidance has

helped me to smoothly transition into starting my PhD. I thank Dr Benjamin Low, who collected Holter and demographics of study patients. I also thank the consultants who supervised every research case and for providing patients to recruit to my studies: - Dr Zachary Whinnett, Dr Norman Qureshi and Dr Michael Koa-Wing.

I experienced dynamic teamwork like no other with the physiologists, namely Elaine Lim, Michelle Todd and Robert Edwards. Their contribution allowed every research case to run as smoothly and effortlessly as possible, which was an essential element to continue performing my research cases to completion. In addition, I cannot forget their kindness and humour which made every day an absolute joy. I also thank the Biosense Webster team, namely Andrew Arnott, Danielle Segal, Katie Vaughan and Rebecca Risberg - who provided their technical expertise for operating CARTO™ and for troubleshooting any problems that arose during GP ablation cases.

I could not have conceived the idea for my Langendorff porcine heart experiments without the generosity of Dr Rasheda Chowdhury. I am grateful for her reaching out to me for this exciting collaborative project, which not only challenged me to learn new skills but also connected me to the world of basic science. I thank her for allowing me to use her Langendorff apparatus for all my experiments, and to work with her PhD student, Joe Brooks, who has helped to set-up and perform my experiments. I thank my excellent BSc student, James Nesbitt, for his perseverance and hard work collecting and analysing immunohistochemistry data for the Langendorff porcine heart experiments. I am grateful to Dr Fu Siong Ng, who has co-supervised my BSc student and for his expertise, guidance and encouragement on this project when it all felt impossible. I thank Dr Rheeda Ali and Dr Chris Cantwell for their programming expertise, which has helped to create our novel probability distribution atlases for GP, and for our ongoing collaboration with machine

learning and GP mapping. I must also thank Professor Nicholas Peters, who supported this collaborative work from the start and integrated me into the ElectroCardioMaths program at Imperial College London.

Lastly but not least, to my parents, Mi-kyeong Yang, Jeong-bae Kim, and brother Kyu-jin Kim – for your endless love and support from day one. Thank you for helping me to reach this far. To my dearest husband, James Hawley – I know that you have, and will always believe in me. Thank you for everything. To my daughter, Isabelle Hawley – you are the greatest gift and joy in my life. Thank you for being born to this world.

ABSTRACT

The ganglionated plexuses (GP) are dense epicardial nerves that are implicated in atrial fibrillation (AF). They can be functionally located from the endocardium using high frequency stimulation (HFS) which can locate distinct GP that trigger atrial ectopy/AF (ET-GP) or atrioventricular (AV) dissociating (AVD-GP). Our aim was to map and understand the histological, anatomical and functional properties of the different types of GP and ablate them with or without pulmonary vein isolation (PVI) in patients with AF. We hypothesised that ablating these specific GP sites is feasible, and prevents AF.

Firstly, to investigate this, we mapped for AVD-GP and ET-GP using HFS in the left atrium of patients with AF. An automated process was used to merge and transform all patient maps onto one reference left atrial shell. A probability density function was applied at each tested site, including GP and negative HFS response sites, to create a probability distribution atlas of AVD-GP and ET-GP. There were distinct anatomical regions according to each GP sub-type, and ET-GP had preponderance to the PV ostia, roof, and mid-anterior wall. These are the areas that would usually be targeted with circumferential PVI.

Therefore, a prospective, randomised, controlled study was performed (GANGLIA-AF) which assessed ET-GP ablation without PVI and PVI alone in patients with paroxysmal AF. Patients were followed-up for 12 months with multiple 48hr Holter monitors. The primary endpoint was any documented atrial arrhythmia >30s, and the secondary endpoints included complications and redo ablations. This showed that there was no statistically significant difference in AF prevention between the two arms, however the GP ablation arm required less ablation on average than the PVI arm. We also performed

a smaller pilot study of redo AF ablation patients, assessing for feasibility and safety of GP ablation in addition to redo PVI. The same follow-up and endpoint criteria were used as in the GANGLIA-AF study. Some patients had permanent PVI, and non-PV triggers of AF were identifiable with HFS.

We also developed a custom-built high frequency stimulator (Tau-20) that was used to identify ectopy-triggering (ET) sites in Langendorff-perfused porcine hearts. We were able to replicate the HFS responses used in the clinical setting in the porcine atria. Transmural cross-sectional dissections were taken from ET and non-ET sites, and the tissues were stained for parasympathetic and sympathetic nerves using immunohistochemistry methods. This showed that the mean density of nerves was greater in ET sites compare to non-ET sites.

The Tau-20 has been successfully trialled in humans in the clinical setting, and with further improvements, it may replace the old Grass S88 stimulator for future GP ablation cases.

In conclusion, ET-GP are upstream triggers of AF that can be ablated without PVI to prevent paroxysmal AF. GP ablation can be achieved with less RF energy than PVI implying a more specific technique on mechanistic grounds. The cross-over rate and clinical outcomes for GP ablation needs further improvement but GANGLIA-AF provides evidence that GP ablation may be an alternative or an adjunct technique to PVI. In addition, our *ex-vivo* evidence of increased nerve density at ET sites may account for the differential functional response of ET-GP stimulation in the clinical setting.

PRIZES

1. Young Investigator Award in Clinical Science; Heart Rhythm Congress, 2020.

   Kim MY, Koutsoftidis S, Chowdhury RS, Tomlinson DR, Coyle C, Sikkel MB, Leong KM, Luther V, Malcolme-Lawes L, Sohaib A, Sandler B, Nesbitt J, Cantwell CD, Ali R, Hunter RJ, Koa-Wing M, Qureshi NA, Whinnett ZI, Lim PB, Peters NS, Drakakis E, Ng FS, Linton NWF, Kanagaratnam P. Ganglionated Plexus Ablation to Prevent Atrial Fibrillation (GANGLIA-AF).

2. Best Poster Prize; European Cardiac Arrhythmia Society Congress, 2018.

   Kim MY, Sikkel MB, Sohaib A, Malcolme-Lawes L, Leong K, Luther V, Sandler B, Koa-Wing M, Whinnett Z, Qureshi N, Ng FS, Peters NS, Davies W, Lim E, Fudge M, Todd M, Wright I, Linton NWF, Lim PB, Kanagaratnam P. Non-pulmonary vein triggers of AF in patients with complete pulmonary vein isolation.

PUBLICATIONS

1. **Kim MY**, Sandler BC, Sikkel MB, Cantwell C, Leong KM, Luther V, Malcolme-Lawes L, Koa-Wing M, Ng FS, Qureshi N, Sohaib A, Whinnett Z, Fudge M, Lim E, Todd M, Wright I, Peters NS, Lim PB, Linton NWF, Kanagaratnam P. The ectopy-triggering ganglionated plexuses in atrial fibrillation. *Auton Neurosci.* 2020 Jul 21. doi: 10.1016/j.autneu.2020.102699.
2. **Kim MY**, Sandler BC, Sikkel MB, Cantwell C, Leong KM, Luther V, Malcolme-Lawes L, Koa-Wing M, Ng FS, Qureshi N, Sohaib A, Whinnett Z, Fudge M, Lim E, Todd M, Wright I, Peters NS, Lim PB, Linton NWF, Kanagaratnam P. The Anatomical Distribution of the Ectopy-Triggering Ganglionated Plexus in Patients with Atrial Fibrillation. *Circ Arrhythm Electrophysiol.* 2020. Jul 27. doi: 10.1161/CIRCEP.120.008715.
3. **Kim MY,** Lim PB, Coyle C, Sandler B, Koa-Wing M, Kanagaratnam P. A single ectopy-triggering ganglionated plexus ablation without pulmonary vein isolation prevents atrial fibrillation. *JACC Case Rep.* 2020. Jul 2. doi: 10.1016/j.jaccas.2020.07.058.
4. **Kim MY**, Sikkel MB, Hunter RJ, Haywood GA, Tomlinson DR, Tayebjee MH, Ali RL, Cantwell CD, Gonna H, Sandler BC, Lim E, Furniss G, Panagopoulos D, Begg G, Dhillon G, Hill NJ, O'Neill J, Francis DP, Lim PB, Peters NS, Linton NWF, Kanagaratnam P. A novel approach to mapping the atrial ganglionated plexus network by generating a distribution probability atlas. *J Cardiovasc Electrophysiol.* 2018. Aug 31. doi: 10.1111/jce.13723.
5. Brook J, **Kim MY,** Koutsoftidis S, Pitcher D, Agha-Jaffar D, Sufi A, Jenkins C, Tzortzis K, Ma S, Jabbour R, Houston C, Handa B, Li X, Chow JJ, Jothidasan A,

Bristow P, Perkins J, Harding S, Bharath A, Ng FS, Peters NS, Cantwell CD, Chowdhury R. Development of a pro-arrhythmic ex vivo intact human and porcine model: Cardiac electrophysiological changes associated with cellular uncoupling. *Pflügers Archiv.* 2020. Oct. doi: 10.1007/s00424-020-02446-6

MANUSCRIPTS UNDER REVIEW

1. **Kim MY**, Sandler B, Sikkel MB, Leong KM, Luther V, Malcolme-Lawes L, Koa-Wing M, Ng FS, Qureshi N, Sohaib A, Whinnett ZI, Fudge M, Lim E, Todd M, Wright I, Peters NS, Lim PB, Linton NWF, Kanagaratnam P. Targeting the ectopy-triggering ganglionated plexuses without pulmonary vein isolation prevents atrial fibrillation.

FIRST AUTHOR ABSTRACTS

1. **Kim MY**, Nesbitt J, Koutsoftidis S et al. The Immunohistochemical Characteristics Of Ectopy-triggering Ganglionated Plexuses In Langendorff-perfused Porcine Hearts. *Heart Rhythm.* 2020 May; 17(5), Supplement, S297; D-PO03-033.
2. **Kim MY**, Sandler BS, Leong K et al. The Ganglionated Plexuses and their Electrophysiological Phenomena: Evidence for their Role in Pathogenesis of Atrial Fibrillation. June 2019*. J Interv Card Electrophysiol.* 2019 June. 55(Suppl 1). Abstract 04-11. doi.org/10.1007/s10840-019-00559-2.
3. **Kim MY**, Sandler BS, Sikkel B et al. Targeting Autonomic Upstream Drivers Of Atrial Fibrillation To Treat Paroxysmal Atrial Fibrillation Without Pulmonary Vein Isolation. *Heart Rhythm.* 2019 May; 16(5); S186; B-PO02-130. doi.org/10.1016/j.hrthm.2019.04.015
4. **Kim MY**, Sandler BS, Sikkel B et al. Non-pulmonary vein triggers of AF in patients with complete pulmonary vein isolation. *EP Europace*, Volume 20, Issue suppl_4, October 2018, Page iv8. doi.org/10.1093/europace/euy198.011
5. **Kim MY**, Sandler BS, Sikkel MB et al. Ablation of the ganglionated plexus terminates sustained atrial fibrillation. *J Interv Card Electrophysiol*. 2018. 51(Suppl 1):S1-S147. 12-2 Abstract 04-15. doi.org/10.1007/s10840-018-0338-y
6. **Kim MY**, Sandler BS, Sikkel M, et al. Non-pulmonary vein triggers of atrial fibrillation in patients with complete pulmonary vein isolation. J *Interv Card*

Electrophysiol. 2018. 51(Suppl 1):S1-S147. 16-49 Abstract 04-14. doi.org/10.1007/s10840-018-0338-y

7. **Kim MY**, Sikkel MB, Hunter RJ et al. A novel approach to mapping the ganglionated plexus network by generating a probability atlas. *Heart Rhythm*. 2018 May; 15(5); S223-S224; B-PO02-105. doi.org/10.1016/j.hrthm.2018.03.025.
8. **Kim MY**, Sandler BS, Sikkel MB et al. Ablation Of The Ganglionated Plexus Terminates Sustained Atrial Fibrillation. *Heart Rhythm*. 2018 May; 15(5); S431-S432; B-PO04-103
9. **Kim MY,** Sikkel MB, Hunter R et al. Generation of the first functional map of left atrial ganglionated plexus sites that induce AV nodal bradycardia. *EP Europace*. October 2017. Volume 19, Issue suppl_1, 1, Pages i24

LIST OF FIGURES

Larger versions of figures with electrograms are shown in the Appendix.

LIST OF TABLES

ABBREVIATIONS

AERP = atrial effective refractory period
AF = atrial fibrillation
ANS = autonomic nervous system
AP = action potential
ARGP = anterior right ganglionated plexus
AT = atrial tachycardia
AV = atrioventricular
AVD = atrioventricular dissociating
AVN = atrioventricular node
AVNERP = atrioventricular nodal effective refractory period
BB = betablocker
BP = blood pressure
CABG = coronary artery bypass graft
CAD = coronary artery disease
CAT = choline acetyl transferase
CPVA = circumferential pulmonary vein ablation
CPVI = circumferential pulmonary vein isolation
CS = coronary sinus
CTI = cavotricuspid isthmus
DCCV = DC cardioversion
DM = diabetes mellitus
ECG = electrocardiography
ECNA = extrinsic cardiac nerve activity
EP = electrophysiology
ERP = effective refractory period
ET = ectopy triggering
FAM = fast anatomical mapping
GA = general anaesthesia
GP = ganglionated plexus
GPA = ganglionated plexus ablation
GUI = graphical user interface
HF = heart failure
HFS = high frequency stimulation
HRA = high right atrium
HRV = heart rate variability
HTN = hypertension
ICNA = intrinsic cardiac nerve activity
IHD = ischaemic heart disease
ILGP = inferior lower ganglionated plexus
INF = inferior
IQR = interquartile range
IRGP = inferior right ganglionated plexus
ITT = intention to treat
IVC = inferior vena cava
LA = left atrium
LAA = left atrial appendage
LAO = left anterior oblique
LIPV = left inferior pulmonary vein
LL = left lateral
LSPV = left superior pulmonary vein
LV = left ventricle
LVEF = left ventricular ejection fraction
LVSF = left ventricular systolic function
MAP = mapping
MV = mitral valve
PA = posterior anterior
PV = pulmonary vein
PVI = pulmonary vein isolation
PVT = pulmonary vein tachycardia
RA = right atrium
RAA = right atrial appendage
RAO = right anterior oblique
RF = radiofrequency
RIGP = right inferior ganglionated plexus
RIPV = right inferior pulmonary vein
RL = right lateral
RLGP = right lower ganglionated plexus
RSPV = right superior pulmonary vein
RV = right ventricle
SR = sinus rhythm
STD = standard deviation
SUP = superior
SVC = superior vena cava
TH = tyrosine hydroxylase
TIA = transient ischaemic attack
TRE = transformation registration error
TSP = transseptal puncture
VF = ventricular fibrillation

Table of Contents

1. BACKGROUND

1.1. Introduction

Atrial fibrillation (AF) is the most common arrhythmia in the world that causes significant morbidity and mortality from stroke, heart failure and acute coronary syndrome. AF also causes significant discomfort in patients, leading to repeated hospitalisations. It affects 0.5-1% of the developed worldwide population and has reached an epidemic proportion[1]. In the UK, it is estimated that AF accounts for 1% of the National Healthcare System budget[2] and in the US, $16-26 billion of expenses per annum[3]. In the past decade, the costs and healthcare burden attributable to AF has markedly increased and is predicted to continue to escalate due to ageing populations[1]. Despite technology advancements in mapping systems and ablation techniques, no single strategy has translated into consistent, superior clinical outcomes in AF freedom to the conventional pulmonary vein isolation, which remains stagnant at 50-60% success rate[4]. Recently, there has been an increasing interest in the investigation of the role of the autonomic nervous system in AF. One of the biggest challenges in AF is knowing what to target and how to approach these safely, and effectively, that is reproducible outside single-centres. This is particularly true for targeting the autonomic nervous system (ANS), a complex network of nerves that has important structure-function relationship with cardiac physiology. Decades of experimental work highlighted the importance of the role of the ANS in AF. However, translation into clinical application has lost its way from carefully identifying selective nerves that are responsible for the complex structure-function relationship of the cardiac ANS, to adopting an empirical catheter-ablation strategy termed, “anatomical ganglionated plexus ablation” as a neuromodulation procedure in AF. This approach

makes important assumptions that all patients have fixed, common anatomical regions of nerves that are implicated in AF, and that ablation of these regions is enough to achieve a therapeutic effect. Experimental and clinical studies suggest the otherwise in the former[5,6], and in the latter, not only is this approach inferior to the conventional treatment with pulmonary vein isolation[7,8], but also harmful in thoracoscopic AF ablations[9]. As Capa and Callans[10] have stated, we must "harness the elegance of the neural-cardiac interface to better manage our patients more safely, effectively and *thoughtfully*."

The experimental and clinical work in this thesis explore the detailed structure-function relationship in the ANS of the heart, and test the hypothesis that mapping and ablating selective neural structures can prevent AF; an alternative approach to anatomical ganglionated plexus ablation and pulmonary vein isolation in AF.

1.2. Atrial Fibrillation: The History

"When the pulse is irregular and tremulous and the beats occur at intervals, then the impulse of life fades; when the pulse is slender (smaller than feeble, but still perceptible, thin like a silk thread), then the impulse of life is small."

- *Huang Ti Nei Ching Su Wen*

The first description of AF stretches back to over 2000 years B.C. in the oldest known Chinese medicine document in history: 'Huang Ti Nei Ching Su Wen' ('The Yellow Emperor's Classic of Internal Medicine'), said to have been written by the famous Chinese Emperor, Huang Ti, "when the pulse is irregular and tremulous and the beats occur at intervals, then the impulse of life fades; when the pulse is slender"[11]. In 1628, William Harvey established the right atrium as the origin of the heart beat and was first to describe AF in a dying animal heart; "I noticed that after the heart proper, and even the right auricle were ceasing to beat and appeared on the point of death, an obscure movement undulation or palpitation had clearly continued in the right auricular blood itself for as long as the blood was perceptibly imbued with warmth and spirit"[12]. In 1669, Richard Lower stated in the *Tractatus de Corde* that the movement of the heart muscle is due to the "abundance of nerves which are inserted into it."[13] Perhaps one of the most remarkable early insights into linking clinical observations and pathophysiology of AF in humans was by Jean Baptist de Sénac, the physician to Louis XV in the mid eighteenth century. He found that mitral valve disease, dilated ventricles, and atria that are "strained and increased in volume" induce AF and the "causes of palpitation are not the causes of the natural heart-beat"; a prophetic statement for the ectopic origin of AF[14]. He was also first to use quinidine in treatment of AF. De Sénac further built on the ideas of Richard Lower that the heart was innervated like other muscles and understood the importance

of the role of the autonomic nervous system in the heart. He questioned, “why does the heart not stop after cutting nerves?” and “how does a non-innervated embryo heart of a chick visibly contract?”[12]. In 1785, William Withering, an English physician discovered the therapeutic effects of digitalis leaf (digitalis purpurea) to patients with symptomatic heart failure, and also observed that the pulses of patients who likely had AF became "more full and more regular" with digitalis[11]. In 1827, Robert Adams used a stethoscope invented by Laénnec, to identify that AF was "almost pathognomonic of mitral stenosis". Then in 1863, Étienne-Jules Marey published the first recorded irregular arterial pulse of AF using a sphygmograph from a human with mitral stenosis (Figure 1.1). James Mackenzie in 1894 was the first to describe the absence of the presystolic 'a' wave, in the jugular venous pulse using a phlebogram, during AF[15].

A significant breakthrough in the history of electrophysiology was the invention of the electrocardiograph (ECG), by Augustus D. Waller. In 1887, he recorded the first human ECG with a mercury capillary electrometer in 1887, at St Mary’s Hospital, London[16]. William Einthoven improved the clinical applicability of Waller’s ECG by devising a string galvanometer in 1900, and Thomas Lewis, the father of modern electrocardiography first recorded an ECG in a patient with AF in 1908. With improvements in the recording technique, he was able to discern fibrillatory f-waves with normal R waves throughout the cardiac cycle in AF (Figure 1.2). He deduced that f-waves originate from the atria, and not the atrioventricular node as Mackenzie earlier suggested[17,18].

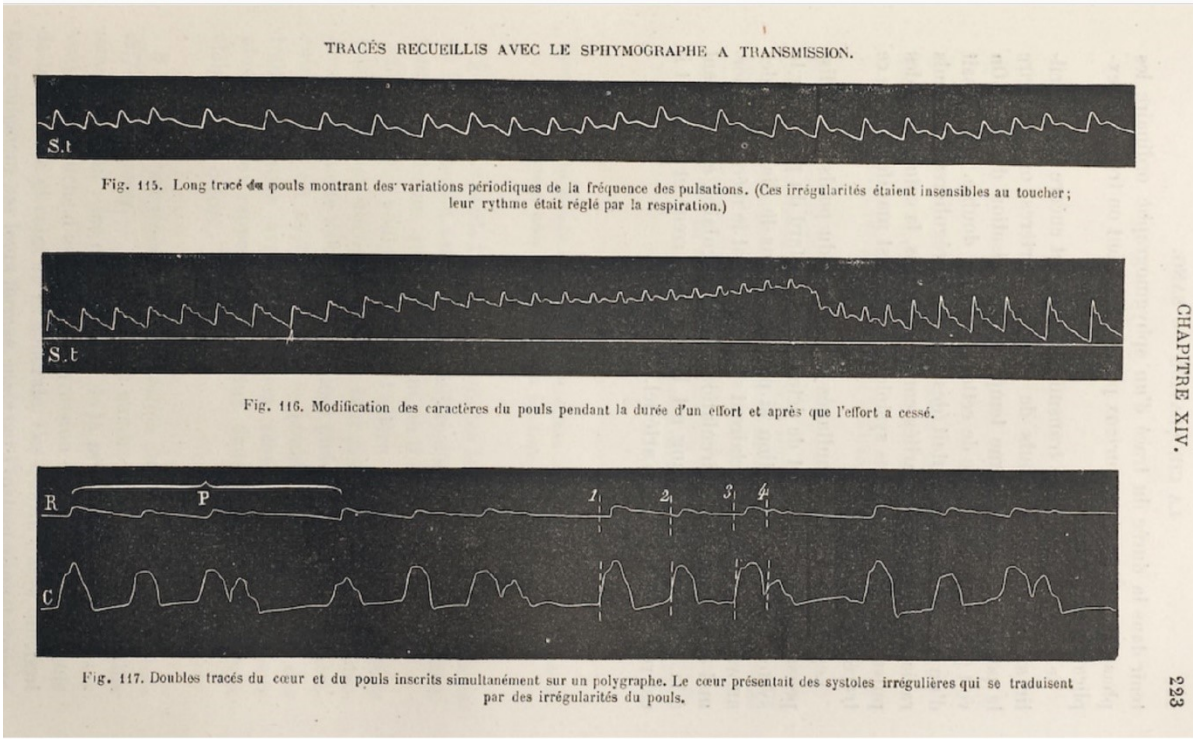
TRACÉS RECUEILLIS AVEC LE SPHYMOGRAPHE A TRANSMISSION.

S.t

Fig. 115. Long tracé du pouls montrant des variations périodiques de la fréquence des pulsations. (Ces irrégularités étaient insensibles au toucher; leur rythme était réglé par la respiration.)

S.t

Fig. 116. Modification des caractères du pouls pendant la durée d'un effort et après que l'effort a cessé.

R P 1 2 3 4

C

Fig. 117. Doubles tracés du cœur et du pouls inscrits simultanément sur un polygraphe. Le cœur présentait des systoles irrégulières qui se traduisent par des irrégularités du pouls.

CHAPITRE XIV.

223

Figure 1.1 The first arterial tracing of atrial fibrillation using a sphygmograph

This is the first published arterial pulse trace using a sphygmograph showing an irregularity of the pulse consistent with atrial fibrillation by Étienne-Jules Marey.

Translation of the Figure 115 legend: “Long pulse trace showing periodic changes in pulse frequency. (These irregularities were insensitive to touch; their rhythm was regulated by respiration).

Translation of the Figure 117 legend: “Double traces of heart and pulse simultaneously written on a polygraph. The heart had irregular systoles which resulted in pulse irregularities.”

Adapted from Marey[19].

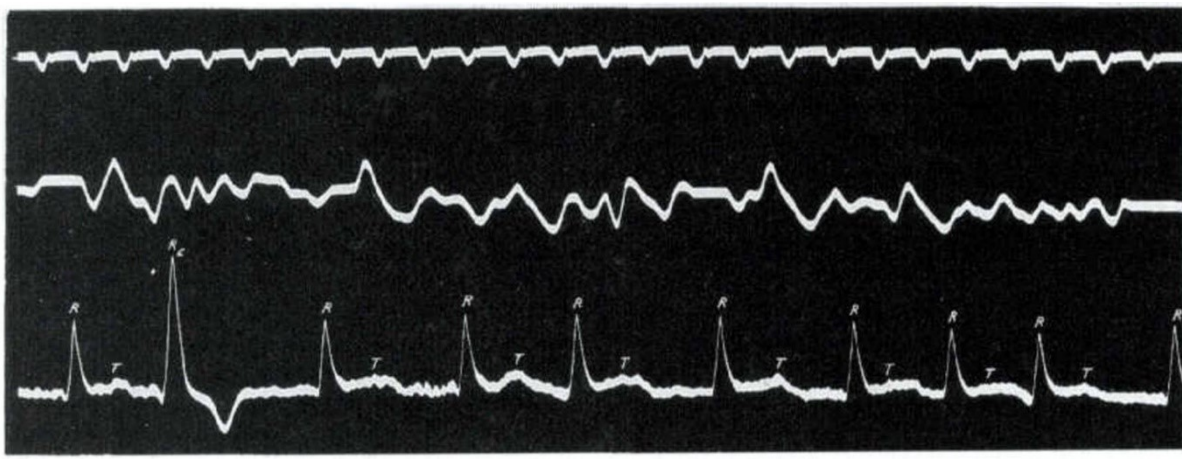

Figure 1.2 The first electrocardiograph of AF.

This electrocardiograph demonstrates f-waves but absence of p waves in AF. Adapted from Hering[20].

1.3. Mechanisms of AF

Theories in the mechanism of AF have prevailed since the early 1900's, and still fiercely debated today. Historically, three main concepts competed to explain the mechanism of AF; multiple re-entrant wavelet theory, rapidly discharging automatic foci, and a single re-entrant circuit with fibrillatory conduction (Figure 1.3)[21]. Since then, significant progress has been made in our understanding of the initiation, maintenance and progression of AF, particularly from the seminal work by Haïsaguerre *et al*[22] in the key role of pulmonary veins (PV) in AF, and also as the first direct evidence of AF initiation and mechanism.

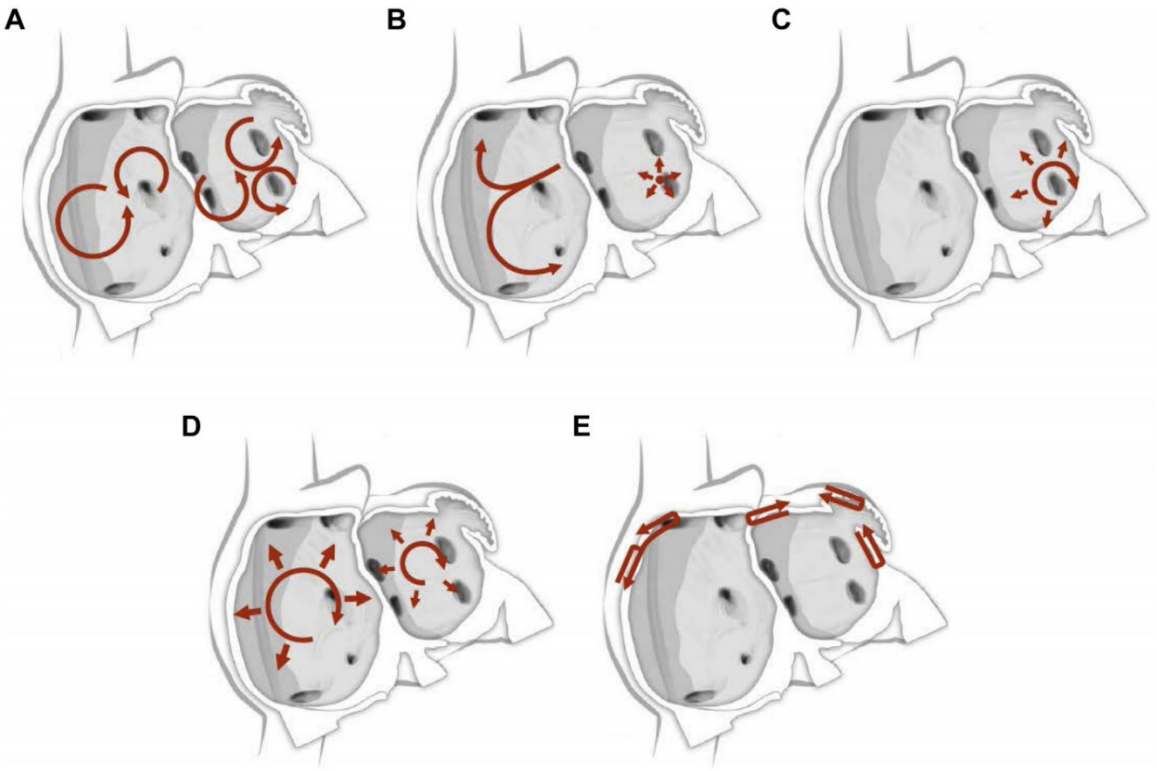

Figure 1.3 Historical concepts on the mechanisms of atrial fibrillation

A: Multiple wavelets hypothesis. B: Rapidly discharging automatic foci. C: Single reentrant circuit with fibrillatory conduction. D: Functional reentry resulting from rotors or spiral waves. E: AF maintenance resulting from dissociation between epicardial and endocardial layers, with mutual interaction producing multiplying activity that maintains the arrhythmia. Adapted from 2017 HRS expert consensus document in AF[21].

1.3.1. "AF Begets AF"

The pace of discovery in AF mechanisms accelerated greatly during the 90's. In 1995, Wijffels *et al* published a seminal observation that "AF begets AF"; maintenance of AF progressively shortened the atrial effective refractory period (AERP) and increased the inducibility and stability of AF.[23] Morillo *et al* also confirmed that sustained atrial tachycardia or AF leads to shortened AERP, higher inducibility of AF, and biatrial enlargement with atrial cardiomyopathy[24]. These findings were the first evidence for atrial remodelling and AF.

1.3.2. Multiple Wavelet Theory

In 1924, Garrey recognised the inter-relationship between atrial flutter and AF, and described that AF is maintained by: 1) local ectopic foci (multiple or single with fibrillatory conduction), 2) a single re-entry circuit (a "mother wave") with fibrillatory conduction, or 3) multiple simultaneous functionally determined re-entry circuits[25]. In 1964, Moe *et al*[26] published their first 2D computerised mathematical model of AF, which exhibited self-sustained turbulent activity having many similarities to AF. The authors found that irregularly drifting eddies which varied in position, size and number sustained the AF-like activity, and increasing the refractory periods whilst retaining nonuniformity terminated the AF-like activity. The presence of independent wavelets supporting this theory have been demonstrated more recently[27–29]. This established the "multiple wavelet" hypothesis that became the most dominant concept in the mechanism of AF for over three decades[30]. However, Chen *et al*[27] in 2000 analysed individual wavelets during sustained AF by identifying phase singularities using optical mapping. In their models, the wavelets existed for less than one rotation in 98% of the cases. In addition, the number of wavelets decreased between the entrance and the exit of the mapping field. These results suggested that wavelets result from the breakup of high frequency organized waves and as such they are not an independent mechanism that maintains AF. Multiple wavelets during PV firing is an example that supports the passive role of these wavelets.

1.3.3. Pulmonary Vein Arrhythmogenicity

In 1998, Haïssaguerre et al[22] published their seminal paper on the role of the pulmonary vein (PV) ectopy in AF, which formed the basis of our ablative strategies for AF today. The authors studied 45 patients with drug-refractory, paroxysmal AF, by mapping for the

earliest depolarisation of atrial ectopy or AF using multielectrode catheters. Out of 69 ectopic foci mapped, 94% were from 2-4cm within the PVs (Figure 1.4).

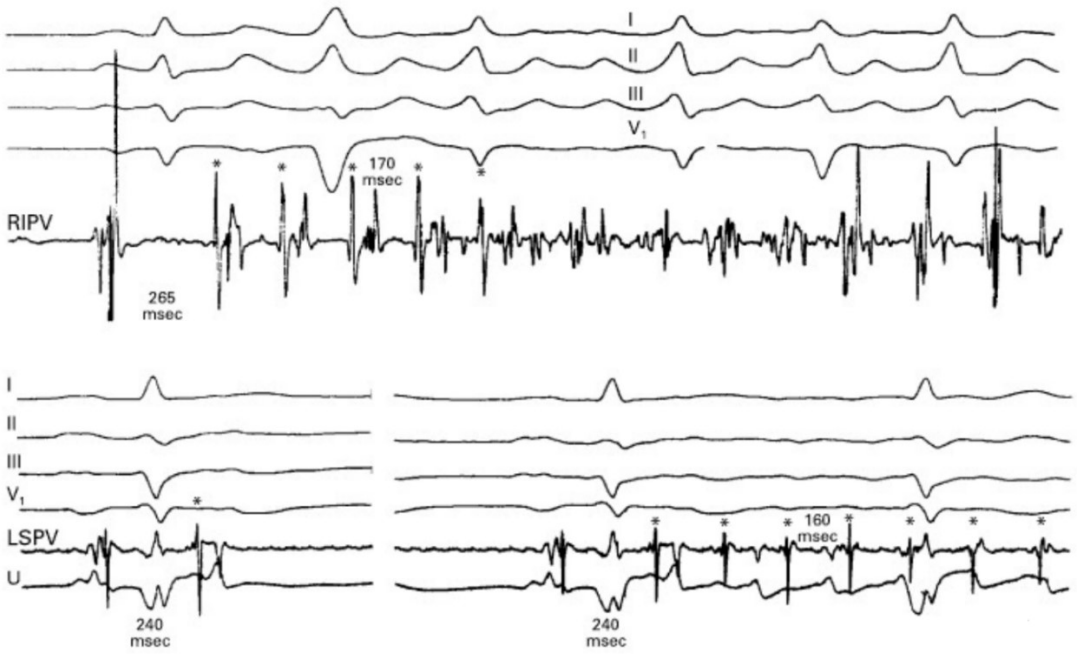

Figure 1.4 Pulmonary vein ectopy initiating atrial fibrillation

The top panel shows an electrogram with initiation of PV ectopy in the RIPV during sinus rhythm. A burst of five ectopy (asterisked) with a mean cycle length of 170msec is induced, which causes coarse atrial fibrillation on the surface electrocardiogram. The coupling interval of the first spike was 265msec.

In the bottom panel on the left, a sinus beat (with a terminal spike) is followed by an isolated atrial ectopic beat (asterisk) at a coupling interval of 240msec. The electrogram of the ectopic beat characteristically shows temporal reversal, with the rapid deflection spike preceding the lower-amplitude, slower far-field atrial activity.

In the bottom panel on the right (same patient), a burst of ectopy (asterisks) at a cycle length of 160msec triggers atrial fibrillation. The spike discharges are also characterized by temporal reversal but exhibit a progressively prolonged conduction time to the atria. The coupling interval of the first spike on the right (240msec) is identical to that of the isolated ectopic beat on the left. Adapted from Haïssaguerre *et al*[22]. (LSPV=left superior pulmonary vein; U=unipolar left atrial activity)

The left superior PV was the most common source of ectopic foci, followed by the right superior PV, left inferior PV and right inferior PV. 29 (64%) patients had a single ectopic

focus. The rest of the patients had two or more ectopic foci. The individual ectopic foci were locally ablated and successful ablation was achieved in 38 patients. After mean 8 months follow-up, 28 (62%) patients were free from AF. The patients who had recurrence of AF had recurrence of ectopy.

Chen *et al.*[31] demonstrated interesting structural and electrophysiological differences between different PVs and the atria in patients with or without AF. The superior and left PVs had longer myocardial sleeves than inferior and right PVs, distal PVs had the shortest effective refractory periods (ERPs), and right superior PVs had higher intra-PV conduction block than left superior PVs. These properties possibly explained the highest likelihood of ectopic foci to trigger from the left superior PV and the lowest in the right inferior PV, as reported by Haïssaguerre *et al*[22]. Interestingly, there were no differences in these parameters between patients with and without AF. However, only 10 control patients were assessed. Jaïs *et al*[32] studied 20 patients without AF and compared their atrial electrophysiological properties to 20 patients with AF and found that the PV ERPs were shorter in patients with AF, leading to more frequent AF induction by pacing the PVs compared to patients without AF. No statistically significant difference in the left atrial ERP was seen between the two groups.

The underlying histological and anatomical structure of the PVs are considered an important factor to their arrhythmogenicity. Histological data showed that myocardial tissue of the left atrium extends into the pulmonary venous walls at variable distances[33,34], and longer myocardial sleeves correlated to larger number of ectopic foci[31]. Larger diameter and thicker wall of PVs correlated to the arrhythmogenicity of PVs[35,36]. There have been reports of PVs harbouring specialised, pacemaker-like cells in animals and humans[37–39]. However, there were some technical limitations and unanswered questions

from the studies[40,41], with conflicting evidence from other studies reporting the absence of any specialised cells or unique features that differentiate PV from other atrial cells[42,43].

Different electrophysiological mechanisms for PV ectopy have been proposed; triggered activity, abnormal automaticity, or microreentry[44]. Double potentials and fractionated electrograms in PVs suggested a complex architecture of the myocardial sleeves in the veins, which supports the microreentry mechanism. A computer simulation showed that reduced coupling of cells at sites with abrupt changes in fibre orientation facilitate the escape of a ectopic focus and subsequent activation of the surrounding tissue[45].

Another computational technique incorporating 3-dimensional atrial structure and detailed ionic-current model of an atrial myocyte studied initiation of AF, by ectopic foci from various atrial locations including the PV. This model demonstrated that AF was most likely to be initiated from the PV region[46]. From animal models, spontaneous PV activity has been recorded, from phase 4 depolarisation as well as early after depolarisations[47]. Pharmacological interventions often provoked non-spontaneous PV activity, and the cycle length of PV ectopic were often irregular, supporting a focal mechanism of the ectopic beats.

Other ion current mechanisms involved in atrial remodelling were described in detail[48,49], indicating that the PVs also have properties favouring local microreentry, which likely contribute to their participation in AF.

1.3.4. Reentry Mechanism and Rotors

In 1977, Allessie *et al*[50] described the "leading circle" hypothesis as a re-entry mechanism for AF, by inducing and mapping isolated rabbit atria. The authors detected an activation sequence that suggested centripetal direction of wavelet propagation. It was proposed

that these centripetal wavelets activated tissue at the centre of the circuit, resulting in double responses (double potentials) of subnormal amplitude. Because the centripetal wavelets were unable to propagate beyond the centre, they prevented the impulse from shortcutting the circuit, resulting in the maintenance of reentry. This suggested that functional reentry naturally establishes itself in the shortest circuit that can maintain reentry, defined by the distance a cardiac impulse travels during the refractory period[51,52]. However, subsequent studies utilising high-density mapping and mathematical models failed to confirm the "leading circle" theory, or the presence of centripetal wavelets in the maintenance of reentrant excitation.

Since the 1960s, "rotors" or "spiral waves" became a popular theorised re-entry mechanism for arrhythmias[53–55]. Although they are similar form of functional re-entrant activity as in the "leading circle" theory, one critical difference is that the curved wavefront and wavetail meet each other at a singularity and the tissue at the centre is not refractory[56]. The terms spiral wave and rotor have been used interchangeably by some; however in the context of cardiac arrhythmias, rotors are "drivers" or organizing sources of fibrillation, and a spiral wave is a 2D representation of the curved vortices generated by the spinning rotor in its immediate surroundings[57] (Figure 1.5). The concept of rotor can also be applicable to anatomical reentry in the atria; a pectinate muscle or the orifice of a PV can stabilise a reentrant rotor[58,59].

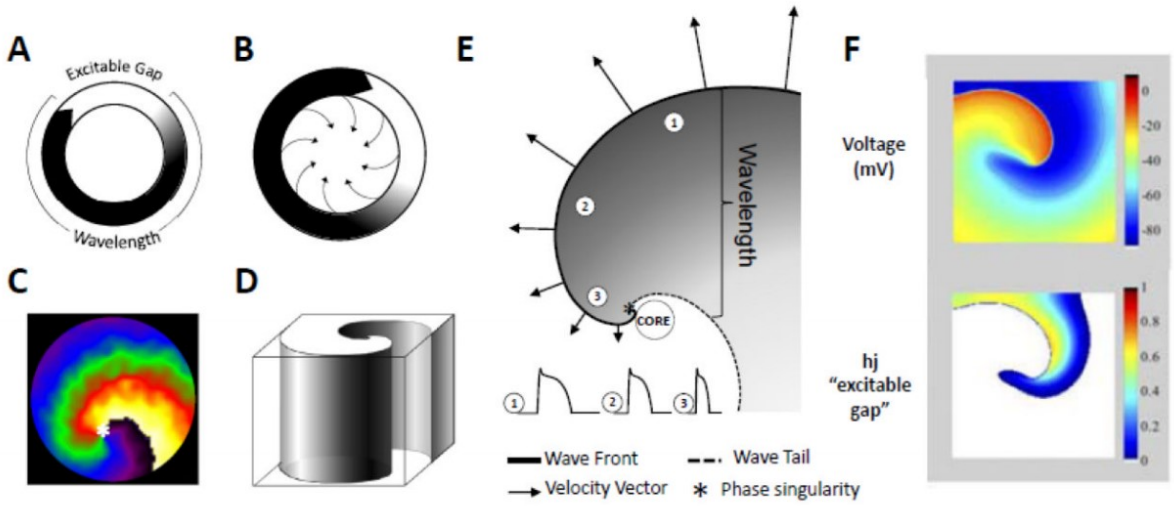

Figure 1.5 Rotors and spiral waves

A) A schematic representation of reentry around a ring-like anatomical obstacle where the wavelength (black) is shorter than the path length allowing for a fully excitable gap (white). B) Leading circle reentry around a functional obstacle, with centripretal forces pointing inwards toward a refractory centre. C) 2D spiral wave, along with the rotor tip at the centre "*". D) Schematic of a 3D scroll wave. E) Snapshot of the spiral wave: Electrotonic effects of the core decrease conduction velocity (arrows), action potential duration (representative examples shown from positions 1, 2 and 3) and wavelength (the distance from the wave front (black line) to the wave tail (dashed line)). Conduction velocity (CV) decreases and wavefront curvature becomes more pronounced, near the rotor, which is a phase singularity at the point where the wave front and the wave tail meet "*". F) Computer simulation of re-entry. Top panel: snapshot of the transmembrane voltage distribution during simulated reentry in chronic AF conditions in a 2D sheet incorporating human atrial ionic math models. Bottom panel: snapshot of inactivation variables of sodium current, "hj" (fast-slow) during re-entry. Adapted from Pandit *et al*[58].

1.3.5. The Autonomic Nervous System

One of the earliest recorded observations in the role of the autonomic nervous system in AF was made by McWilliams[60] in 1850, of the vagus nerve. He found that stimulation of the vagus nerve had dual effects in AF; 1) temporary inhibition or "weakening" of AF, which would appear again after cessation of the vagal effect or terminate AF and sustain normal rhythm. 2) the opposite effect was also true in some cases, where vagal

stimulation caused AF. No vagal effect was observed in ventricular fibrillation (VF). Over the next six decades, McWilliams' findings were verified by several authors[25]. Winterberg in 1907[61] noted that atropine could abolish the effect of vagal stimulation, and physostigmine, pilocarpine rendered it easier to induce AF with vagal stimulation.

In 1905, Kronecker and Spallitta[62] showed that vagal stimulation lowered the ventricular rate during AF, and Robinson and Draper[63] showed in humans, that vagal stimulation induced atrial-ventricular conduction delay and block, whilst the atrial activity continued in the ECG. Robinson and Draper studied children with chronic endocarditis who were susceptible to vagal stimulation with pressure. The authors highlighted the differences between the left and right vagal nerve stimulation; the right vagus had more profound effect on slowing the sinus rate than the left, and atrioventricular (AV) dissociation was observed in both left and right vagal stimulation (Figure 1.6 An ECG of a child with chronic endocarditis having right vagus nerve stimulation inducing AV dissociation.Figure 1.6).

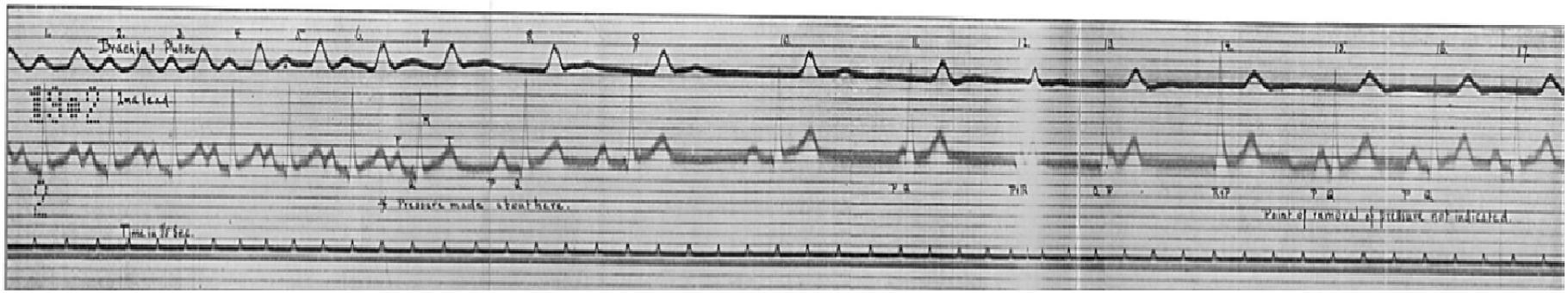

Figure 1.6 An ECG of a child with chronic endocarditis having right vagus nerve stimulation inducing AV dissociation.

At the 7th beat, pressure is exerted on the right vagus nerve. An immediate slowing of the sinus rate is observed in the next few beats. AV dissociation is evident from the 11th beat. At 15th beat, pressure is relieved from the right vagus nerve. There is immediate recovery from AV dissociation and normal sinus rhythm resumes. Adapted from Robinson and Draper[63].

(AV=atrioventricular dissociation; ECG=electrocardiograph)

The authors hypothesised that this difference in functional effects correlates to the anatomical distribution of the vagal nerves to the heart. However, despite these early efforts to understand the effects of vagal stimulation, the paradoxical role of the vagus nerve in being able to both provoke and inhibit AF was not explained[25]. This phenomenon was later explained in 1975, when Armour *et al* performed direct electrical stimulation of the smaller cardiac branches from the vagus nerve in canines, eliciting highly localised, and differential responses from individualised segments of the atrial myocardium[64]. As previously shown, both negative dromotropic and positive inotropic, chronotropic changes were observed when selectively stimulating cardiac branches from the vagus nerve. The negative dromotropic responses were eliminated with atropine, leaving positive inotropic, chronotropic changes unchanged. This revealed that the smaller cardiac branches of the vagus nerve contained both parasympathetic and sympathetic components which were responsible for these variation in the heart's physiological response.

Further work by the authors throughout the 1980's was paramount to our understanding of the detailed neural connections within the heart, that are highly specific and discriminatory in their functional correlation. The sinoatrial node was found to be preferentially sensitive to parasympathetic regulation and the atrioventricular node (AVN) preferentially sensitive to sympathetic regulation. Furthermore, selective and restricted injections of lidocaine (general neuronal blocker) and hexamethonium (ganglionic blocker) indicated that the vast majority of vagal ganglia supplying the sinoatrial node reside in the pulmonary vein fat pad and associate adipose tissues. In contrast, the vagal ganglia supplying AVN were found within a smaller fat pad overlying epicardium at the junction of inferior vena cava-inferior left atrium[65].

In 1990, Coumel highlighted the importance of the sympathetic nervous system in promoting arrhythmias in diseased tissues by promoting ectopy foci activity[66]. He recognised the complexity of the vagosympathetic interaction in the heart, and that a nonuniform neural distribution in combination with diseased atrial cells were major contributors to atrial arrhythmias. Coumel described that most patients he studied with paroxysmal AF were young males, without structural heart disease, who experienced symptoms at night, at rest, ending in the morning or during digestive periods (particularly after dinner). This pattern of AF inducibility was attributed to enhanced vagal activity during rest, and the short-term high-frequency heart rate variability was a marker for enhanced vagal activity, which manifested shortly before the onset of arrythmia. Much less frequently, another subset of patients had high sympathetic tone triggering AF as seen in Holter recordings (Figure 1.7). These patients experienced symptoms during the day, with emotional stress or exertion.

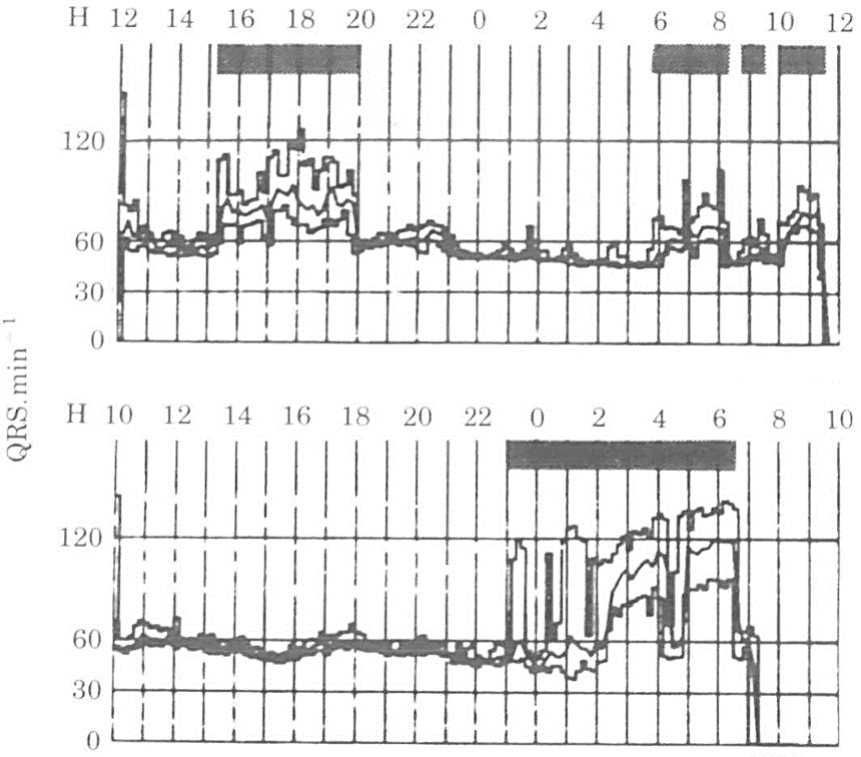

Figure 1.7 Diurnal variation seen in patients with paroxysmal AF.

Heart rate plot from Holter recordings in two patients with paroxysmal AF. AF episodes with high heart rate under black strips. The upper diagram shows what is likely an adrenergically mediate AF that occurs mostly during the day, and the bottom diagram shows what is likely a vagally mediated AF that occurs mostly during the night. Adapted from Coumel[67].

Coumel also stated that both vagal and sympathetic nerve activity can shorten the action potential, though vagal stimulation shortens the wavelength of the atrial impulse, leading to macro re-entrant circuits such as atrial flutter. On the other hand, sympathetic nerve activity seemed to favour micro re-entry, automatic and triggered activity. Overall, Coumel observed that there was predominance of vagal influence in healthy atria, but this was also first to withdraw in diseased hearts before sympathetic nerve activity increased. Adrenergically driven arrhythmia was thought to be a rare occurrence in healthy hearts.

Patterson *et al*[68] proposed a theory behind the neuro-electrophysiological mechanism in induction of PV ectopy and AF. When there is action potential shortening within the PV

sleeve, a temporal disparity between repolarisation and the Ca transient is created, that is not observed in other myocardial sites. The intracellular calcium concentration $[Ca^{2+}]_i$ remains elevated at a time when the membrane potential is negative to the equilibrium potential for Na/Ca exchange. This becomes arrhythmogenic when the myocardial repolarisation is accelerated with parasympathetic nerve stimulation, releasing acetylcholine. When the sympathetic nerves are stimulated, catecholamines are released and the Ca transient elevated. The elevated extracellular Ca^{2+} concentration $[Ca^{2+}]_o$ drives the Na^+-Ca^{2+} exchange current (I_{NCX}) inward in the absence of significant outward repolarising membrane currents, initiating EAD and arrhythmia (Figure 1.8).

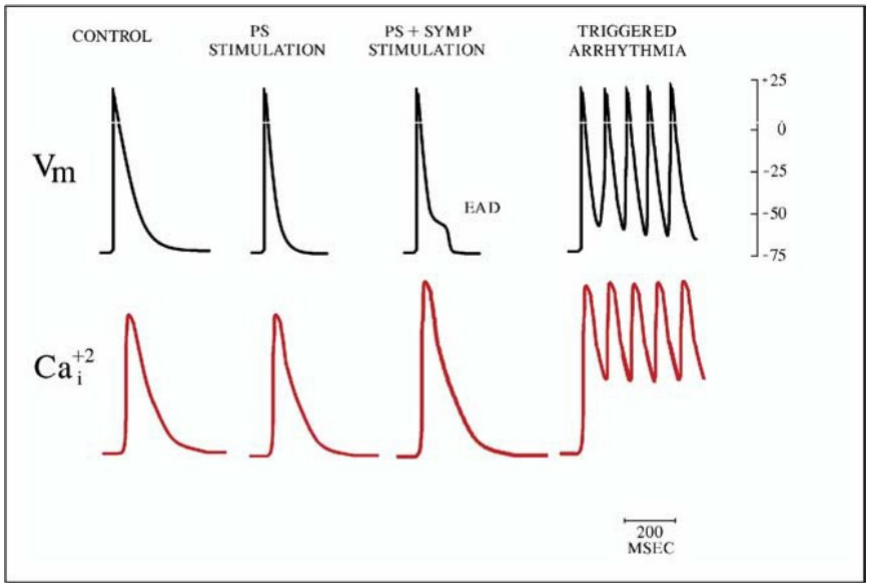

Figure 1.8 Mechanism of the autonomic nervous system provoking arrhythmia

Depicted are membrane voltage (V_m) and cytoplasmic calcium [Ca_i^{+2}] under control conditions, during parasympathetic nerve (PS) stimulation, during combined parasympathetic and sympathetic nerve (PS+SYMP) stimulation, and during triggered arrhythmia formation. Under control conditions, the Ca transient slightly exceeds action potential duration. The disparity between action potential duration and the Ca transient increases with parasympathetic nervous system stimulation. Early afterdepolarization (EAD) formation is apparent only with (1) an increase in Ca transient with sympathetic nerve stimulation and (2) shortening of action potential with increased parasympathetic nerve stimulation. If sufficient inward Na/Ca exchange current is present, rapid arrhythmia is initiated.

EAD and arrhythmia may also be enhanced by a relative absence of inwardly rectifying potassium current (I_{K1}) current within PV cells compared to the atrium, and a failure to activate significant time-dependent outward currents capable of off-setting the inward I_{K1}[69].

The experimental evidence behind the proposed mechanism is as follows:

1. Activation of parasympathetic nerves with electrical stimulation triggers arrhythmia. Hyperpolarisation and action potential duration shortening occurs with the known electrophysiologic actions of acetylcholine in atrial tissues[70–72], precede EAD and arrhythmia associated with stimulus trains incapable of stimulating myocardium. The hyperpolarisation and action potential shortening are prevented by atropine, a nonspecific muscarinic receptor antagonist[70,73], although complete arrhythmia suppression may require blockade of both muscarinic and α1- adrenergic receptors.

2. Sympathetic nerve stimulation lead to norepinephrine release, which enhances Ca transient. Atenolol, a selective α1-adrenergic receptor antagonist, prevents triggered arrhythmia without preventing hyperpolarisation and action potential shortening, as seen with stimulation of parasympathetic nerves.

3. Arrhythmia is prevented with suppression of the Ca transient by ryanodine and suppression of Na/Ca exchange by a transient increase in $[Ca^{2+}]o$. Suppression of Na/Ca exchange prevents EAD formation and arrhythmia from pacing, nonspecific autonomic nerve stimulation and acetylcholine plus norepinephrine administration within the canine PV sleeve.

4. Tetrodotoxin administration, at a concentration less than that needed to suppress sodium currents in myocardium, prevents shortening of the action potential duration and arrhythmia associated with HFS trains seen to excite local autonomic nerves within the PV.

5. HFS introduced to the proximal region of the PV ostium and overlying a GP neural connected to the PV sleeve, shortens the action potential and induce PV ectopy. This observation dissociates the site of autonomic effect from the local anatomical site of HFS[74].

In 2008, Lemola *et al* conducted an elegant study which assessed the effects of targeted GP ablation and PVI without GP damage in canine models of vagal AF. This study sought to differentiate the role of PV tissue in vagal AF, and the role of GP near the PV in vagal AF.

In vitro model of dogs, coronaries were perfused with carbachol in left atrial PV preparations and *in vivo,* with cervical vagal stimulation*.* Carbachol caused dose-dependent AF promotion *in vitro,* which was not affected by excision of all PVs. Sustained AF could be induced easily in all dogs during vagal nerve stimulation *in vivo* both before and after isolation of all PVs, using radiofrequency ablation.

GP were identified before PVI, and PVI was performed without damaging GP. As a result, the atrial effective refractory period did not change, nor its responses to cholinergic stimulation.

GP were selectively identified using continuous HFS in the epicardial fat pad, at a threshold that was less than direct atrial capture. GP were identified as mean RR >50% increase from baseline during AF, AV block or sinus bradycardia. Ablation of GP that overlay PVs suppressed shortening of the refractory period and AF-promoting effects of

cervical vagal stimulation. However, ablation of only left, *or* right PV GP did not suppress AF. Dominant-frequency analysis suggested that the success of ablation in suppressing vagal AF depended on the elimination of high-frequency driver regions.

Therefore, the PVs were not essential for AF maintenance in the presence of strong vagal tone. These results suggested that ablation of GP near PV ostia may be an important contributor to the efficacy of PV-directed ablation procedures in clinical AF.

1.4. The Ganglionated Plexuses

The earliest recorded study on the cardiac autonomic nervous system was in 1794 by Scarpa[75]. Numerous nerves were seen to covering the whole surface of the heart of various mammals and humans by naked eye, and he considered "swellings" on these nerves as ganglia[76]. Later throughout 1800s, Remak[77], Lee[78] and Kolliker[79] reported that the nerves course into the myocardium and carry the nerve cells with them, though this was challenged in 1853 by Cloetta[80], one of the earliest authors to study the heart microscopically.

Since the latter part of the nineteenth century, extensive literature in the topographical and anatomical examination of the extrinsic and intrinsic cardiac autonomic nervous system have been published[5,76,81,82]. In the human heart, extrinsic cardiac autonomic nervous system comprises of nerves that branch from the left and right vagus nerves, recurrent laryngeal nerves, and both sympathetic trunks at the cervico-thoracic and thoracic levels[83,84]. In 2000, Pauzal *et al*[81] studied the largest number of human hearts (21 in total), including adult, foetal, neonatal, infant autopsied whole human hearts that suffered no cardiac complications. The authors stained nerves with acetylcholinesterase, and used stereoscopic, contact and bright-field microscopy for nerve examination. GP

were described to originate from “seven main subplexuses” that start from the hilum of the heart. In general, 2 ganglionated subplexuses innervated the right atrium, 3 in the left atrium, 1 in the right ventricle, and 3 in the left ventricle. Although the seven ganglionated subplexuses were consistent topographically from heart to heart, the individual ganglia and branching nerves varied considerably, and in relation to age. Ganglia were interconnected with one another via thin nerves, but there was generally distinct regions of ganglia clusters or “fields”, that were clearly separated from each other by wide regions of the heart surface. These wide regions were usually devoid of ganglia and only sparse, thin nerves interconnected the GP clusters. The densest cluster of ganglia were in the regions coloured in Figure 1.9.

There were two main routes of nerves identified. Some epicardial nerves originated from numerous intrinsic ganglia and were frequently thicker and stained more positive for acetylcholinesterase than those that coursed between the heart hilum and the ganglia clusters. The nerves that coursed between the heart hilum and ganglia clusters were considered as preganglionic nerves. The nerves that coursed from ganglia clusters to penetrate into the myocardium or gradually become thinner in the epicardium were mostly devoid of ganglia, and considered as postganglionic nerves (Figure 1.10). Thicker nerves were directed more to the postganglionic nerves, whilst thinner nerves interconnected ganglia.

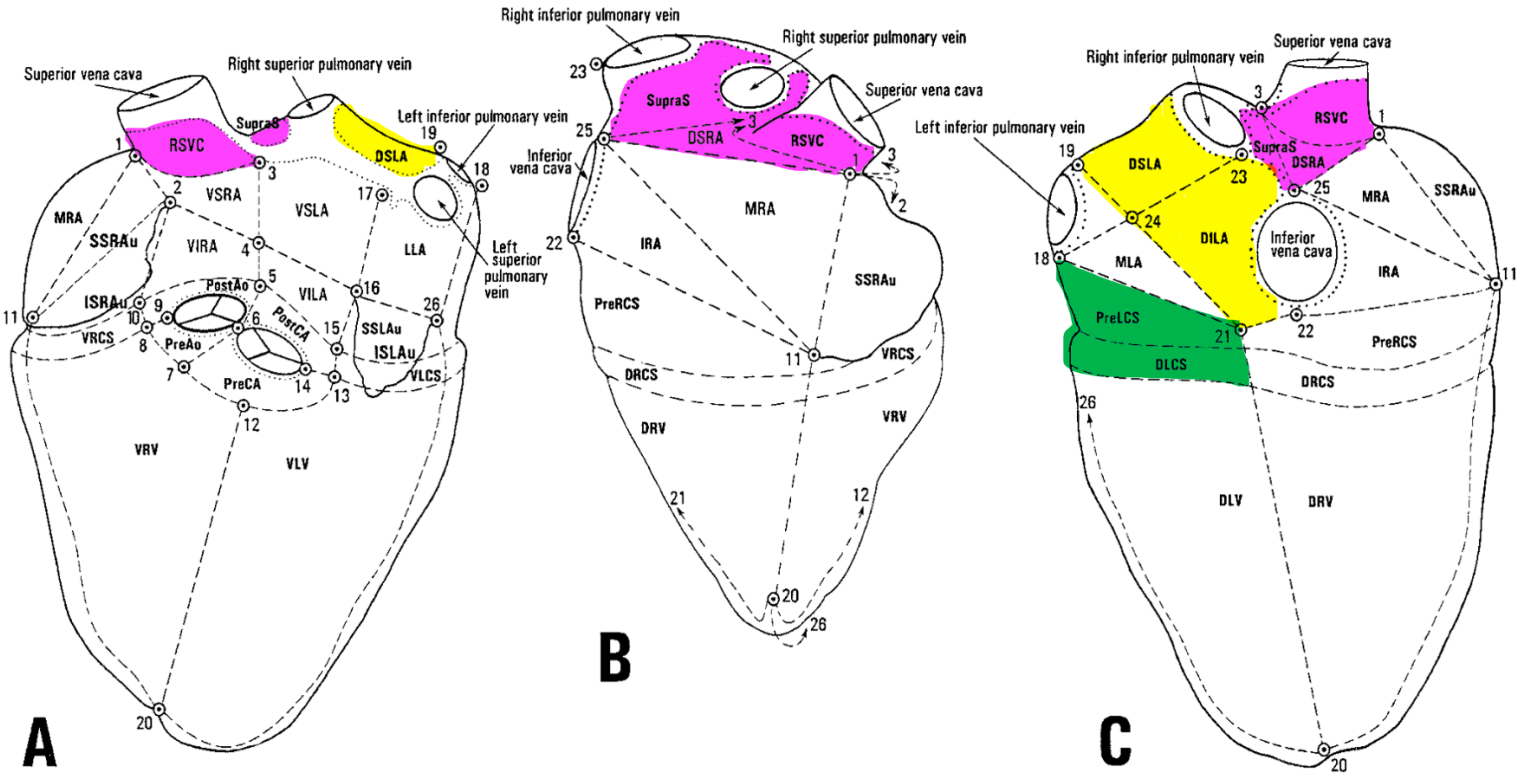

Figure 1.9 Top three dense clusters of ganglia in the human heart.

Drawings of a ventral (A), right lateral (B), and dorsal (C) view of the pressure-inflated human heart illustrating the subdivision of the heart surface into 31 regions. Dotted lines indicate the limits of the heart hilum. The densest cluster of ganglia was in PreLCS and DLCS (green; 30%), followed by SupraS, DSRA, RSVC (pink; 26%) and DSLA, DILA (yellow; 21%). Adapted from Pauza *et al*[81].

(DILA = dorsal inferior left atrial region; DLCS = region of dorsal left coronary sulcus; DSLA = dorsal superior left atrial region; DSRA = dorsal superior right atrial region; PreLCS = region laying over the left coronary sinus; RSVC = root of the superior vena cava; SupraS = region over the interatrial septum)

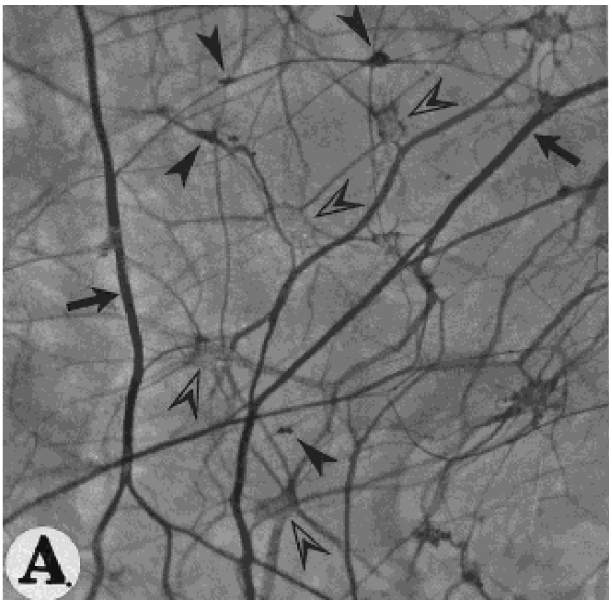

Figure 1.10 Epicardial ganglionated plexus in a 4-year-old boy's heart in the dorsal wall of the left atrium.

The nerves were stained with acetylcholinesterase. Large ganglia are marked by open arrowheads, small ganglia by black arrow heads, and arrows point toward thick nerves, distributed within the epicardium in different depths. The layered structure of this plexus is revealed by differences in staining intensity of ganglia. Adapted from Pauza *et al*[81].

The highest density of ganglia was near the heart hilum, especially on the dorsal and dorsolateral surfaces of the left atrium, where up to 50% of all cardiac ganglia were located. Most ganglia were in the epicardium, some in the myocardium and none were found in subendocardial or endocardial layers[82]. In contrast to previous findings[76,82], Pauza *et al* did not identify any ganglia in the interatrial septum or at the atrioventricular node region. The average number of ganglia was 836 ± 76 per heart (range 706 to 1,560) and 43,000 intrinsic neurons. Interestingly, adult hearts had less number of epicardial neurones than younger hearts (children/infants/foetuses/neonates), that had almost twice as many neurones (Figure 1.11 Contact photomicrographs of epicardial ganglia from a child and an adult heart.Figure 1.11). However, the diameter of adult neurones were larger than younger hearts[81].

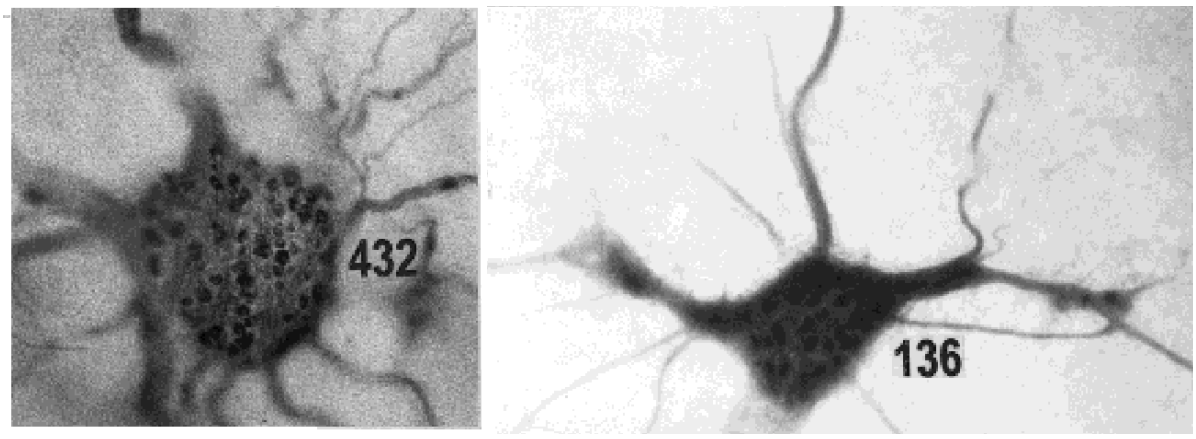

Figure 1.11 Contact photomicrographs of epicardial ganglia from a child and an adult heart.

On the left, is an epicardial ganglia of a 3-month-old and on the right, a 73-year-old. The nerves and ganglia have been stained histochemically for acetylcholinesterase and subsequently examined in serial sections. Numbers indicate the number of neurons counted within them. Larger number of neurones were identified on average, in younger hearts. Adapted from Pauza *et al*[81].

1.4.1. Histology of the Epicardial Ganglia

Histologic features of epicardial ganglia included adipocytes surrounding ganglia and a capsule of connective tissue around each ganglia (Figure 1.12). Satellite cells and neuropils, consisting of axonal and dendritic arborisations, were found throughout the ganglia. Ganglia were generally oval to circular in shape and branched in grapelike clusters from large-diameter nerves.

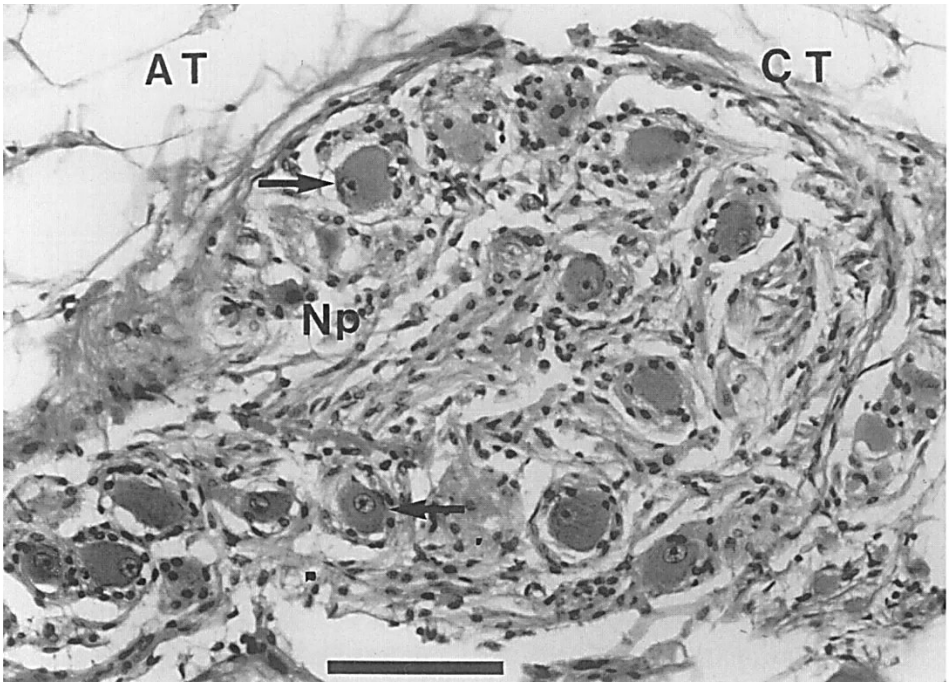

Figure 1.12 Histological features of a cardiac ganglion surrounded by epicardial adipose tissue.

A haematoxylin and eosin stained photomicrograph of a ganglion from the para-sinoatrial node of an adult human heart. There is a capsule of connective tissue (CT) around the ganglion and peripherally located postganglionic neurons (arrow). Neuropil (Np) is found throughout the ganglion. Bar represents 100 µm. Adapted from Singh *et al*[82].

(AT=adipose tissue, CT=connective tissue, Np=neutrophil).

Neurons were generally located at the periphery of the cardiac ganglia. Multipolar neurons predominated, although pseudo-unipolar neurons were also present. Neurons were oval to circular in shape and contained eccentrically located nuclei. A thin capsule of connective tissue surrounded each neuron within the ganglia (Figure 1.13).

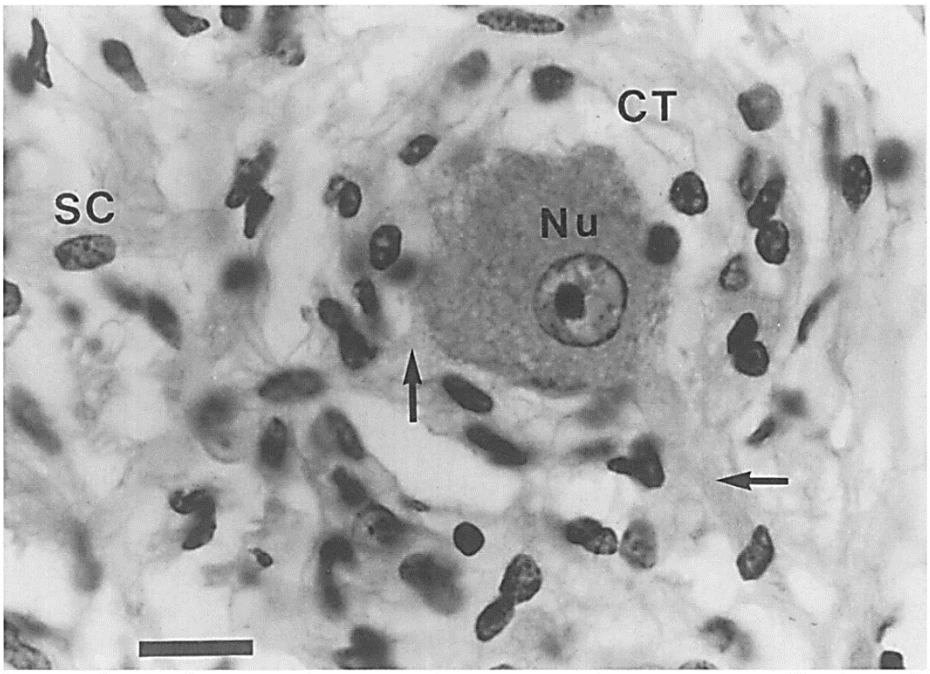

Figure 1.13 Histological features of a neuron within a ganglion in an adult human heart.

A haematoxylin and eosin stained photomicrograph of a multipolar postganglionic neuron within a ganglion from the para-sinoatrial node of an adult human heart. Eccentrically located nuclei (Nu) and nucleoli are clearly visible. Note the two neuronal processes (arrows) visible at this level. A thin layer of connective tissue (CT) surrounds the neuron, whereas satellite cells (SC) are intermingled within the neuropil. Bar represents 10 µm.

(CT = connective tissue, Nu = nuclei, SC = satellite cell)

The sizes of the human ganglia varied, and the mean area was $0.07mm^2 \pm 0.02$. This was comparatively small to canine right atrial ganglia, where a medium sized epicardial ganglia was more than $0.25mm^2$ from a study by Pauza *et al* in 1999[85].

1.4.2. Functional Identification of the Ganglionated Plexuses

In 1963, Vincenzi *et al*[86] first demonstrated the technique of using selective neural stimulation to identify nerves, at a subthreshold level to avoid direct myocardial capture in mammalian cardiac tissues. Since then, various methods using this stimulation technique has been described throughout late 1990s and early 2000s. This made it

possible to conduct detailed studies of the mammalian and human intrinsic cardiac autonomic nervous system to identify specific nerves and examine their functional effects and assess how this impact trigger and maintenance of AF. HFS is a valuable tool that allows functional identification of GPs that are not easily identifiable by eye on the epicardial surface, and can also be used endocardially, as a less invasive approach.

In 2001, Schauerte *et al*[74] first tested in dogs that short bursts of high-frequency electrical stimulation (HFS) in PVs and left and right atrial appendages during the local myocardial refractory period was capable of inducing atrial ectopy, atrial tachycardia (AT) and AF[74]. HFS (100Hz, impulse duration 0.1msec, 10-44V) was coupled to pacing stimulus to ensure that this was delivered within the local refractory period. HFS shortened the local refractory period of the PVs, leading to PV ectopy and tachycardia as seen in the clinical setting (Figure 1.14). Most ectopy originated from PVs, especially in the left superior PV. The highest probability of induction of AF was in the left superior PV, and the lowest in the right inferior PV. These responses to HFS was blunted with betablockade and abolished by atropine. At a site that induced single atrial ectopy, higher voltage stimulation with HFS caused AT or AF. This suggested that a greater degree of neural stimulation was achieved with higher voltage stimulation, leading to repeated after depolarisations and/or progressive shortening of the atrial refractoriness.

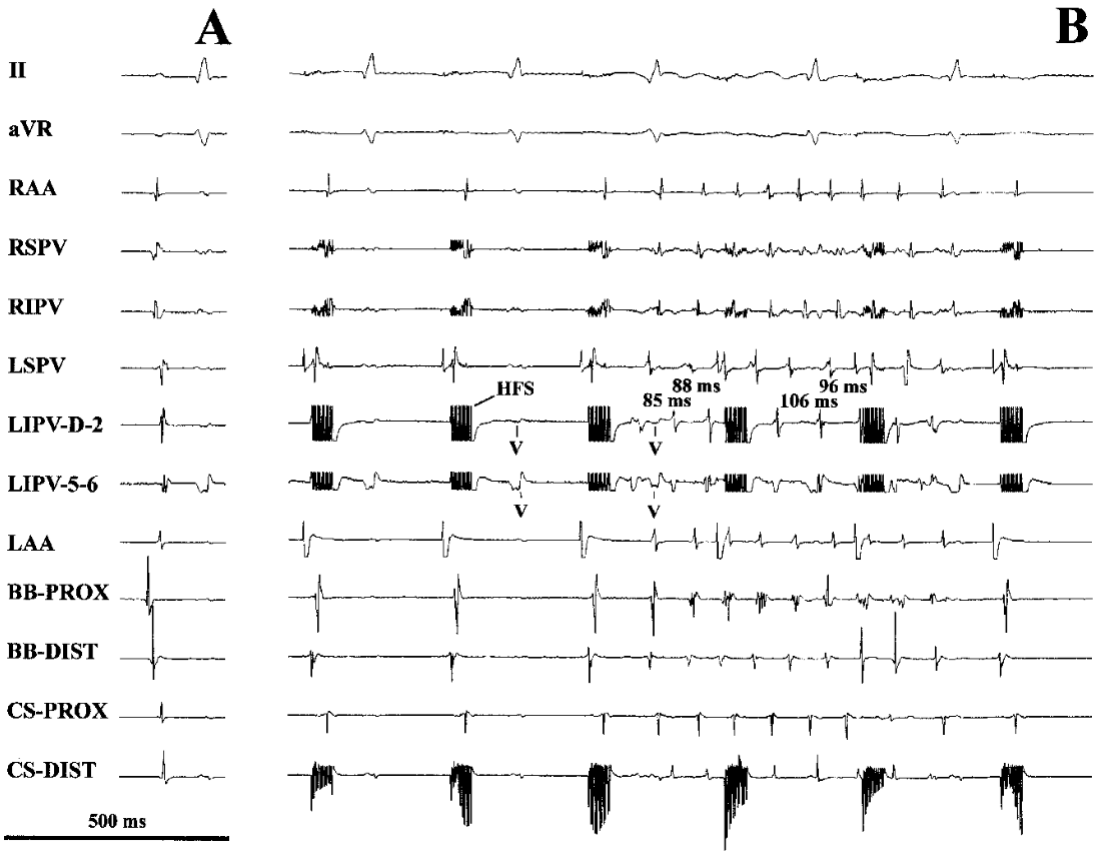

Figure 1.14 High frequency stimulation delivered within the local refractory period of canine PV which triggers PV ectopy and AF

(A) Electrograms during sinus rhythm. (B) Pacing from the left atrial appendage (LAA). HFS (6 V) was delivered in LIPV, over the electrode pair LIPV-3-4 (not shown because of huge stimulus artifact), which was located between electrode pair LIPV-D-2 and LIPV-5-6. LIPV-5-6 was closer to the ostium of the LIPV (approximately 2 cm away from the ostium), whereas LIPV-D-2 was closer to the pulmonary hilus. During HFS, rapid and irregular nonsustained atrial tachycardia with earliest onset of the local activity in the LIPV was induced. In this case, onset of the ectopic surface ECG P wave preceded the earliest local activity in the LIPV electrogram by 25 ms. Subsequent local potentials in the LIPV electrograms have a slightly different morphology, which suggests the ectopic focus may have originated from a different site within the LIPV, possibly closer to LIPV-3-4 over which HFS was delivered. Adapted from Schauerte *et al*[74].

(BB = Bachmann's bundle; CS = coronary sinus; RAA = right atrial appendage; LSPV = left superior pulmonary vein; LIPV = left inferior pulmonary vein; RSPV = right superior pulmonary vein; RIPV = right inferior pulmonary vein; PROX = proximal; DIST = distal)

The authors also performed HFS *in vitro* by measuring the action potential in PV and atrial cells. HFS shortened the action potential in some cells and prolonged this in others, which led to atrial ectopy or AT. Again, atropine abolished the effects of HFS on the cellular action potential. It was not clear from this study why there was a heterogeneous action potential response to HFS. The authors hypothesised it was due to heterogeneous innervation to the atrial structures, or varying cellular response to muscarinic stimuli.

This method of HFS "synchronised" to pacing stimuli was replicated by Lim *et al*[87] in patients with AF. Synchronised HFS was performed at presumed GP sites in the left atrial endocardium of patients, which triggered atrial ectopics and AF. 76% of triggered atrial ectopy were observed to come from the nearest PV to the site of HFS. In one patient, both ectopy and AV block was observed using synchronised HFS.

Another method of HFS, which is more commonly utilised in the literature, is "continuous" HFS (20Hz, 12V, pulse width 1-10ms). However, HFS endocardially directly captures the myocardium and cause AF, and the only useful measure of its neural stimulatory effect during AF, is ventricular slowing with AV block. Po *et al*[88] used this method in in the left atrium of patients with AF, using an "arbitrary" definition of >50% increase in RR interval from baseline during AF, as a GP site. This was described as a parasympathetic response, due to hypotension and AV block.

1.5. Non-Invasive Evaluation of Autonomic Activity

1.5.1. Heart Rate Variability

Heart rate variability (HRV) is a beat-to-beat variation in the heart rate, that is a reflection of the heart's sympathovagal balance on the sinus node. There is marked interindividual variability of HRV[89–91], and it is greater in females than males[92]. It is a useful non-invasive

tool to assess for an individual's cardiac autonomic regulation during sinus rhythm. The high frequency (HF) component of HRV has been linked to respiration-related alterations in primarily parasympathetic cardiovagal outflow[93], and the low frequency (LF) to the sympathetic activity, although the latter relationship is less clear. LF reduces during high-intensity exercise and during immediate recovery with sympathetic activation[94], which also correlates to muscle sympathetic activity[95]. This suggests reduction in LF correlates to increased sympathetic nerve activity. However, LF as a marker of sympathetic activity is only reliable using long ECG recordings, as short recordings may reflect baroreflex responses instead of cardiac sympathetic innervation[93]. Atropine administration also almost completely abolishes LF (and HF) of HRV, which should not occur with purely a sympathetic nerve component in LF[96].

It was shown that LF component of HRV is a predictor of new-onset AF in middle-aged populations. Perkiomaki *et al* in 2014, analysed 784 patients with a mean follow-up of 16.5 years. Decreased LF oscillation independently predicted new-onset AF, requiring hospitalisation. Other components of the frequency domain lost their predictive power after adjusting for other risk factors. A larger study in 2017, analysing 11,715 middle-aged patients by Sunil *et al*[97] also showed that an elevated LF/HF ratio (sympathetic : parasympathetic) was associated with AF incidence.

HRV has been shown to alter significantly before and after PVI[98–101], with surgical AF ablations[102], as well as with GP modulation[103–105]. In one study, reduction of the LF/HF ≥0.26 at 3 months was independently associated with clinical recurrence of AF after pulmonary vein isolation[98]. In another study, a sustained change in HRV parameters such as LF up to 6 months, LF/HF up to 3 months correlated to AF freedom[99]. However, HRV

eventually recovers, in both PVI and GP modulation procedures, which is postulated to be a marker of neural re-connection and associated with AF recurrence.

1.5.2. Sympathetic Skin Activity

The skin of the thorax and upper extremities are well innervated by sympathetic nerves, and their somata of originate in the cervical and stellate ganglia[106]. Measurement of the skin sympathetic nerve activity is thought to be a more accurate assessment of cardiac sympathetic tone than HRV[107]. Uradu *et al* have devised a new method to simultaneously record ECG and the skin sympathetic nerve activity using "neuECG". It overcomes the limitations of HRV by not relying on the sinus node for its interpretation. Patients with AF and heart failure often have sinus node dysfunction. Therefore, HRV in patients with AF may not be a truly accurate representation of their autonomic regulation.

In a prospective study utilising neuECG to record the pattern of skin sympathetic nerve activity in patients with AF and VF[108], there was a significant latency between the onset and offset of skin sympathetic nerve activity of the occurrence and termination, respectively. It was hypothesised that this latency is due to a higher threshold of neurotransmitter accumulation required in the myocardium to lead to electrophysiological changes that trigger the arrhythmia, and similarly, takes time to eliminate the neurotransmitters after cessation of the sympathetic nerve activity. There was a longer latency with AF than in VF. The authors also performd HRV analysis on their patients, which did not pick up on the sympathetic nerve activity changes identified with neuECG. Further studies are required which correlates clinical outcome with skin sympathetic nerve activity monitoring.

1.6. Evolution of Catheter Ablation in AF

1.6.1. Pulmonary Vein Isolation

Since the landmark observation by Haïssaguerre *et al* that PV ectopy are the most common triggers of AF[22], circumferential PV isolation (CPVI) for electrical isolation of the PVs has remained the standard treatment for drug-refractory AF[21].

One of the first approaches to PV isolation was with segmental ostial PV ablation by identifying which PV were triggers to AF[22,109,110]. However, challenges to this approach included being able to consistently induce arrhythmogenic PV foci, increased risk of symptomatic PV stenosis, and AF triggers in the more proximal antral region were not targeted with this strategy. In addition, subsequent repeat AF ablations for AF recurrence showed that different ectopic foci from the same or different PVs were often identified. Therefore, empiric, wide antral isolation of all PVs became the preferred strategy[110–112].

However, the success rate of PVI in large, randomised, multi-centre trials have consistently shown 50-60% for AF prevention at 12 months follow-up[4,113]. A more recently published trial (CIRCA-DOSE) assessed contact-force guided RF ablation for PVI and reported 53.9% at 12 months follow-up[114]. The most dominant mechanism for AF recurrence from PVI is thought to be PV reconnection[115], due to recovery of conducting tissue over time. A small study on patients with recurrent AF undergoing surgical thoracoscopic AF ablations showed that PVs that maintained electrical isolation were more likely to show transmural scar (5/7; 71%) than PVs that had reconnected (6/15; 40%; p = 0.36)[116]. However, re-connection is also observed in patients without AF recurrence[117–119], and durable complete PVI is not invariably associated with AF freedom[116]. In one randomised prospective study, up to 70% PV re-connection was

identified within 3 months from PVI, and out of these patients, 40/65 (62%) patients had early AF recurrence within this period[120]. These findings suggest that perhaps other substrate modification occurs during PVI that contributes to its success and raises a question in successful PVI as a sole endpoint for AF ablation.

1.6.2. Non-Pulmonary Vein Triggers

Despite achieving permanent PVI, small subset of patients still continue to experience symptoms and recurrence of arrhythmia[121]. Search for non-PV triggers of AF identified discrete anatomical clusters in the coronary sinus, inferior mitral annulus, interatrial septum, left atrial appendage, crista terminalis, ligament of Marshall and the superior vena cava as potential sources[122–124]. All these sites have been shown to contain cardiomyocytes that can exhibit arrhythmogenic activity. This may arise from the combined effects of enhanced automaticity, triggered activity and localised microreentrant circuits[43]. Once these non-PV arrhythmia triggers have been eliminated, the incremental value of additional substrate modification with linear ablation, ablation of complex fractionated atrial electrograms, rotors, and autonomic targets remains unproven[125–127].

Intra-Cardiac Neuromodulation in AF

1.6.3. Endocardial Catheter Ablation

There were several endocardial GP ablations in AF attempted in the literature, with two main approaches to GP ablation: ‘anatomical’ and ‘selective’. Anatomical GP ablation approach, as in the AFACT study, is performed by locating clusters of common GP sites known to exist in human and animal hearts. This is an empirical strategy that does not

involve functional testing to confirm GP sites. Selective GP ablation approach utilises HFS to map around the atria and identify a functional 'vagal' response from AV-block, to locate the GP sites.

Clinical studies comparing anatomical and selective GP ablation in AF have suggested that anatomical GP ablation is superior to selective GP ablation. However, there are several important limitations to the selective GP ablation technique utilised by the studies.

Two studies performed 'selective' GP ablation in the human left atrium to map for GPs that produce AV-block or 'vagal' response[105,128]. The larger study of eighty patients[105] limited their functional testing to anatomical regions of the atria thought to contain GPs. They tested on average 37 sites with HFS (Figure 1.15), which was spread across both right and left atria and yielded approximately 5 (14%) GPs per patient.

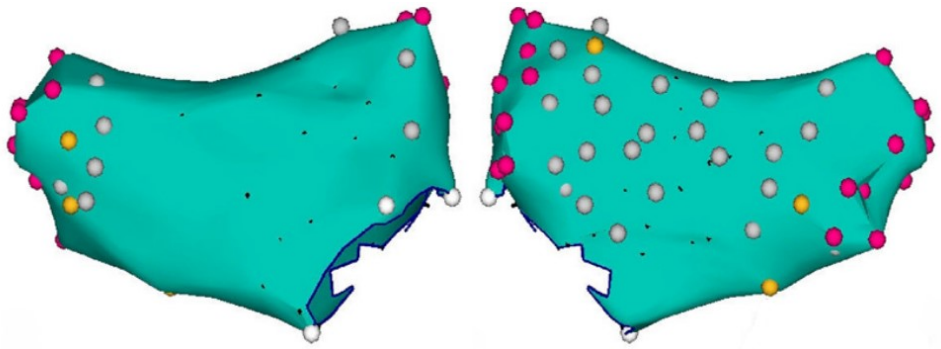

Figure 1.15 Distribution of selective GP mapping with continuous HFS by Pokushalov *et al.*

This is an anterior-posterior (left) and posterior-anterior (right) views of a 3D electroanatomic map of the left atrium. Pink dots represent pulmonary vein boundaries. White dots represent continuous HFS tested sites and yellow dots represent positive atrioventricular block or 'vagal' response from GP stimulation. The authors limited their selective testing of GPs to anatomical regions where GPs are thought to be. Large portion of the anterior wall and the lower border of the posterior wall of the left atrium were not tested. Adapted from Pokushalov *et al*[105].

(GP = ganglionated plexus, HFS = high frequency stimulation)

These selectively identified GPs were ablated and performed statistically significantly worse than anatomical GP ablation at preventing AF (Selective GP = 42.5% vs Anatomical GP = 77.5%; p=0.02).

The same group later showed that anatomical GP ablation performed statistically significantly worse at preventing AF than PVI[7,8]. However, addition of PVI to anatomical GP ablation produced more promising results, achieving significantly higher success at preventing AF than PVI alone[8,129] (74% vs 56%; p=0.004). The technique for anatomical GP ablation was PVI first, then the line extended to cover four main anatomical GP sites as demonstrated in Figure 1.16. The appearance of the ablation lesions is reminiscent of the wide area circumferential ablation (WACA) for PVI. Large amount of ablation was performed, indicated by the prolonged average radiofrequency (RF) time of 67 minutes, compared to 41 minutes with PVI only (p<0.001). Despite this, there were no procedure-related complications in the GP in addition to PVI group.

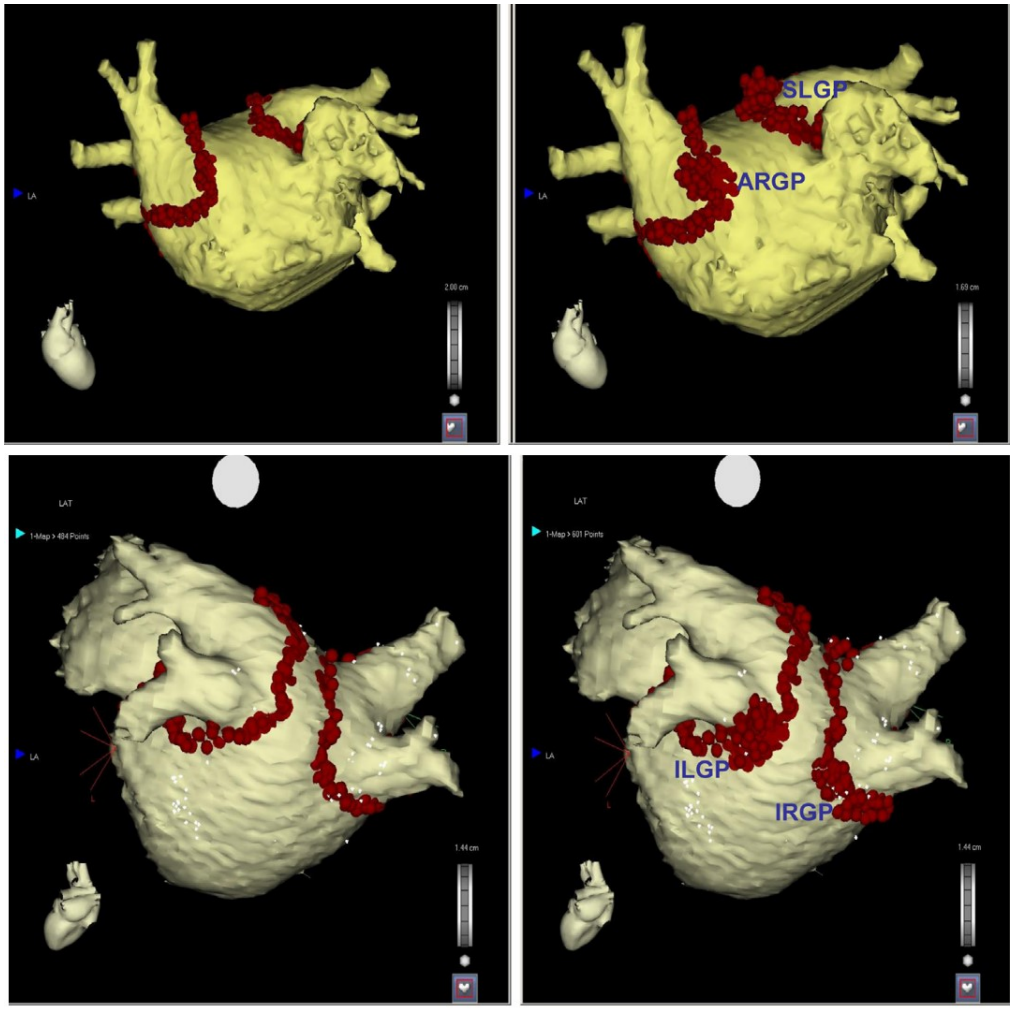

Figure 1.16 Anatomical GP ablation technique by Katrisis *et al*.

3D electroanatomical geometries of the left atrium. Top is the anterior-posterior view, bottom is the posterior-anterior view. The authors performed anatomical GP ablation by first performing pulmonary vein isolation, then extending the line out to 'cover' four main GP clusters though to occupy those anatomical regions. Adapted from Katritsis *et al*[8].

(ARGP = anterior right GP; SLGP = superior left GP; ILGP = inferior lower GP; IRGP = inferior right GP)

1.6.4. Thoracoscopic Epicardial Catheter Ablation

One single-centre clinical trial (AFACT study) ablated GPs thoracoscopically in the epicardial fat pad of patients with advanced, persistent and paroxysmal AF[127]. This study randomised 240 patients to either PVI or anatomical GP ablation in addition to PVI. High frequency stimulation (HFS) was not used routinely to identify GP sites, but was used as a functional confirmation of anatomically located GP sites. The authors located GP sites using approximate anatomical landmarks (Figure 1.17). Functional testing with continuous HFS was performed at the anatomically identified GP sites, but the AV-blocking response was not mandated to ablate the GP sites. No patient who had anatomical GP ablation had AV-blocking response at the end of the procedure, but 87% in the PVI group still had this response.

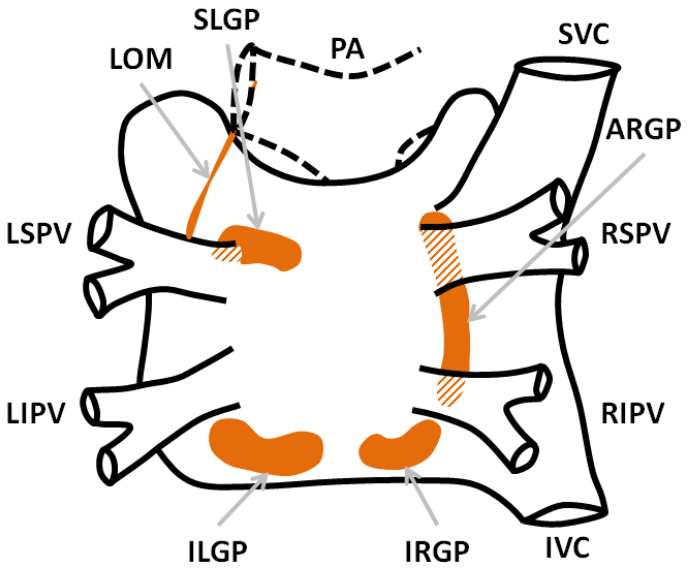

Figure 1.17 'Anatomical' ganglionated plexus localisation in the AFACT Study.

This is a posterior view of the left and right atria with orange regions marking the anatomical GP sites that the investigators ablated in the GP ablation group. These areas were targeted with or without functional AV-block response observed with continuous high frequency stimulation. Adapted from Driessen *et al*[127].

(AFACT = Atrial Fibrillation Ablation and Autonomic Modulation via Thoracoscopic Surgery; ARGP = anterior right GP; GP = ganglionated plexus; ILGP = inferior left GP;

IRGP = inferior right GP; IVC = inferior caval vein; LIPV = left inferior PV; LSPV = left superior PV; PA = pulmonary artery; PV = pulmonary vein; RIPV = right inferior PV; RSPV = right superior PV; SLGP = superior left GP; SVC = superior caval vein)

After 12 months follow-up, freedom from AF was not statistically different between the two groups (GP = 70.9% vs PVI = 68.4%; p = 0.696). GP ablation group had 4 deaths; 1 from sepsis from decompensated restrictive cardiomyopathy, 2 from metastatic cancer, and 1 sudden death from unknown causes. There was no death in the PVI group (p = 0.055). There were statistically significantly higher major procedure-related complications in the GP group compared to PVI group (19% vs 8%; p = 0.022). 55% of the major procedure-related complications in the GP group were sinus node dysfunction, requiring admission for isoprenaline and/or temporary wire pacing. Some required permanent pacemaker implantations as a result.

It was clear from this study that thoracoscopic GP ablation in addition to PVI carries a greater risk of developing conduction disease, without conferring additional benefit over PVI alone. This implies that a more selective GP ablation approach is required to prevent these major complications, at least thoracoscopically. Also, abolition of AV-blocking response remained in majority of patients with PVI only, with statistically non-significant difference in freedom from AF to GP ablation in addition to PVI. This suggests that most AV-blocking GP are not within the regions of PVI and specifically targeting them in addition to PVI does not prevent AF better than PVI alone.

1.6.5. Meta-Analyses of Catheter Ablation

A meta-analysis of four randomised controlled studies (RCT)[130] with 718 patients showed that anatomical GP ablation in addition to PVI had significantly higher freedom from AF/atrial tachycardia (AT), than PVI alone (75.8 vs 60.0%; OR [95% CI]: 2.22 [1.36-

3.61]; p=0.001). In persistent AF patients, anatomical GP ablation in addition to PVI did not show statistically significant higher freedom from AF/AT than PVI alone (54.7% vs 43.3%; OR [95% CI]: 1.55 [0.96-2.52]; p=0.08). In all cases, heterogeneity was low (I^2 of 32% or lower), but three of the four RCT were from the same group of investigators and centres[8,131,132]. Another meta-analysis evaluating 1615 patients who had anatomical GP ablation as a stand-alone procedure, anatomical GP ablation in addition to PVI, and non-GP ablation strategies for AF were analysed[133]. Overall, anatomical GP ablation did not improve freedom from AF at 12 months (p=0.12). Again, four out of six studies from this analysis were from the same group of investigators and centres[7,8,131,132].

1.6.6. Botulinum Toxin and Lidocaine Epicardial Fat Pad Injection

Botulinum toxin is a neurotoxin produced by *Clostridium botulinum* that blocks the exocytotic release of acetylcholine stored in synaptic vesicles and interferes with cholinergic neurotransmission. In the last two decades, it has been utilised in different formulations and preparations to treat various medical conditions, such as headaches, blepharospasm, cervical dystonia and adult spasticity[134]. Its role in treating cardiac conditions are not yet clear. In experimental canine models, Botulinum toxin injection into the cardiac fat pad responsible for the sinus node activity was capable of preventing bradycardia, as well as AF inducibility via stimulation of the parasympathetic nerves[135,136]. However, the botulinum toxin effects are thought to vary between 1 to 6 months, depending on the injection location[136].

Oh *et al*[137] injected botulinum toxin or normal saline into the fat pads of dogs and found that the cervical vagal stimulation effects on the sinus and atrioventricular node were inhibited in those injected with botulinum toxin. Significant AF suppression was achieved with botulinum toxin injection up to 1 week. These changes were not evident in the

normal saline injection group. Pokushalov *et al*[103,138,139] performed the first "in-man" injection of botulinum toxin into patients with a history of AF undergoing coronary artery bypass surgery (CABG). The authors randomised patients to either botulinum toxin injection into the four major GP areas in the fat pad, or normal saline injection as placebo. An implantable loop recorder was used to identify reoccurrence of AF. Patients with AF burden of ≤0.5% were considered AF free, which corresponded to maximum cumulative time in AF of 3.6hrs in 1 month and to >99.5% spent in sinus rhythm during the 12 months follow-up period. Outcomes showed that within the early post-operative period of 30 days, 2 out of 30 patients (7%) in the botulinum toxin group and 9 out of 30 (30%) patients in the placebo group had AF recurrence ($p = 0.024$). After 30 days and up to 12 months follow-up, 7 out of 30 (27%) patients in the placebo group had AF recurrence and none of the 30 patients in the botulinum toxin group had AF recurrence ($p = 0.002$). At 36 months of follow-up, 23.3% had AF recurrence in the botulinum injection group compared to 50% in the placebo group ($p = 0.02$).

Heart rate variability (HRV) is a marker of the parasympathetic nerve activity on the sinus node of the heart[89]. As botulinum toxin works purely on blocking of acetylcholine neurotransmitters from the parasympathetic nerves, one would expect HRV to correlate with the reversal of the botulinum toxin effects. However, patients in this study who received botulinum toxin injection remained AF free at 12 months, despite the reversal of the time and domain frequency heart rate variability (HRV) parameters after 6 months. The mechanism for this is not clear.

The long-term benefit of botulinum toxin injection in patients has not been reproduced elsewhere. It is not known what effect the same therapy can have on patients with AF, without an indication for CABG.

Lidocaine alters signal conduction in neurons by prolonging the inactivation of the fast voltage-gated Na^+ channels in the neuronal cell membrane responsible for action potential propagation. A small pilot study performed lidocaine injection into the epicardial fat pad, targeting the four major GP areas in 6 long-standing persistent AF patients undergoing CABG with or without valvular surgeries[140]. There was no control group. The mean AF cycle length in the left atrium became significantly more prolonged after lidocaine injection compared to baseline ($p<0.05$). This was not observed in the right atrium. Also, the left to right atrium frequency gradient that was present at baseline disappeared after lidocaine injection ($p=0.08$), but AF did not terminate.

1.6.7. Fat Pad Removal and Retention

Epicardial fat of the heart is adipose tissue that surrounds the heart, locate between the myocardium and the visceral pericardium. This is distinguished from the paracardial fat, which is located external to the parietal pericardium (Figure 1.18). The physiological functions of epicardial fat includes lipid storage for myocardial energy, thermoregulation, regulation of coronary artery vasomotion and luminal size, and protection of the autonomic ganglia as the main integration centres of the intrinsic cardiac autonomic nervous system[141]. It is associated with prevalence of AF, even after adjusting for AF risk factors such as the body mass index (BMI)[141,142]. Briefly, epicardial fat can influence various structural and electrical remodelling of the atria by both direct (e.g. by the infiltration of adipose tissue leading to altered atrial electrophysiological properties) and indirect mechanisms (e.g. by acting as a source for paracrine modulators of myocardial inflammation and oxidative stress). GPs are also known to be most abundant within the epicardial fat of the heart. Interestingly, a study by Nagashima *et al*[143] in persistent and paroxysmal AF patients showed that the epicardial fat distribution correlated to

endocardial high dominant frequency areas. No correlation between the epicardial fat distribution and complex fractionated atria electrogram was found.

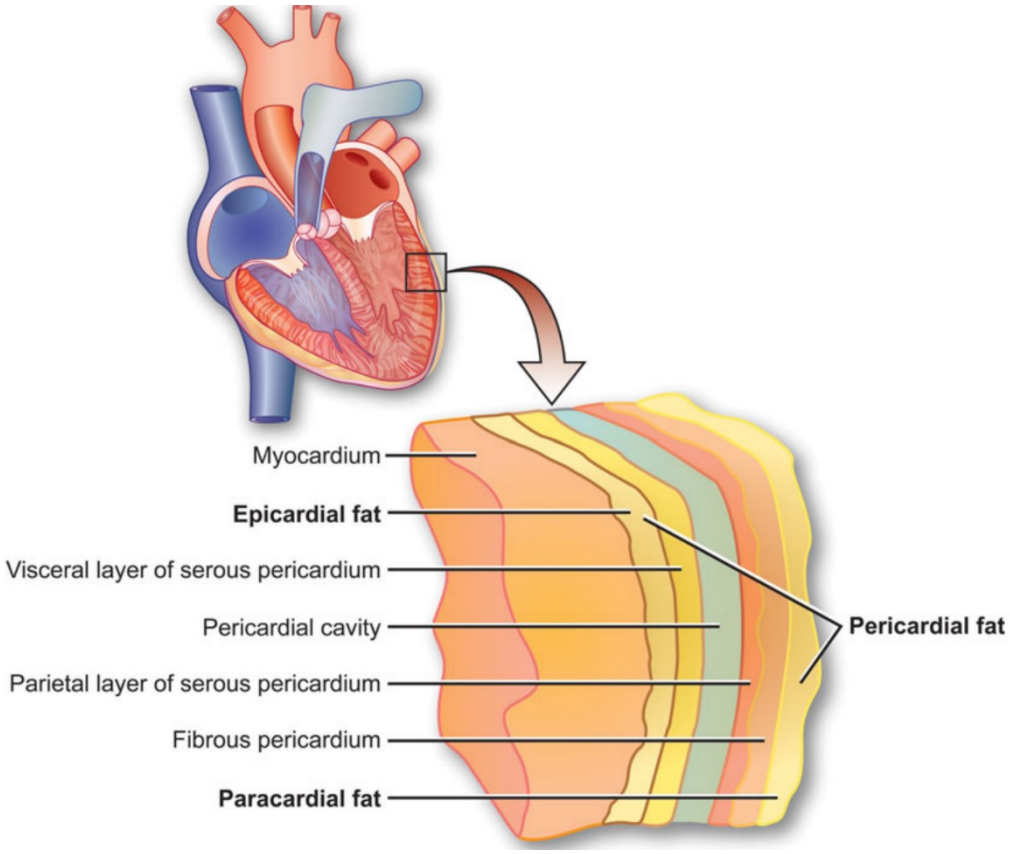

Figure 1.18 Definition of epicardial fat and related adipose tissues

Schematic demonstrating epicardial fat between the myocardium and visceral pericardium, paracardial fat adherent and external to the parietal pericardium, and pericardial fat as the combination of epicardial and paracardial fat components. Adapted from Wong *et al*[141].

1.7. Extra-Cardiac Neuromodulation in AF

1.7.1. Vagus Nerve Stimulation

The auricular branch of the vagus nerve located at the tragus, the anterior protuberance of the outer ear, is capable of affecting neural pathways at a distance[144,145]. Yu *et al*[146] delivered 2 hours of low-level tragus stimulation (LLTS) in the ear of anaesthetised dogs, and this reversed the effects of rapid atrial pacing-induced atrial remodelling (shortened effective refractory period, increased neural activity from baseline) and inhibited AF inducibility. Bivagal transection prevented this reversal. Stavrakis *et al*[147] studied patients with paroxysmal AF presenting for AF ablations. Under general anaesthesia, AF was induced by rapid atrial pacing at baseline and after 1 hour of low-level tragus stimulation in the right ear. Sham tragus stimulation acted as controls in a separate group of patients. Inflammatory markers including C-reactive protein (CRP) and tumour necrosis factor-alpha were measured from the coronary sinus and femoral veins at baseline. After 1 hour of LLTS, there was significant decrease in the inflammatory markers centrally from the femoral vein, pacing induced AF duration significantly reduced by 6.3mins compared to the baseline, and AF cycle length significantly prolonged by 28.8ms from the baseline. There was no difference in the sham group. The authors went onto testing LLTS for 1 hour daily in 53 patients with AF, over 6 months[148]. AF burden was assessed by non-invasive continuous ECG Monitoring at baseline, 3 and 6 months, over 2 week periods. After combining across the 3- and 6-month time-points, the median AF burden was reduced by 75% in the LLTS group compared to the sham group (ratio of medians: 0.25, 95% CI: 0.08 to 0.77, p=0.016). Adherence to the stimulation protocol was 75% in LLTS and 83% in the sham group. Figure 1.19 shows a diagram of the mechanism of LLTS in AF.

The effects of manipulation and sectioning of the vagus nerve has been reported as early as 1970s, though in one case report, targeting the upper vagal rootlets in patients led to hypotension, increased ventricular ectopy, and right bundle branch block[149]. Therefore, it is important to understand the subtleties of this novel therapy as more than just the binary effect of on/off stimulation or high/low energy, to comprehensively understand its correct application in a clinical setting[10].

This non-invasive, self-administered therapy for AF shows promising results, though the optimal LLTS settings for maximal beneficial effect is yet to be determined. How LLTS will compare with the standard PVI in AF patients, is unknown.

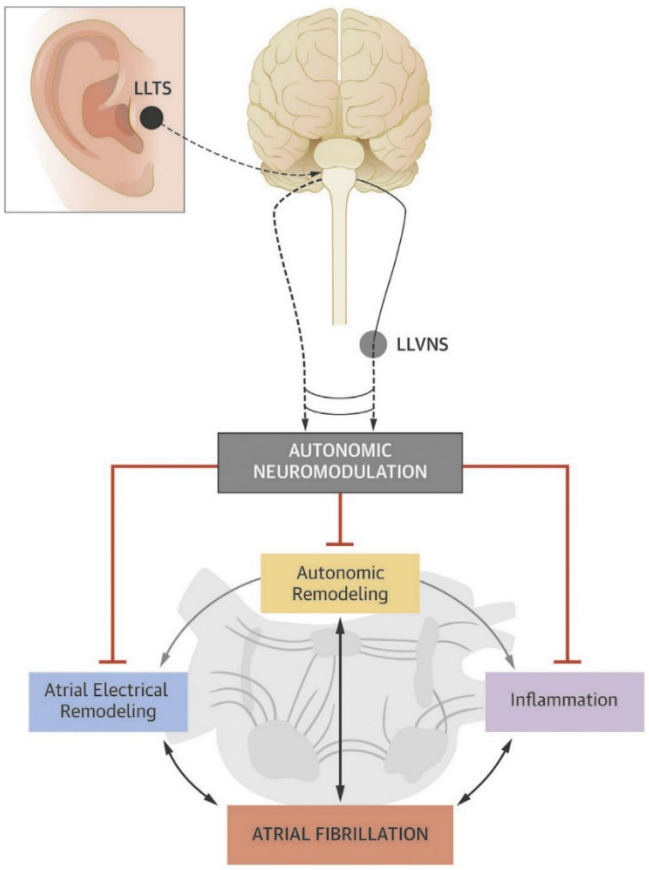

Figure 1.19 Mechanism of autonomic modulation via low-level tragus stimulation

LLTS acts upon the vagus nerve, which is part of the extrinsic cardiac autonomic nervous system and interacts with the intrinsic cardiac autonomic nervous system. This leads to reversal of autonomic and atrial electrical remodelling, reduce inflammation, and AF suppression. Adapted from Stavrakis *et al*[150].

(LLTS = low level tragus stimulation; LLVNS = low level vagus nerve stimulation)

1.7.2. Renal Denervation

Renal denervation has been studied for treating resistant hypertension in the past, with mixed results[151]. Recently, in a single-blinded, randomised controlled trial (ERADICATE-AF) studying 300 paroxysmal AF patients, renal artery denervation added to PVI had significant greater freedom from AF compared to PVI alone (71.4% vs 57.8%; p = 0.011). However, it is not yet known what effect renal denervation had on the blood pressure of the patients who had recurrence vs non-recurrence with AF. Hypertension is a well-

established risk factor for AF, and its modulation with renal denervation may have influenced the outcomes of the study.

1.8. Scope of Thesis

This thesis sets out to address the hypothesis that GP are upstream triggers of AF and can be safely mapped and specifically targeted to prevent AF.

Chapter 1 explores the history and background of our understanding of AF, with specific focus on the autonomic nervous system and its role in AF. Current strategies for treatment of AF are also explored, including our knowledge of autonomic modulation techniques to date.

Chapter 2 addresses the common Methodology used throughout the clinical studies performed in this Thesis. This includes patient selection and follow-up details, detailed mapping technique for different types of GP and ablation. This is followed by description of our custom-built, automated algorithm used for creating the probability distribution atlases of the different types of GP. Lastly, the technical aspects of Langendorff whole-heart retrograde perfusion set-up for the porcine heart experimentation is outlined.

Chapter 3 investigates the anatomical distribution of atrioventricular dissociating GP (AVD-GP). This is achieved by functional mapping with HFS globally around the left atrium of patients with AF. We define what constitutes an AVD-GP by functional response from HFS. By collating together multiple patients' 3D electroanatomic maps of AVD-GP and negative HFS sites, a probability distribution atlas of the AVD-GP is created. We describe the highest and lowest probability of AVD-GP by anatomical regions in the left atrium. This atlas gives a clear visual representation of the discrete anatomical distribution of AVD-GP and can be used to guide clinicians to map for AVD-GP.

Chapter 4 investigates the anatomical distribution of ectopy-triggering GP (ET-GP) in the left atrium of patients with paroxysmal AF, using HFS during sinus rhythm. Reproducible

atrial ectopy and arrhythmia triggers are observed with ET-GP stimulation. We categorise different types of responses to HFS at ET-GP sites, and construct a probability distribution atlas using the same automated process as with AVD-GP, to identify high and low probability ET-GP anatomical distribution around the left atrium. This is compared with AVD-GP, which shows marked contrast in their anatomical distribution. Reproducible atrial arrhythmia triggered from ET-GP stimulation and their distinct anatomical distribution gives scope for further investigation of their clinical role in AF treatment.

Chapter 5 investigates the hypothesis that ET-GP ablation without PVI prevents AF in paroxysmal AF patients, as a prospective, randomised, controlled, multi-centre study. Patients are randomised to ET-GP ablation without PVI, or PVI alone. Primary, secondary outcomes and complications are reported. Factors that may contribute to AF/AT recurrence with ET-GP ablation and PVI are explored.

Chapter 6 investigates the hypothesis that ET-GP ablation in addition to PVI prevents AF in redo AF ablation patients, as a prospective, feasibility study. Patients are randomised to ET-GP ablation in addition to redo PVI, or redo PVI alone. Regardless of the randomisation, all patients receive HFS mapping before and after PVI, which assesses the effect of PVI on ET-GP. Interesting cases are reported, such as sustained PV tachycardia triggered by ET-GP stimulation outside the PVs, and ET-GP ablation in patients with all PVs permanently isolated.

Chapter 7 describes interesting phenomena observed during GP ablation in the clinical studies. In some patients, acute modification of AF is observed with GP ablation, which is correlated with long-term AF/AT freedom. We also analyse patterns of GP recovery after initial GP ablation procedures, in patients returning with AF recurrence.

Chapter 8 investigates the hypothesis that atrial arrhythmia with ET-GP stimulation can be replicated with HFS in Langendorff-perfused whole porcine hearts, and that histologically, there are increased nerve density at ET sites compared to non-ET sites. The same HFS technique used in the clinical setting to identify ET-GP are used in this experimental model to replicate the functional effects of ET-GP stimulation. A custom-built neural stimulator (Tau-20) is used to perform HFS. Both left and right atria are mapped with HFS. ET and non-ET cross-sectional tissues are dissected, fixed, and immunofluorescence technique used to stain for sympathetic and parasympathetic nerves. Nerves are quantified and compared between ET and non-ET tissues. The clinical implication of the findings is discussed.

Chapter 9 summarises the development of a custom-built neural stimulator (Tau-20) with aims to replace the old Grass S88 stimulator used commonly for HFS. The Tau-20 uses a digital graphical user interface and engineered to accurately deliver the exact HFS parameters as specified. It is also capable of performing basic pacing functions during electrophysiology studies, and has an intracardiac electrogram recording function. Set-up and results from the whole live pig experiment with the Tau-20 and first successful human cases using the Tau-20 are outlined.

Chapter 10 is the conclusion of this thesis, summarising the major findings. Future projects based on the evidence found in this thesis are also outlined.

2. METHODS

2.1. Introduction

Methods and protocols that have been repeatedly used in more than one clinical study are described in this chapter.

2.2. Patient Selection and Clinical Follow-up

2.2.1. Patient Recruitment

Patients with symptomatic paroxysmal atrial fibrillation (AF), resistant to at least one anti-arrhythmic agent, and referred for AF ablation were screened for inclusion in the clinical studies. All patients stopped their anti-arrhythmic agents and betablockers five half-lives prior to the procedure. Amiodarone was stopped at least 2 months prior to the procedure. All patients provided written informed consent for participation in the study, which was approved by the Health Research Authority and the Local Research Ethics Committee. Details of the inclusion and exclusion criteria are outlined in the chapters, which differed between studies.

2.2.2. Clinical Procedures

All patients undergoing AF ablation in the clinical studies had general anaesthesia and a transoesophageal echocardiogram to rule out cardiac thrombus. A decapolar catheter was positioned in the coronary sinus in all cases. After transseptal puncture, a 20-pole circumferential catheter (LassoNav, Biosense Webster, Diamond Bar, CA, USA) was used to create a respiratory-gated 3-dimensional electroanatomic map of the left atrium (CARTO™, Biosense Webster, CA, USA). It was then placed in one of the PVs. A bipolar

3.5mm irrigated-tip contact force sensing ablation catheter (Smart-Touch™, Biosense Webster, CA, USA) was positioned on a stable endocardial surface with a target contact force ≥3g for HFS and ablation protocols. Blood pressure was continuously monitored using a radial arterial line. Heparin was administered throughout the cases to maintain the activated clotting time >300s. All data were recorded at 1,000Hz by the EP recording system (Bard EP, Lowell, MA, USA). At the end of the procedure, heparin was reversed with protamine, and patients were discharged the next morning if well.

2.2.3. Clinical Follow-Up

All clinical study patients were followed-up for 12 months. At four time points throughout the year (3,6,9,12 months post-ablation), each patient received 48hr Holter monitors and had their symptoms and progress checked via telephone and/or email communication with a doctor. If patients reported symptoms between these time points, further investigations were ordered such as additional Holter monitors. All patients attended at least one out-patient appointment to see a cardiology consultant within the 12 months of follow-up. Anyone presenting with symptomatic recurrence of AF or atrial tachycardia (AT) was considered for a further ablation procedure.

2.2.4. Definitions for Endpoint

The primary endpoint was any documented atrial arrhythmia (AF, AT, atrial flutter) for ≥30s consecutively recorded on a Holter monitor or 12 lead ECG after a 90-day blanking period. The 90-day blanking period was included as atrial arrhythmia during this period are common whilst undergoing extensive physiological healing process after ablation, as per the expert consensus statement on AF ablation[21].

The secondary endpoints included repeat ablation for AF/AT/atrial flutter after a 90-day blanking period, mortality, any complications related to the procedure (bleeding, thrombosis, phrenic nerve palsy, cardiac tamponade) requiring intervention or a prolonged hospital stay.

2.3. Identification of The Ganglionated Plexus

High frequency stimulation (HFS) was performed to identify the ganglionated plexuses (GPs) in the left atrial endocardium of patients undergoing AF ablation. Endocardial HFS stimulates the epicardial GP[152] via the complex neural network that branches out throughout the left atrial tissue. Two different types of HFS protocols were used throughout the clinical studies: continuous HFS and synchronised HFS, which were used to detect atrioventricular dissociating GP (AVD-GP) and atrial ectopy/AF/AT triggering GP (ET-GP) respectively. A S88 Grass stimulator (Astro-Med, RI, USA) was used to deliver HFS from the distal electrode of an ablation catheter for all clinical studies. Approximately 6mm spacing was used between each HFS test site to achieve an evenly spaced global left atrial map of GP. This was confirmed by measuring distances between random HFS sites on the CARTO™ system.

2.3.1. Grass S88 Stimulator Set-up

The Grass S88 stimulator used for HFS studies contained two primary output channels; S1 and S2. S1 was used to pace and perform continuous HFS, and S2 used exclusively to deliver short and repeated bursts of HFS synchronised to paced stimuli in S1. "S1 Function" was always set to "S1 Repeat" and "S2 Function" set to "S1 & S2 Train". Channel rate, delay, duration and voltage parameters for continuous and synchronised HFS are outlined later in this chapter.

Each channel was connected to two separate isolation units, which minimised current leakage from the stimulator. The isolation unit parameters did not change according to which HFS protocol was used. “Coupling” was set to “Direct”, “Polarity” set to “Normal”, and “Multiply Input Volts” was set to x1.0. The small black and red (+/-) electrode ports on the isolation unit was used to connect with the CARTO™ PIU unit (Figure 2.1). Specifically, on the PIU unit, the “RF generator” ports were used for S1 channel input, and “MAP” ports used for S2 channel input. A jumping cable was used from the RF generator electrodes that also connected to the junction box of the intracardiac recording system (Bard EP, Lowell, MA, USA) amplifier station. This allowed pacing to be performed via the intracardiac recording system as well as the Grass S88 stimulator.

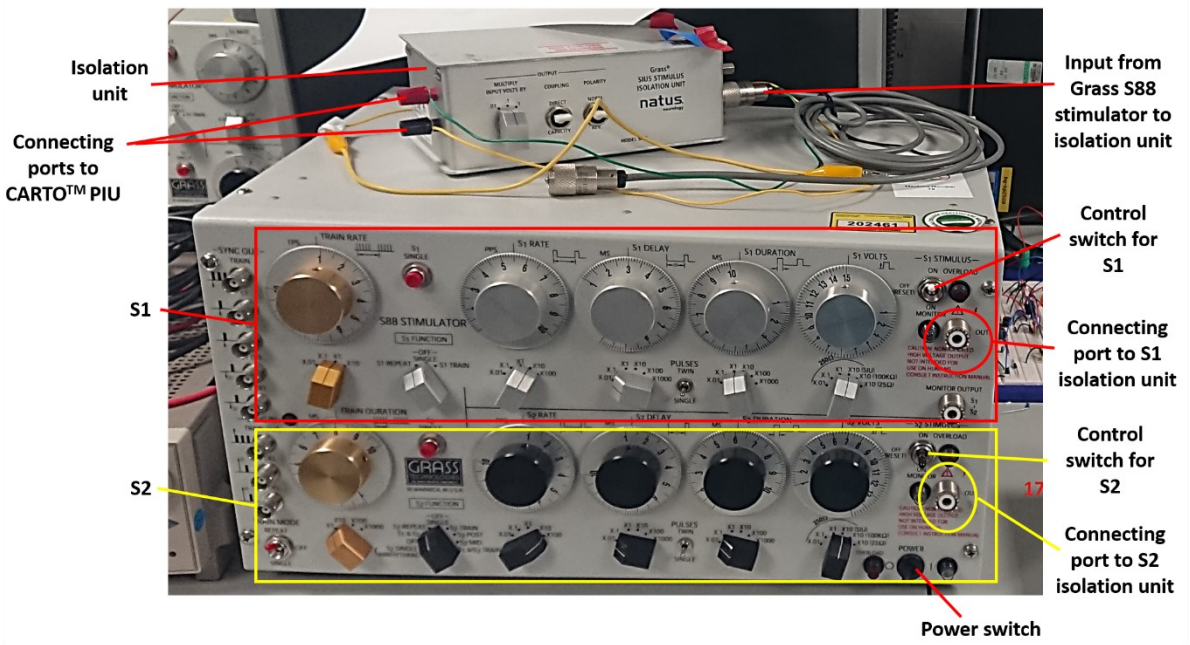

Figure 2.1 The Grass S88 stimulator and the isolation unit used for high frequency stimulation.

The Grass S88 stimulator comprises of two output channels; S1 and S2. S1 is boxed in red at the top of the stimulator, and S2 boxed in yellow at the bottom of the stimulator. The analogue dials are used to adjust the stimulation parameters in both S1 and S2, and the control switches used to turn on/off for S1/S2 stimulations. Flicking the switch upwards enabled the user greater manual control of how long to stimulate the impulses for, as letting the switch go immediately ceased stimulation. Flicking the switch downwards enabled fixed continuous stimulation without needing to hold the switch down for longer stimulations. Two isolation units connected to respective S1

and S2 connecting ports to minimise current leakage from the Grass S88 stimulator. The black and red (+/-) connecting ports at the front of the isolation units allowed direct connection of the Grass S88 stimuli to the catheters via the CARTO™ PIU unit.

2.3.2. CARTO Set-up

For all HFS cases, a 3D electroanatomic map was created of the left atrium using CARTO™. Respiratory gating was performed for all patients to produce more accurate 3D electroanatomic map. A template specific to all HFS cases was saved onto the system, which saved the default Tag setup as shown in Figure 2.2. Hotkeys assigned to individual Tags allowed quick and efficient way of tagging anatomical sites and visually indicating response to HFS (positive or negative).

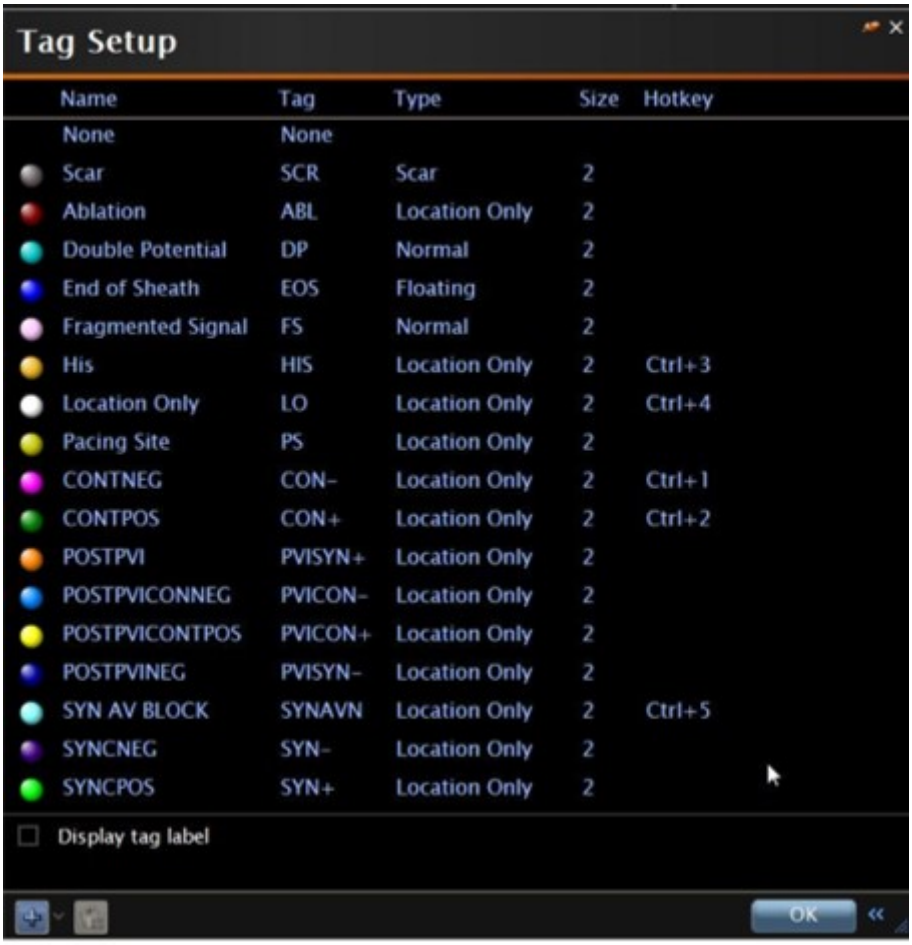

Figure 2.2 CARTO default tag set-up example for HFS studies

For all clinical HFS studies, a Tag template was set-up prior to starting each case. This allowed a convenient "hotkey" to be assigned to different Tags to allow quick and efficient case protocol completion. Different colours assigned to each Tag allowed visual differentiation of responses to HFS on the 3D electroanatomic map. For example, "CONTNEG" and "CONTPOS" indicated continuous HFS negative, and continuous HFS positive response. (HFS = high frequency stimulation)

A grey "Scar" Tag was used to mark any site that did not capture the left atrium with high output pacing with Grass S88 stimulator. Synchronised HFS was not performed in these areas as atrial capture was essential with pacing to deliver HFS within the local atrial refractory period. With the Grass S88 stimulator, it was not possible to pace from another catheter to the catheter delivering HFS.

2.3.3. Continuous High Frequency Stimulation

Continuous HFS was performed to locate AVD-GP. Before delivering HFS, at least four pacing stimuli at high output (12V) was delivered to ensure there was no ventricular capture. HFS was then applied at 20Hz, amplitude 12V, pulse duration 10ms, for up to 10s or until significant atrioventricular (AV) dissociation or asystole occurred. This autonomic effect was usually apparent on the arterial blood pressure trace, or the surface ECG. Sometimes, an additional quadripolar catheter was inserted in the right ventricle for easier visualisation of the ventricular signals within the continuous HFS artefact. Continuous HFS always induced AF due to direct myocardial capture. If there was no obvious asystole, but suspected slowing of the ventricular rate during continuous HFS, RR intervals were measured from the maximum peaks of the arterial BP trace, or the right ventricular electrogram. In the event of any measurement uncertainty, HFS was repeated at the tested site.

2.3.4. Synchronised High Frequency Stimulation

Synchronised HFS was performed to locate ET-GP. Patients were in sinus rhythm for this protocol. If in AF/AT at start of the procedure, they were DC cardioverted up to three times to restore sinus rhythm. A 20-pole circumferential catheter (LassoNav; Biosense Webster Inc, Diamond Bar, CA) or a PENTARAY® catheter was inserted into the nearest pulmonary vein to where synchronised HFS was being tested. This was to maximise the chances of identifying the earliest triggered pulmonary vein ectopy with HFS, with the assumption that GPs are more likely to have neural connections to adjacent structures.

Before HFS, at least four pacing stimuli at high output (12V) was delivered to ensure there was no ventricular capture. Once confirmed, the atrium was paced at a fixed rate that was higher than the intrinsic rate. HFS was coupled to each pacing stimuli with 20ms delay

(to ensure HFS delivery within the local atrial refractory period), 40Hz, 12V amplitude, pulse duration 10ms, for up to 15 trains, or until atrial ectopy or AF/AT occurred. If there was ≤3 atrial ectopy, synchronised HFS was repeated to ensure the response was reproducible. Sometimes, progressive Wenckebach occurred with synchronised HFS with or without AV block. This confirmed an AVD-GP site with synchronised HFS. Repeat testing with continuous HFS at the same site produced a more pronounced AV dissociation with longer HFS duration. An example of this is shown in Chapter 4.

2.3.5. Definition of AVD-GP

During continuous HFS, any asystole lasting several seconds, or significant ventricular slowing defined as >50% increase in the average RR interval during HFS from the baseline was defined as an AVD-GP. Examples and calculation of this threshold is detailed in Chapter 3.

During synchronised HFS, any asystole, progressive Wenckebach with or without atrioventricular block was also defined as an AVD-GP.

2.3.6. Definition of ET-GP

During synchronised HFS, any single atrial ectopy, AF or AT triggered were defined as ET-GP. These autonomic responses cannot be observed with continuous HFS, as this mode of HFS inevitably causes AF from direct myocardial capture. If ≤3 atrial ectopy was triggered with synchronised HFS, the same site was re-tested up to three times. If two out of three tests produced atrial ectopy/AF/AT, this was confirmed as ET-GP.

2.4. Catheter Ablation Protocols

2.4.1. GP Ablation Protocol

At each GP site, a cluster of 2-3 point-by-point lesions overlapping the GP site were delivered at 30W, 30s each, >3g contact force, catheter irrigation rate 17ml/min. If GPs were in the posterior wall, power was limited to 25W only. Other ablation parameters such as the interlesion distance, force-time-integral, Ablation Index were not specified for GP ablation, as there is currently no evidence for any specific parameters to be effective for GP ablation. All GPs were retested with HFS afterwards to ensure no further autonomic response was triggerable. If there was still a response, further ablation was performed until there was no further response.

GP ablation was usually performed at the end of the procedure. However, if sustained AF/AT was triggered with synchronised HFS for >2 minutes during HFS mapping, the culprit ET-GP was ablated first followed by other identified ET-GP until restoration of sinus rhythm. If after ablating all identified GP the patient remained in sustained AF/AT, up to three DC cardioversions were performed to restore and maintain sinus rhythm. If this failed, we switched to continuous HFS to map the rest of the left atrium to identify AVD-GP. All GP including ET-GP and AVD-GP were ablated at the end of the procedure. The pulmonary veins were left electrically connected.

2.4.2. Pulmonary Vein Isolation Protocol

Pulmonary vein isolation (PVI) was achieved with circumferential and contiguous point-by-point radiofrequency ablation lesions around the antra of pulmonary veins. Entry and exit block of pulmonary veins was confirmed using a Lasso or PENTARAY® catheter.

2.4.3. Repeat Ablation Protocol

All patients returning for repeat AF ablations regardless of their initial procedure type (GP ablation or PVI) received PVI. If GP ablation was performed previously, ablated sites were re-tested with HFS to identify any recovered GPs prior to PVI.

2.5. Registration of the Left Atrial HFS Maps

The left atrial fast anatomical map (FAM) of patients with AF mapped with HFS were exported from CARTO™. A representative LA anatomy was chosen as a reference shell and all patient data was co-registered onto this geometry using a semi-automated process[153]. This shell was chosen as having a 'typical' distribution of the four pulmonary veins.

Four sets of circumferential landmarks, with each pair of landmarks separated by a constant angle were automatically generated along the intersection of PV-atrial junctions and a plane, at the point of maximum geometric curvature. Landmark registration followed by non-rigid surface registration was used to compute mapping from each patient-specific geometry to the reference LA surface. An automated angle-based fiducial-point selection algorithm was used to choose the optimal landmarks on the PV-atrial junctions for each patient which minimised the target registration error (TRE) when co-registered to the reference shell. TRE is defined as the average distance between the true position of landmarks on the target reference shell, which were not used during the registration process, and their position when the corresponding landmark on the source shell was mapped under the computed transformation.

This enabled GP and negative HFS points to be accurately transformed onto the reference LA shell. An example of a registration with data points transformed on to the common shell is shown in Figure 2.3.

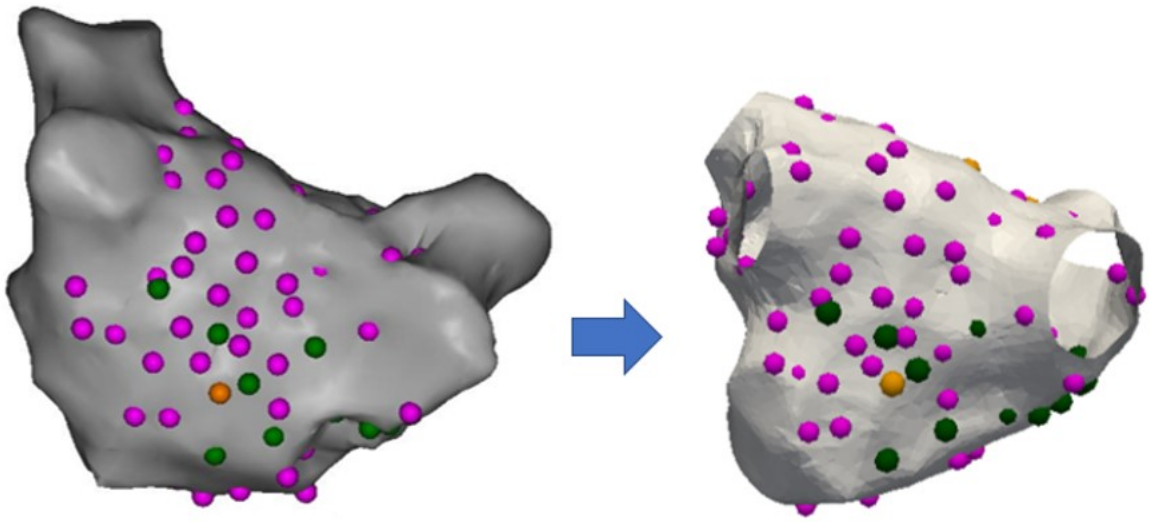

Figure 2.3 Registration of HFS tested points onto a reference left atrial shell

An example of a patient's CARTO™ left atrial image (posterior-anterior view) with AVD-GP (green and orange) and high frequency stimulation negative response sites (pink) registered and transformed onto a reference left atrial shell (right).

(AVD-GP = atrioventricular dissociating ganglionated plexus)

2.6. The Probability Distribution Atlas of GP

A probability of 1 was applied to AVD-GP and ET-GP sites and 0 for sites tested with HFS that did not evoke a positive response. Each measurement site was weighted by a Gaussian kernel with a variance of 5mm, which characterised the uncertainty in the measurement of the site location as a result of catheter movement. The probability that an arbitrary test point within the reference atrial surface that has a positive response was then computed per-patient. This was the sum of the product of probabilities of nearby measured sites with their respective weight kernels evaluated at the required point

which was then normalised by the sum of the weight kernels evaluated at the point. Resulting maps were then averaged across the patients.

3. THE ATRIOVENTRICULAR DISSOCIATING GANGLIONATED PLEXUS

3.1. Introduction

The autonomic nervous system (ANS) regulates normal cardiac function, but is also implicated in pathological processes such as arrhythmogenesis.[67,152,154–156] Such pro-arrhythmic changes are likely to be mediated by the intrinsic cardiac ANS (IC-ANS), which is a complex network of ganglionated plexuses (GP) around the epicardium. There is also a constant interaction with the extrinsic GPs (stellate, middle and superior cervical GPs) modulating the electromechanical function of the heart as a result of signals from the spinal cord, medulla and higher centres. These different hierarchical neural centres have afferent, efferent and local circuit neurons that interdependently interact with each other by receiving inputs from physiological and pathological stressors.[157]

The left atrium (LA) innervation is of particular interest as it has been proposed as a potential target for AF therapies. Anatomical studies of post-mortem human hearts identified 800 GPs per heart, with the densest collection (50% of all cardiac GPs) in the hilum between the posterior and posterolateral surfaces of the LA. GPs sites varied widely between the hearts but three main common clusters (superior left, posteromedial left and posterior right) and extending anteriorly into the interatrial septum (interatrial septal GP).[7,8] Further studies indicated the highest density of nerve fibres were in the ostium and antrum of the pulmonary veins (PV) and posterior portion of the LA.[159,160] Although the GPs are epicardial, smaller nerve fibrils penetrate the endocardium allowing for conduction of electrical stimulation from the endocardium to the epicardial GPs[159,161,162].

High frequency stimulation (HFS) of canine epicardial GPs reduces heart rate and blood pressure (BP).[163–167] Similarly changes occur in patients with endocardial HFS directly under the epicardial GP.[88,100,128,152,168,169] Therefore the neural network can be accessed and influenced by stimulation of endocardial sites.[170,171] The atria will fibrillate when HFS is applied due to high rate capture, but at atrial GP sites there will also be ventricular rate slowing with a ≥50% increase in the mean RR interval compared to baseline. This response has been described as a 'vagal response, vagal reflex, bradycardia, atrioventricular (AV) node block and asystole' in other studies.[7,105,129,172,173] For greater specificity, we will use the term 'atrioventricular dissociating GP' (AVD-GP) for GP sites that show AV dissociation.

In this study, the distribution of AVD-GPs in the human LA with high density HFS mapping in patients having AF ablations was studied. The LA geometries were then combined to create a probability distribution atlas of AVD-GPs.

3.2. Methods

28 patients with symptomatic, paroxysmal AF undergoing first ablation procedure were recruited to the study from four centres. Patients gave written informed consent and the study had ethics approval from the Health Research Authority and the Local Research Ethics Committee. Antiarrhythmics were stopped for five half-lives before each procedure. Patient characteristics are in Table 1.

Demographic characteristics	
Age (yrs)	64±10
Sex (Male/Female)	17/11
BMI (kg/m^2)	27.5±4.8
LVEF (%)	61±4.5
LA diameter (mm)	3.8±0.6
CHA_2DS_2-VASc	1.7
Stroke/TIA	2
CAD	3
HTN	12
DM	3
Fluoroscopy time (min)	23.2±13.9
Procedure time (min)	248.9±123.4
HFS mapping time (min)	63.3±24.8

Table 3.1 Demographic characteristics of patients recruited to this study

Numbers in the right column represent mean ± SD.

(BMI = body mass index; CAD = coronary artery disease; DM = diabetes mellitus; HFS = high frequency stimulation; HTN = hypertension; LA = left atrium; LVEF = left ventricular ejection fraction)

3.2.1. Mapping for AVD-GP

Patients had general anaesthesia and transoesophageal echocardiogram to rule out cardiac thrombus. All patients underwent the AF ablation "Clinical Procedures" protocol and Continuous HFS was used to identify AVD-GP as outlined in Chapter 2.

AF was induced with the first application of continuous HFS due to local myocardial capture. RR intervals were measured from the maximum peaks of the arterial BP trace, or the right ventricular electrogram. In the event of any measurement uncertainty, HFS was repeated at the tested site.

Ablation was performed after the HFS mapping protocol. Retrospectively, the number of AVD-GPs distal or proximal to the PV isolation (PVI) ablation lines were manually counted.

3.2.2. Defining an AVD-GP

In animal experiments, GP sites were defined as causing ≥50% increase in the mean RR interval during HFS from the baseline[152]. The mean RR interval during HFS was measured from the time between the first R during HFS and the first R after the cessation of HFS. The baseline RR interval was defined as the mean of the 10 RR intervals immediately preceding HFS.

Asystole was the most frequent response to HFS. When this occurred, HFS was stopped and RR intervals and BP recovered quickly. We termed these sites as 'asystole atrioventricular dissociating ganglionated plexus' or 'A-AVD-GPs'.

Some GP sites gave a milder prolongation of RR intervals, with no asystole. These showed a stable bradycardic response throughout continuous HFS. As with A-AVD-GP, RR

intervals recovered quickly after HFS stopped. We termed these sites as 'bradycardia atrioventricular dissociating ganglionated plexus or 'B-AVD-GPs'.

In order to distinguish the two responses objectively, the normal RR variability in patients during AF was observed. Random 75 samples of 20s AF electrograms from patients were selected. For each sample, the first 10s RR intervals were averaged and the longest RR interval was measured in the last 10s. The ratio of the latter to the mean 10s RR interval was calculated. This was repeated for all 75 samples. The Shapiro-Wilk test was performed to confirm that the log-transformed ratios were not significantly different to normal distribution ($p=0.56$). This confirmed a log-normal distribution of the ratios. In a one-tailed log normal distribution, 2.33 standard deviations above the mean gave the ratio of 2.6 whereby <1% of single RR prolongation during HFS is a false-positive AVD-GP. Therefore, any single RR prolongation during HFS that was >2.5 times the average 10s RR interval before HFS was defined as an A-AVD-GP site. This was equivalent to >150% increase in the single RR prolongation from the baseline Figure 3.1. Any ratio below this threshold and within the definition of an AVD-GP (>50% increase in the average RR interval from the baseline) was termed 'B-AVD-GP' Figure 3.2.

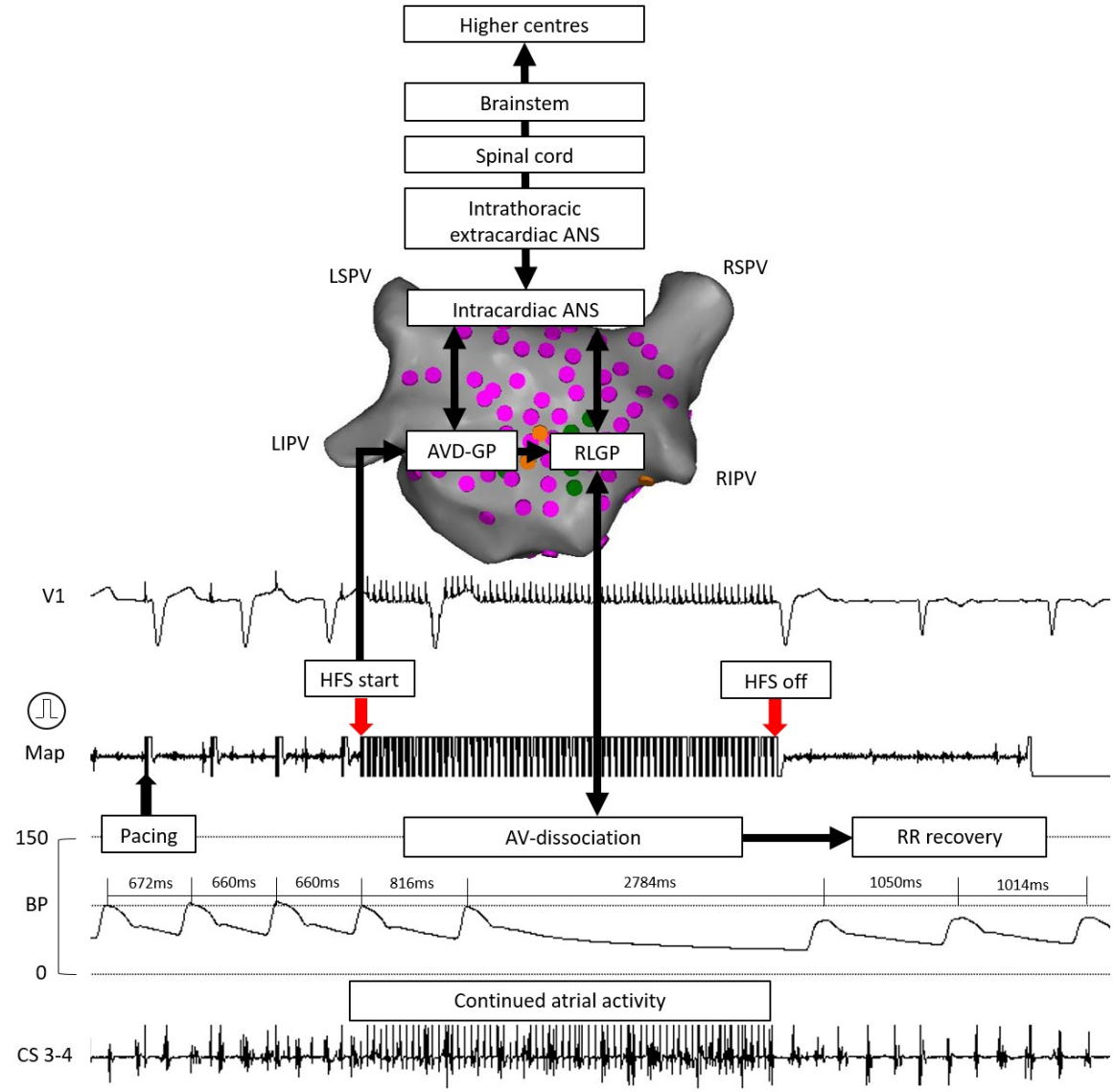

Figure 3.1 Hierarchical stages of the ANS from the central to the peripheral system

First, a Mapping catheter was used to pace in the endocardium of the left atrium for four beats to ensure that there was no ventricular capture. HFS was then delivered at 20Hz, 12V. Asystole occurred almost immediately after starting HFS. This was due to direct AV dissociation or via stimulation of the RLGP acting as the common "gateway" to the AV node. During HFS and AV dissociation, there was continued atrial activity as observed in CS 3-4. Due to the high voltage output, the Map electrogram only showed output signals during pacing and HFS. The RR interval recovered following cessation of HFS. This site was determined as an A-AVD-GP site.

(A-AVD-GP=asystole atrioventricular dissociating ganglionated plexus, ANS=autonomic nervous system, AV=atrioventricular node, AVD-GP=atrioventricular dissociating ganglionated plexus, B-AVD-GP=bradycardia atrioventricular dissociating ganglionated plexus, BP=blood pressure, CS=coronary sinus, HFS=high frequency stimulation, GP=ganglionated plexus, LA=left atrium, RLGP=right lower ganglionated plexus)

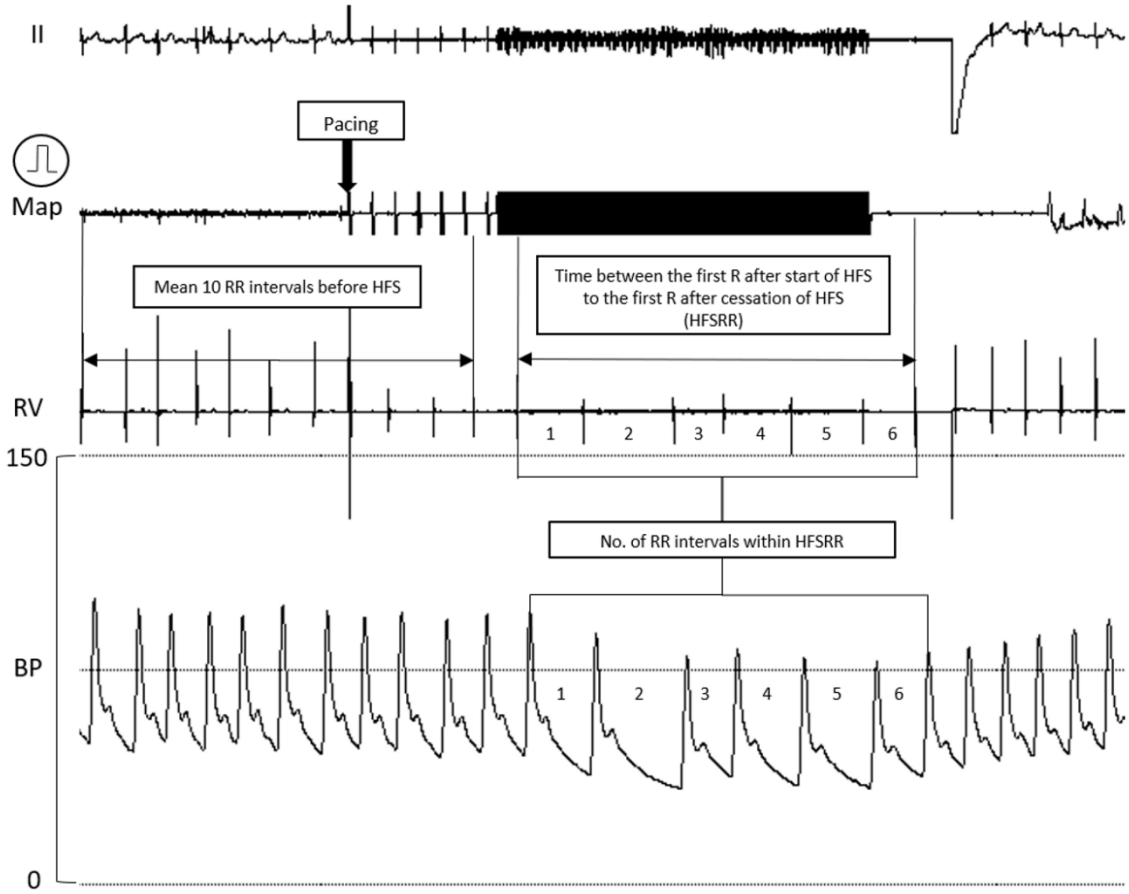

Figure 3.2 An intracardiac recording of determination of a B-AVD-GP site

HFS was performed with the same parameters as Figure 3.1 but for 10s. The mean of 10 RR intervals preceding HFS was 952ms. The total time duration between the first R after starting HFS and the first R after cessation of HFS (HFSRR) was measured and averaged to calculate the mean RR interval (1610ms). There was increase in >50% of the RR interval during HFS from the baseline which determined it as an AVD-GP site. However, there was no asystole like in A-AVD-GP. This was therefore determined as a B-AVD-GP site.

(B-AVD-GP=bradycardia atrioventricular dissociating ganglionated plexus, BP=blood pressure, CS=coronary sinus, HFS=high frequency stimulation, GP=ganglionated plexus, LA=left atrium, RLGP=right lower ganglionated plexus)

Using the CARTO™ Tag system, A-AVD-GP were marked green and B-AVD-GP were marked orange. Negative responses to HFS were marked pink.

3.2.3. Registration and The Probability Distribution Atlas of AVD-GP

LA fast anatomical map (FAM) of all the patients were exported from CARTO™. A representative LA anatomy was chosen as a reference shell and all patient data was co-registered onto this geometry using a semi-automated process[153]. This shell was chosen as having a 'typical' distribution of the four pulmonary veins. Details of the registration process and creation of the probability distribution atlas with examples is shown in Chapter 2.

3.2.4. Statistics

All continuous variables were expressed as mean and standard deviation (mean±SD) or median and interquartile range (IQR), unless otherwise explicitly stated. Shapiro-Wilk test was used for normality test of log-transformed figures.

3.3. Results

28 patients (17 males, 11 females, mean age 64±10yrs) were recruited. Full demographics and clinical characteristics are in Table 5.2. The total number and the median number of HFS points tested per patient was 2108 and 74 (IQR 27) respectively. The total number and the median number of AVD-GPs identified was 283 (13%) and 6.5 (IQR 12) respectively. The number of AVD-GPs ranged widely from 1 to over 30 (Figure 3.3).

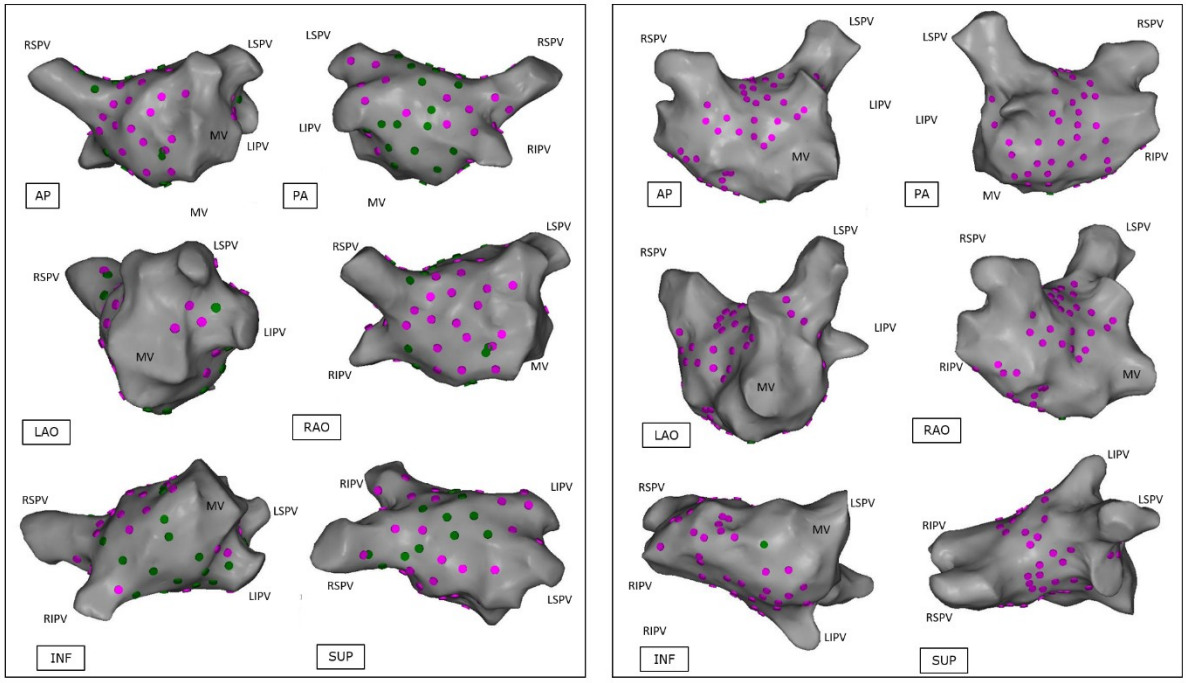

Figure 3.3 Examples of patients with the lowest and the highest number of AVD-GPs

The left panel shows the highest number of AVD-GPs (31) and the right panel shows the lowest number (1) of AVD-GPs. Pink dots indicate negative HFS sites, green dots are A-AVD-GPs. Neither patients had B-AVD-GP. Clinical characteristics of the patients are as follows: Left panel patient = 67yrs old, male, BMI 28.1, good LVSF, LA size 3cm, hypertensive. 72 points tested in total. 29 were A-AVD-GP. Right panel patient = 77yr old, male, BMI 25.5, good LVSF, LA size 3.9cm, previous stroke, previous percutaneous coronary intervention, hypertensive. 71 points tested in total.

(A-AVD-GP = asystole atrioventricular dissociating ganglionated plexus; AP = anterior-posterior; AVD-GP = atrioventricular dissociating ganglionated plexus; B-AVD-GP = bradycardia atrioventricular dissociating ganglionated plexus; INF = inferior; LSPV = left superior pulmonary vein; LAO = left anterior oblique; LIPV = left inferior pulmonary vein; MV = mitral valve; PA = posterior-anterior; PVI = pulmonary vein isolation; RAO = right anterior oblique; RSPV = right superior pulmonary vein; RIPV = right inferior pulmonary vein; RLGP = right lower ganglionated plexus; SUP = superior)

There was no correlation between the number of HFS tested sites and the number of AVD-GPs (Figure 3.4). Registration of all our patients to one reference shell revealed that 48% of the total area of the left atrium contained 90% of AVD-GPs. The average Target Registration Error (TRE) was 2.7±1.0mm (where '0' is perfect registration).

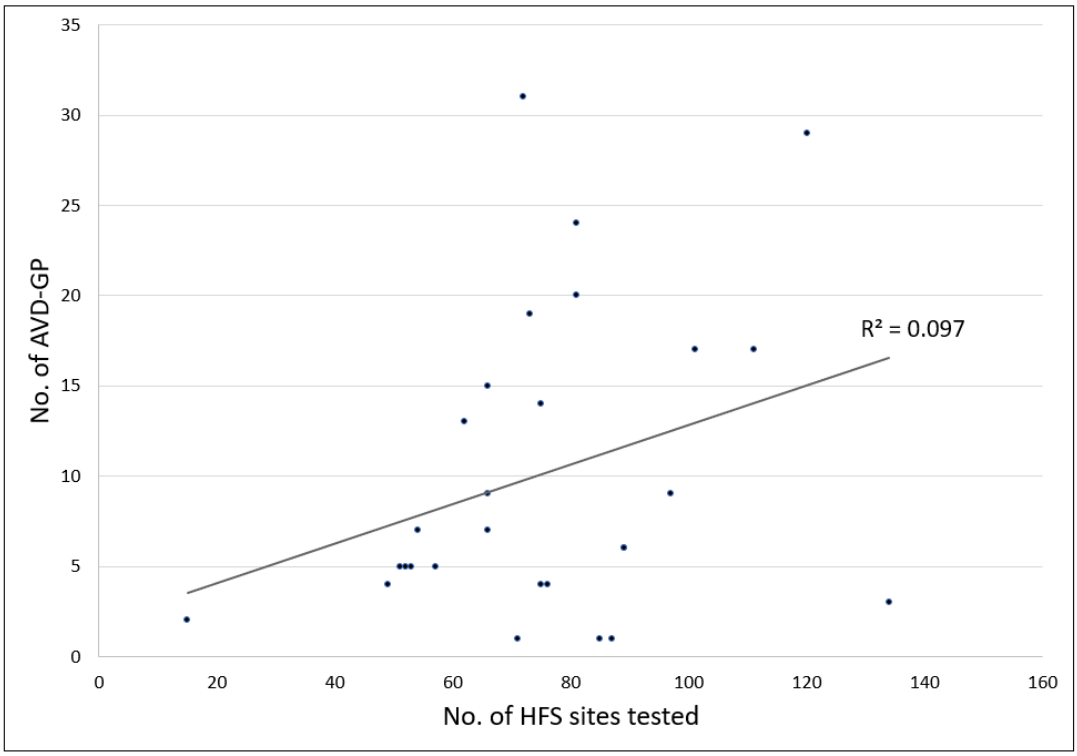

Figure 3.4 Relationship between no. of AVD-GP and no. of HFS sites tested

A scatter plot with 28 patients and the number of AVD-GPs identified out of the total number of high frequency stimulation sites tested per patient. There was no clear linear relationship between the two variables.

(AVD-GP = atrioventricular dissociating ganglionated plexus; HFS = high frequency stimulation)

The total number of A-AVD-GP and B-AVD-GP was 226 (80%) and 57 (20%) respectively. The mean number per patient was 8±7 (median 6; IQR 9) and 2±4 (median 0, IQR 3) respectively (Table 3.2).

HFS and AVD-GP (n=28)	Total (%)	Mean per patient (SD)	Median per patient (IQR)
HFS points tested	2108	75 (24)	74 (27)
AVD-GP identified	283 (13)	10 (8)	6.5 (12)
A-AVD-GP	226 (80)	8 (7)	6 (9)
B-AVD-GP	57 (20)	2 (4)	0 (3)

Table 3.2 The breakdown of HFS points tested and AVD-GPs identified

(A-AVD-GP = asystole atrioventricular dissociating ganglionated plexus; AVD-GP = atrioventricular dissociating ganglionated plexus; B-AVD-GP = bradycardia atrioventricular dissociating ganglionated plexus; HFS = high frequency stimulation; IQR = interquartile range; SD = standard deviation)

The total distribution of A-AVD-GP and B-AVD-GP in the reference LA shell is shown in Figure 3.5A and B respectively. The colours around each tested point demonstrate the degree of uncertainty (5mm radius) from the catheter movement during live cases. The general distribution of A-AVD-GP and B-AVD-GP were in the similar regions of the LA. The combined map is shown in Figure 3.5C. This represents all the AVD-GP sites from 28 patients. The largest number of AVD-GPs were in the posterior wall of the LA and the least were in the anterior wall.

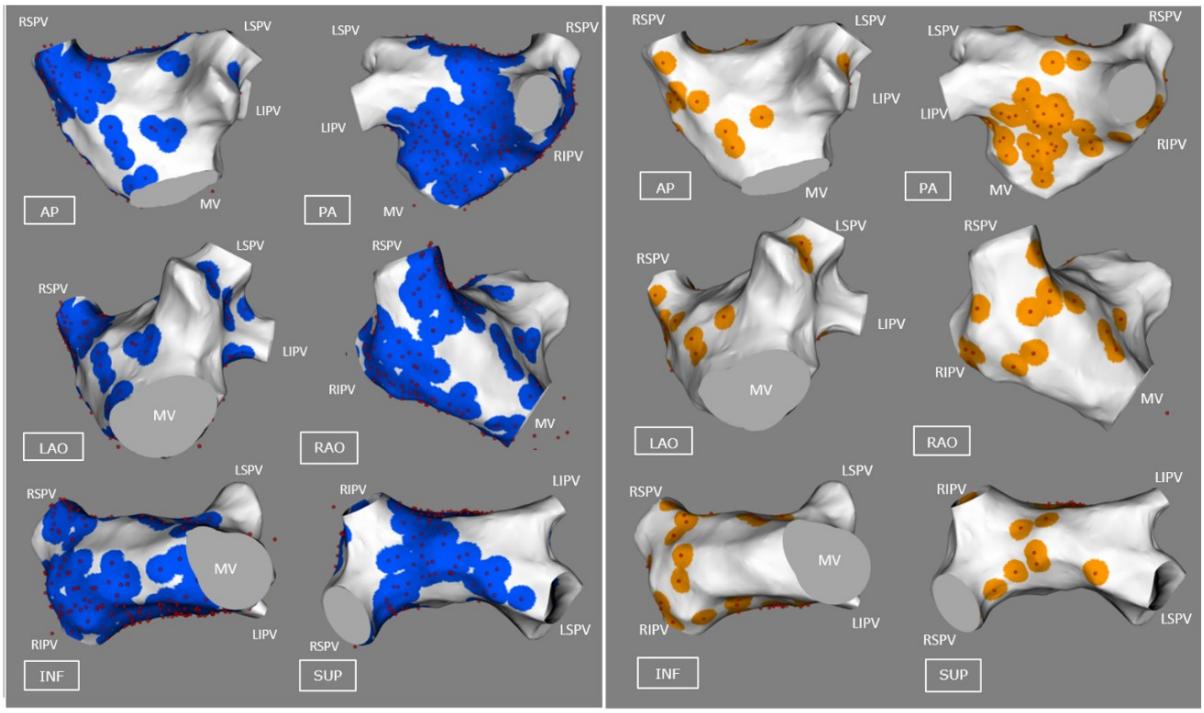

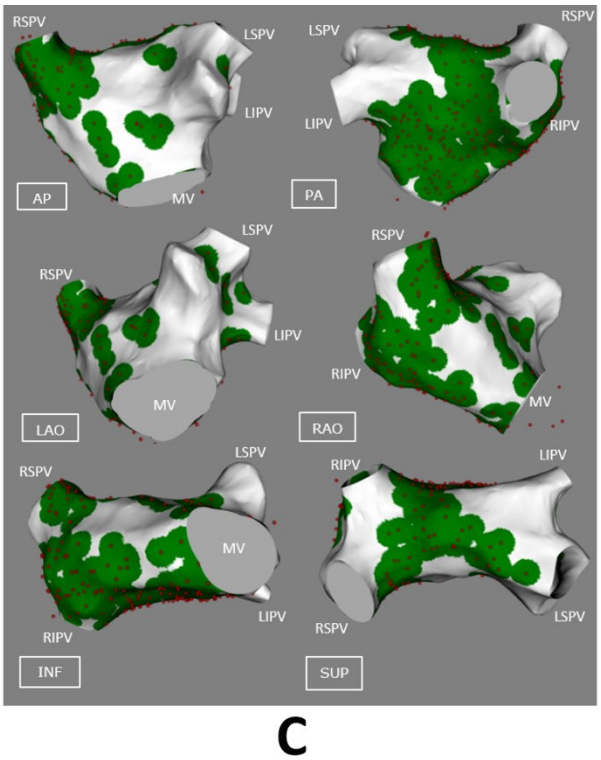

Figure 3.5 A-AVD-GP and B-AVD-GP distributions in the left atrium

A) All the A-AVD-GPs identified from 28 patients on the reference left atrial shell. The red spots indicate A-AVD-GPs and the blue circle around each point represents the 5mm kernel variance.

Similarly, B) shows all the B-AVD-GPs identified. The red spots indicate B-AVD-GPs and the orange circle around each site represents the 5mm kernel variance. Areas in white are absent of any AVD-GPs.

C) shows the combination of A) and B) into one map of AVD-GPs.

(A-AVD-GP = asystole atrioventricular dissociating ganglionated plexus; AP = anterior-posterior; AVD-GP = atrioventricular dissociating ganglionated plexus; B-AVD-GP = bradycardia atrioventricular dissociating ganglionated plexus; INF = inferior; LSPV = left superior pulmonary vein; LAO = left anterior oblique; LIPV = left inferior pulmonary vein; MV = mitral valve; PA = posterior-anterior; RAO = right anterior oblique; RSPV = right superior pulmonary vein; RIPV = right inferior pulmonary vein; RLGP = right lower ganglionated plexus; SUP = superior)

By incorporating negative HFS sites to the AVD-GP map, we constructed a probability atlas of AVD-GPs across the entire LA. This identified three distinct peaks with greater than 30% in probability of AVD-GPs with a gradual decreasing gradient of probability branching outward from the peaks. These were 1) the infero-septal aspect of the posterior wall (41%), 2) the RSPV antrum (31%) and 3) the base of the RIPV in the posterior wall (30%) (Figure 3.6).

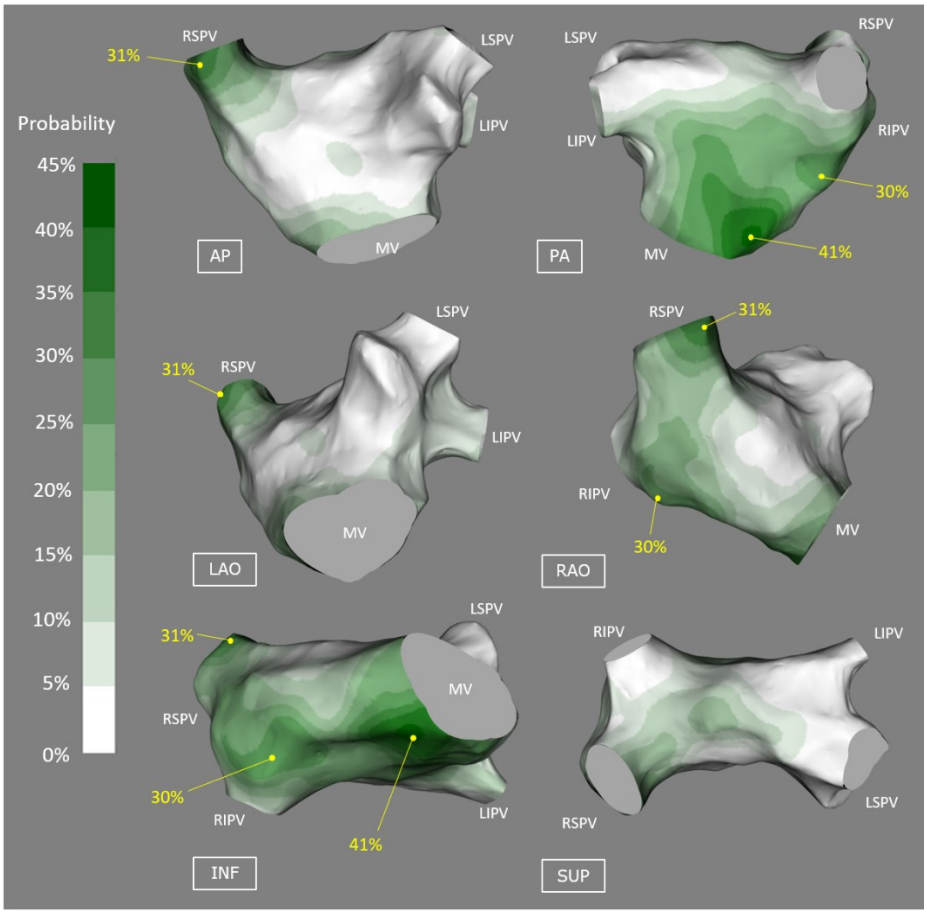

Figure 3.6 A probability distribution atlas of AVD-GP

The probabilities are shown in the figure from 0-45%, white to dark green. This resulted in clear identification of the highest probability sites of AVD-GP to the lowest. "High probability AVD-GP sites" were ≥30% in probability, labelled with yellow dots with corresponding probabilities. These were: infero-septal posterior wall (41%), the RSPV antrum (31%), and the base of the RIPV in the posterior wall (30%).

(AP = anterior-posterior; AVD-GP = atrioventricular dissociating ganglionated plexus; INF = inferior; LSPV = left superior pulmonary vein; LAO = left anterior oblique; LIPV = left inferior pulmonary vein; MV = mitral valve; PA = posterior-anterior; RAO = right anterior oblique; RSPV = right superior pulmonary vein; RIPV = right inferior pulmonary vein; RLGP = right lower ganglionated plexus; SUP = superior)

The operators performed their circumferential ablation approach as per their standard practice and with the location of GP sites hidden. The location of AVD-GP sites in relation to the circumferential ablation lines was categorised post-hoc as being either included within the isolated PV antrum or being outside and unaffected by the ablation. 53% of AVD-GP were outside the boundary of the PVI ablation line (Table 3.3). We tested most of the left atrium (Figure 3.7).

Locations of AVD-GP in patients undergoing PVI (n=19)	n (%)
AVD-GP proximal to the PVI line	
Total	103
A-AVD-GP	90 (87)
B-AVD-GP	13 (13)
AVD-GP distal to the PVI line	
Total	118
A-AVD-GP	91 (77)
B-AVD-GP	27 (23)

Table 3.3 Locations of AVD-GPs in 19 patients undergoing PVI

The AVD-GPs were manually counted retrospectively after PVI. These were categorised into "proximal to the PVI line" and "distal to the PVI line". Ablation Visitags of CARTO™ were used as boundaries of PVI lines. The right-hand column represents the number of AVD-GPs and their percentages in brackets.

(AVD-GP = asystole atrioventricular dissociating ganglionated plexus; B-AVD-GP = bradycardia atrioventricular dissociating ganglionated plexus; HFS = high frequency stimulation; PVI = pulmonary vein isolation)

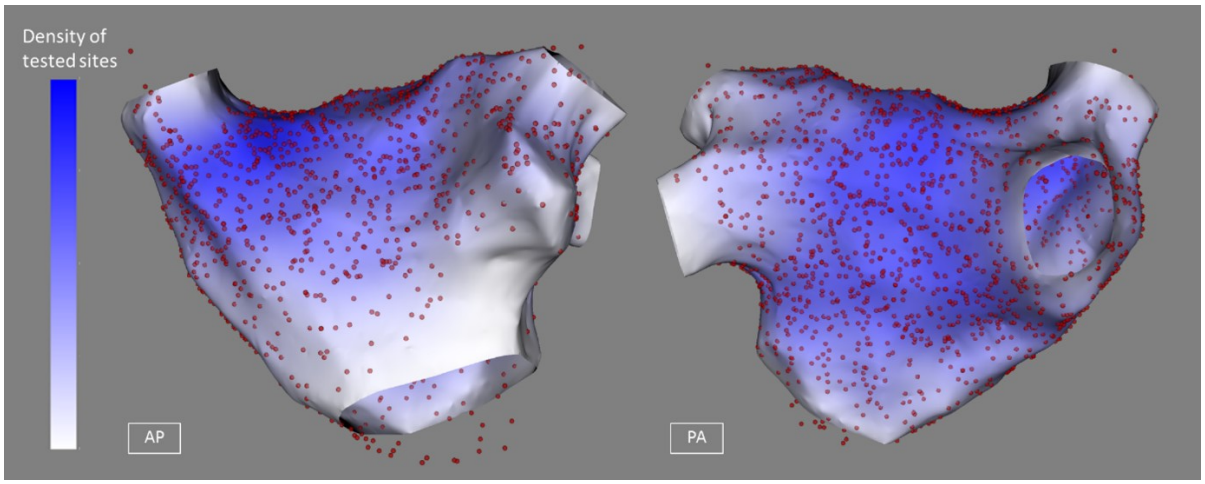

Figure 3.7 All AVD-GPs and high frequency stimulation negative sites in 28 patients on the reference left atrial shell

Red spots represent high frequency stimulation site tested and the colour scale on the left-hand side represent the density of high frequency stimulation points tested (darkest blue representing highest density) in the left atrium.

(AVD-GP=atrioventricular dissociating ganglionated plexus)

3.4. Discussion

In this study, we created a probability atlas showing the regions of the LA where AVD-GPs are most likely to be found. These areas were similar to those described in histological studies. However, the most striking finding was the marked variation in number and location of AVD-GPs between individual patients.

GP sites are defined as having a ≥50% increase in the average RR interval from the baseline in response to HFS. However, the degree of AV dissociating effect varies with what appears to be two distinct responses; asystole and bradycardia. In our study, these were characterised separately as A-AVD-GP and B-AVD-GP. Combining all the patients' maps, we deduced that these two functional classes of GPs that cause AV dissociation appear to be co-located. An alternative explanation for this finding is that there is only

one type of AVD-GP, with differences in response reflecting the distance from the atrial lumen to GP, affecting the amount of current transmitted.[174,175]

3.4.1. Other Functional Classes of GP

GP can also be identified by delivering HFS within the refractory period of the atrium to induce atrial premature depolarisation and atrial arrhythmia.[68,87,174,175] It has previously been shown that these GPs identified as 'ectopy-triggering ganglionated plexus (ET-GP)' co-locate with less than half of GP sites with AV dissociating effect.[87] It is also known that ablation of GPs near the right upper PV influences the sinus node heart rate variability. This suggests that GPs have a spectrum of functional effects which are likely to be determined by the local neural architecture that is activated by HFS at that site. These further underlines the importance of functionally mapping the LA prior to considering autonomic modification.

3.4.2. High Probability Regions of AVD-GP

We have identified three main regions of the LA that are abundant in AVD-GPs, and all these sites were in close proximity to the right atrium.[5,158] The two high probability peaks in the posterior wall were located at the site where the right lower GP (RLGP) is expected to be. The RLGP acts as the 'integration centre' or 'common gateway' to the AV node[170,173], which is an important site where ablation at this site can prevent any further induction of vagal response to HFS at other GP sites.

3.4.3. GP Modification in The Treatment of AF

Inadvertent injury to GP sites has been assumed to occur during PVI and contribute to successes in treatment of AF.[100] In our patients, we noted that some AVD-GPs had been

'encircled' as a part of the ablation procedure. Interestingly, more than half of AVD-GPs remained distal to the antrally isolated myocardium.

Animal studies have shown that stimulation of GP is capable of shortening the refractory period at PVs and the atrium and ablation at these sites can abolish the effects.[22,176,177] These studies led to the assumption that autonomic drive was a pre-requisite for human AF. Vagal symptoms and sympathetic stressors are well-described associations in patients with AF and have been cited as circumstantial evidence for autonomic changes being an upstream trigger in AF pathogenesis.

Although AVD-GPs are epicardial structures, studies have shown that ablation guided by HFS mapping can eliminate the AV dissociating effects.[173,20,21] This has led to a series of studies attempting autonomic modification as a therapy for AF. However, outcomes have been conflicting and has led to a Class IIb classification in the 2017 HRS expert consensus for AF treatment.[21]

Even though GPs are epicardial structures, the only studies showing benefit utilised endocardial ablation.[7,129] Improved outcomes were noted in those patients who received PVI and additional ablation to 'presumed GP sites' using anatomical description without any functional confirmation of GP sites.[129] Such an approach could be considered a limited endorsement of autonomic modification, as no formal confirmation of autonomic changes was obtained. In this study, we have shown that it is feasible to perform global LA mapping to determine AVD-GP sites followed by a standard ablation procedure. Therefore, it would be possible to perform more targeted ablation procedures with formal testing rather than 'blind' ablation. The study of 'selective' AVD-GP ablation tested an average of 37 sites and ablated 5 AVD-GP sites.[105] In contrast, our study needed an average of 75 sites to be tested to get sufficient coverage of the LA, identifying average 10

AVD-GPs per patient. Therefore, studies of AVD-GP ablation that did not perform whole chamber mapping are unlikely to achieve their endpoint, making results difficult to interpret. However, there was no linear relationship between the number of HFS sites tested and the number of AVD-GPs. There were no identifiable clinical characteristics that predisposed patients to have more AVD-GP than others.

The AFACT study was a large randomised controlled study that performed adjunctive GP ablation to PVI in AF patients undergoing thoracoscopic AF ablation. There was no benefit in adjunctive GP ablation, but there was an increased complication rate associated with surgical exploration for GP sites. This confirms that the endocardial approach is a safer means for understanding the role of the ANS in AF, but also underlines the importance of understanding the functional pathways triggering AF[38,39].

3.5. Conclusion

It is safe and feasible to map the entire LA for AVD-GP using endocardial HFS prior to performing a standard circumferential antral PVI procedure. The distribution of AVD-GPs is highly variable between patients, mandating patient-specific mapping if the GP sites are to be clinically targeted. Also, we identified three distinct regions with the highest probability of locating AVD-GPs which correlates to the findings of previous anatomical human heart studies. The AVD-GP atlas may be used as a guide for patient-specific mapping to identify AVD-GPs more effectively and efficiently. Defining the neural network by whole-chamber functional mapping may become an important first step in autonomic modification procedures.

4. THE ECTOPY-TRIGGERING GANGLIONATED PLEXUS

4.1. Introduction

Atrial fibrillation (AF) is most commonly caused by rapid electrical discharges from the pulmonary veins (PV)[22]. One of the proposed drivers of PV arrhythmogenicity are ganglionated plexuses (GP), which are epicardial neural structures[5] that upon stimulation can shorten the PV refractory period leading to PV tachycardia and AF[177].

Clinical studies have commonly used continuous high frequency stimulation (HFS) to functionally identify GPs by observing for atrioventricular (AV) dissociation or block[152]. These AV dissociating GPs (AVD-GP) were previously mapped in the left atrium (LA) of patients with AF, and were not present in all the anatomical regions where GPs are assumed to be.[5,6] This suggested that not all GPs can be functionally identified with continuous HFS.

An alternative HFS technique called "synchronised HFS" can map for GPs in sinus rhythm and does not cause AF through high-rate myocardial capture, like continuous HFS. This technique can reproducibly trigger atrial ectopy or AF from sites distant to stimulation[68,74,87,152]. It is not known where the ectopy-triggering GPs (ET-GP) are in the LA, and how these differ to AVD-GP.

In this study, ET-GP were mapped and characterised, then their anatomical distribution was compared with AVD-GP.

4.2. Methods

Patients with symptomatic, paroxysmal AF undergoing first ablation procedure were recruited to the study. Patients gave written informed consent and the study had ethics approval from the Health Research Authority and the Local Research Ethics Committee. Antiarrhythmics were stopped five half-lives before each procedure.

All patients had general anaesthesia and underwent synchronised HFS mapping of the whole LA as detailed in Chapter 2.

4.2.1. Definition of ET-GP

ET-GP was defined as a site reproducibly inducing atrial ectopy or atrial arrhythmia with synchronised HFS. If there was no response, it was deemed a "negative HFS" site. Both ET-GP and negative HFS sites were tagged on the CARTO™ 3D atrial geometry. We tested for reproducibility by re-testing any site that induced ≤3 ectopy.

4.2.2. The Probability Distribution Atlas of ET-GP

The LA fast anatomical map (FAM) of all patients were exported from CARTO™. We used a custom-built software to create the probability distribution atlas of ET-GP, using methods described from Chapter 2.

4.2.3. Statistics

All continuous variables were expressed as mean and standard deviation (mean±SD) or median and interquartile range (IQR), unless otherwise explicitly stated.

4.3. Results

26 patients were recruited. Table 4.1 shows their demographics and clinical characteristics.

Demographic characteristics	
Age (yrs)	60±9
Sex (Male/Female)	18/8
Body mass index (kg/m^2)	27.7±5.3
Left Ventricular Ejection Fraction (%)	64.5±1.2
Left atrial diameter (cm)	3.69±0.41
CHA_2DS_2-VASc	1.2±0.9
0	8
1	9
≥2	9
Stroke/ Transient Ischaemic Attack	1
Coronary artery disease	1
Hypertension	6
Diabetes Mellitus	1

Table 4.1 Demographics of patients recruited to the study

Continuous variables represented as mean ± SD.

A range of reproducible responses with synchronised HFS at GPs were observed, which were characterised as follows.

4.3.1. Atrioventricular Dissociation with Synchronised HFS

AV dissociation is the hallmark GP stimulation effect observed with continuous HFS but is also seen occasionally during synchronised HFS.

A shows progressive Wenckebach until asystole. Re-testing the same site with continuous HFS produced a more pronounced AV dissociation, confirming the site as AVD-GP. Less frequently, Wenckebach was also followed by atrial ectopy and AF with synchronised HFS (Figures B and C), identifying both AVD-GP and ET-GP at a single test site.

Figure 4.1 Intracardiac electrograms of synchronised HFS at a GP site

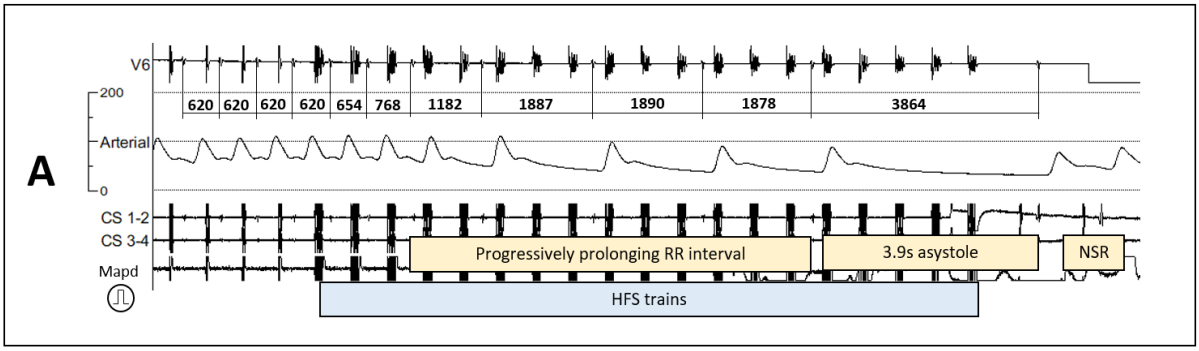

Figure 4.1A. Asystole with synchronised HFS

Pacing and HFS are delivered from Map distal.

A) Pacing before the onset of HFS does not cause Wenckebach (620ms). HFS is delivered after the fourth paced beat. There is a progressive RR prolongation during HFS until 3.9secs asystole. RR interval recovers after cessation of HFS. No atrial ectopy or arrhythmia is observed. Therefore, this site was tagged as "AVD-GP" and not "ET-GP".

(AVD-GP = atrioventricular dissociating ganglionated plexus; CS = coronary sinus; ET-GP = ectopy triggering ganglionated plexus; GP = ganglionated plexus, HFS = high frequency stimulation; Map = mapping catheter)

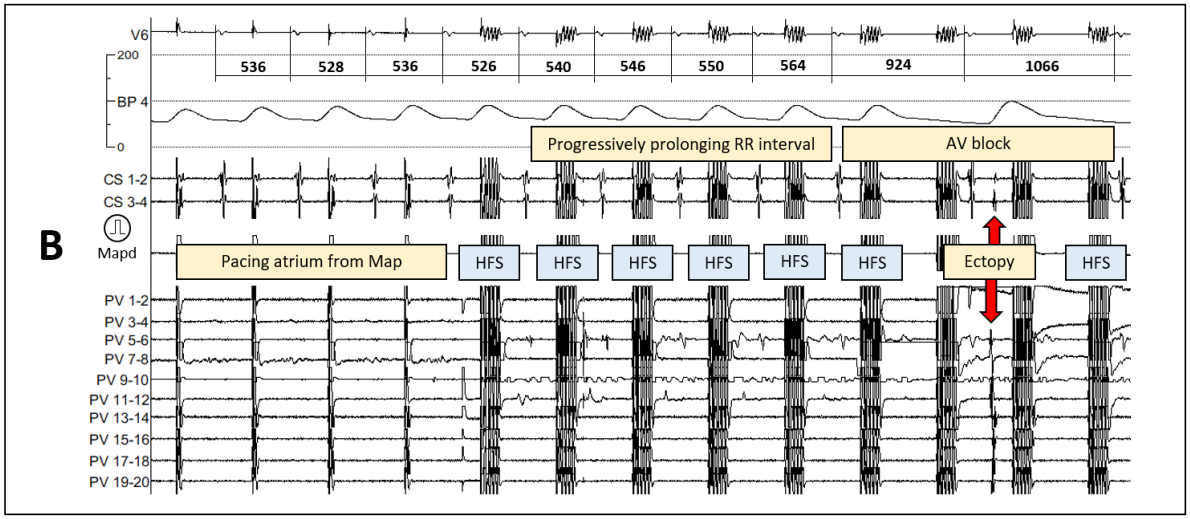

Figure 4.1B. AV block and atrial ectopy with synchronised HFS

Pacing and HFS are delivered from Map distal.

B) Pacing before the onset of HFS does not cause Wenckebach (528-536ms). There is a progressive RR prolongation during HFS until it reaches 1066ms; almost twice as long as the RR interval before HFS. An atrial ectopy is triggered after the 7th train of HFS.

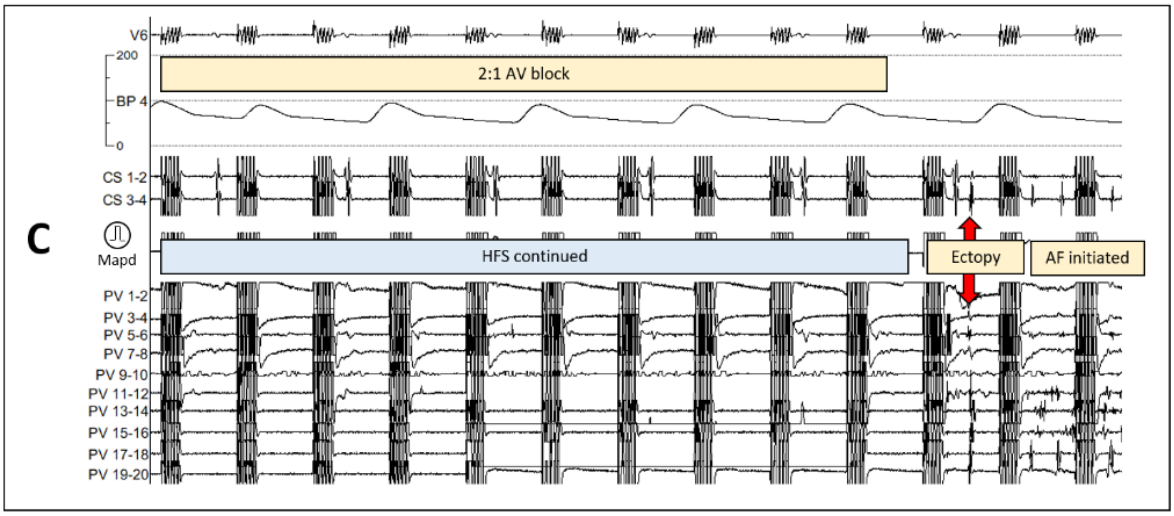

C) Continuation from the trace from B). AV block continues in 2:1 block fashion after the initial ectopy in B). Another ectopy is triggered after the 20th train of HFS, which induces atrial fibrillation. Therefore, this site was tagged both as "ET-GP" and "AVD-GP".

(AV = atrioventricular; AVD-GP = atrioventricular dissociating ganglionated plexus; CS = coronary sinus; ET-GP = ectopy triggering ganglionated plexus; GP = ganglionated plexus, HFS = high frequency stimulation; Map = mapping catheter; PV = pulmonary vein)

4.3.2. Atrial Ectopy and Arrhythmia with Synchronised HFS

A PV ectopy triggered by synchronised HFS at an ET-GP site was mapped and visualised using CARTOFINDER®. Figure 4.2 shows a step-by-step PV ectopy activation sequence and confirms that atrial ectopy induced by HFS is not the result of direct myocardial capture, but a distant neural effect that occurs remotely to the stimulation site.

Figure 4.2 Sequential PV ectopy activation with ET-GP stimulation

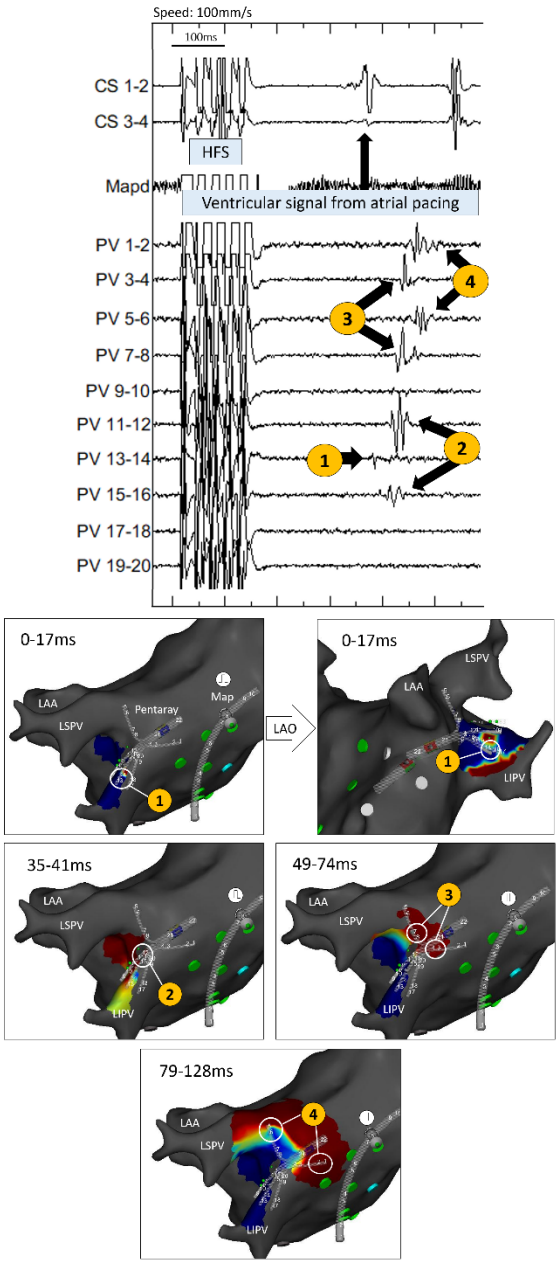

A 20-pole PENTARAY® catheter was situated in the LIPV and the Map catheter was situated in the mid-roof. The intracardiac electrogram at the top shows the earliest ectopy initiating at PV 13-14. The sequence of ectopy activation travels from 1 to 4, as labelled, directly correlating to the time of red wavefront in the bottom images 1 to 4 (red correlates with the circled PENTARAY® bipoles). This demonstrates the neural network with GP stimulation in the left atrium leading to myocardial activation from within the PV.

(ET-GP = ectopy triggering ganglionated plexus; HFS = high frequency stimulation; LAA = left atrial appendage; LAO = left anterior oblique; LSPV = left superior pulmonary vein; LIPV = left inferior pulmonary vein; Map = mapping catheter; PV = pulmonary vein)

Further example of PV ectopy triggered by synchronised HFS is shown in Figure 4.3. Similar PV activation sequence is seen after stimulating three different HFS sites in the LA. However, in Figure 4.3A, HFS triggers single PV ectopy only, whereas Figure 4.3B and C trigger short run of AF and incessant AF respectively. The mechanism for these varied responses is yet to be determined but illustrates how the neural network can act on a single PV from multiple sites. Also, fewer HFS trains were needed for a more profound myocardial response each time at the same PV end-location. Similar phenomenon was also seen by stimulating the same HFS site and the examples are in the reproducibility section.

Figure 4.3 Intracardiac electrograms of the range of responses to HFS at ET-GP

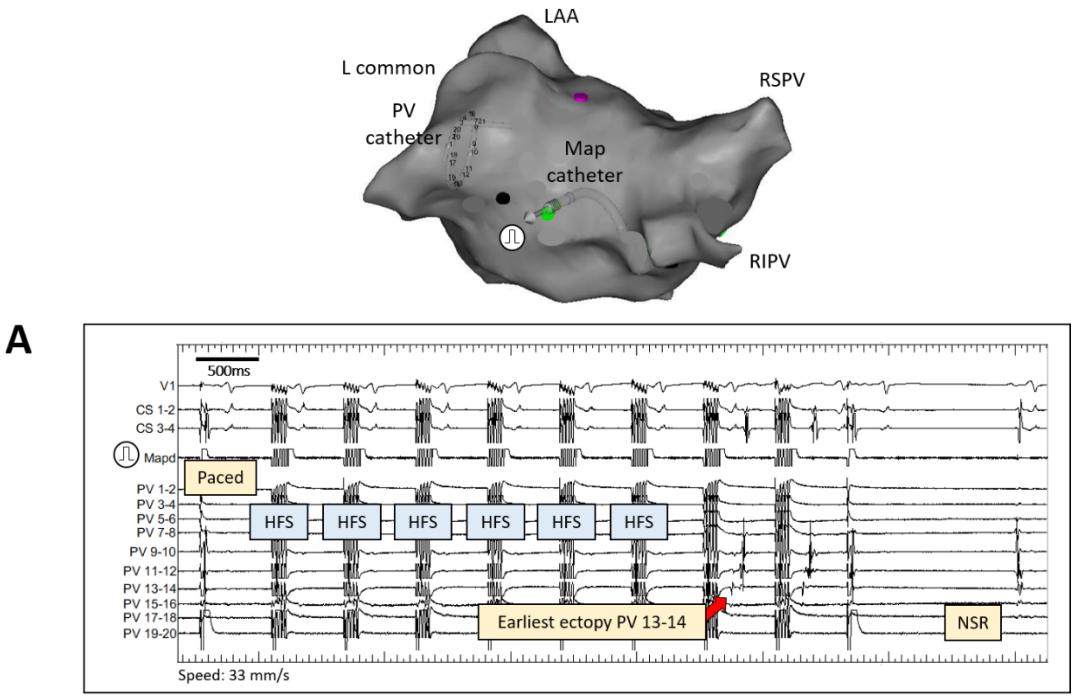

Figure 4.3A. Single ectopy triggered with ET-GP stimulation

A) Map distal was used to pace and deliver HFS. This was positioned in the middle between the left common and RIPV near the posterior wall. The PV catheter was in the lower branch of the left common PV. After the first paced beat, the subsequent trains are synchronised HFS. The earliest ectopy activation is in PV 13-14. There are just two beats of the same ectopy before stopping both HFS and pacing.

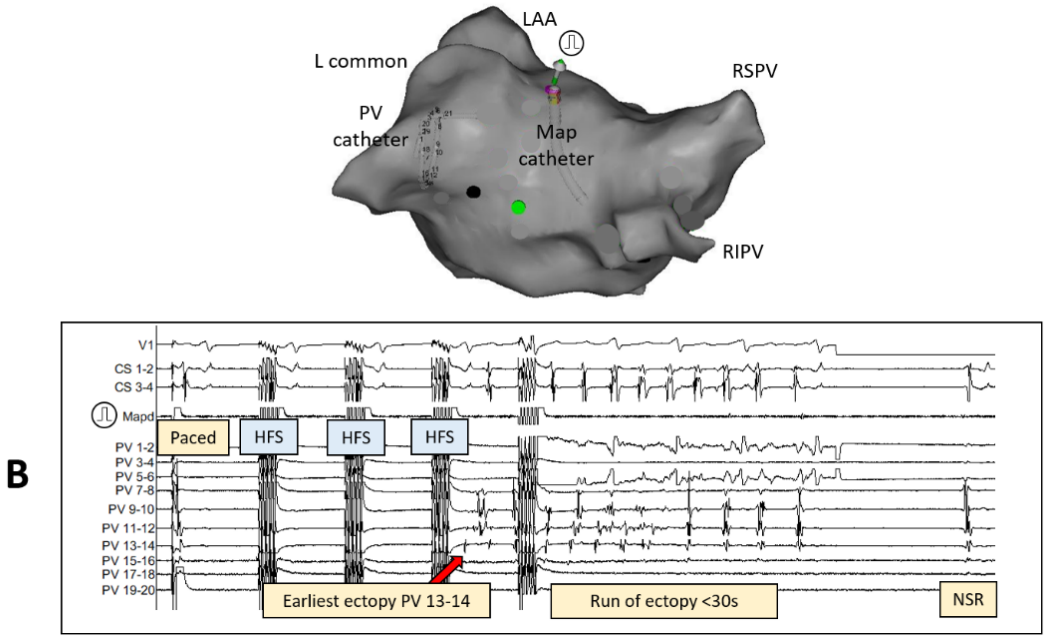

Figure 4.3B. Non-sustained AF triggered with ET-GP stimulation

B) The Map catheter was positioned near the anterior ostium of the upper branch of the left common PV. After the first paced beat, the subsequent trains are synchronised HFS. Again, the earliest ectopy activation is seen in PV 13-14. The PV rapidly fires causing few seconds of AF that regularises towards the end then terminates.

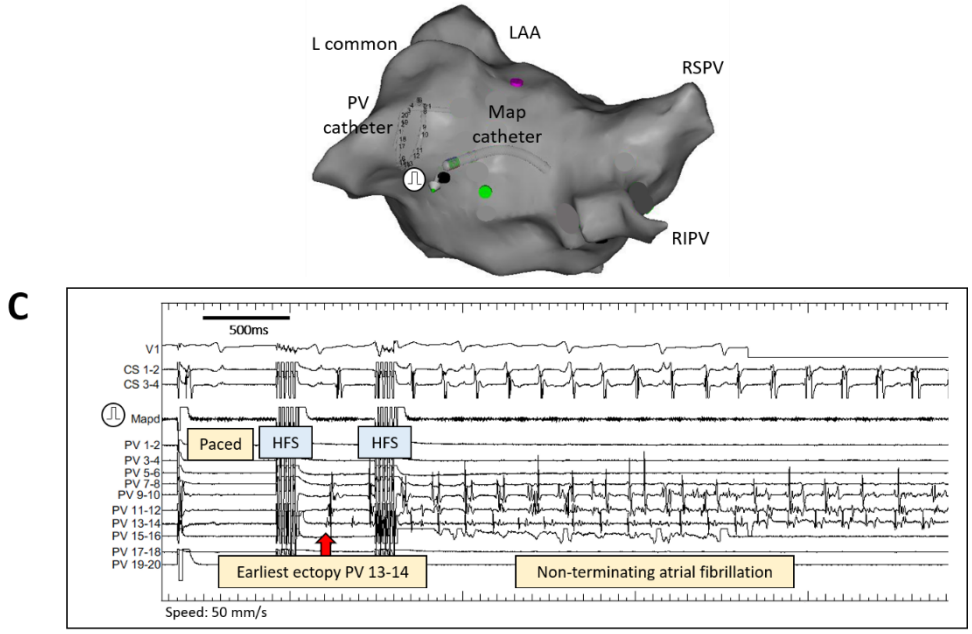

Figure 4.3C. Sustained AF triggered with ET-GP stimulation

C) The Map catheter was positioned at the posterior ostium of the lower branch of the left common PV. This trace shows the first paced beat followed by one synchronised HFS train which triggers ectopy. The earliest ectopy activation is again in PV 13-14. These initiates sustained AF lasting >2mins. The patient had direct DC cardioversion to restore sinus rhythm.

The range of responses to ET-GP stimulation was seen in most patients and the distribution of this range in a single patient is shown in Figure 4.4. We analysed and categorised 464 HFS sites into: <3 beats of atrial ectopy (187 sites, 40%), <30s of atrial arrhythmia (203 sites, 44%), >30s of atrial arrhythmia (74 sites, 16%).

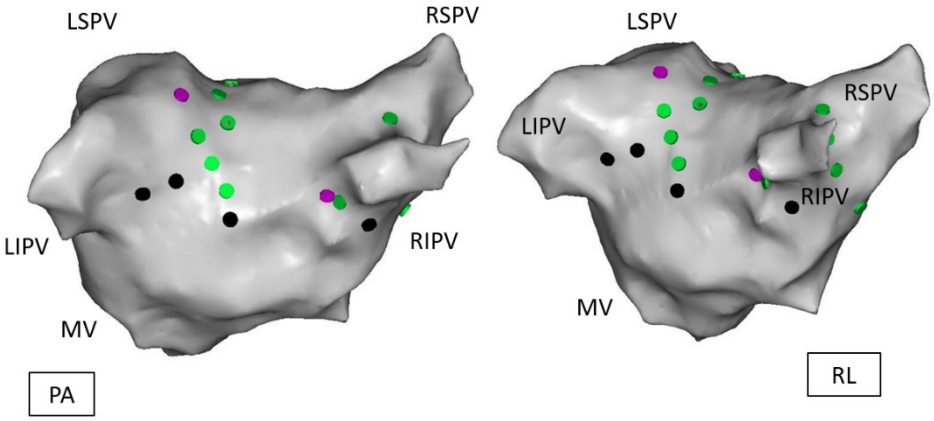

Type of GP response to HFS	No. of GPs
<3 ectopy	187 (40%)
≤30s AF/AT	203 (44%)
>30s AF/AT	74 (16%)
Total no. of GPs	464

Figure 4.4 Distribution of three different types of ET-GP responses to HFS in a single patient

The left and right panels are 3D CARTO™ LA geometries in the PA view and the RL view respectively. All range of ET-GP responses to HFS were found: <3 ectopy (green), <30s AF (pink), >30s AF (black). The number of these ET-GPs responses are shown in the table. All ET-GPs triggering >30s AF were near the LIPV. Areas in grey are absent of ET-GPs.

(AF = atrial fibrillation; AT = atrial tachycardia; ET-GP = ectopy-triggering ganglionated plexuses; HFS = high frequency stimulation; LIPV = left inferior pulmonary vein; LSPV = left superior pulmonary vein; MV = mitral valve; PA = posterior-anterior view, RSPV = right superior pulmonary vein; RIPV = right inferior pulmonary vein; RL = right lateral view)

4.3.3. Reproducibility of Ectopy from ET-GP Stimulation

Spontaneous ectopy occurs during AF mapping procedures. Therefore, it is important to prove that these are reproducible and are driven by neural stimulation via synchronised HFS, rather than as spontaneous events. All synchronised HFS site provoking single and short run of ectopy were re-tested from the same location at least twice for reproducibility (Figure 4.5A). Sometimes, this triggered non-sustained AF (Figure 4.5B). This type of potentiation confirms the reproducibility of neural stimulation even though the effect is more pronounced. Figure 4.5C demonstrates an example from a different patient where the same location triggers an almost identical ectopy followed by non-sustained AF on both occasions. These observations confirm that ET-GP sites are anatomically fixed. In total, 150 ET-GP sites were tested at least twice in 26 patients. 118 (79%) retested positive, and 32 (21%) retested negative.

Similarly, negative HFS sites were also reproducible and anatomically fixed (Figure 4.5D). We tested a negative site five times and no ectopic responses were elicited. This was repeated in 10 patients to prove that negative sites remain negative.

Figure 4.5 Intracardiac recordings of ET-GP response reproducibility with synchronised HFS

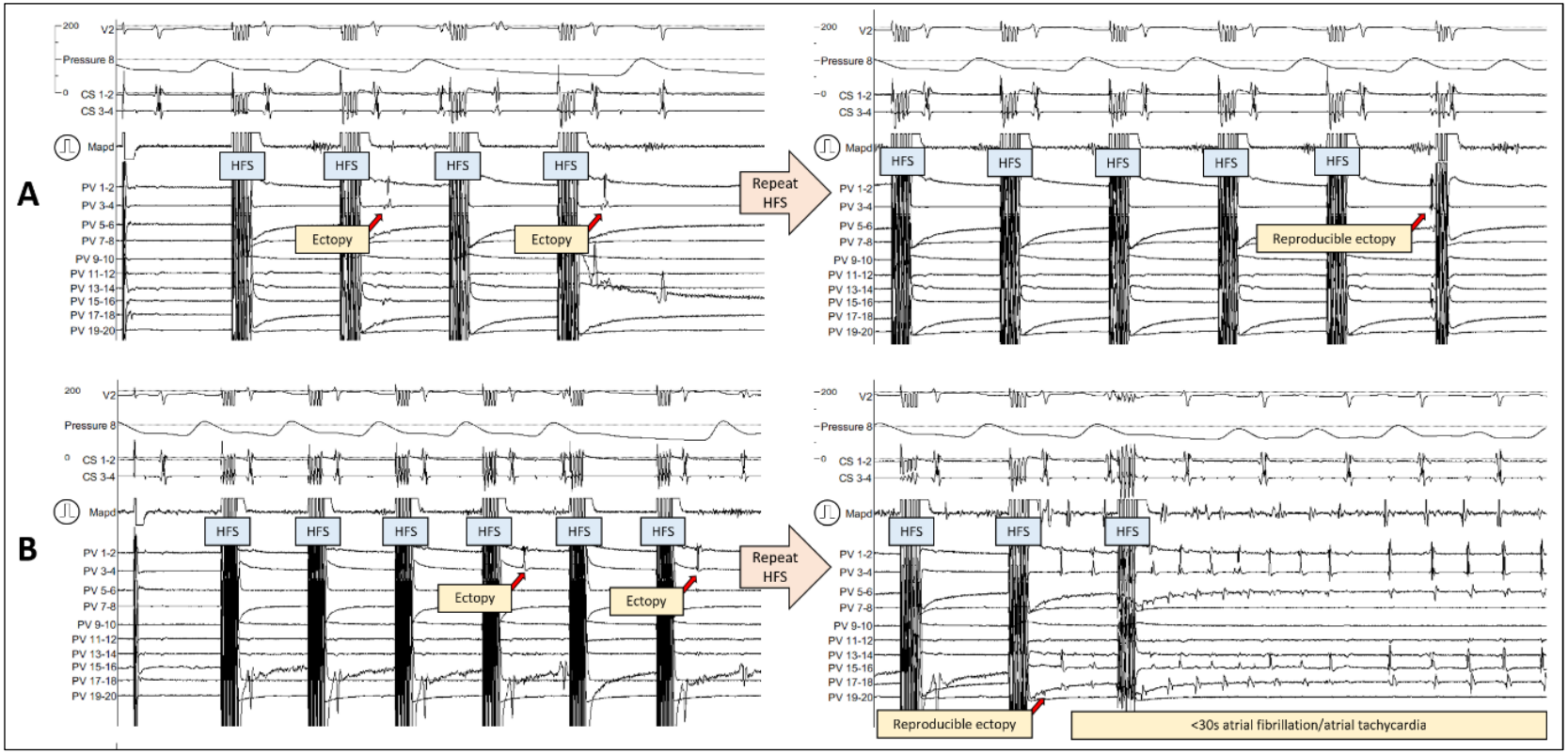

Figure 4.5A and B. PV ectopy and non-sustained AF with repeat synchronised HFS

A) In the left panel, a second train of HFS produces a PV ectopy which repeats itself after two further HFS. This response is reproducible upon re-testing the same site with HFS in the right panel. The PV ectopy in the right panel has different activation pattern to the left panel PV ectopy. The Map catheter is in the left side of the mid-posterior wall. The PV catheter is in the LIPV.

B) In the same patient as A), a different site is tested with HFS in the left panel. This produces a PV ectopy after the 4th train of HFS, which repeats after 2 further HFS trains. Upon re-testing the same site with HFS, the right panel shows an early PV ectopy in PV 17-18 which initiates rapid PV discharges, causing 3.5secs of AF. The Map catheter is near the base of the LIPV in the posterior wall, 10mm superior to the Map position from A). The PV catheter is the LIPV.

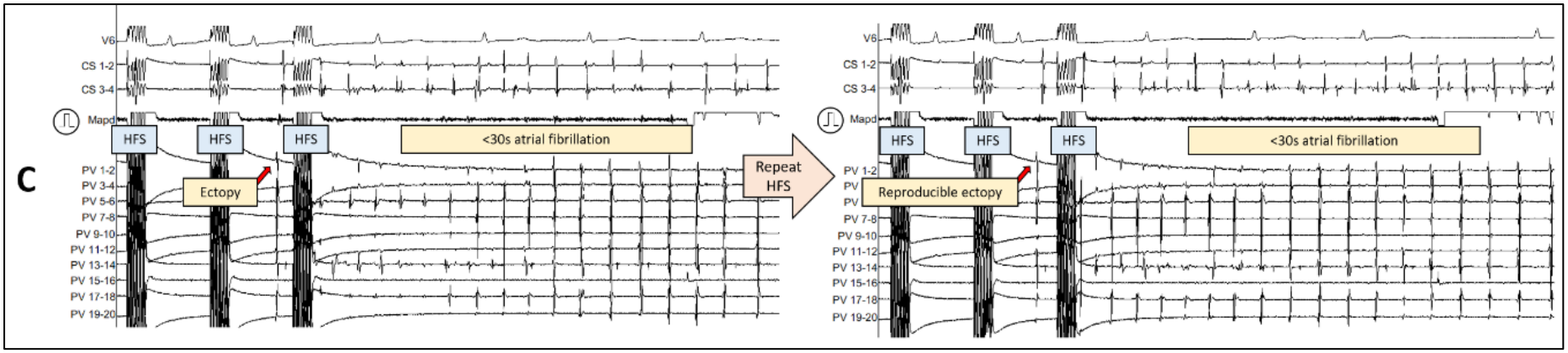

Figure 4.5C. PV ectopy that triggers non-sustained AF with repeat synchronised HFS

C) In a different patient to A/B, a PV ectopy initiates after several trains of HFS which induces 7.6secs of AF. Re-testing this site in the right panel shows repeated PV ectopy which induces 4.5secs of AF. The Map catheter is at the base and ostium of the LIPV in the posterior wall. The PV catheter is in the LIPV.

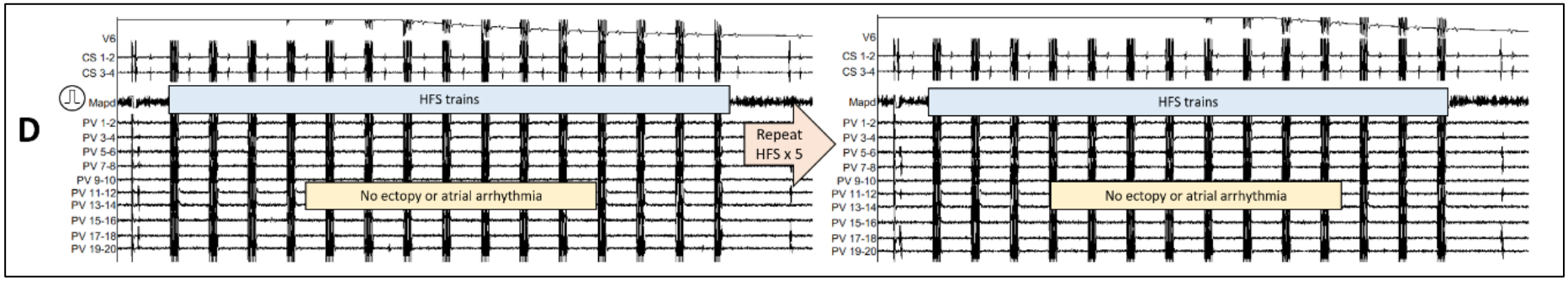

Figure 4.5D. Negative HFS site reproducibility

D) In a different patient to A/B and C, one negative HFS site was re-tested five times, with no positive response to HFS in each re-test. The Map catheter was medial to the appendage in the anterior wall and the PV catheter was in the left superior PV. This was repeated in 9 other patients which produced the same outcome of negative responses to HFS with up to five re-tests at the same site. (CS = coronary sinus; ET-GP = ectopy triggering ganglionated plexus; GP = ganglionated plexus, HFS = high frequency stimulation; Map = mapping catheter; PV = pulmonary vein)

4.3.4. Quantification of ET-GP in the LA

A total of 2302 sites were tested with synchronised HFS in the LA, which identified 579 (25%) ET-GPs. A median of 97 (IQR 55) HFS sites were tested per patient, which identified a median of 19 (20%; IQR 12) ET-GP per patient. The number of ET-GPs ranged widely from one patient to another (Figure 4.6). There was no direct relationship between the number of HFS tested and the number of ET-GPs identified (Figure 4.7).

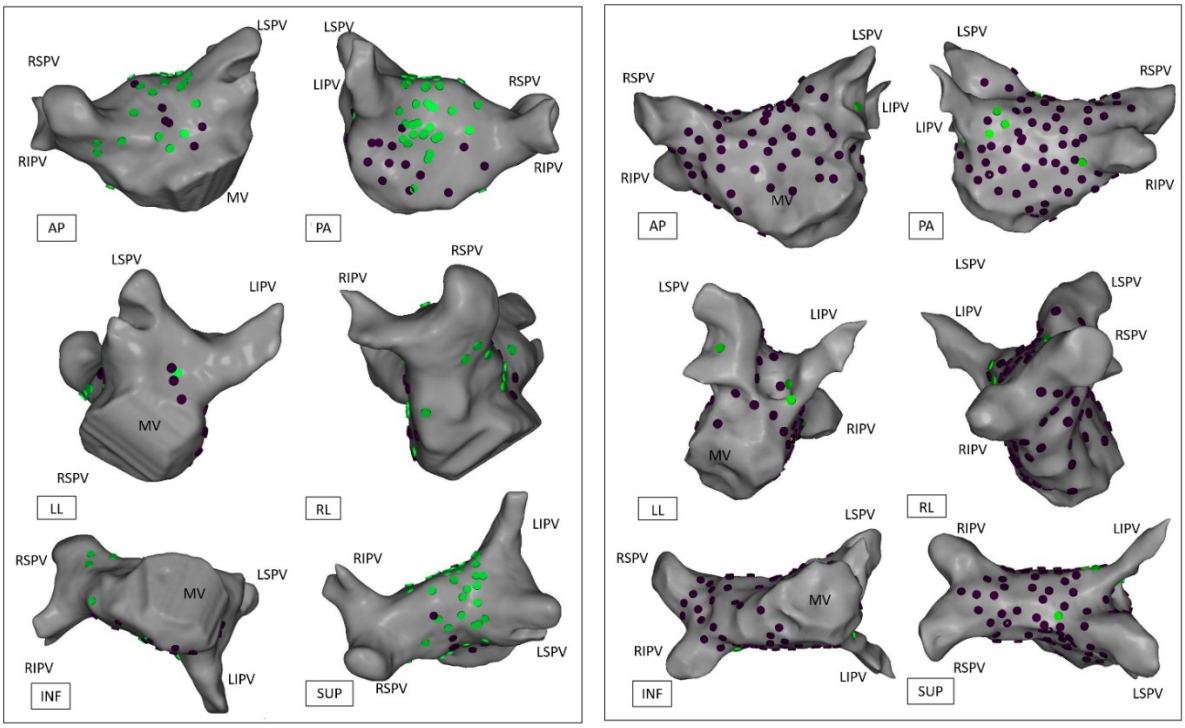

Figure 4.6 Examples of high and low numbers of ET-GP found in patients

The top panel shows the LA of a patient with high number of ET-GPs and the bottom panel shows an example with low number of ET-GPs. Green and purple dots are ET-GPs and negative HFS sites respectively.

(AP=anterior-posterior, INF=inferior, LSPV=left superior pulmonary vein, LAO=left anterior oblique, LIPV=left inferior pulmonary vein, LVSF=left ventricular systolic function, MV=mitral valve, PA=posterior-anterior, PVI=pulmonary vein isolation, RAO=right anterior oblique, RSPV=right superior pulmonary vein, RIPV=right inferior pulmonary vein, RLGP=right lower ganglionated plexus, SUP=superior)

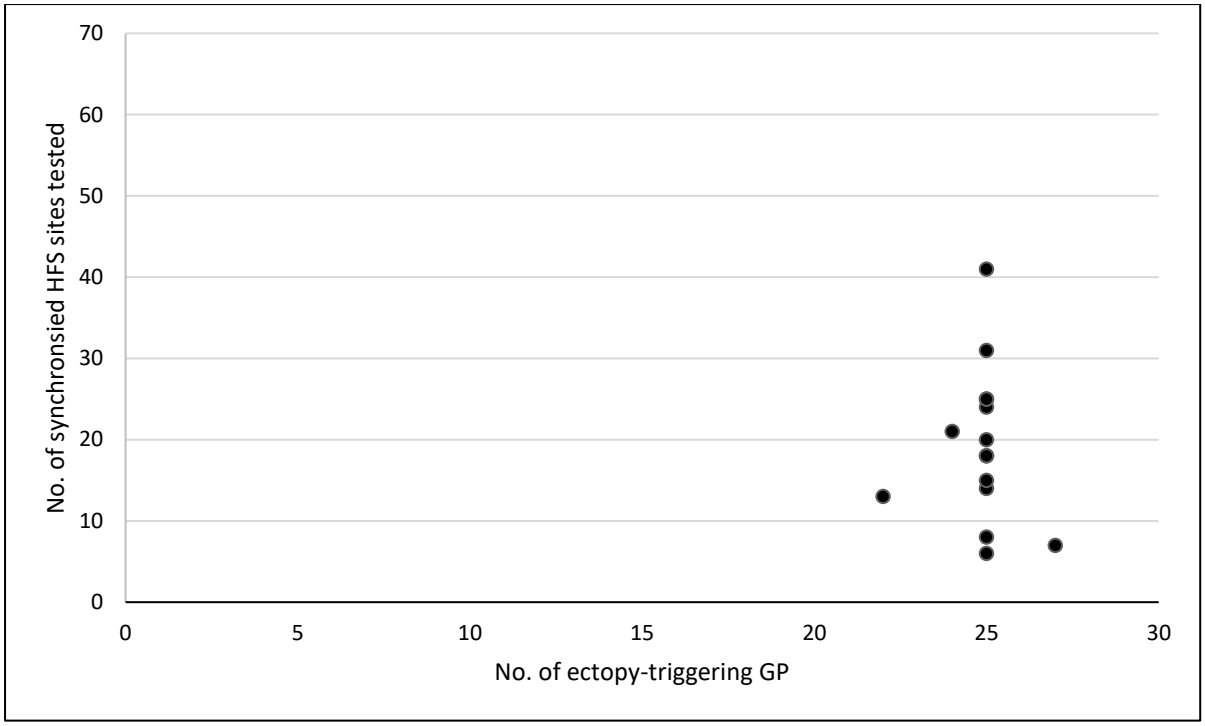

Figure 4.7 A scatter plot of the total number of HFS sites tested and the total number of ET-GPs per patient

There was no direct relationship between the two variables.

(ET-GP = ectopy-triggering ganglionated plexus; HFS = high frequency stimulation)

4.3.5. The Probability Distribution Atlas of ET-GP

Registration of all our patients to one reference shell revealed that 58.3% of the total surface area of the LA contained 90% of ET-GPs. The average target registration error was 2.78±1.05mm (where '0' is perfect registration). The probability atlas of ET-GPs across the whole LA revealed 30-40% probability of ET-GPs in the following anatomical regions: the roof, around the ostia of all PVs except for the base of the right inferior PV in the posterior wall, left side of the anterior wall near the right superior PV and left side of the posterior wall near the left inferior PV. Smaller, discrete patches of ≥40% probability of ET-GP was confined to the PV region: left sided PV carina, right superior PV antrum and its ostium in the roof (Figure 4.8).

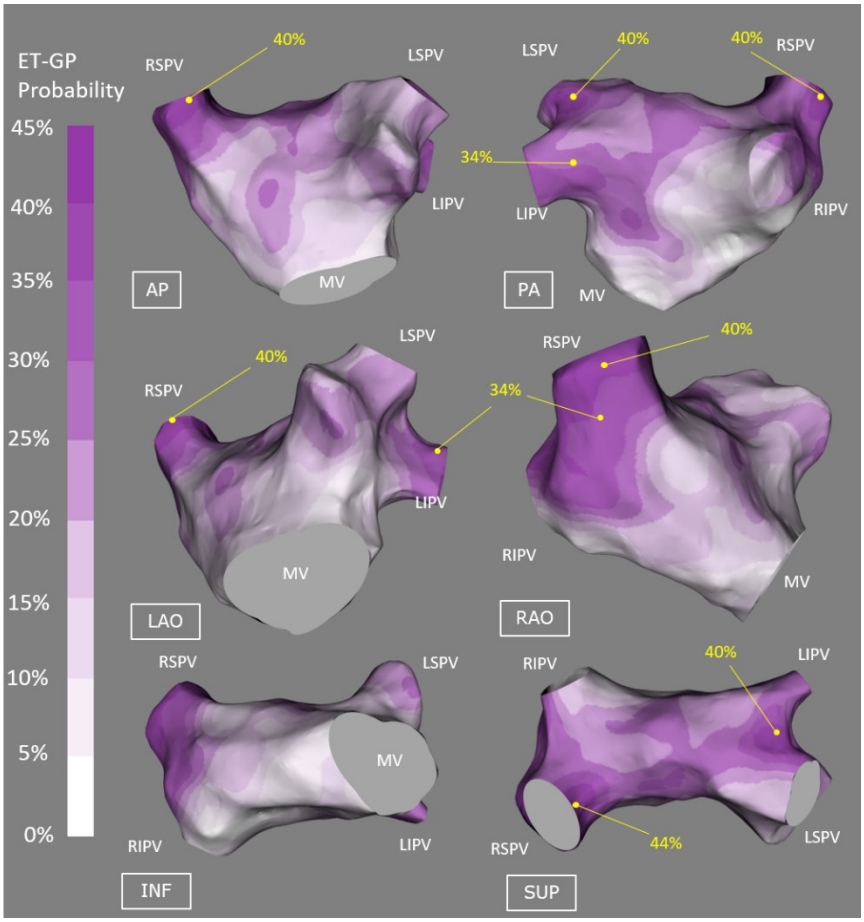

Figure 4.8 The probability distribution atlas of ET-GP

The probabilities are between 0-45%, white to dark purple. "High probability ET-GP sites" were defined as >30% in probability, labelled with yellow dots on the atlas. The highest probability of finding ET-GPs were in the roof and around the PV ostia.

(AP = anterior-posterior; ET-GP = ectopy triggering ganglionated plexus; INF = inferior; LSPV = left superior pulmonary vein; LAO = left anterior oblique; LIPV = left inferior pulmonary vein; MV = mitral valve; PA = posterior-anterior; RAO = right anterior oblique; RSPV = right superior pulmonary vein; RIPV = right inferior pulmonary vein; SUP = superior)

4.3.6. A Comparison Between ET-GP and AVD-GP Probability Distribution

A comparison was made between the ET-GP and the AVD-GP probability distribution atlases[6] (Figure 4.9). A clear contrast is seen in the anatomical distribution of the two GP subtypes. This is particularly apparent in the roof, floor and the posterior wall of the LA. This illustrates the complexity of the neural network from a functional perspective.

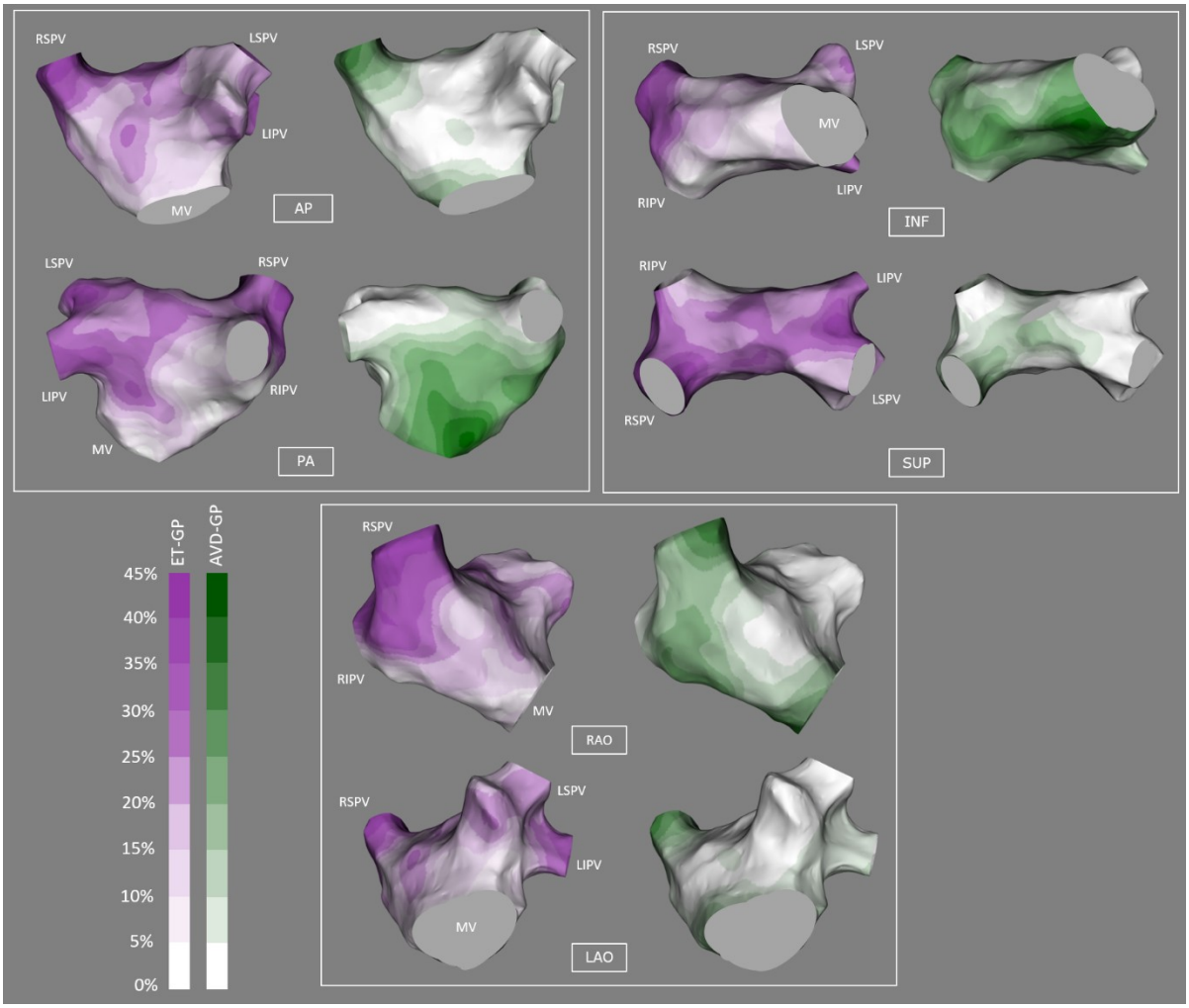

Figure 4.9 ET-GP and AVD-GP probability distribution comparison

The purple and the green atlases represent ET-GP and AVD-GP respectively. The probability ranges from 0-45%, lowest (white) to highest probability (darkest purple/green). The same projection views of ET-GP and AVD-GP atlases are displayed next to each for comparison. The biggest differences are seen in PA, INF, SUP views.

(AP = anterior-posterior; AVD-GP = atrioventricular dissociating ganglionated plexus; ET-GP = ectopy triggering ganglionated plexus; INF = inferior; LSPV = left superior pulmonary vein; LAO = left anterior oblique; LIPV = left inferior pulmonary vein; MV = mitral valve; PA = posterior-anterior; RAO = right anterior oblique; RSPV = right superior pulmonary vein; RIPV = right inferior pulmonary vein; SUP = superior)

4.4. Discussion

It was not the aim of this study to prove that the triggered effects of synchronised HFS are neurally mediated, as this has been demonstrated previously[152,154,175]. However, the phenomena observed with synchronised HFS are highlighted in this study as evidence of the underlying neural mechanism. The distribution and characteristics of ET-GP in patients with AF help to explain some of the clinical phenomena described during and after PV isolation (PVI) for AF and develop a strategy for autonomic modulation.

4.4.1. The Ganglionated Plexus

GP sites that cause AV-dissociation (AVD-GP) have been frequently cited in clinical studies for AF ablation, with the assumption that it is involved in the arrhythmogenesis of AF. However, PV ectopy is known to trigger AF and this can be replicated by HFS stimulation within the local myocardial refractory period at an ET-GP site[87,167,175]. HFS within the local myocardial refractory period can stimulate the intracardiac nerves without direct myocardial capture. Nerve stimulation lead to acetylcholine and catecholamine release, causing shortening of the action potential of the local and adjacent myocardial cells[68,156,178]. This can induce atrial ectopy and arrhythmia. The action potential normalises within two beats of HFS cessation[175].

This study gives further insight into the variation and complexity of the intrinsic cardiac autonomic network in humans. ET-GP stimulation with synchronised HFS displays a wide range of responses from few beats of ectopy to incessant AF, and occasionally AV dissociation with or without ectopy. These are reproducible phenomena.

ET-GP and AVD-GP are co-located and separate from the other[87]. Therefore, the two different types of GP have to be characterised independently.

4.4.2. The Interconnecting Neural Network of GP

The GPs are part of the intricately interconnected autonomic network. The "right lower GP" near the base of the right inferior PV act as an 'integration centre' for AV dissociating effects from other GP areas in the atria[170]. Similarly, stimulation of the GP near the anterior portion of the right superior PV act as the integration centre for slowing of the heart rate and shortening the effective refractory period via the sinoatrial node[162,163,179]. Ablation at these integration centres abolish their stimulation effects at distant sites[170,173] .

The current study also demonstrated that ET-GP stimulated at one location in the LA can trigger electrical changes at another without any apparent effect on the myocardium in between the two locations. PVI can transect the neural communication between ET-GP and the isolated PV, and direct ablation over an ET-GP site abolishes its effects of triggering ectopy[25]. The probability atlas from this study shows a preponderance of ET-GP in the PV antra and may explain why circumferential PV antral (CPVA) ablation is superior to segmental isolation, by transecting the GP neural connections into the PVs. This model may explain why 58.6% patients can have of at least one PV re-connected at follow-up mapping without recurrence of AF[119]. These findings from the ET-GP distribution and behaviour may finally explain some of the inconsistencies from PV isolation simply being about preventing activation exiting the veins.

4.4.3. Functional and anatomical locations of ET-GP and AVD-GP

We densely mapped the whole LA with synchronised HFS to identify their distinct anatomical sites. The higher probability (>30%) sites of ET-GP was consistent with previous anatomical and clinical studies of GP[22,180,181]. Interestingly, there were discrete regions that were absent from ET-GP such as the right side of the posterior wall and the

base of the right inferior PV. These regions are likely occupied by AVD-GP, as we described previously.[6] Similarly, the regions that are absent of AVD-GP are likely occupied by ET-GP. These anatomical differences are important to distinguish to deliver the correct HFS technique to identify all GP.

4.4.4. Differences in GP responses to HFS

We demonstrated a range of responses with synchronised HFS at an ET-GP site. This may be related to the degree of GP stimulation which can be controlled by the amount of current delivered to the site[167,175], which in turn affects the actional potential and atrial effective refractory period shortening. Therefore, a single ectopy-triggering GP site with HFS may be capable of inducing AF with more prolonged HFS or increased current delivery to the GP site[175].

Occasionally, we observed a progressive Wenckebach with or without ectopy when testing a GP site with synchronised HFS, as previously reported by Lim *et al*[87]. Re-testing the site with continuous HFS showed a more pronounced RR prolongation, reaching the threshold for an AVD-GP site. As synchronised HFS can identify both ET-GP and AVD-GP, we would have expected to see more AVD-GP in the posterior wall but found only a few. This may be due to not adequately reaching the threshold for stimulating AVD-GP with shorter bursts of HFS trains used with synchronised HFS.

4.4.5. Neural Composition of ET-GP

A detailed study on the muscle connection and autonomic nerve distribution in the PV-LA junction of the LA showed that both adrenergic and cholinergic nerves were equally spatially distributed along the longitudinal and transmural axes of the PV-LA segments and circumferentially around the PV orifice[160]. We are likely stimulating both types of

nerves with HFS, and this is likely the neural composition of ET-GPs as we found these to be mostly in the PV-LA junction.

4.4.6. Clinical implications

In clinical studies, continuous HFS has been commonly used to identify AVD-GPs as targets for autonomic modulation in AF[7,9,128]. However, it is clear from our study that continuous HFS does not identify all GP. ET-GP and AVD-GP have very different anatomical and functional characteristics that need to be distinguished to target the relevant GP.

The current standard ablative treatment for AF is complete PVI via CPVA. CPVA invariably ablate many ET-GP that are located in the roof and around the PV ostia. This is in effect, both PVI and GP ablation procedure. However, the results from this study demonstrate that there are ET-GP outside the conventional CPVA lines. It is not known whether ET-GP ablation may confer additional benefit to CPVA alone in prevention of AF.

4.4.7. Limitations

We do not know what effect general anaesthetic have on the patients' ectopy-triggering threshold with HFS. We have not mapped the right atrium with HFS, and we know from previous studies that there are GPs at this site[5]. Co-location of ET-GP and AVD-GP has been identified in some patients, but this has not been consistently tested across all patients as the focus of this paper was in the ET-GP distribution of the LA.

4.5. Conclusion

There are distinct high and low probabilities regions of ET-GP in patients with AF. Comparison with AVD-GP showed marked contrast in their anatomical distributions. ET-

GP preponderance to the roof and the PV ostia suggest that they are inadvertently ablated during PVI procedures. This is electrophysiological evidence that ET-GP are upstream triggers of AF and may contribute to success of AF ablations.

5. GANGLIONATED PLEXUS ABLATION TO PREVENT AF (GANGLIA-AF)

5.1. Introduction

The autonomic nervous system is increasingly recognised as an important therapeutic target for prevention and treatment of atrial fibrillation (AF)[182]. Attempts to target ganglionated plexuses (GP) that are key integration centres of the intrinsic cardiac nerves have produced mixed results. "Selective" GP ablation has only targeted GPs with atrioventricular dissociating effects with stimulation, and our work previously identified that these GPs occupy discrete regions of the left atrium; a small proportion of the human GP anatomical sites[6] (Chapter 3). Other studies have shown that catheter ablation of atrioventricular dissociating GPs alone does not prevent AF.[8,105,128]

One group demonstrated that "anatomical" GP ablation in addition to pulmonary vein isolation (PVI) conferred benefit over PVI alone[8]. However, anatomically locating GP by approximation is subjective and does not account for inter-patient variability, with no definite endpoint to ablation. The role of GPA in AF prevention remains unclear.

In Chapter 4 of this thesis, we showed that pulmonary vein (PV) and non-PV ectopy can be triggered by stimulating discrete areas of postganglionic nerves from the endocardium, using high frequency stimulation (HFS) within the local atrial refractory period (synchronised HFS)[87,175]. These "ectopy-triggering" postganglionic nerves communicate with the epicardial GP (ET-GP), and stimulation of ET-GP led to reproducible AF. Our first single-centre feasibility study on 67 patients confirmed that ET-GP mapping and ablation was clinically safe and prevented AF in 49% of patients with paroxysmal AF at 12 months follow-up[183].

In this Chapter, we addressed some of the limitations of the feasibility study in protocol design. This included high rate of crossovers from GP ablation arm to PVI arm due to sustained AF. We tested the hypothesis that ET-GP are part of the triggering mechanism for AF, by performing selective endocardial ablation of ET-GP without PVI and observed for AF recurrence.

5.2. Methods

This was a prospective, multi-centre, randomised, single-blinded clinical study (NCT02487654) recruiting patients with paroxysmal AF indicated for AF ablation. Recruitment period was between May 2017 to May 2019. Three centres (Hammersmith Hospital, Imperial College London Trust; Derriford Hospital, University Hospitals Plymouth NHS Trust; St Bartholomew's Hospital, Barts Health NHS Trust) participated in the study. All patients gave written informed consent and the study was approved by the Local Research Ethics Committee. Patients with symptomatic, drug-refractory paroxysmal AF, indicated for ablation were recruited to the study. The inclusion and exclusion criteria are in Table 5.1.

5.2.1. Randomisation

Patients were randomised to PVI or ganglionated plexus ablation (GPA) without PVI. Randomisation was performed using the 'sealed envelope' approach. The first block of randomisation was performed on 21 consecutive patients, randomised 2:1 for GPA (GPA = 14, PVI = 7). This was in anticipation for high-rate of cross-over from the GPA group as experienced in the feasibility study. Afterwards, randomisation was switched to 1:1 in blocks of ten, for the remainder of the recruitment. Patients and their cardiologists

providing their usual care were blinded to their randomisation. Operators on the day of the ablation, the data collector and analyst were unblinded to randomisation.

Table 5.1 Inclusion and exclusion criteria

Inclusion criteria	Exclusion criteria
• Males or females from 18 to 85yrs old • Paroxysmal atrial fibrillation • Off amiodarone for at least 60 days • Suitable candidate for catheter ablation • Signed informed consent	• Contraindication to catheter ablation • Contraindication for general anaesthetic • Presence of a left ventricular thrombus • Previous left atrial ablation • Valvular disease that is grade moderate or greater • Any form of cardiomyopathy • Severe cerebrovascular disease • Active gastrointestinal bleeding • Serum Creatinine >200umol/L or on dialysis or at risk of requiring dialysis • Active infection or fever • Life expectancy shorter than the duration of the trial • Allergy to contrast • Moderate to severe heart failure and/or NYHA Class III-IV • Bleeding or clotting disorders or inability to receive heparin • Uncontrolled diabetes (HbA1c ≥73mmol/mol or HbA1c ≤64mmol/mol and Fasting Blood Glucose ≥9.2mmol/L) • Malignancy needing therapy • Pregnancy or women of childbearing potential not using a highly effective method of contraception • Unable to give informed consent or has insufficient comprehension

(NYHA = New York Heart Association)

5.2.2. Protocol for All Patients

Peri-procedural, intra-procedural and post-operative protocols were the same for all centres. Details of these protocols, including PVI and GP mapping and ablation are in Chapter 2. Local policies were followed for anticoagulation and assessment of left atrial appendage thrombus using transoesophageal echocardiography.

5.2.3. Clinical Follow-Up

Patients were followed-up and monitored for 12 months, with continuous remote contact with a clinician. Patients were fitted with 48hr Holter monitors at 3, 6, 9, 12-month intervals. If patients experienced symptoms between these 3-monthly timepoints, they were offered further Holter monitors in attempt to record their symptomatic arrhythmia. Patients with pacemaker and loop recorder devices had these interrogated throughout their follow-up. Any significant arrhythmia identified on interrogation of implanted devices counted towards the primary endpoint regardless of the Holter results. Some patients were also in possession of AliveCor ECG monitoring device. Any significant arrhythmia identified through these recorders were also counted towards the primary endpoint.

5.2.4. Definitions for Endpoint

The primary endpoint was any documented atrial arrhythmia (AF, atrial tachycardia, atrial flutter) ≥30s consecutively recorded on: Holter monitor, 12 lead ECG, pacemaker and loop recorder device, AliveCor ECG, after a 90-day blanking period.

The secondary endpoints included repeat ablation for AF/atrial tachycardia/atrial flutter after a 90-day blanking period, mortality, any complications related to the procedure (bleeding, thrombosis, phrenic nerve palsy, cardiac tamponade) requiring intervention.

5.2.5. Statistics

Data analyses were conducted using the modified intention-to-treat (ITT) and per-protocol (PP) study populations. The ITT evaluation consisted of patients that were enrolled and randomised, including: consent withdrawn (n=3), received Cryoballoon ablation for PVI (n=1), did not attend for ablation (n=1), significant HFS protocol deviation (n=1) and persistent AF for >5 days prior to day of ablation (n=1). Cross-over patients were also included (n=6). However, the ITT population excluded those who did not undergo AF ablation due to the following reasons (n=5): 4 had symptomatic improvement and were not clinically indicated for AF ablation, and 1 had atrioventricular nodal re-entry tachycardia instead of AF. The PP population only included patients who were randomised and completed their ablations without any protocol deviation.

For sample size calculation, it was estimated that at a statistical power of 80% at a 5% significance level, 108 patients were required to detect 25% difference in primary endpoint, where 45% in PVI and 20% in GPA are predicted to have recurrent AF/AT.

Statistical analysis was performed using GraphPad 5 (Prism, San Diego, California) and SPSS v25.0 (SPSS Inc., Chicago, IL). Continuous variables were expressed as mean ± SD. Categorical variables were expressed as numbers and percentages. D'Agostino & Pearson omnibus and Shapiro-Wilk tests were performed to assess normality of continuous variables prior to comparison of means tests. Mann-Whitney *U* test, Fisher's exact test and unpaired t-test were used for comparison of means. An event-free survival was

estimated using a Kaplan-Meier curve for the primary endpoint. Clinical parameters associated with AF recurrence and other procedural parameters were studied using univariate and stepwise multivariate analysis in a Cox regression model. Continuous variables such as age, left atrial diameter were dichotomised into categories, based on their median value. All variables with p values ≤0.10 in univariate analysis and left atrial size as a well-established risk factor for AF recurrence was entered into the multivariate regression analysis. A p value <0.05 indicated statistical significance.

5.3. Results

5.3.1. Patients Studied

121 patients were included and randomised. 66 patients were randomised to GPA and 55 to PVI. In the ITT population, 2 patients were excluded after randomisation to PVI and 3 patients excluded after randomisation to GPA as patients were not clinically indicated for AF ablation any longer. Therefore, 53 patients in the PVI group and 63 patients in the GPA group were analysed for primary outcomes in the ITT population (Figure 5.1).

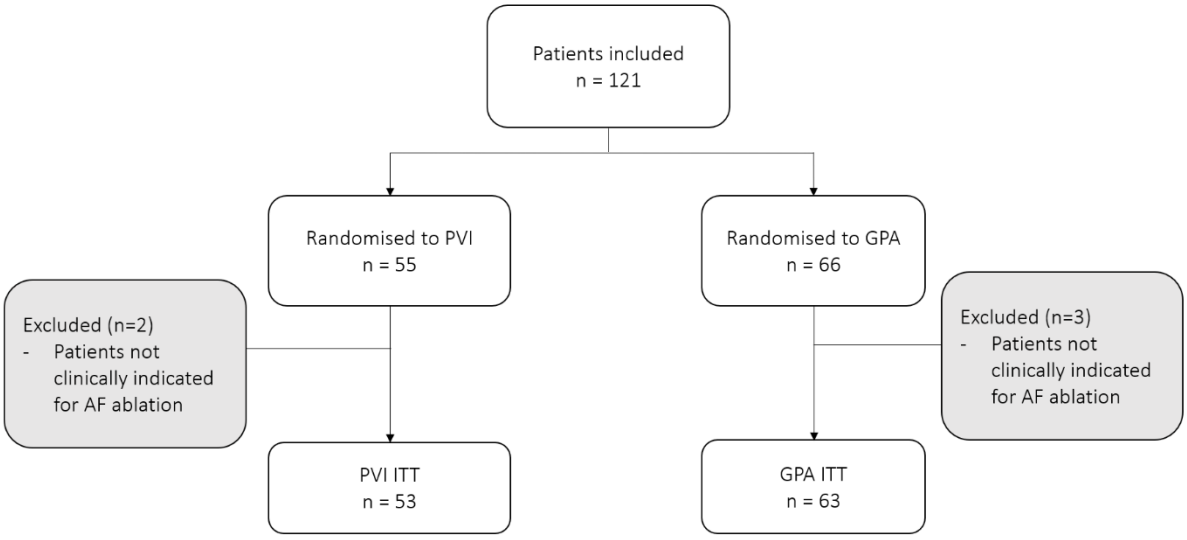

Figure 5.1 Study flow chart for Intention-to-Treat primary analysis

Out of 121 patients recruited, 53 patients were analysed for PVI and 63 patients for GPA in the ITT population.

(AF = atrial fibrillation; GPA = ganglionated plexus ablation; ITT = intention to treat; PVI = pulmonary vein isolation)

In the Per Protocol (PP) population, 12 patients randomised were excluded. 5 were randomised to PVI, 7 were randomised to GPA. The reasons were as follows: 5 were not clinically indicated for AF ablation any longer. 3 refused further participation in the study, 1 had cryoballoon ablation for PVI instead of radiofrequency ablation due to the technical malfunction of the 3D mapping system, 1 was in persistent AF for >7 days, 1 did not attend for their AF ablation procedure, and 1 did not have HFS performed correctly.

6 randomised to GPA crossed over to PVI; 4 patients had incessant AF or repeated sustained AF despite multiple cardioversions. Synchronised HFS could not be performed to map for ET-GP. Therefore, continuous HFS was performed to map for AVD-GP but none were identifiable. 1 patient also had repeatedly inducible sustained AF during the procedure despite multiple cardioversions, and developed ST segment depression with high ventricular rate in AF. There was no evidence of myocardial ischaemia from arterial

blood tests and transoesophageal echocardiography. The patient was deemed clinically unstable to be further mapped with HFS. 1 patient had malfunction of the 3D mapping system in the middle of HFS mapping and therefore HFS was abandoned. No GPs were ablated at this point. All crossed-over patients received complete PVI as per PVI protocol.

Following the above exclusions and crossovers, 56 and 53 patients received PVI and GPA respectively in the PP population (Figure 5.2). In this population, 39 patients had purely synchronised HFS mapping, 4 patients had purely continuous HFS mapping, and 10 patients had combined synchronised and continuous HFS mapping.

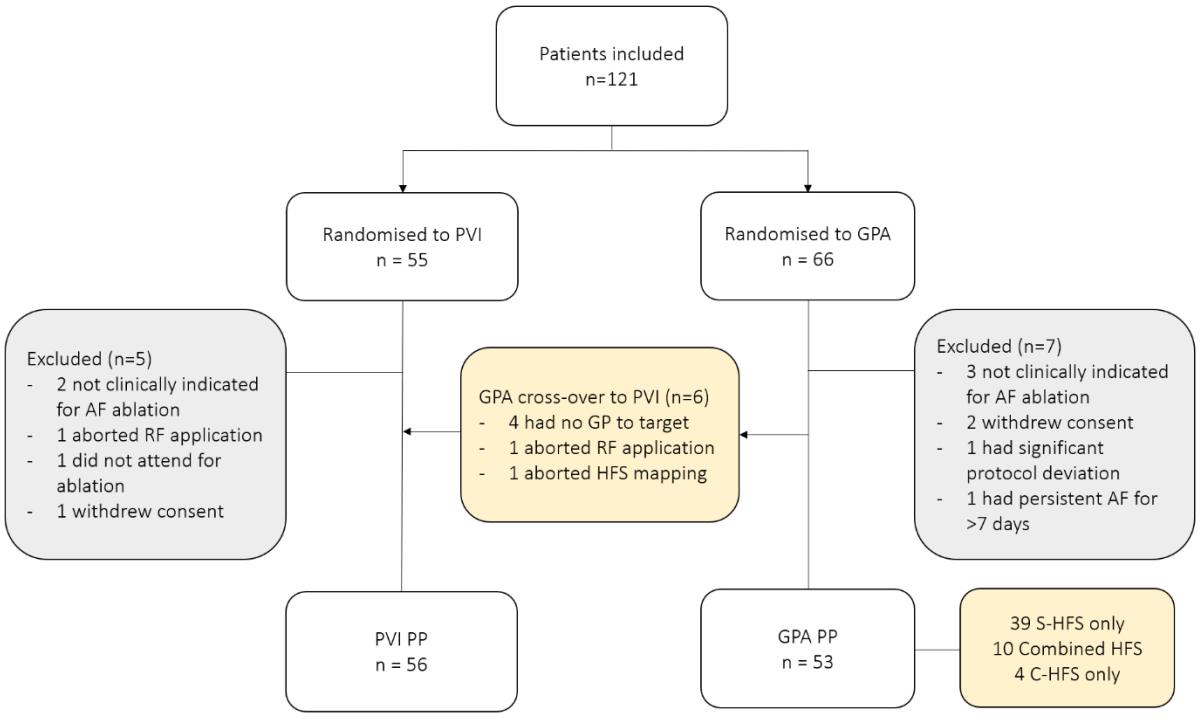

Figure 5.2 Study flow chart for Per Protocol primary analysis

Out of 121 patients recruited, the primary outcome analysis was performed on 56 patients for PVI and 53 patients for GPA in the PP population.

(AF = atrial fibrillation; C-HFS = continuous high frequency stimulation; GPA = ganglionated plexus ablation; PP = per population; PVI = pulmonary vein isolation; S-HFS = synchronised high frequency stimulation)

Patients were 64 ± 10 years of age and 62 (61%) were men. There was no difference in the baseline demographics of patients who completed PVI and ET-GP ablation (Table 5.2).

Table 5.2 Baseline patient demographics

	PVI (n=53)	GP ablation (n=63)	p Value
Demographics			
Age, yrs	62 ± 11	64 ± 12	0.47
Male	34 (64%)	38 (60%)	0.56
BMI, kg/m^2	27.9 ± 4.9	27.4 ± 4.2	0.62
LA diameter, mm	4.1 ± 0.1	3.8 ± 0.5	0.11
LVEF, %	56.4 ± 4.3	56.5 ± 4.1	0.48
CHA2DS2-VASc			
0	9 (17)	15 (24)	0.49
1	25 (5)	15 (24)	0.01
2	6 (11)	14 (22)	0.14
≥3	9 (17)	16 (25)	0.37
HTN	20 (38)	18 (29)	0.33
IHD (previous PCI)	3 (6)	6 (9.5)	0.51
T2DM	3 (6)	4 (6)	1.00
Stroke/TIA/embolus	2 (4)	5 (8)	0.45
Sleep apnoea	3 (6)	1 (2)	0.33
Symptoms			
Autonomic triggers	8 (15)	15 (24)	0.35
Antiarrhythmic drugs			
Class 1C	15 (28)	25 (40)	0.24
Class II	29 (55)	30 (48)	0.46
Class III	5 (9)	8 (13)	0.59
Class IV	4 (7.5)	5 (8)	1.00
Digoxin	0 (0)	4 (6)	0.13

Values are mean ± SD, n (%), or median (interquartile range), unless otherwise indicated.

(BMI = body mass index; CHA2DS2-VASc = congestive heart failure, hypertension, age >75 years, diabetes mellitus, prior stroke, transient ischemic attack, or thromboembolism, vascular disease, age 65-75yrs, sex category (female); GP = ganglionated plexus; HTN = hypertension; IHD = ischaemic heart disease; LA = left atrial; LVEF = left ventricular ejection fraction; PVI = pulmonary vein isolation)

5.3.2. Procedure Details

Patients randomised to GPA had on average 88 ± 28 HFS sites tested per patient, identifying 18 ± 9 (20.5%) GPs. In total, 4182 HFS sites were tested, which identified 829 (20%) GPs. Out of all GPs, 683 (82%) were exclusively ET-GP, 25 (3%) were ET-GP co-located with AVD-GP, 121 (15%) were AVD-GP identified with synchronised or continuous HFS. Examples of synchronised HFS and continuous HFS for identification of ET-GP and AVD-GP are shown in Figure 5.3 and Figure 5.4 respectively.

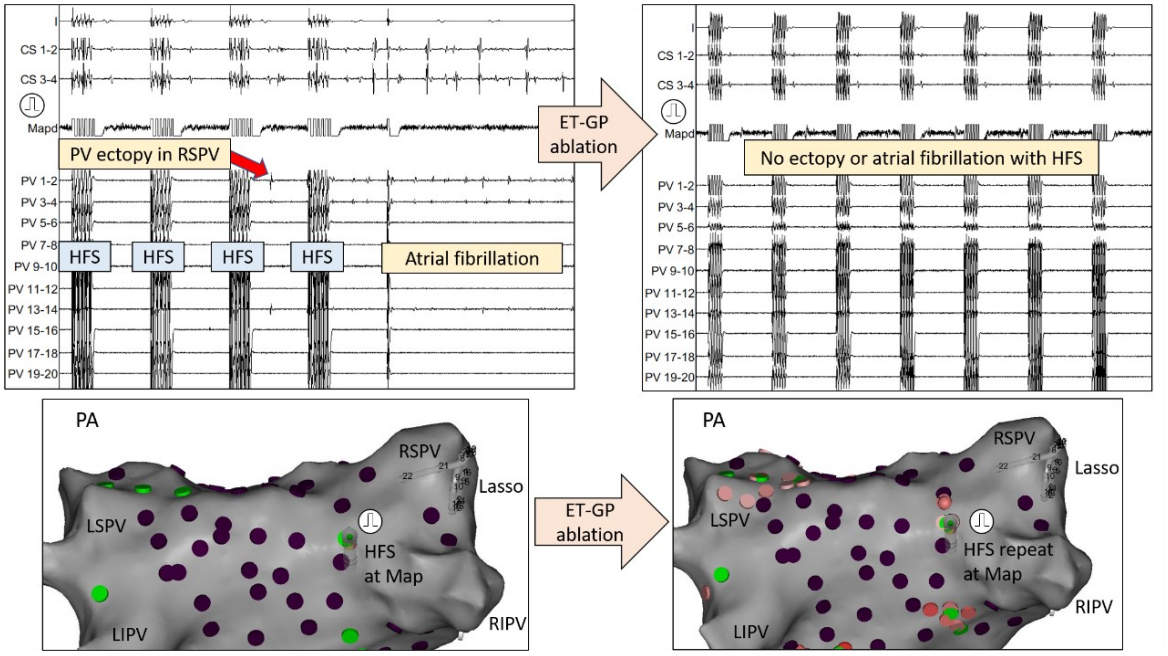

Figure 5.3 Synchronised HFS mapping for ET-GP and its ablation effects

An example of mapping for an ET-GP site using synchronised HFS is shown on the left-hand side. PA view of the left atrium at the bottom shows that the ablation catheter (Map) was positioned near the mid-point between the RSPV and RIPV in the roof. The pulmonary vein catheter (Lasso) was inserted into the RSPV. Pacing was performed first, followed by delivery of HFS coupled to each pacing stimulus (synchronised HFS). After the third HFS train, PV ectopy was initiated (earliest PV 13-14) which triggered atrial fibrillation. This site was marked as an "ET-GP" site, tagged green in the CARTO geometry. After performing ablation at this site, re-testing with synchronised HFS could not trigger the same response as before ablation. This confirmed adequate ablation at this site. Purple tags on CARTO represented negative responses to HFS. (ET-GP = ectopy triggering ganglionated plexus; HFS = high frequency stimulation; RSPV = right superior pulmonary vein; RIPV = right inferior pulmonary vein; PA = posterior-anterior; PV = pulmonary vein)

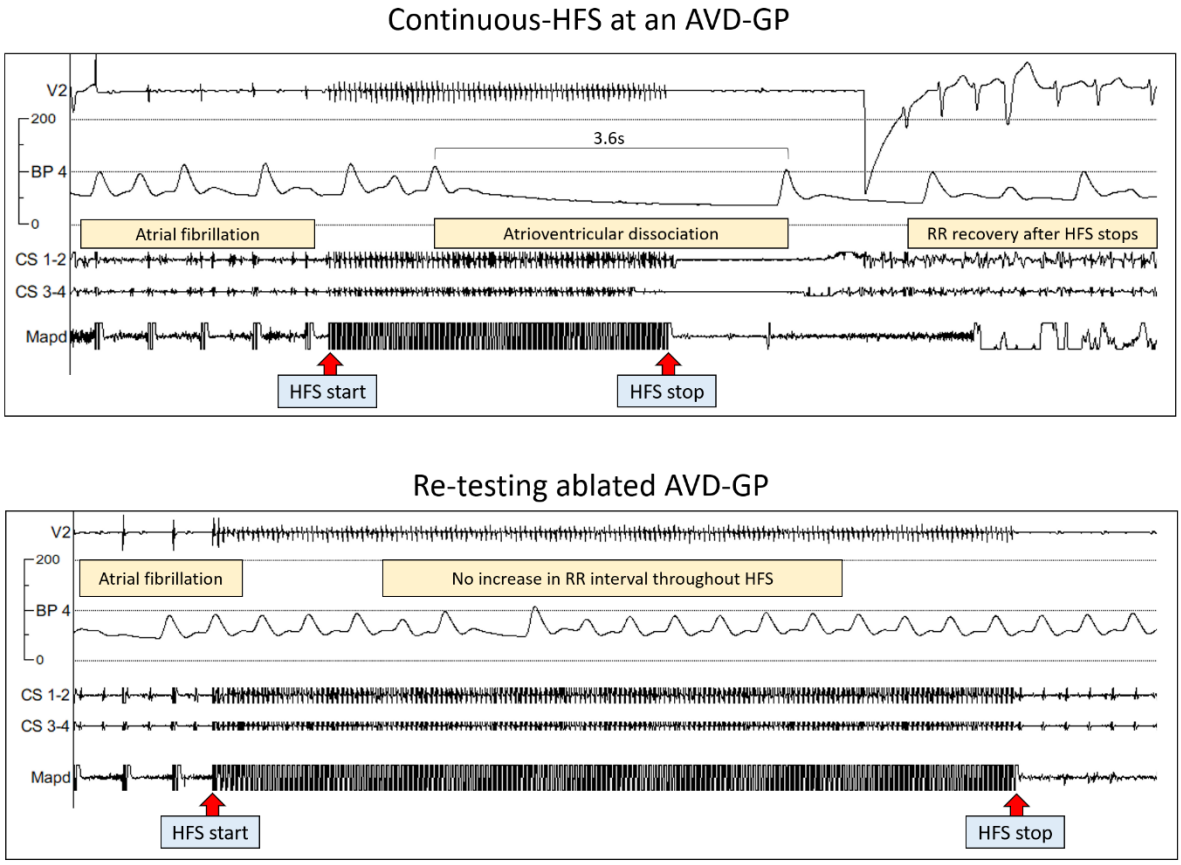

Figure 5.4 Continuous HFS mapping for AVD-GP and its ablation effects

During atrial fibrillation, continuous HFS was performed to identify AVD-GPs as in the top panel. Here, pacing was performed for at least five beats to ensure that there was no ventricular capture. A continuous train of HFS was then delivered at the end of an ablation catheter (Map). A significant atrioventricular dissociation occurred, causing asystole of 3.6secs. HFS was stopped at this point and there was a rapid RR interval recovery and continuation of atrial fibrillation. This site was determined as an AVD-GP site and ablated at the end of the procedure. The bottom panel shows that re-testing with continuous HFS at this ablated site did not trigger any atrioventricular dissociation again. This confirmed adequate ablation at this site.

(AVD-GP = atrioventricular dissociating ganglionated plexus; BP = blood pressure; HFS = high frequency stimulation)

17 patients randomised to GPA had evidence of repeated sustained AF despite multiple DC cardioversions to maintain sinus rhythm (including 3 patients who were crossed over to PVI due to having no GP sites identifiable).

Most GP were ablated with 2-3 lesions of ablation, 30s each. However, in one patient, there was a large nest of ET-GP in the posterior wall, which would have required

significant amount of cluster ablations individually. A circumferential ablation was performed around the large cluster of GP sites to “box-isolate” the ET-GP inside. Testing several ET-GP with HFS within the box of ablation did not re-trigger any atrial ectopy or AF (Figure 5.5). This patient completed 12 months follow-up with multiple 48hr Holter monitors without AF/AT recurrence.

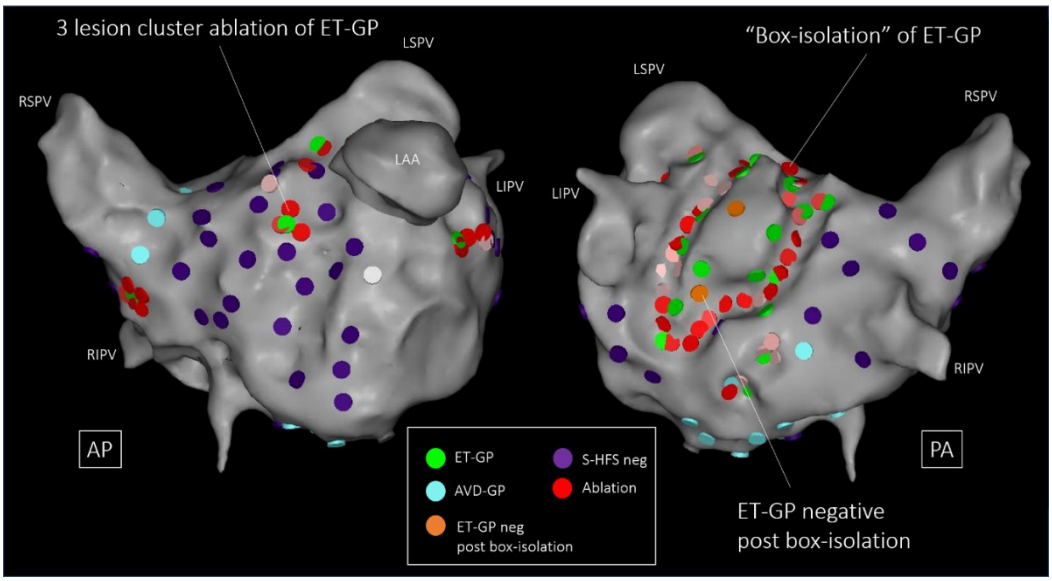

Figure 5.5 Typical cluster ablation at ET-GP and atypical "box-isolation" of a large nest of ET-GP

This patient had a large nest of ET-GP in the roof and posterior wall of the left atrium that triggered atrial ectopy and AF. This would have required a lot of cluster ablations for each individual ET-GP site. In this case, ablation was performed circumferentially around the nest of ET-GP, thereby performing a “box-isolation” of ET-GP. ET-GP were re-tested within the box lesion after ablation with synchronised HFS, and it did not trigger any further ectopy or AF. The remaining ET-GP outside this box-isolation were ablated as normal; 2-3 lesions of ablation for each ET-GP. Each coloured dot represents different responses to HFS and red for ablation lesions, which are labelled at the bottom of the diagram.

(AVD-GP = atrioventricular dissociating ganglionated plexus; ET-GP = ectopy triggering ganglionated plexus; LAA = left atrial appendage; LIPV = left inferior pulmonary vein; LSPV = left superior pulmonary vein; RIPV = right inferior pulmonary vein; RSPV = right superior pulmonary vein; S-HFS = synchronised high frequency stimulation)

All patients randomised to PVI had successful PV isolation, with confirmation of entry and exit PV block. We aimed for contiguous lesions with no gaps between ablation lesions during circumferential ablation (Figure 5.6).

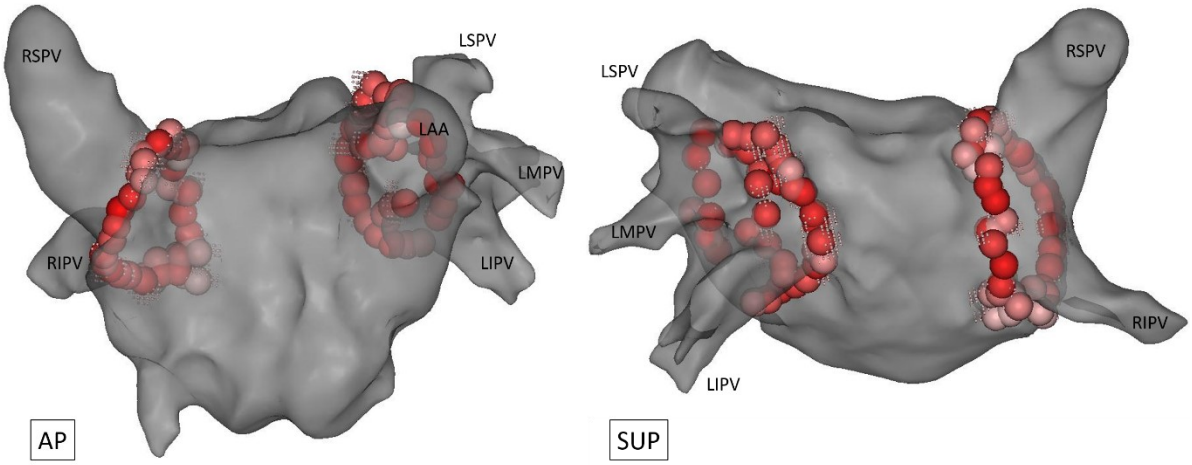

Figure 5.6 Example of a successful circumferential pulmonary vein isolation

Example of a patient randomised to PVI with contiguous lesions during circumferential PVI. Transparency was applied to the left atrial 3D geometry for clear views of the circumferential lesions. This patient did not have any AF/AT recurrence at 12 months follow-up with multiple 48hr Holter monitors.

(AP = anterior posterior; LAA = left atrial appendage; LMPV = left middle pulmonary vein; LSPV = left superior pulmonary vein; LIPV = left inferior pulmonary vein; RSPV = right superior pulmonary vein; RIPV = right inferior pulmonary vein; SUP = superior)

The duration of procedure was 132 mins ± 33in PVI and 179 mins ± 37in GPA (p < 0.0001). The duration of fluoroscopy was 14.9 mins ± 7.1 in PVI and 19.9 mins ± 13.2 in GPA (p = 0.26). The total radiofrequency energy used in PVI was 64.1 kWs ± 24.0 and in GPA, 35.3 kWs ± 15.7 (p < 0.0001). Similarly, in only the successful procedures without AF/AT recurrence, the average RF energy used in PVI was 56.2 kWs ± 19.7 and in GPA, 37.5 kWs ± 14.9 (p = 0.005). (Figure 5.7).

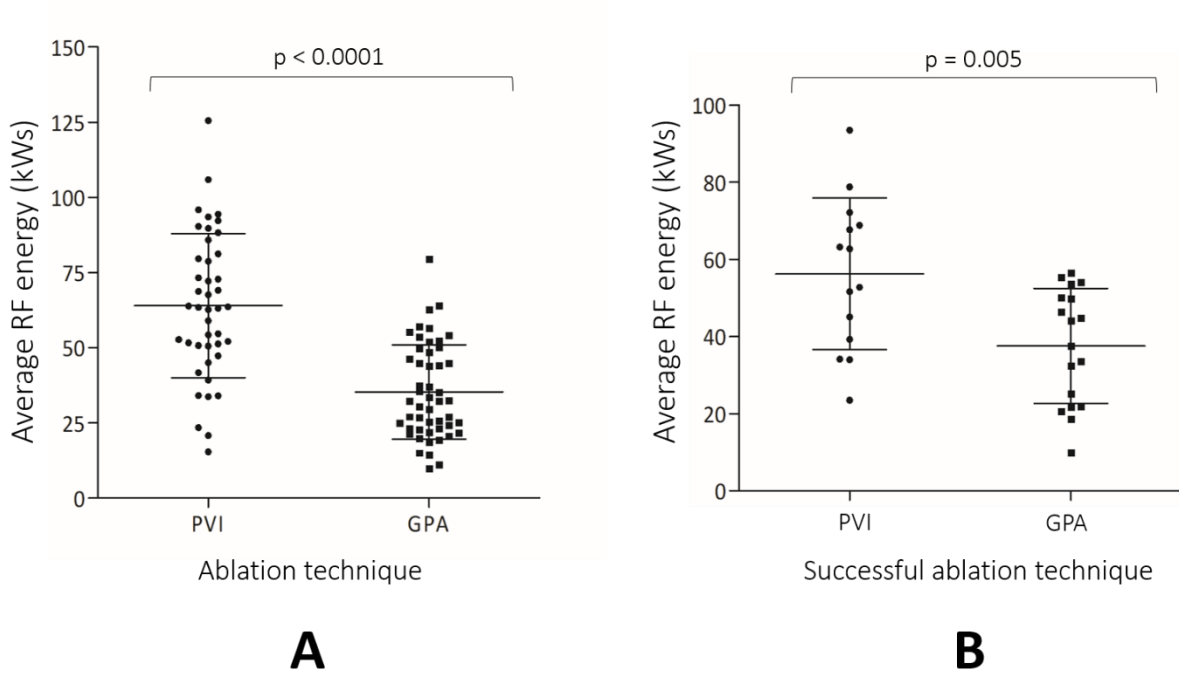

Figure 5.7 Average radiofrequency energy used in PVI and GPA

In A, patients randomised to PVI had average 64.1 kWs ± 24.0 and in GPA, 35.3 kWs ± 15.7 (p < 0.0001) RF energy.

In B, only successful PVI and GPA are shown. The average RF energy used in successful PVI was 56.2 kWs ± 19.7 and in successful GPA, 37.5 kWs ± 14.9 (p = 0.005).

The long bar in the middle of the plots represent mean, and the upper and lower bars represent the standard deviation.

(GPA = ganglionated plexus ablation; PVI = pulmonary vein isolation; RF = radiofrequency)

Within PVI procedures, the average RF energy used in successful PVI was 56.2 kWs ± 19.7, and in unsuccessful PVI 68.9 kWs ± 26.8 (p = 0.16). Within GPA procedures, the average RF energy used in successful GPA was 37.5 kWs ± 14.9 compared to 30 kWs ± 13.0 in unsuccessful GPA (p = 0.15) (Figure 5.8).

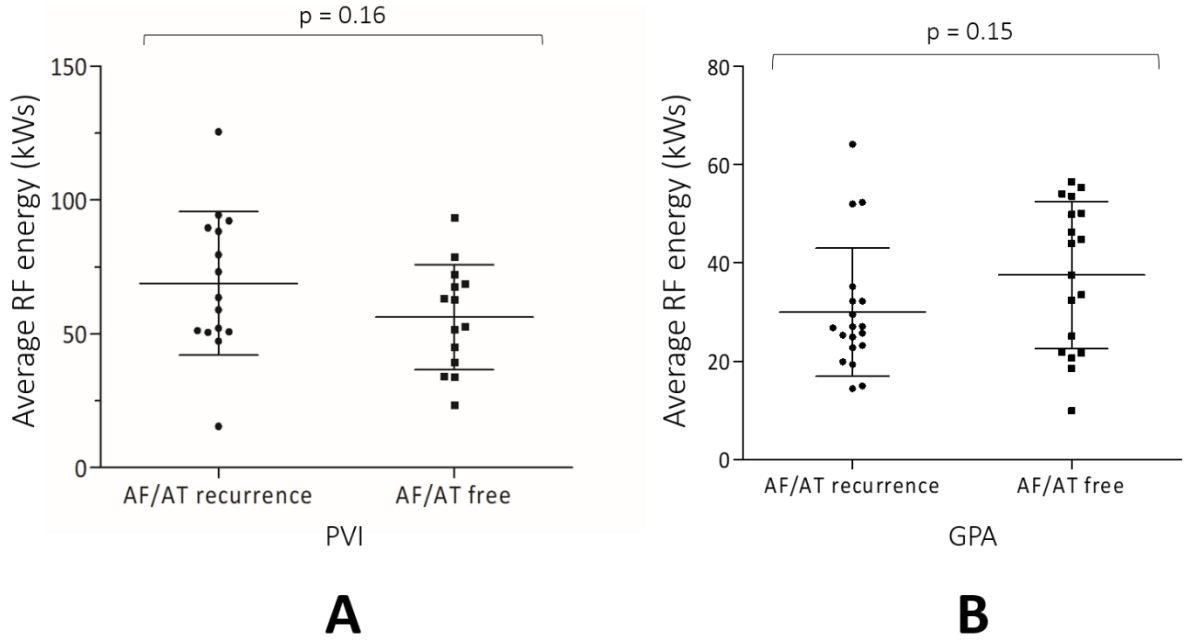

Figure 5.8 The average RF energy used in successful and unsuccessful PVI and GPA

In A, comparison between successful and unsuccessful PVI procedures and average RF energy used are shown. Unsuccessful PVI procedures had average 68.9 kWs ± 26.8 RF compared to successful PVI procedures with average 56.2 kWs ± 19.7 RF energy used per procedure (p = 0.16). Likewise in B, comparison between unsuccessful and successful GPA procedures were made. Unsuccessful GPA had average 30 kWs ± 13.0 compared to successful GPA with 37.5 kWs ± 14.9 (p = 0.15).

(GPA = ganglionated plexus ablation; PVI = pulmonary vein isolation; RF = radiofrequency)

5.3.3. Follow-up

116 patients in the ITT population were evaluated for primary endpoint. 73 (63%) patients completed 12 months follow-up so far (PVI = 30, GPA = 43). 15/30 (50%) and 21/43 (49%) patients randomised to PVI and GPA respectively, were free from primary endpoint (log rank p = 0.71).

103 patients in the PP population were evaluated for primary endpoint. 67 (65%) patients completed 12 months follow-up so far (PVI = 30, GPA = 37). 15/30 (50%) and 18/37 (49%) patients randomised to PVI and GPA respectively were free from primary endpoint (log rank p = 0.71)(Figure 5.9).

There was no significant difference in outcomes between ITT and PP populations. These are the outcome data at the time of writing the thesis. There is ongoing follow-up of patients.

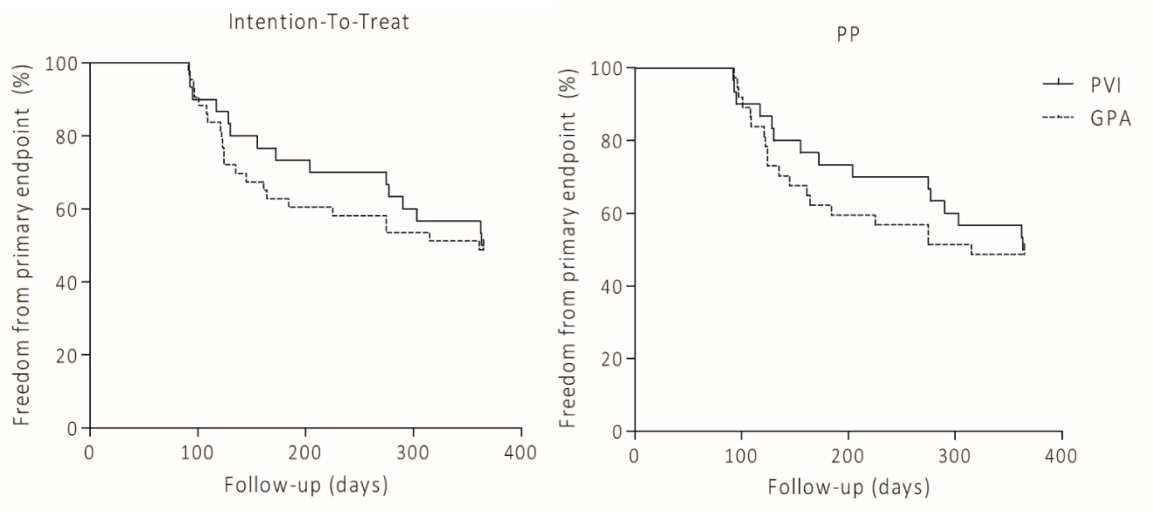

Figure 5.9 Kaplan-Meier curves of freedom from primary end point in the Intention-To-Treat and Per Protocol groups

73/116 (63%) patients completed 12 months follow-up in the Intention-To-Treat group (30 randomised to PVI, 43 randomised to GP ablation). 15 (50%) and 21 (49%) patients randomised to PVI and GPA respectively were free from primary endpoint (log rank p = 0.71)

67/102 (66%) patients completed 12 months follow-up in the Per Protocol group (30 randomised to PVI, 37 randomised to GPA). 15 (50%) and 18 (49%) patients randomised to PVI and GPA respectively were free from primary endpoint (log rank p = 0.71).

(AF = atrial fibrillation; AT = atrial tachycardia; PVI = pulmonary vein isolation; GPA = ganglionated plexus ablation)

Patients who reached primary end point did not get further Holter monitors fitted. Patients who did not reach primary end point had on average 3 ± 1 48hr Holter monitors fitted per patient. There was no significant difference in the average number of Holter monitors between PVI and GPA groups (p = 0.74).

12 patients had additional ECGs to Holter monitors, including: 9 patients with AliveCor ECG recorders, 3 patients with permanent pacemaker device and 1 patient with an implanted loop recorder. 4 (33%) of these patients had PVI and 8 (67%) patients had GPA (p = 0.36).

5.3.4. Repeat procedures

67 patients in the PP population completed 12 months follow-up (PVI = 30, GPA = 37). 10/30 (33%) who had PVI and 13/37 (35%) who had GPA underwent repeat AF ablations (n=24). All 13 (100%) patients from GPA had PVI (including further GPA if any GP recovered from previously ablated sites) without any additional AT ablations. However, 5/10 (50%) patients from PVI required PVI and/or AT ablation. This difference in repeat ablation strategies was statistically significant (p=0.0075). Further repeat ablation details are shown in Table 5.3.

One patient randomised to PVI had repeat PVI and AT ablation at their 2nd ablation and had further recurrence of persistent AF and AT requiring a 3rd AF and AT ablation (575 days post index procedure). No other patients required more than one repeat AF ablation so far. Time between patients' first randomised ablations and their repeat ablations ranged from 182 days to 673 days.

Table 5.3 Repeat ablation type for all patients

Type of redo ablation	PVI (n=10)	GPA (n=13)
PVI only*	5 (50)	13 (100)
PVI and/or AT ablation	5 (50)	0 (0)
PVI + CTI line	2	0
PVI + left AT ablation	1	0
PVI + CTI + left AT ablation	1	0
Left AT ablation only	1	0

Values are n (%). * GPA group had previously ablated GP re-mapped with HFS and further ablated if any recovered, in addition to PVI. PVI group did not receive any GP ablation.

(AT = atrial tachycardia; CTI = cavotricuspid isthmus line; GPA = ganglionated plexus ablation; PVI = pulmonary vein isolation)

5.3.5. Successful GP Ablation Cases

An example of a successful ET-GP ablation with clear AF burden reduction is shown in Figure 5.10. This patient was an 85yrs old male with hypertension, non-flow limiting mild to moderate mid left anterior descending coronary artery disease, a permanent pacemaker device implanted with minimal ventricular pacing, good left ventricular systolic function and 2.6cm left atrial diameter. The patient previously had multiple repeated admissions to hospital with AF symptoms.

He was randomised to GPA and synchronised HFS map was performed globally around the left atrium. 135 sites were tested, which identified 13 (10%) ET-GP. Discrete clusters were present in the carinal portion of the left sided PVs, septum, mid-line of the posterior wall and the anterior wall. Some ET-GP triggered sustained atrial tachycardia, which was acutely terminated with ET-GP ablation. All ET-GP were ablated and re-tested with synchronised HFS afterwards, which did not trigger further AF/AT/atrial ectopy.

The patient was followed-up for 12 months with multiple 48hr Holter monitors and the pacemaker device interrogated, which identified brief AF/AT episodes within the 3-month blanking period post ET-GP ablation, but no other significant arrhythmia since. The patient reported improvement in symptoms and was not hospitalised again. This ET-GP ablation without PVI led to clear reduction in AF burden as evidenced by continuous ECG monitoring and significant symptom improvement.

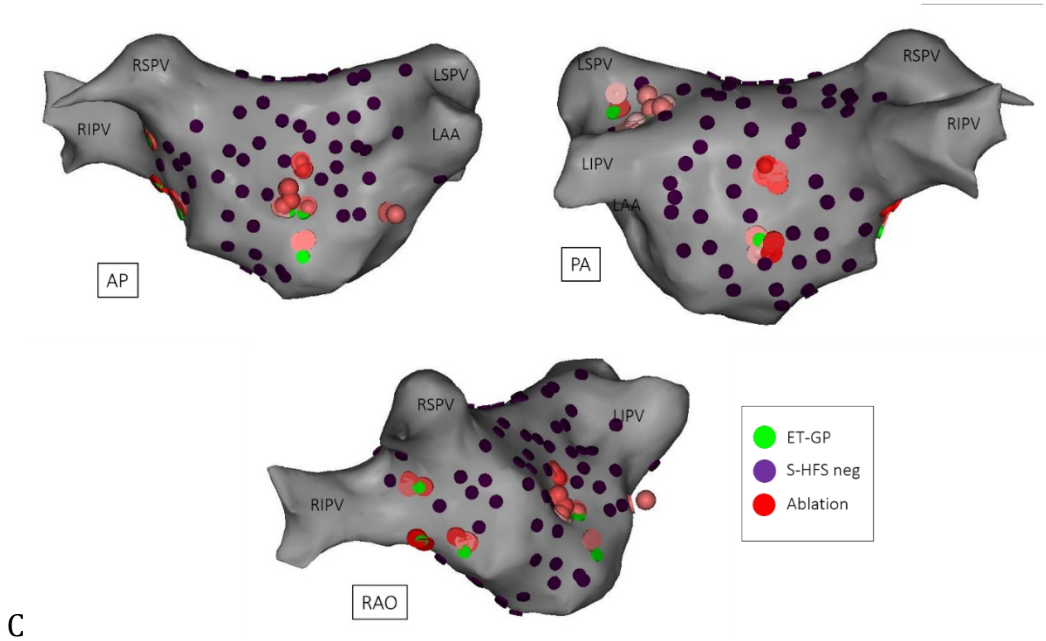

C

Figure 5.10 Successful ET-GP ablation without AF/AT recurrence after 12 months follow-up

This patient was randomised to GPA and synchronised HFS map was performed globally around the left atrium. We tested 135 sites, which identified 13 (10%) ET-GP. Discrete clusters were present in the carinal portion of the left sided PVs, septum, mid-line of the posterior wall and the anterior wall. Some ET-GP triggered sustained atrial tachycardia, which was acutely terminated with ET-GP ablation. All ET-GP were ablated and re-tested with synchronised HFS afterwards, which did not trigger further AF/AT/atrial ectopy.

This patient had a permanent pacemaker device implanted prior to the ablation. The patient was hospitalised over 8 times prior to the ablation with symptomatic AF. There were brief x2 AF/AT episodes within the 3-month blanking period post ET-GP ablation, but there was no other significant arrhythmia post-blanking period for 12 months. The patient also had follow-up with multiple 48hr Holter monitors which identified no arrhythmia, and the patient reported symptomatic improvement since the ablation.

(AP = anterior posterior; ET-GP = ectopy triggering ganglionated plexus; LAA = left atrial appendage; PA = posterior anterior; PV = pulmonary vein; S-HFS = synchronised high frequency stimulation)

An example of a successful AVD-GP ablation is shown in Figure 5.11. This patient was a 73yrs old lady with paroxysmal AF and hypertension. She had good left ventricular systolic function and 2.7cm left atrial diameter. She took regular flecainide to control her symptoms prior to the ablation. On the day of the ablation, the patient was in sinus rhythm but triggered sustained AF with minimal catheter movement or normal pacing. Despite multiple electrical cardioversions, she was unable to maintain sinus rhythm for more than few seconds. Synchronised HFS could not be performed, so continuous HFS was used to map for AVD-GP in AF. 65 HFS sites were tested in total, identifying 4 AVD-GP, which produced significant RR prolongation with HFS. These AVD-GP were in a discrete cluster on the floor of the left atrium and one on the septum.

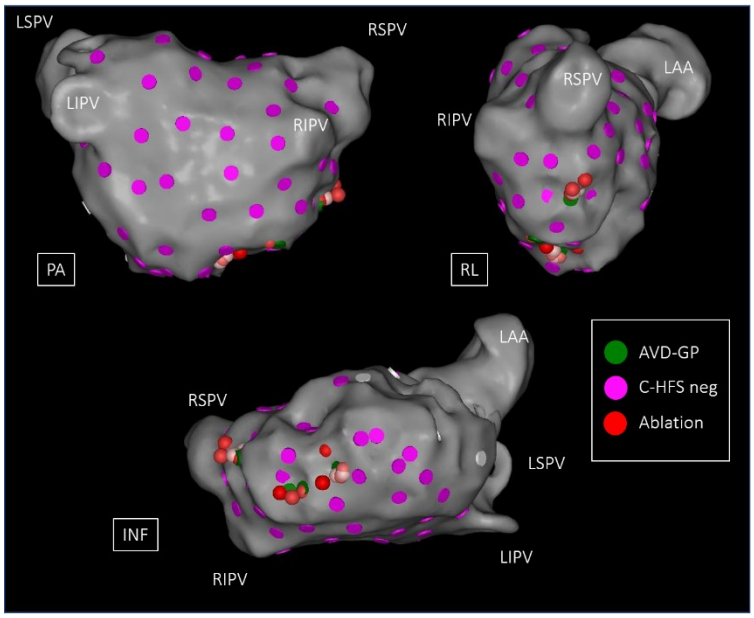

Figure 5.11. AVD-GP locations of a patient with no AF/AT recurrence

The pink dots represent negative continuous HFS test sites, dark green are AVD-GP that caused significant RR prolongation with continuous HFS, and red dots are radiofrequency ablation lesions. We tested 65 HFS sites and ablated 4 AVD-GP only. These AVD-GP were discretely located in the floor of the left atrium and along the septal region. The pulmonary veins were left electrically connected.

(AVD-GP = atrioventricular dissociating ganglionated plexus; C-HFS = continuous HFS; INF = inferior; LL = left lateral; PA = posterior anterior)

All AVD-GP were ablated, and the pulmonary veins were left electrically connected. After electrically cardioverting the patient back to sinus rhythm, all ablated AVD-GP were re-tested with continuous HFS. At 2 sites, AF/AT from rapid atrial capture during continuous HFS did not sustain after cessation of HFS (Figure 5.12). 2 other AVD-GP site triggered

sustained AF with continuous HFS, but self-terminated within 1min 30secs. There was no RR prolongation any longer at AVD-GP sites. Multiple 48hr Holter monitors since ablation have not shown any recurrence of AF/AT and the patient has been symptom free.

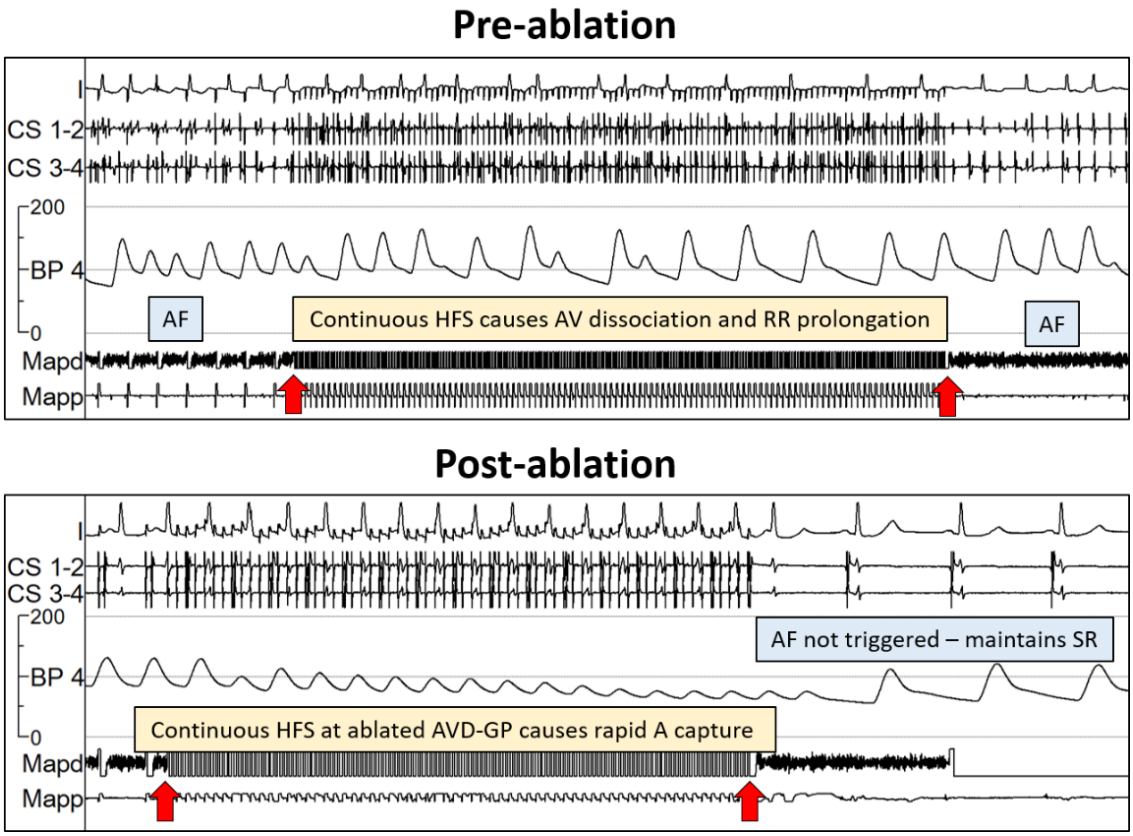

Figure 5.12 Non-inducible AF with rapid atrial pacing after AVD-GP ablation

This is the same patient as in Figure 5.11. The top trace "Pre-ablation" shows continuous HFS at an AVD-GP site, which causes significant RR prolongation due to AV dissociation. AF continues during and after continuous HFS. The red arrows indicate start and stop of HFS.

The bottom trace "Post-ablation" shows repeat of continuous HFS after ablation of the AVD-GP site from the "Pre-ablation" trace. Continuous HFS is performed during SR, which rapidly captures the atrium with HFS, but does not sustain AF/AT after stopping HFS. The red arrows indicate start and stop of HFS.

This patient had no recurrence of AF/AT after 12 months follow-up with multiple 48hr Holter monitors and reported symptomatic improvement since the ablation.

(AVD-GP = atrioventricular dissociating ganglionated plexus; HFS = high frequency stimulation)

5.3.6. Determinants of AF/AT Recurrence

Univariate and multivariate regression analysis was performed on all patients who completed 12 months follow-up on AF recurrence (Table 5.4). Patients aged 64yrs and older had over two times the risk of developing AF recurrence (HR 2.01 [CI 1.03-3.94]; p = 0.04). Interestingly, patients with a history of hypertension were less likely to develop AF recurrence (HR 0.4 [CI 0.22-0.90]; p = 0.02).

Univariate	HR	95% CI	P Value
Age			
≥ 64 yrs	2.01	[1.02 – 3.94]	0.04
< 64 yrs	0.50	[0.25 – 0.98]	0.04
Sex			
Male	0.95	[0.49 – 1.82]	0.87
Female	1.06	[0.55 – 2.04]	0.87
HTN			
Yes	0.44	[0.22 – 0.90]	0.02
No	2.25	[1.11 – 4.57]	0.02
CHA2DS2-VASC score			
0	0.86	[0.36 – 2.05]	0.73
1	0.74	[0.37 – 1.46]	0.38
2	1.60	[0.67 – 3.85]	0.29
≥ 3	1.22	[0.61 – 2.43]	0.57
GP ablation			
Yes	1.13	[0.59 – 2.18]	0.72
No	0.89	[0.46 – 1.71]	0.72
Left atrial size			
≥ 4.0 cm	0.82	[0.39 – 1.76]	0.62
< 4.0 cm	1.21	[0.57 – 2.58]	0.62
Total RF energy application			
≥ 49 kWs	0.85	[0.45 – 1.62]	0.62
< 49 kWs	1.18	[0.62 – 2.25]	0.62
Presence of autonomic triggers			
Yes	1.16	[0.51 – 2.66]	0.72
No	0.86	[0.38 – 1.96]	0.72

Multivariate	HR	95% CI	P Value
Age (≥ 64 yrs)	1.95	[0.86 – 4.41]	0.11
HTN	0.28	[0.12 – 0.68]	0.005
Left atrial size (≥ 4.0 cm)	1.13	[0.52 – 2.45]	0.76

Table 5.4 Univariate and multivariate regression analysis on AF recurrence

In the univariate analysis, patients aged 64yrs and older had over two times the risk of developing AF recurrence (HR 2.01 [CI 1.03-3.94]; p = 0.04). Patients with a history of hypertension were less likely to develop AF recurrence (HR 0.4 [CI 0.22-0.90]; p = 0.02). No other variable significantly impacted AF recurrence.

Age, hypertension and left atrial size as one of the most common risk factors for AF were entered into the multivariate regression analysis, which showed that patients with history of hypertension was the only independent factor that significantly reduced the risk of AF recurrence (HR 0.28 [CI 0.12-0.68]; p = 0.005).

(GP = ganglionated plexus; HTN = hypertension; RF = radiofrequency)

5.3.7. Adverse events

In the PP population of patients, 2 patients had procedure-related major complications with GPA. 1 patient had cardiac tamponade during ablation requiring pericardiocentesis. The patient was discharged the next day. 1 patient had middle cerebral artery stroke as a result of interrupting anticoagulation a day after ablation. The patient was also found to be in AF on the day of stopping the anticoagulation. This patient had successful thrombolysis and made a full neurological recovery. There were no major complications with PVI ($p = 0.50$).

7 patients with GPA had hospitalisation with symptoms consistent with pericarditis. 1 patient with PVI was hospitalised for pericarditis ($p = 0.02$).

5.4. Discussion

This is the first study to functionally localise and observe the effects of ablating ET-GP, with or without AVD-GP ablation in patients with paroxysmal AF. It is safe and feasible to map for ET-GP, and that GPA provides similar AF freedom to PVI. Similar proportion of patients in each group required repeat AF ablation, but patients with previous GPA required no AT ablation. 50% of patients with previous PVI required AT ablations.

GPA used 1.8 times less ablation energy than PVI per procedure to achieve a similar outcome. However, the average procedure time was 43 minutes longer in the GPA group compared to PVI, likely attributed to time duration for detailed HFS mapping. A larger proportion of ET-GP were identified per patient (20%) compared to AVD-GP (13%) which we mapped previously in a demographically similar cohort of patients (13%)[6] (Chapter 3).

The precise location of GP vary between hearts significantly, as found in this study[5,6,157,184]. The usage of synchronised and continuous HFS enabled the identification of both functional types of GP; ET-GP and AVD-GP. It is known that AVD-GP have discrete anatomical distribution in the left atrium which does not conform to all the anatomical areas that are known to contain GPs[6]. ET-GP were present in different regions to AVD-GP, as discussed in detail in Chapter 4 . ET-GP stimulation produced PV and non-PV ectopy that are reminiscent of typical AF initiation. Therefore, our mapping and ablation was focused on ET-GP as our primary target for GPA. AVD-GP were targeted only if ET-GP could not me mapped with synchronised HFS in sinus rhythm. Although majority of our cases was ET-GP ablation only, some included combination of both ET-GP and AVD-GP ablation, or AVD-GP ablation alone. Long-term success was demonstrated in both ET-GP and AVD-GP ablation.

5.4.1. Catheter Ablation for GP

Two studies have previously performed 'selective' GP ablation in the human left atrium to map for AVD-GP using continuous HFS[105,128]. The larger study of eighty patients[105] limited functional testing to specific regions of the atria thought to contain GPs and tested a small number of sites (average 37 HFS sites) spread across both atria, which yielded approximately 5 AVD-GP per patient. This method of 'selective' GP ablation performed significantly worse than 'anatomical' GP ablation at preventing AF (42.5% vs 77.5%; p=0.02). However, the two studies from the same group showed that 'anatomical' GP ablation alone performed significantly worse at preventing AF than PVI[7,8]. Addition of PVI to anatomical GP ablation produced more promising results, achieving significantly higher success at preventing AF than PVI alone[8,129] (74% vs 56%; p=0.004). This was not a reproducible finding in the thoracoscopic GP ablation in addition to PVI for advanced

AF (AFACT study)[127]. In fact, GP ablation in addition to PVI had significantly higher complication rates than PVI alone, including major bleeding, sinus node dysfunction and pacemaker implantations. 4 patients died after 1 year in the GP ablation group and none in the PVI group (p=0.055). Continuous HFS was used to verify anatomical GP locations, though not all expected GP areas provoked an atrioventricular dissociating response which were ablated regardless. These data suggested the importance of functional HFS mapping for GP, and endocardial catheter ablation as a more favourable approach to epicardial catheter ablation for GP.

5.4.2. Mechanisms of AF Prevention with ET-GP Ablation

The similar success rate in GPA and PVI indicates that ET-GP ablation predominantly prevents PV triggers of AF, via interrupting the neural communication between the ablated nerves and PVs. However, significantly less RF ablation was required in GPA than PVI, which suggests that GPA is a more specific and targeted approach to abolishing PV triggers of AF. Importantly, GPA did not lead to development of any macro or micro re-entry circuits with AT. 50% of patients with PVI returned with AT. AF as the recurring rhythm with GPA suggests several possible mechanisms: (1) regeneration of postganglionic nerves from incomplete epicardial GP damage from endocardial ablation (Chapter 7). (2) Incomplete targeting of all responsible autonomic triggers of AF, including ET-GP, AVD-GP, right atrial GP. (3) Formation of AF promoting substrates with patchy GPA across the left atrium. (4) Non-neurally mediated PV triggers of AF. Whilst (4) may be better targeted by PVI, (1) and (3) may be improved with adjustments to GPA technique, after evaluating power, duration of each lesion, number of lesions at each GP site. Large nests of GP may be "box-isolated" as in the example in Figure 5.5, preventing large amount of ablation and achieving AF freedom.

It would be difficult to address (2) without significant prolongation to procedure time. It is possible to increase the density of HFS testing in the left atrium, but the spacing between each HFS site is already very small, considering the natural catheter movement (5-6mm). Cluster ablation at each ET-GP site also affects a wider region, negating the need for denser mapping between negative HFS sites and adjacent ET-GP. AVD-GP can be mapped with synchronised HFS, which sometimes co-locate with ET-GP (Chapter 4). However, the short duration of HFS trains with synchronised HFS may not be enough stimulation to cross the threshold for AVD-GP to produce significant RR prolongation. Therefore, the most reliable way of mapping for AVD-GP would be with continuous HFS, and this may be restricted to the high probability distribution regions of AVD-GP[6] (Chapter 3). An alternative way of targeting all AVD-GP without significantly prolonging HFS mapping time, is to empirically ablate the right inferior GP; the "common gateway" to all AVD-GP. This is situated inferiorly to the right inferior PV[170,173]. Right atrial GP were not mapped in this study, but are known to be present from topological studies[5,157]. The functional characteristics of right atrial GP are not known but may be mapped using the same technique as in the left atrium with synchronised and continuous HFS.

PVI inadvertently ablates many ET-GP that are densely clustered around the pulmonary veins and the roof, and also targets the right inferior PV, the common gateway to all AVD-GP. In addition, electrical isolation of PVs prevents any PV trigger to exit and cause AF. PVI is effectively a double barrier for AF. However, PV reconnection occurs over time, and not all PV ectopy triggering GP lie within circumferential PVI line. This also includes non-PV triggering GP which may not be affected at all by PVI.

Combination of both PVI and GPA as single or separate procedures may target autonomic triggers of AF medial and lateral to PVI lines, including PV and non-PV triggers which may improve AF freedom.

5.4.3. Adverse Effects of GP Ablation

There was no significant difference between PVI and GPA in major complications, but GPA had significantly larger number of patients presenting with symptoms consistent with pericarditis. This is despite the significantly smaller average RF energy used in GPA compared to PVI, which suggests that it is the anatomical location and concentration of GPA in the left atrium that predisposes patients to pericarditis. Overall, the patients who had pericarditis with GPA had the mid-anterior portion of the left atrium ablated whereas PVI patients avoided this region. However, myopercarditis is a common phenomenon post ablation, and does not usually cause significant complications long-term.

5.4.4. Variables that Predict AF Recurrence

Hypertension and AF often co-exists, and is regarded as one of the main risk factors in developing AF[185]. Despite the well-known association between hypertension and AF, several pathogenetic mechanisms underlying the higher risk of AF in hypertensive patients are still incompletely understood[186]. However, despite these strong correlations, our multivariable regression analysis demonstrated that the history of hypertension in our patients was an independent variable that predicted favourable outcomes for AF prevention, regardless of the ablation technique. Patients diagnosed with hypertension and AF were often on treatment to control their blood pressures, with normal mean left atrial size (3.9cm). This indicates that the patients were on appropriate treatment to prevent progressive hypertensive atrial disease that can lead to AF. However, this still

does not explain why treated hypertension should confer better AF prevention compared to those without a history of hypertension at all.

Older age (median age 64yrs or older) was a significant variable that predicted AF recurrence in the univariate analysis, but not in the multivariate regression analysis, when left atrial size and hypertension were factored into the analysis.

5.4.5. Limitations

Patients mapped with continuous HFS to identify AVD-GP had repeatedly sustained AF despite multiple cardioversions. This suggests that they were a subgroup of higher risk cohort that may have influenced the outcome of GPA.

Reproducibility of atrial ectopy triggered by ET-GP was demonstrated with HFS programmed to deliver within the local atrial refractory period, but this does not completely exclude the possibility of mechanical irritation from the catheter.

Electrical connection of PVs in the GPA group was not routinely checked at the end of every procedure. As a lot of GPs were clustered around PVs and the roof, their ablation may have led to inadvertent isolation of PVs. Similarly, PVI inadvertently ablates GP, but GP were not checked routinely in the PVI group.

The threshold for triggering PV ectopy and AF may be affected by general anaesthetic, although we avoided using any adrenergic or cholinergic suppressing anaesthetic agents. Identification of GP under general anaesthetic may be an underestimation of the total autonomic input that is relevant to the patient's clinical AF.

5.5. Conclusion

It is feasible to perform a global functional mapping and ablation of ET-GP to prevent AF. This provides direct evidence that ET-GP are part of the AF mechanism. Freedom from AF/AF with PVI and GPA was similar, but GPA required 1.8 times less ablation than PVI. This indicates that GPA is a more specific target in the mechanism of AF. These results justify further investigation of the role of ET-GP in AF pathophysiology.

6. PVI IN ADDITION TO GP ABLATION: A FEASIBILITY STUDY (ADD-GP)

6.1. Introduction

Out of all autonomic modulation studies via endocardial catheter ablation in paroxysmal atrial fibrillation (AF), "anatomical" ganglionated plexus (GP) ablation in addition to pulmonary vein isolation (PVI) has demonstrated the most benefit when compared to PVI alone[129,130]. Katrisis *et al*[8] conducted the largest randomised controlled trial in this domain. They studied 82 patients randomised to anatomical GP ablation in addition to PVI, and 78 patients randomised to PVI alone. Location of the anatomical sites of GP were identified based on the "4 major left atrial GP" as described by Po *et al*[88]. These included 1) superior left GP: on the roof of the left atrium, medial to left superior pulmonary vein (PV) and extending to the medial aspect of left atrial appendage. 2) Anterior right GP: anterior to the right superior PV and extends inferiorly to the region anterior to the right inferior PV. 3) Inferior left GP: inferior aspect of the posterior wall, 1-3cm below the left inferior pulmonary vein. 4) Inferior right GP: inferior aspect of the posterior wall, 1–3 cm below the right inferior pulmonary vein. The justification of adding PVI to anatomical GP ablation was from their previous data, which showed that anatomical GP ablation alone does not prevent AF more than PVI at 12-month follow-up[7], but adding PVI to anatomical GP ablation conferred a significant benefit (PVI = 45.5% vs PVI+GP = 73.5%; log rank p = 0.02)[131]. However, the anatomical GP sites as in Figure 1.16 in Chapter 1 are largely extensions of the PVI line, and this may have provided more durable PVI as the mechanism of achieving AF freedom, rather than autonomic modulation itself.

In Chapter 6, we saw that there was no statistically significant difference between selective ectopy-triggering GP (ET-GP) ablation compared to PVI alone. We concluded that perhaps not all GP responsible for PV or non-PV ectopy triggering AF were identified, leading to AF in this group of patients. We hypothesised that elimination of possible unidentified PV triggers to AF with PVI, in addition to selective ET-GP ablation that targets both PV and non-PV triggers may confer improved success in AF freedom, compared to PVI alone.

6.2. Methods

This was a prospective, single-centre, randomised, single-blinded, feasibility study. Recruitment period was between May 2017 to May 2019. All patients gave written informed consent and the study was approved by the Local Research Ethics Committee. Patients with symptomatic, drug-refractory paroxysmal AF, who had previous PVI (cryoballoon or radiofrequency ablation) indicated for repeat ablation were recruited to the study. The inclusion and exclusion criteria are shown in Table 6.1.

Table 6.1 Inclusion and exclusion criteria

Inclusion criteria	Exclusion criteria
• Males or females from 18 to 85yrs old • Paroxysmal atrial fibrillation • One or more previous pulmonary vein isolation procedures • Previous left sided atrial ablations other than pulmonary vein isolation • Off amiodarone for at least 60 days • Suitable candidate for catheter ablation • Signed informed consent	• Contraindication to catheter ablation • Previous surgical AF ablation • Contraindication for general anaesthetic • Presence of a left ventricular thrombus • Valvular disease that is grade moderate or greater • Any form of cardiomyopathy • Severe cerebrovascular disease • Active gastrointestinal bleeding • Serum Creatinine >200umol/L or on dialysis or at risk of requiring dialysis • Active infection or fever • Life expectancy shorter than the duration of the trial • Allergy to contrast • Moderate to severe heart failure and/or NYHA Class III-IV • Bleeding or clotting disorders or inability to receive heparin • Uncontrolled diabetes (HbA1c ≥73mmol/mol or HbA1c ≤64mmol/mol and Fasting Blood Glucose ≥9.2mmol/L) • Malignancy needing therapy • Pregnancy or women of childbearing potential not using a highly effective method of contraception • Unable to give informed consent or has insufficient comprehension

6.2.1. Randomisation

Patients were randomised to PVI or PVI in addition to GP ablation (ADD-GP). Randomisation was performed using the 'sealed envelope' approach in blocks. Patients were initially randomised 2:1 for ADD-GP in the first consecutive twenty patients recruited in anticipation for high-rate of cross-over from the GP ablation group as in the

prior feasibility study. Afterwards, we switched to 1:1 randomisation for the remainder of the recruitment period. Patients and their cardiologists providing their usual care were blinded to their randomisation. Operators on the day of the ablation, the data collector and the data analyst were unblinded to randomisation.

6.2.2. Protocol for All Patients

All patients received general anaesthesia. Warfarin was stopped for one to two days, or continued, depending on the INR within seven days before the ablation. All novel oral anticoagulants were stopped the evening before the ablation. Details of the peri-operative investigations, usage of the 3D electroanatomic mapping system, intracardiac electrogram recording system, and transseptal puncture method are the same as in the Methods section of Chapter 2.

All patients except for the first patient had paced bipolar voltage mapping during sinus rhythm and 3D electroanatomic mapping of the left atrium. If patients were in AF, they were electrically cardioverted once to attempt mapping in sinus rhythm. If AF returned, a bipolar voltage map was not collected.

Total duration of procedure was defined as time from transseptal to heparin reversal with protamine and included additional ablations such as cavotricuspid isthmus line ablation, roof line, mitral line ablations. Patients randomised to PVI only had additional left atrial ablations if the operators thought it was clinically relevant for their intraprocedural arrhythmia (e.g. roof-dependent or mitral isthmus dependent AT). In the ADD-GP group, additional left atrial ablations were avoided. Following ablation, patients stayed overnight and were discharged in the morning if well.

6.2.3. High Frequency Stimulation Mapping Protocol

All patients in both randomised groups underwent high frequency stimulation (HFS) mapping globally around their left atrium before and after PVI, to evaluate the number and anatomical locations of GP prior to PVI, and assess how PVI affects the GPs, and what proportion of these were non-PV triggers. HFS mapping in PVI patients was incorporated after the second patient was recruited to the study. Mapping was performed globally around the left atrium with HFS prior to PVI. However, post-PVI HFS mapping was not mandated, due to time-constraints. Post-PVI HFS mapping was restricted to anatomical regions where GPs were identified pre-PVI.

If patients developed incessant AF with synchronised HFS, they followed the "Incessant AF Protocol" as detailed in Chapter 2 for HFS mapping.

6.2.4. Ganglionated Plexus Ablation Protocol

This protocol was performed as detailed under the Methods section in Chapter 2. However, GP ablations were only performed after PVI and after GPs pre-PVI were re-mapped with HFS. New CARTO™ Tags were allocated to pre-PVI GP sites and labelled according to response to HFS (e.g. "post-PVI ET-GP still positive").

6.2.5. Pulmonary Vein Isolation Protocol

PVs that had re-connected from previous procedure were noted at the start of the procedure. Then, PVI was performed only after completing a global left atrial map with HFS to identify GPs. Depending on the number and magnitude of re-connected sleeves in PVs, a full circumferential PVI (CPVI) or a touch-up radiofrequency (RF) ablation was performed until all PVs were isolated. The ablation method, placement of catheters and confirming isolation of PVs are as detailed under the Methods section in Chapter 2.

6.2.6. Repeat AF Ablation Protocol

If patients returned with recurrence of AF since the study procedure, all had previously mapped GPs re-mapped with HFS whether or not they were ablated as part of their study randomisation. However, only the patients who were randomised to the ADD-GP group received additional ablations on the GPs if they had recovered. Any additional lines of ablations were left to the operator's discretion.

6.2.7. Clinical Follow-Up

Patients were followed up for 12 months, with 3, 6, 9, 12-month 48hr Holter monitors as detailed under the Methods section of Chapter 2.

6.2.8. Definitions for End-Point

The primary endpoint was any documented atrial arrhythmia (AF, atrial tachycardia, atrial flutter) >30s consecutively recorded on a Holter monitor or 12 lead ECG after a 90-day blanking period.

The secondary endpoints included repeat ablation for AF/atrial tachycardia (AT)/atrial flutter after a 90-day blanking period, mortality, any complications related to the procedure (bleeding, thrombosis, phrenic nerve palsy, cardiac tamponade) requiring intervention.

6.2.9. Statistics

Statistical analysis was performed using GraphPad 5 (Prism, San Diego, California) and SPSS v25.0 (SPSS Inc., Chicago, IL). Continuous variables were expressed as mean ± SD. Categorical variables were expressed as numbers and percentages. D'Agostino & Pearson omnibus and Shapiro-Wilk tests were performed to assess normality of continuous

variables prior to comparison of means tests. Mann-Whitney *U* test, Fisher's exact test and unpaired t-test were used for comparison of means. An event-free survival was estimated using a Kaplan-Meier curve for the primary endpoint. Clinical parameters associated with AF recurrence and other procedural parameters were studied using univariate and stepwise multivariate analysis in a Cox regression model. All variables with p values ≤0.10 in univariate analysis and three well-established risk factors for AF recurrence (age, sex, hypertension) were entered into the multivariate regression analysis. A p value <0.05 indicated statistical significance.

6.3. Results

45 patients were recruited to the study. 44 were randomised to PVI (n = 18) or ADD-GP ablation (n = 26). 16 in the PVI group and 23 in the ADD-GP group completed ablation as per protocol (Figure 6.1).

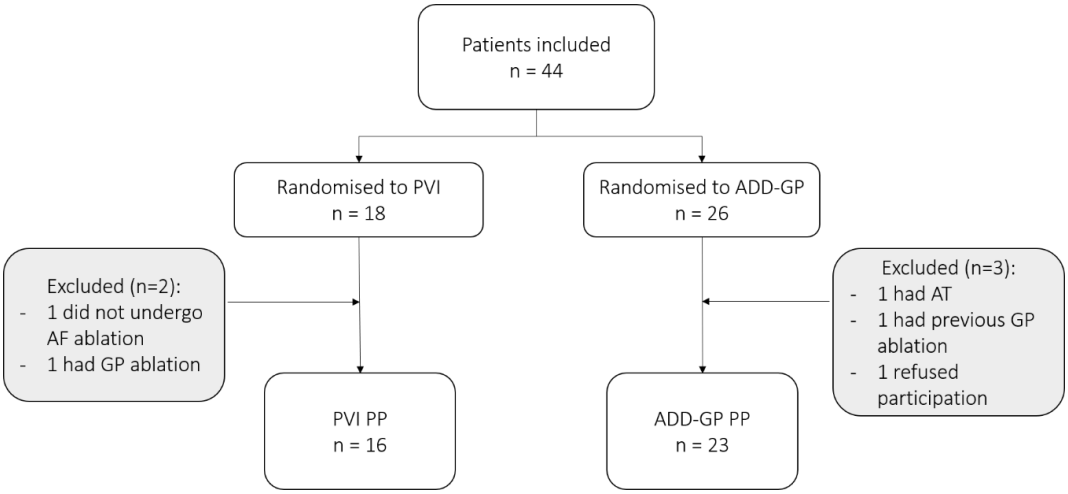

Figure 6.1 ADD-GP study flowchart

Flowchart of the ADD-GP study from recruitment to completion of research protocol.
(ADD-GP = PVI in addition to ganglionated plexus ablation; AT = atrial tachycardia; AF = atrial fibrillation; GP = ganglionated plexus; PVI = pulmonary vein isolation)

Patients were 64 ± 8yrs old and 30 (68%) were male. The baseline demographics of patients are in Table 6.2.

Table 6.2 Demographics of patients in the ADD-GP study

Demographics	All (n=44)	PVI (n=18)	ADD-GP (n=26)	p Value
Age (yrs)	64 ± 8	64 ± 9	63 ± 10	0.81
Male (%)	30 (68)	8 (44)	22 (85)	0.008
No. of previous PVI procedures	1.3 ± 0.6	1.1 ± 0.3	1.4 ± 0.7	0.08
≥2 PVI	11 (25)	2 (11)	9 (35)	0.15
Duration between the most recent PVI and this study procedure (yrs)	4.2 ± 3.2	4.6 ± 3.7	4.0 ± 3.0	0.96
CTI line	9 (20)	2 (11)	7 (27)	0.26
Left sided AT ablations	7 (16)	0 (0)	7 (27)	0.03
No. of bipolar voltage points ≤0.15mV : total no. of bipolar voltage points (%)*	39.9 ± 14.8	38.9 ± 15.8	41.2 ± 14.9	0.70
AF/AT before or after GA induction	11 (25)	4 (22)	7 (27)	1.00
No. of PVs re-connected at start of procedure	2.2 ± 2.1	2.7 ± 1.1	1.8 ± 1.2	0.02
All PVs re-connected	10 (23)	6 (33)	4 (15)	0.27
All PVs isolated	4 (11)	0 (0)	4 (15)	0.13
No. of cardioversions	2.9 ± 2.3	3.4 ± 2.1	2.5 ± 2.4	0.27
LA diameter (cm)	3.8 ± 0.5	3.6 ± 0.5	3.9 ± 0.5	0.28
LV ejection fraction (%)	57.5 ± 7.1	59.3 ± 4.3	56.2 ± 7.1	0.06
BMI (kg/m^2)	27.8 ± 5.3	28.6 ± 7.6	27.3 ± 3.0	0.87
Hypertension	9 (21%)	3 (18%)	6 (33%)	0.71
Stroke/TIA	3 (7%)	2 (11%)	1 (4%)	0.56
Diabetes	1 (2%)	1 (6%)	0 (0%)	0.41
CHA2DS2-VASC score				
0	12 (27%)	3 (17%)	9 (35%)	0.30
1	16 (36%)	7 (39%)	9 (35%)	1.00
≥2	14 (32%)	7 (39%)	7 (37%)	0.52
Autonomic symptoms**	9 (21%)	4 (22%)	5 (19%)	1.00

Table values are mean ± STD, n (%).

*From paced bipolar voltage maps of the left atrium at the beginning of procedures before ablations.
**Autonomic symptoms include, vagal/adrenergic triggers of AF such as nocturnal, stress, exertion, postprandial.

(ADD-GP = PVI in addition to GP ablation group; AF = atrial fibrillation; AT = atrial tachycardia; BMI = body mass index; CTI = cavotricuspid isthmus; GP = ganglionated plexus; LA = left atrial; LV = left ventricular; PV = pulmonary vein isolation; PVI = pulmonary vein isolation; TIA = transient ischaemic attack)

6.3.1. Non-PV Ectopy in Patients with Complete PVI

Four patients had no PVs re-connected at the start of their procedures. Therefore, with complete PVI, their AF recurrence was assumed to be due to non-PV triggers. Patients were all randomised to the ADD-GP group.

The first patient had one PVI procedure previously and had weekly AF symptoms prior to repeat ablation. He had 87 HFS sites tested, of which 16 (18%) was with synchronised HFS, and 71 (82%) with continuous HFS. This identified 19 (22%) GPs, 5 of which were non-PV ET-GP, and 14 were AVD-GP. The ET-GP with HFS stimulation triggered sustained AT, which degenerated into incessant AF. Ablation of ET-GP did not terminate AF. Up to three electrical cardioversions were performed as per protocol, however sinus rhythm could not be maintained. Therefore, we mapped the rest of the left atrium with continuous HFS to identify AVD-GP. Most AVD-GP were in the inferior border of the posterior wall, as expected. Several sites produced significant asystole of up to 5.5s. At the start of ablation of AVD-GPs, the patient was in an organised AT with cycle length 198ms. During ablation, this degenerated into AF and organised again to AT periodically, with a slower cycle length of 218ms (20ms slower). After approximately 16 minutes of ablation at multiple AVD-GP, incessant AF terminated to normal sinus rhythm. Interestingly, re-testing ablated AVD-GP with continuous HFS during sinus rhythm triggered AF/AT (from high-output, rapid pacing causing direct myocardial capture), which self-terminated after stopping HFS (Figure 6.2). This inability to re-induce sustained atrial arrhythmia is a phenomenon that we observed in multiple other GP ablation cases, which will be discussed further in Chapter 7.

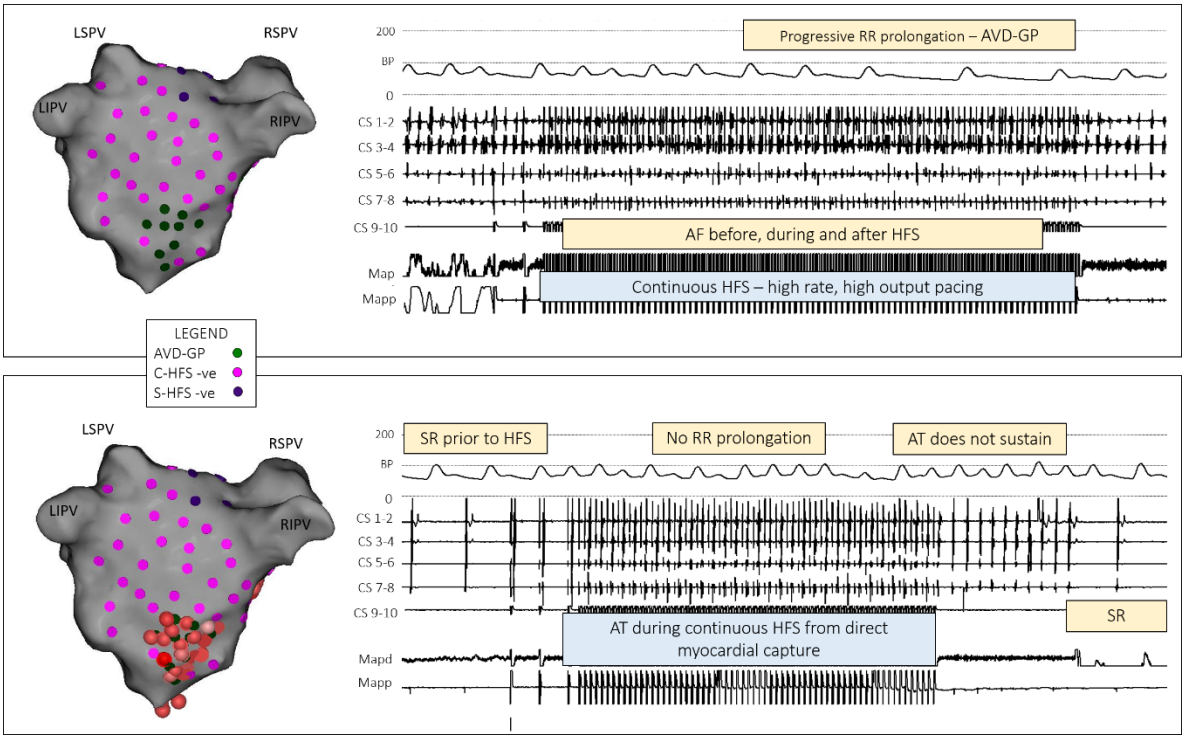

Figure 6.2 Successful AVD-GP ablation leading to acute and long-term freedom from AF

This patient had complete PVI at start of their repeat procedure. AVD-GP (green) were mapped with continuous HFS during AF, in the inferior border of the posterior wall. There was progressive RR prolongation with AV block during HFS at these sites. We ablated all GPs and re-tested the AVD-GP with continuous HFS during sinus rhythm. AF/AT was triggered during continuous HFS due to direct, high-rate/high-output capture of the atrium, but the arrhythmia did not sustain after cessation of HFS.

(AF = atrial fibrillation; AT = atrial tachycardia; AVD-GP = atrioventricular dissociating ganglionated plexus; C-HFS = continuous high frequency stimulation; GP = ganglionated plexus; HFS = high frequency stimulation; LIPV = left inferior pulmonary vein; LSPV = left superior pulmonary vein; RIPV = right inferior pulmonary vein; RSPV = right superior pulmonary vein; S-HFS = synchronised high frequency stimulation; SR = sinus rhythm)

This patient had a brief occurrence of AF documented on his AliveCor ECG monitoring device after 149 days of follow-up, however he was free of AF for another 430 days of follow-up, and symptom free.

The second patient had 51 HFS sites tested (mixture of continuous and synchronised HFS) which identified 7 (14%) ET-GP, and no AVD-GP (Figure 6.3). Some ET-GP triggered a single non-PV ectopy only, and others triggered persistent AF or AT. The patient completed 206 days follow-up so far, with one 48hr Holter monitor, well without symptoms or AF/AT recurrence.

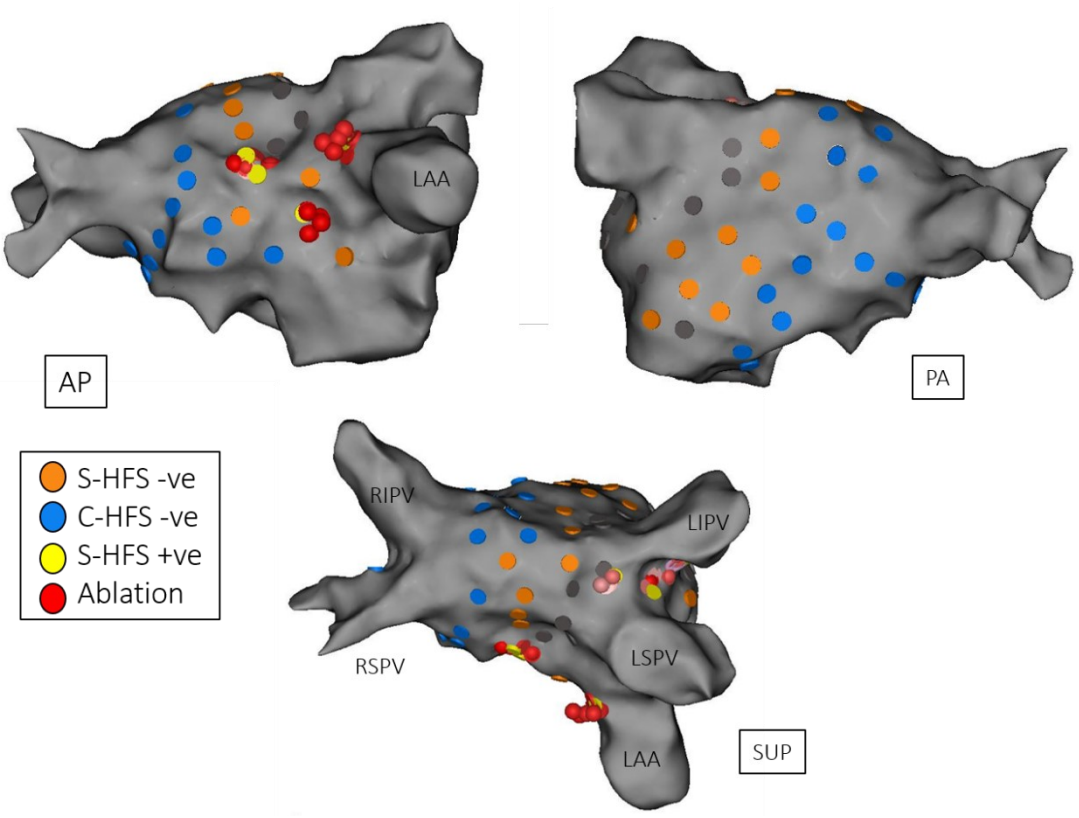

Figure 6.3 Successful ET-GP ablation for non-PV triggers of AF

This patient with previous PVI had persistent complete PVI at start of their repeat procedure. 51 HFS sites were tested, which identified 7 (14%) ET-GP, and no AVD-GP. Some ET-GP triggered a single non-PV ectopy only, and others triggered persistent AF or AT. All ET-GP were ablated, which was primarily in the mid-anterior wall and left side carina. The patient completed 206 days follow-up so far, with one 48hr Holter monitor, well without symptoms or AF/AT recurrence.

(AP = anterior posterior; C-HFS = continuous high frequency stimulation; S-HFS = synchronised high frequency stimulation; LAA = left atrial appendage; LIPV = left inferior pulmonary vein; LSPV = left superior pulmonary vein; RSPV = right super pulmonary vein; RIPV = right inferior pulmonary vein; PA = posterior anterior; SUP = superior)

The third patient had 2 previous PVI procedures in the past. 107 HFS sites were tested, which identified 11 (10%) non-PV ET-GPs. In addition, there were 8 AVD-GP identified with synchronised HFS. There was a variety of responses to synchronised HFS including single repeated ectopy, and AV block followed by AF/AT (Figure 6.4). All ET-GP were targeted, but the patient had documented recurrence of AF after 110 days.

Figure 6.4 Example traces of non-PV ectopy and AF triggered by synchronised HFS, with and without AV block

This patient had all PVs isolated from multiple previous PVI procedures. The left panels show the positions of the catheters on the left atrium, and the right panels show intracardiac electrograms recorded at the time of HFS, with changing Mapd and Lasso PV catheter positions as shown in the left panels. ET-GP = green, negative HFS test = purple, no atrial capture with pacing = grey, AVD-GP without atrial ectopy = blue.

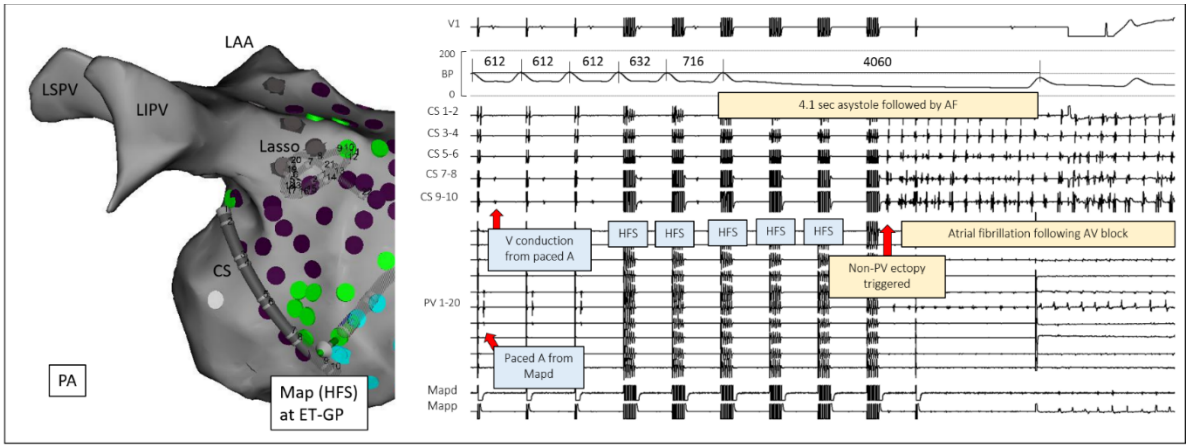

Figure 6.4A. Asystole followed by AF with synchronised HFS

A) Due to stenosed LIPV, the PV catheter was left at the ostium outside the LIPV. HFS was stimulated from the Mapd in mid-inferior posterior wall. There was a progressive prolongation of the RR interval until a sudden significant increase to 4.1s asystole after only two trains of HFS. AF was triggered after the 6th train of HFS, which organised into AT with variable cycle length, then self-terminated after 1 minute.

(AVD-GP = atrioventricular dissociating ganglionated plexus; CS = coronary sinus; ET-GP = ectopy triggering ganglionated plexus; HFS = high frequency stimulation; LAA = left atrial appendage; LIPV = left inferior pulmonary vein; LSPV = left superior pulmonary vein; PV = pulmonary vein; RIPV = right inferior pulmonary vein; RSPV = right superior pulmonary vein;)

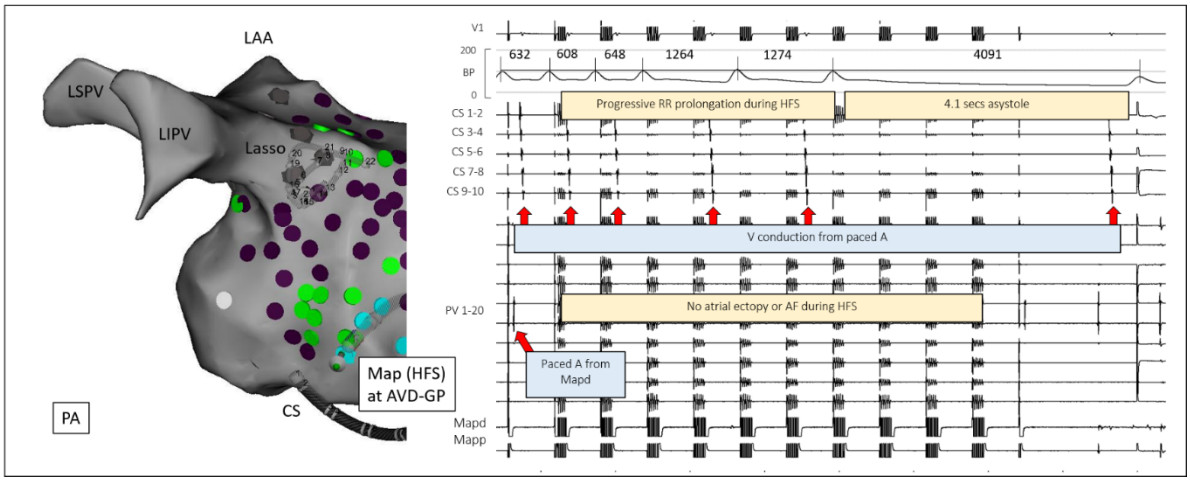

Figure 6.4B Progressive AV block followed by asystole with synchronised HFS

B) Moving the Map catheter only 3-4mm inferiorly to A), synchronised HFS was repeated. This time, there was a more gradual RR prolongation as depicted in the trace. After the 7th train of HFS, 4.1s asystole occurred, however there was no ectopy or AF. The RR prolongation recovered soon after stopping HFS.

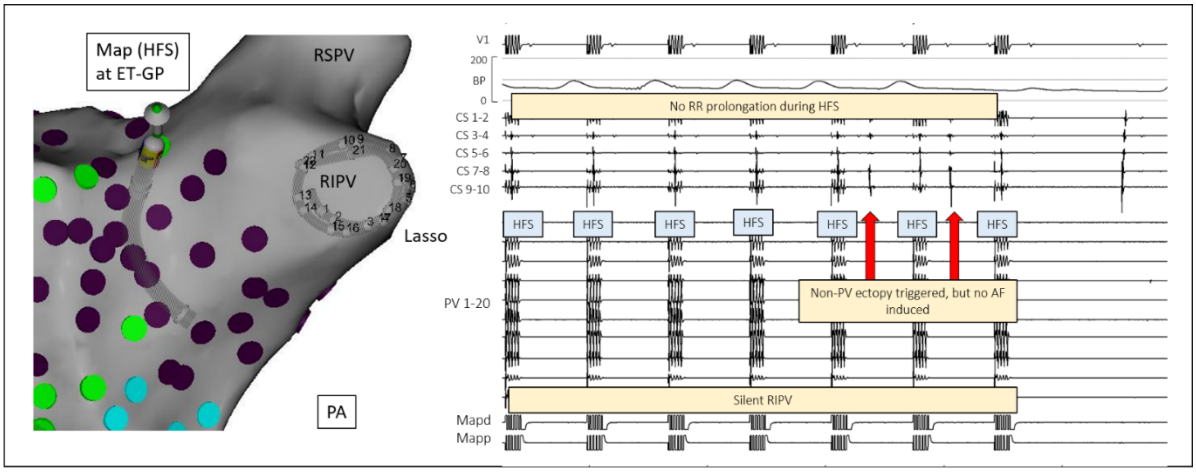

Figure 6.4C Non-PV ectopy without AV block or AF with synchronised HFS

C) The Map catheter was positioned at the ostium of the RIPV in the roof, close to the posterior wall. The PV catheter was moved to the isolated RIPV. HFS at this site did not trigger any RR prolongation as in A) and B), but triggered a single non-PV ectopy after the 9th HFS train (the trace shows HFS starting from the 5th train). The earliest activation was in CS 7-8 which did not induce AF. The RIPV remained silent.

(AVD-GP = atrioventricular dissociating ganglionated plexus; CS = coronary sinus; ET-GP = ectopy triggering ganglionated plexus; HFS = high frequency stimulation; LAA = left atrial appendage; LIPV = left inferior pulmonary vein; LSPV = left superior pulmonary vein; PV = pulmonary vein; RIPV = right inferior pulmonary vein; RSPV = right superior pulmonary vein)

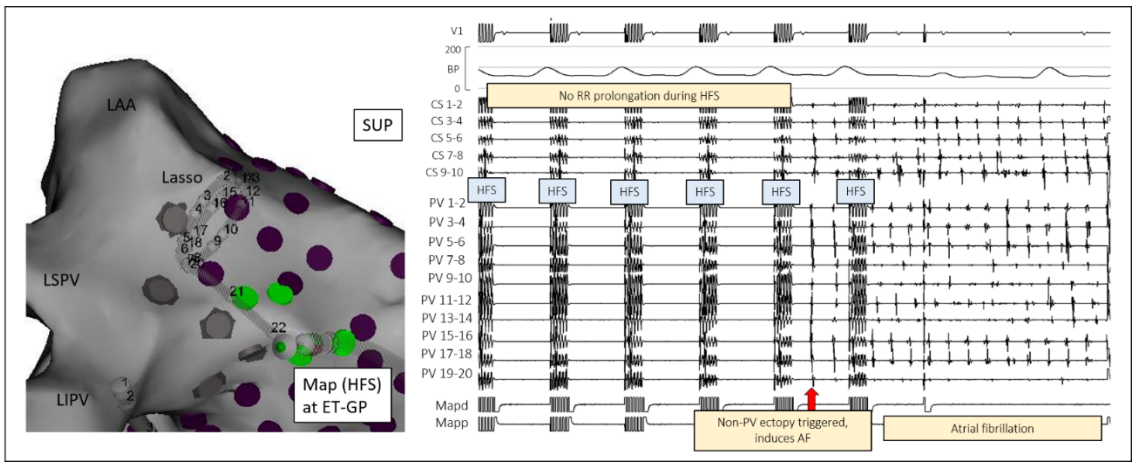

Figure 6.4D Non-PV ectopy and AF without AV block with synchronised HFS

D) The Map catheter was moved to a more medial position in the roof from C). The PV catheter was also moved to the left hand side of the left atrium, outside of the stenosed left PVs. After the fifth HFS train, a non-PV ectopy with the earliest activation in PV 15-16, and in the CS, CS 3-4. The different CS activation pattern made it a different non-PV ectopy from C). This induced AF which self-terminated after 10s.

(CS = coronary sinus; ET-GP = ectopy triggering ganglionated plexus; HFS = high frequency stimulation; LAA = left atrial appendage; LIPV = left inferior pulmonary vein; LSPV = left superior pulmonary vein; PV = pulmonary vein; RIPV = right inferior pulmonary vein; RSPV = right superior pulmonary vein;)

The fourth patient had one previous Cryoballoon PVI with AT that was easily inducible with catheter movement during the procedure. This was a focal AT from the inferior portion of the RIPV region, where there were areas of long, fractionated electrograms. Cluster RF application in this region was performed and AT was no longer inducible. This patient did not undergo HFS mapping and was subsequently withdrawn from the study.

6.3.2. PV Tachycardia with High Frequency Stimulation

In 5 patients (3 randomised to the ADD-GP group, 2 randomised to the PVI group), HFS mapping was performed after re-isolating all PVs. 4 patients demonstrated PV tachycardia (PVT) with exit block, and 1 patient demonstrated PV early depolarisation (PV ectopy) with exit block. 4 patients demonstrated PV early depolarisation/tachycardia

from the left PVs, and 1 patient in the right superior PV (RSPV). The location of GPs that triggered the PV ectopy/tachycardia was generally in the left side of the roof, and in one patient, in the left lateral position. The GP location of the patient with RSPV tachycardia was in the roof, near the RSPV. In 3/4 patients with PVT and exit block, PVT self-terminated shortly after cessation of HFS.

One patient who was randomised to the PVI group had reproducible PV tachycardia that sustained for >20mins, even after cessation of HFS. This patient was a 64yrs old male who had one previous PVI procedure with AF recurrence. After induction with general anaesthesia, the patient was in slow junctional rhythm (35-40bpm). The patient required pacing in the atrium as a result. When pacing stopped, 5.2s pause occurred followed by a sinus beat, then another 3.8s pause, followed by a sinus beat. Then, an atrial ectopy was triggered which degenerated into AF. The patient was cardioverted back to sinus rhythm and when paced, triggered sustained AF again. The patient had two re-connected right-sided PVs, and a decision was made to isolate them first before starting HFS mapping. AF continued after re-isolation of the right-sided PVs. Therefore, he was electrically cardioverted back to sinus rhythm to start HFS mapping. 55 synchronised HFS sites were tested which identified 14 ET-GP (25.5%). With the Lasso PV catheter inserted into the LSPV, HFS in the left side of the roof identified several ET-GP situated in a cluster, that triggered PV tachycardia in the LSPV with exit block. This was re-tested several times and was a reproducible finding. An example of this is shown in Figure 6.5.

Figure 6.5 Sustained PV tachycardia with exit block >20mins from ET-GP stimulation

The Lasso PV catheter was inserted into the LSPV in A) and B).

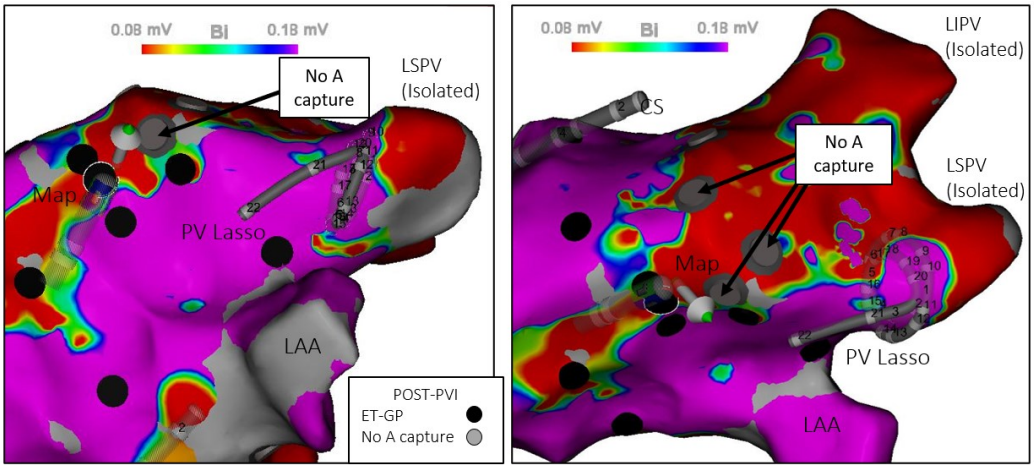

Figure 6.5A. Anatomical positions of the Map catheter in relation to isolated PVs

A) AP and PA views of the 3D electroanatomic map of the left atrium. Circled yellow, the cluster of three ET-GP lateral to previous PVI line triggered PV ectopy and sustained PV tachycardia with exit block, with synchronised HFS. Different colours of the CARTO™ Tags are labelled in the legend between the two views.

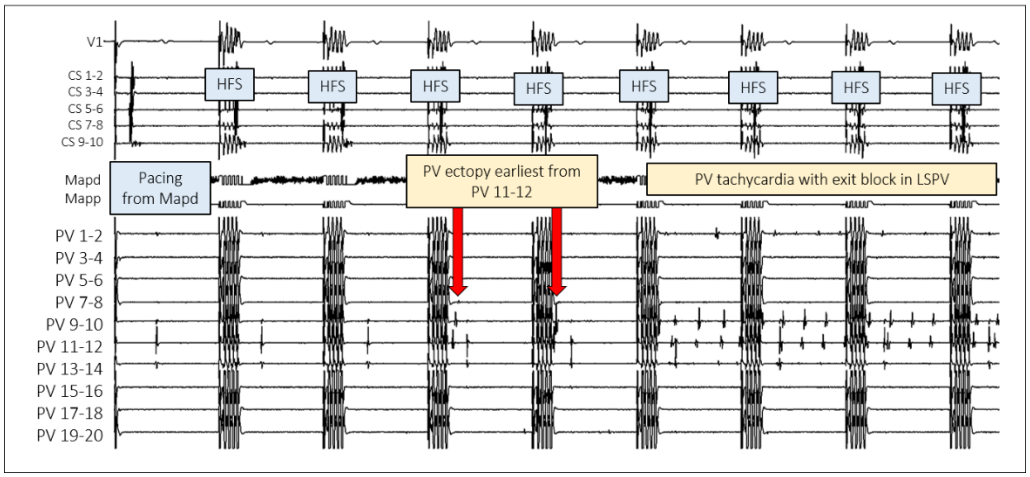

Figure 6.5B. PV ectopy initiating PV tachycardia with exit block at an ET-GP

Intracardiac electrogram trace of HFS at one of the yellow-circled ET-GP site from A). During initial high-output (10V) pacing, a far-field ventricular signal from the left atrial appendage is seen in the PV catheter recording. After the third train of HFS, a PV ectopy fires with the earliest activation in PV 11-12, followed by PV 9-10. The ectopy fires again with the fourth and fifth synchronised HFS trains, each time with earlier activation. On the fifth train of HFS, the same PV ectopy induces a sustained atrial tachycardia that continues for >20minutes.

(CS = coronary sinus; ET-GP = ectopy-triggering ganglionated plexus; HFS = high frequency stimulation; LAA = left atrial appendage; LSPV = left superior pulmonary vein; LIPV = left inferior pulmonary vein; Map = mapping catheter PV = pulmonary vein)

The PV catheter inserted into the LIPV also demonstrated PV tachycardia in the LIPV, with exit block. The PV tachycardia in both the LSPV and LIPV had a cycle length of 130ms (Figure 6.6A and B). However, when the PV catheter was moved to RSPV and RIPV, both PVs were electrically silent (Figure 6.6C). This suggests that the left sided PVs were electrically connected, and the GP cluster that triggered the PV tachycardia was exclusively connected to either the LSPV and/or LIPV. As per protocol, GPs were mapped but not ablated, as the patient was randomised to PVI.

Figure 6.6 The same PV tachycardia in left-sided PVs, right-sided PVs silent

A cluster of GPs in the left side of the roof near the LSPV triggered PV tachycardia which self-sustained for >20minutes. ECG lead V1 are shown at the top of the traces.

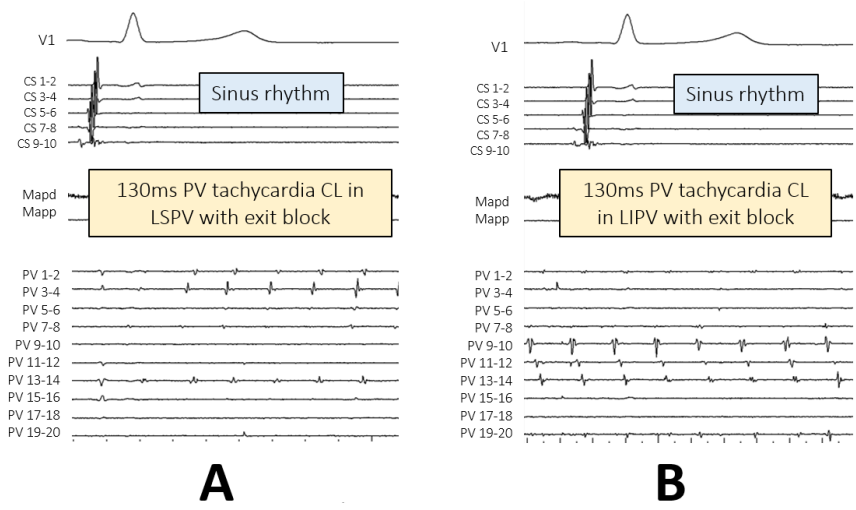

In A), the Lasso PV catheter was positioned in the LSPV. In B), the Lasso PV catheter was withdrawn from A) and inserted into the LIPV. The cycle length was the same in both PVs at 130ms as the PV tachycardia continued. The difference in the activation pattern during the PV tachycardia between A) and B) is reflects the different bipole positioning within the PVs.

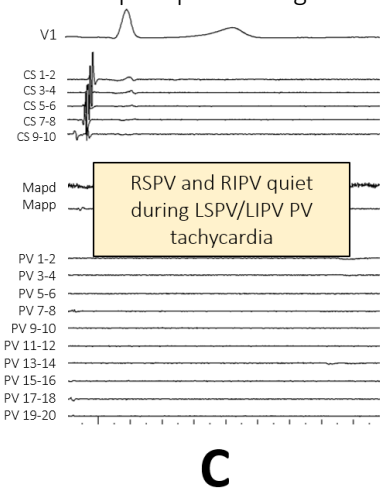

C) shows silent PVs during the same PV tachycardia from A) and B) in both RSPV and RIPV. During the PV tachycardia, the remaining body of the atrium continued in slow, sinus rhythm (as can be seen in the surface ECG and the CS activation).

(CL = cycle length; CS = coronary sinus; LIPV = left inferior pulmonary vein; LSPV = left superior pulmonary vein; Map = mapping catheter; RSPV = right superior pulmonary vein; RIPV = right inferior pulmonary vein

1 month after the ablation, the patient had permanent pacemaker implantation due to 4s pause associated with syncope. This was not thought to be related to the AF ablation, but from a pre-existing conduction abnormality. During the procedure, there was junctional rhythm and several second pauses prior to performing PVI. After the 3-month blanking period, the patient had recurrence of AF, documented from device check. The patient continues to have nocturnal palpitations at least once a month and is awaiting further follow-up to discuss repeat AF ablation. The most likely explanation for this recurrence is re-connection of the left sided PVs which has led to PV tachycardia conducting into the left atrium, causing AF.

In another patient randomised to ADD-GP ablation, the left-side PVs were re-connected. Upon testing for GPs, a cluster of ET-GPs was identified around the antrum of the RSPV, and one within the RSPV. Stimulation of these ET-GP triggered PV tachycardia originating from the RSPV which remained electrically isolated from their previous PVI procedure. This patient had all ET-GPs ablated, except for the ET-GP identified within the RSPV to avoid PV stenosis. The patient also had touch-up RF on the re-connected left-sided PVs to isolate them. All GPs were re-tested with HFS at the end of the procedure, including the ET-GP within the RSPV (Figure 6.7). PV tachycardia was no longer inducible. However, after 200 days of follow-up, the patient had a documented symptomatic recurrence of AF and is awaiting a repeat AF ablation.

Figure 6.7 ET-GP ablation abolishes PV tachycardia

All left sided PVs were re-connected since their previous PVI procedure. The right sided PVs remained electrically isolated. A cluster of ET-GP around the RSPV antrum all triggered PV tachycardia in the RSPV, with exit block. One ET-GP was tested within the RSPV, close to the ostium (circled).

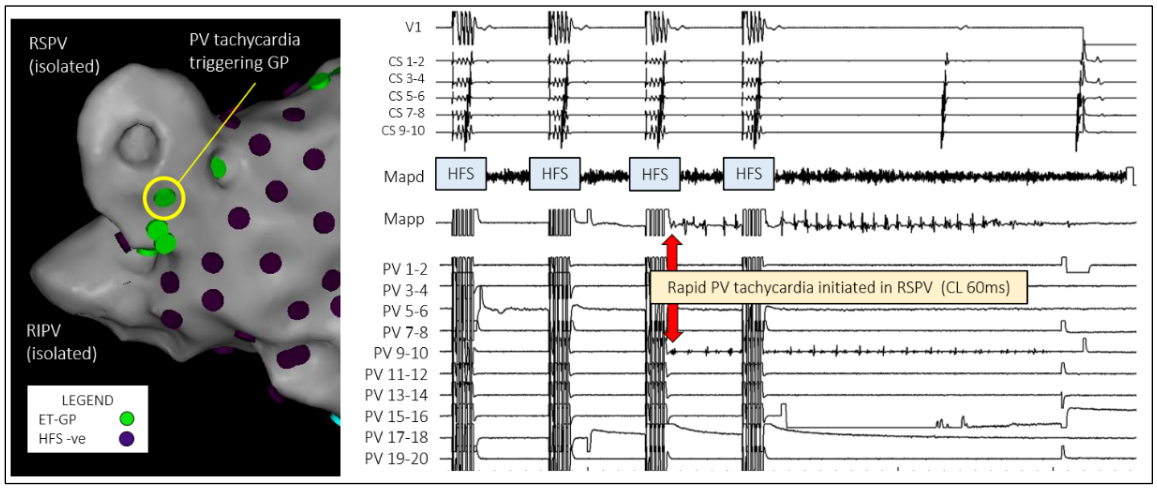

A) At the circled ET-GP site, HFS was performed. After the sixth train of HFS (the trace here starts from the fourth train of HFS), a rapid PV tachycardia was initiated with 60ms cycle length, evident in PV 9-10 and in Mapp. This self-terminated after HFS stopped.

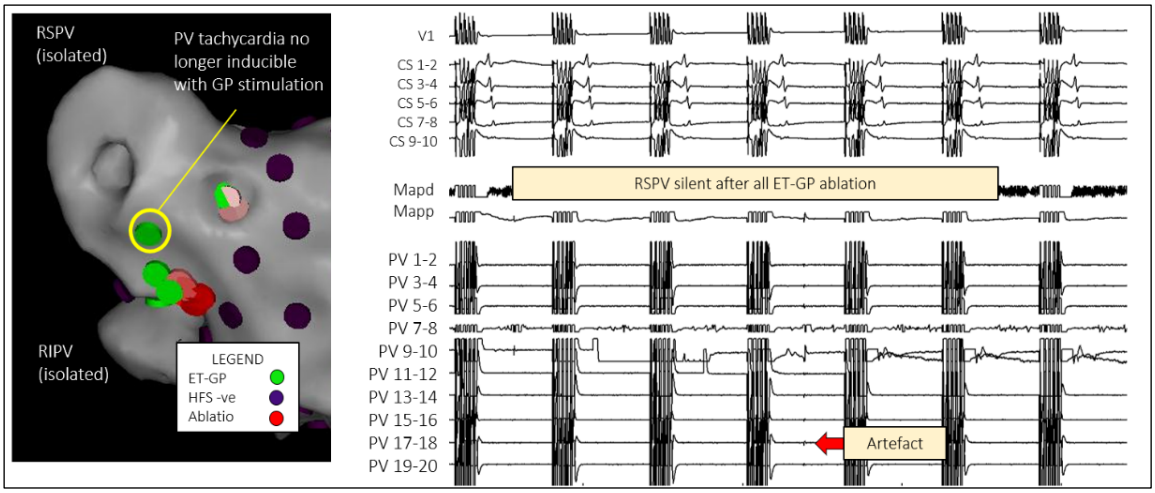

B) All ET-GP except for the circled ET-GP within the RSPV were ablated. The circled ET-GP was re-tested with HFS at the end of the procedure, with the PV catheter positioned in the RSPV again. This showed no inducible PV ectopy or PV tachycardia. The noise seen in the PV electrogram is from artefact, due to Lasso catheter contact with the Map catheter.

(CS = coronary sinus; ET-GP = ectopy-triggering ganglionated plexus; HFS = high frequency stimulation; LAA = left atrial appendage; LSPV = left superior pulmonary vein; LIPV = left inferior pulmonary vein; Mapd = mapping catheter distal; Mapp = mapping catheter proximal; PA = posterior-anterior view; RIPV = right inferior pulmonary vein; RSPV = right superior pulmonary vein; PV = pulmonary vein; PVI = pulmonary vein isolation)

6.3.3. Non-Pulmonary Vein Triggers

26 out of 44 patients (59%) had HFS testing post PVI. There was on average 28 ± 29 HFS sites tested, which identified 7 ± 7 GPs (25%). This included a mixture of ET-GP and AVD-GP. With synchronised HFS, total 114 ET-GP were identified, which induced non-PV triggers. There was median 4 (27%) non-PV trigger per patient (IQR 6). The number of non-PV trigger ranged between 0 to 17. 23 out of 26 (88.5%) patients had non-PV triggers identified. 3 patients did not have any non-PV trigger. This is likely an underestimation of the number of non-PV triggers, as not all patients had them tested consistently prior to their ablation.

The anatomical sites of HFS tested that triggered non-PV ectopy are shown in Figure 6.8. The highest number HFS sites that triggered non-PV ectopy was in the roof of the left atrium (42; 37% in total): 18 near the left PVs, 15 near the right PVs, and 9 in mid-roof), followed by the left side of the anterior wall including in close proximity to the left atrial appendage (24; 21%), the posterior wall (16; 14%), left lateral wall (9; 8%), right side of the anterior wall (8; 7%) and the right lateral wall (3; 3%)

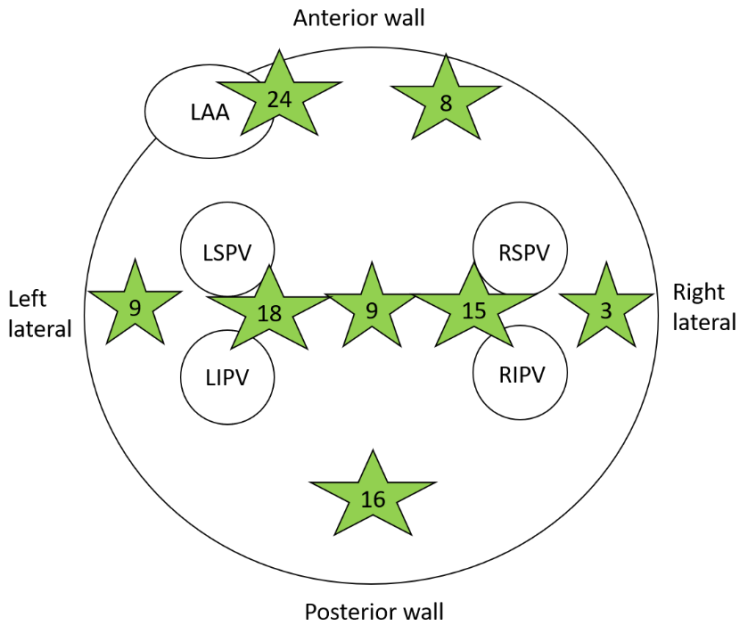

Figure 6.8 Anatomical Sites of Non-PV Triggers induced with HFS

Left atrial diagram of total HFS tested sites that induced non-PV triggers in 26 patients. The highest number of HFS sites that triggered non-PV ectopy was in the roof, followed by the left atrial appendage region and the left side of the anterior wall. The least number of HFS sites that triggered non-PV ectopy was present in the right lateral region.
(LAA = left atrial appendage, LIPV = left inferior pulmonary vein, LSPV = left superior pulmonary vein, RIPV = right inferior pulmonary vein, RSPV = right superior pulmonary vein)

6.3.4. Procedure details

Overall, the average duration of procedure was 169 ± 39 mins. This was significantly longer in the ADD-GP group compared to the PVI group (179 ± 42 mins vs 152 ± 32 mins; p = 0.04). The average fluoroscopy time overall was 16.3 ± 8.3 mins, and there was no significant difference between the two groups (ADD-GP = 17.1 ± 8.8 mins vs PVI = 15.1 ± 8.0 mins; p = 0.47). The total RF energy used per case was significantly greater in the ADD-GP group compared to the PVI group (41.6 ± 17.3 kWs vs 18.7 ± 14.4 kWs; p = 0.004)(Table 6.3).

Table 6.3 Procedure details of the ADD-GP study in the Per-Protocol cohort.

Procedure details	All (n=39)	PVI (n=16)	ADD-GP (n=23)	p Value
Procedure time (min)	169 ± 39	152 ± 32	179 ± 42	0.04
Fluoroscopy time (min)	16.3 ± 8.3	15.1 ± 8.0	17.1 ± 8.8	0.47
RF energy used (kWs)	33.7 ± 19.2	18.7 ± 14.4	41.6 ± 17.3	0.004

Values are expressed in mean ± STD.

(ADD-GP = PVI in addition to GP ablation protocol; PVI = pulmonary vein isolation; RF = radiofrequency)

6.3.5. Re-connection of PVs

10/42 (24%) patients presented with all PVs re-connected. 4 (9.5%) patients presented with all PVs completely isolated.

On average, 2.2 ± 2.1 PVs were re-connected. 7 (17%) patients had left common PV, and out of these patients, all had at least 2 PVs re-connected, and all had left common PVs, and RIPVs re-connected.

35 patients had four PVs. 10 (29%) had 3 re-connected PVs, 9 (26%) had 1 re-connected PV, 7 (20%) had 2 re-connected PVs and 5 (14%) had all four re-connected PVs.

There were 85 re-connected PVs in total, excluding the left common PVs. Re-connection rate for each PV was as follows: 24 (28%) RIPV, 23 (27%) RSPV, 19 (22%) LSPV, 19 (22%) LIPV.

Comparison between the ADD-GP and PVI groups showed that there was a significantly higher number of PV re-connection in the PVI group compared to the ADD-GP group. (2.7 ± 1.1 vs 1.8 ± 1.2; p=0.02) (Table 6.2).

6.3.6. GP mapping

41 patients were mapped with HFS pre-PVI. 19 (46.3%) patients had purely synchronised HFS mapping to identify ET-GP. 19 (46.3%) patients had mixture of synchronised and continuous HFS mapping to identify both ET-GP and AVD-GP. The remaining 3 (7.3%) patients had purely continuous HFS mapping to identify AVD-GP.

Pre-PVI, average 67 ± 29 HFS sites were tested, which identified 12 ± 8 (19%) GPs. 2 patients had no identifiable GP, but these patients had primarily continuous HFS mapping due to incessant AF from start of procedure which enabled identification of AVD-GP only.

Within the ADD-GP group, 11/24 (46%) patients had a mixture of ET-GP and AVD-GP ablated, or AVD-GP ablated alone. The remainder (54%) had purely ET-GP ablated. All pre-PVI GPs identified were ablated, even if they re-tested negative post-PVI.

6.3.7. Follow-up

29 (66%) patients completed 12-month follow-up. 19 were randomised to the ADD-GP group and 10 randomised to the PVI group. In the ITT cohort, 32% of patients in the ADD-

GP group and 50% in the PVI group were free from the primary endpoint at 12 months follow-up (log rank p=0.34). In the PP cohort, 33% of patients in the ADD-GP group and 44% in the PVI group were free from the primary end-point at 12 months follow-up (log rank p = 0.59)(Figure 6.9).

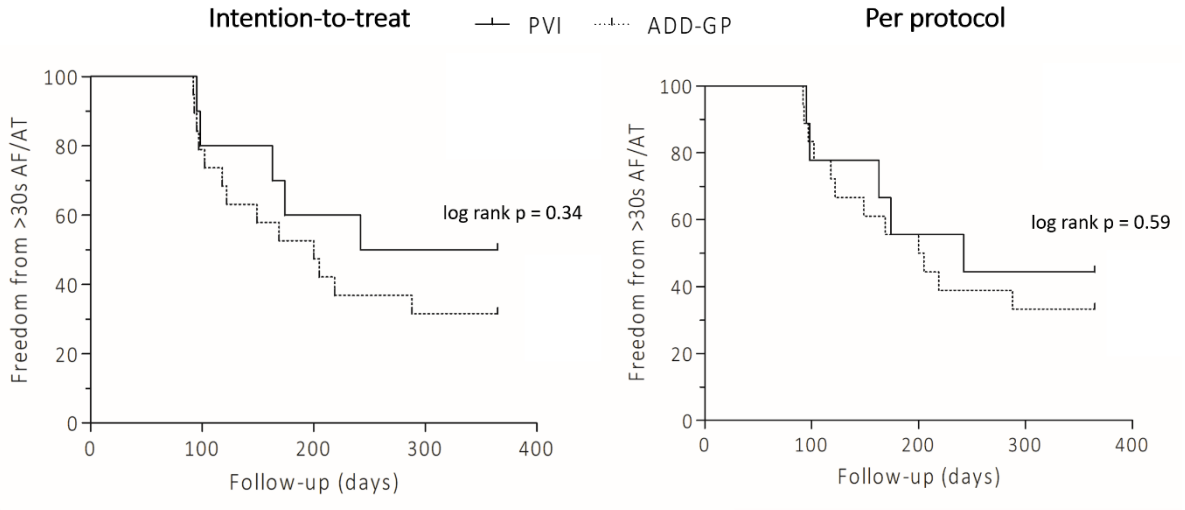

Figure 6.9 12-month follow-up Kaplan Meier curve of freedom from >30s AF/AT

The primary endpoint for the ADD-GP group compared to the PVI group was not significantly different, at completion of 12-month follow-up, in both intention-to-treat and per-protocol cohorts.

(ADD-GP = PVI in addition to GP ablation group; AF = atrial fibrillation; AT = atrial tachycardia; PVI = pulmonary vein isolation)

All patients had on average 3 Holter monitors during their 12-month follow-up, who did not reach primary endpoint. There was no significant difference in the number of Holter monitors between the two groups (PVI=2.8 ± 0.8 vs ADD-GP=3.7 ± 0.8; p = 0.11). Patients had on average 2.2 ± 0.6 AF ablation procedures including this study ablation.

There were 5 events requiring hospitalisation post-operatively. 4 were in the ADD-GP group: 1 urinary tract infection, 1 chest infection, 1 pericarditis and 1 with bradycardia and hypotension which resolved by stopping regular bisoprolol. 1 was in PVI group with a chest infection. There was no statistical difference between the two groups (p = 0.63).

6.3.8. Variables Predicting AF Recurrence

There was no difference in the total RF energy used in patients who reached and did not reach the primary endpoint, regardless of their randomised ablation protocol (33.6 ± 18.7 kWs vs 33.9 ± 21.9 kWs; p = 0.97)(Figure 6.10).

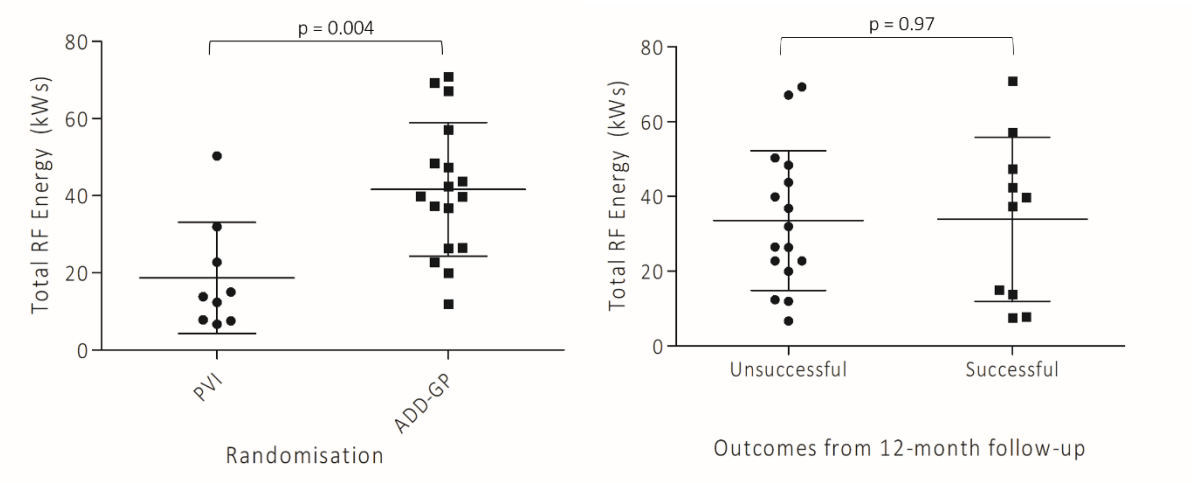

Figure 6.10 Total RF energy used comparison between groups

The left-hand graph shows the difference between the PVI and ADD-GP groups, and the right-hand graph shows the difference between unsuccessful and successful outcomes (reached primary endpoint vs did not reach primary endpoint) in the total RF energy usage. The middle bars in the graphs represent the mean and the bars above and below represent the standard deviation.

(ADD-GP = PVI in addition to ganglionated plexus ablation; PVI = pulmonary vein isolation; RF = radiofrequency)

A univariate Cox regression model with variables commonly associated with AF (age, sex, left ventricular ejection fraction, left atrial diameter, hypertension) and other procedural variables were assessed on AF recurrence (Table 6.4). The only statistically significant predictor of AF recurrence was the total number of electrical cardioversions used during the procedure, as a result of repeatedly inducible incessant AF (HR 1.45 [95% CI; 1.126–1.871], p = 0.004).

Table 6.4 Univariate predictors of AF recurrence

Univariate	B coefficient	HR	95% CI	P Value
Age	0.040	1.040	[0.990 – 1.093]	0.117
Sex (Male)	0.276	0.811	[0.289 - 2.282]	0.692
HTN	0.695	2.004	[0.741 – 5.416]	0.171
BMI	-0.006	0.994	[0.928 – 1.064]	0.855
CHA2DS2-VASC score	1.362	3.905	[0.888 – 17.169]	0.071
ADD-GP ablation	0.499	1.647	[0.586 – 4.629]	0.344
Other left-sided ablations	0.945	2.572	[0.832 – 7.955]	0.101
Left atrial size	-0.481	0.618	[0.196– 1.950]	0.412
Left ventricular ejection fraction	-0.487	0.615	[0.174 – 2.176]	0.451
No. of previous PVI procedures	0.433	1.543	[0.716 – 3.323]	0.268
No. of reconnected PVs	0.338	1.402	[0.924 – 2.128]	0.112
Total RF energy application	0.006	1.006	[0.982 – 1.031]	0.605
No. of ganglionated plexus	-0.045	0.956	[0.899 – 1.017]	0.156
No. of non-PV ectopy	0.183	1.200	[0.985 – 1.464]	0.071
AF/AT with GA induction	0.765	2.149	[0.800 – 5.767]	0.129
Continuous HFS performed	0.777	2.175	[0.811 – 5.832]	0.123
No. of DCCV during procedure	0.373	1.451	[1.126 – 1.871]	0.004

The only significant univariable predictor of AF recurrence was the no. of DCCV used during the procedure ($p<0.05$).

(ADD-GP = PVI in addition to GP ablation protocol; AF = atrial fibrillation; AT = atrial tachycardia; B coefficient = beta coefficient; BMI = body mass index; CI = confidence interval; DCCV = DC cardioversion; HFS = high frequency stimulation; GA = general anaesthesia; HR = hazard ratio; HTN = hypertension; PV = pulmonary vein; PVI = pulmonary vein isolation; RF = radiofrequency)

A multivariate analysis using univariates that reached statistical significance at $p\leq0.10$, including age, sex and hypertension as well-established risk factors for AF were included in the model. Again, the only statistically significant predictor of AF recurrence was the

multiple usage of electrical cardioversions, due to repeated incessant AF induced during procedures (HR 1.80 [95% CI 1.12-2.895], p=0.015) (Figure 6.11).

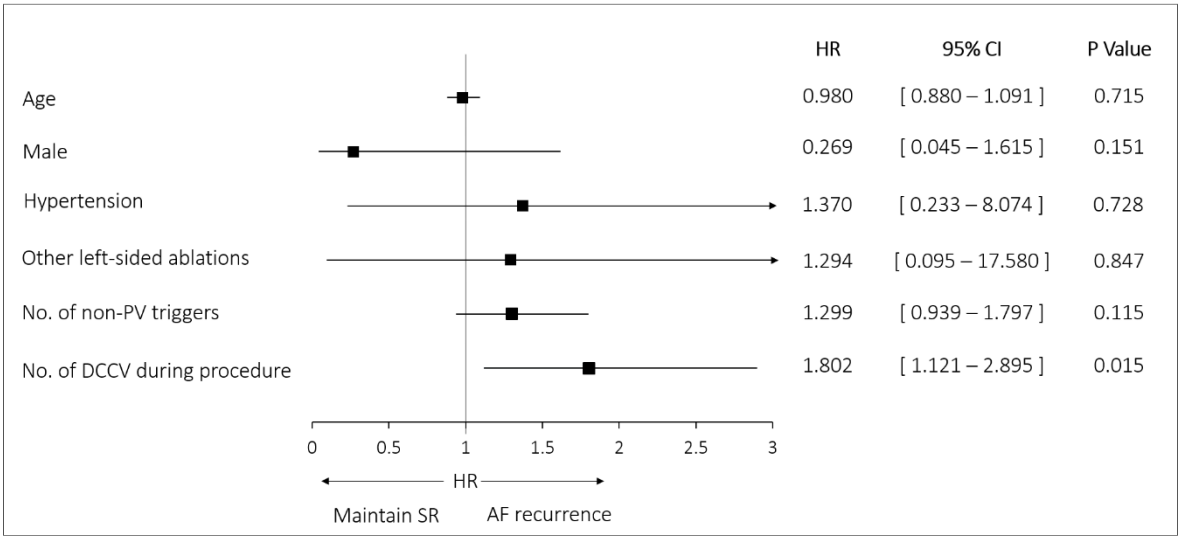

Figure 6.11 Multivariate predictors of AF recurrence

The only significant multivariate predictor of AF recurrence was multiple DCCV during procedures, from recurrent incessant AF.

(AF = atrial fibrillation; CI = confidence interval; DCCV = DC cardioversion; HR = hazard ratio; SR = sinus rhythm)

6.4. Discussion

6.4.1. Patient Characteristics

Due to the initial 2:1 randomisation and the small number of patients recruited to the study, there was significant imbalance in the proportion of patients between the two groups. Subsequently, this has resulted in the imbalance of baseline demographics of patients in the two groups. Overall, the patients recruited were predominantly male (68%), however significantly more were randomised to the ADD-GP group. (85% vs 44%; p = 0.008). Significantly more patients randomised to ADD-GP group had history of left sided AT ablations, such as mitral lines, roof lines, complex fractionated electrogram

ablations with their previous PVI procedures, and/or required these procedures at the time of study protocol (27% vs 0%; p = 0.03). Extensive ablations in the left atrium lead to scarring and AF substrates which have higher recurrence of AT/AF[187]. Cluster of ablations in patches around the left atrium due to additional GP ablation may lead to heterogeneity in refractory periods throughout the left atrial surface, and create substrate for macro re-entry AT. Combination of these factors in the ADD-GP group may have affected the outcomes.

It is known that pre-existing left atrial scarring in patients receiving PVI for AF is an independent predictor of AF/AT recurrence[187–189]. A threshold of 0.15mV as the bipolar voltage amplitude has been used to differentiate left atrial scar in patients having redo AF ablations[190]. For each patient in this study, the proportion of average bipolar voltage amplitude ≤ 0.15mV to the total number of bipolar voltage points collected was expressed as a percentage. Results showed there was no significant difference between the two groups (PVI = 38.9% vs ADD-GP = 41.2%; 0.70).

Other possible indications of patients having more persistent type of AF than paroxysmal AF were explored. For example, whether patients were in AF at start of procedure, and how many electrical cardioversions patients required to complete the research protocol. There were no significant differences between the two groups.

However, the overall demographics of patients recruited to this study had more persistent AF-type of substrate, as evidenced by almost 50% of patients requiring continuous HFS mapping after multiple electrical cardioversions failing to keep them in sinus rhythm. This contrasts the behaviour of patients having their first-time AF ablation patients recruited to the multi-centre GP ablation study (GANGLIA-AF).

6.4.2. Outcomes of Repeat AF Ablation

In the ADD-GP group, the primary endpoint was reached at different time intervals during the 12-month follow-up; most reached endpoint immediately after the 3-month blanking period and becoming less frequent after 200 days of follow-up. In contrast, the PVI group reached the primary endpoint in clusters, immediately after the 3-month blanking period, between 160 to 200 days of follow-up, and just before reaching 250 days of follow-up.

There was little difference between the outcomes of patients in the ADD-GP group between the ITT and PP cohorts.

In one cohort study, 301 patients had a single PVI procedure, and 208 had multiple PVI[191] procedures. Patients with multiple procedures were followed-up for average 4.5 years. Compared to a single PVI procedure, multiple PVI procedures increased the long-term success from 41.3% to 58.3%. 70 patients received "additional substrate modification", which included complex fractionated atrial electrogram ablation, roof or mitral line ablations, and non-PV trigger ablations such as the superior vena cava ablation. This increased patient success to 62.5%. There was also an incrementally reduced proportion of PV re-connection with increasing number of repeat PVI procedures. After a single procedure, 89.4% of PVs were re-connected, whilst after the second and third procedure, 58.3% and 33.3% were re-connected respectively. This was comparable to our study data, as patients had average 1.3 PVI procedures at the time of enrolment and 91% of patients had PV re-connection. However, in our randomised study, the procedural success with PVI after 12-month follow-up was 50% in the ITT cohort. GP ablation as our method of "additional substrate modification" had worse outcome than PVI only, with 32% freedom from AF at 12 months follow-up.

6.4.3. Pulmonary Vein Re-connection and AF

PV re-connection rates at repeat AF ablations have been reported to range from 36% to over 95%[192–195]. In our study, 91% of patients had re-connected PVs, after average 4.2 years since their most recent PVI. In 2017, an observational cohort study by Kim *et al*[194] reported that larger number of PV re-connection at second AF ablation procedures correlated to more success from AF freedom compared to smaller number of PV re-connections (HR 0.41, 95% CI 0.19–0.87, P = 0.021). Patients with re-connected PVs also had shorter time interval between their *de novo* procedures and their repeat procedures (21 months ± 19.8 vs 28.2 months ± 19.6; p = 0.039). However, there was no correlation between the number of PV re-connection and AF freedom in persistent AF patients.

Similarly, in this study, we found significantly larger number of PV re-connections in the PVI group compared to the ADD-GP group, and better success in the PVI group. It is possible that patients with higher number of re-connected PVs received greater number of RF lesions leading to more durable PVI in the subsequent follow-up, than the patients with lesser number of PV re-connections. There are also greater number of PV triggers than non-PV triggers in patients for repeat AF ablation[195]. Lesser number of PV re-connections indicate non-PV triggers playing a greater role in the patient's AF. However, ADD-GP ablation did not effectively target non-PV triggers, or targeting them led to increased pro-arrhythmic substrates in the atrium.

6.4.4. Pulmonary Vein Tachycardia After Pulmonary Vein Isolation

The PVs are the most common cause of AF[22], yet little is known about the significance of conduction block of PV depolarisations and PV tachycardia (PVT) within an electrically isolated vein. PVT has been observed in case reports and in small prospective studies[196–198]. The largest of these studies (85 patients) found that in paroxysmal AF patients

undergoing PVI, 10% of treated PVs (113/1105) demonstrated PV arrythmias dissociated from the sinus rhythm[198]. 25% of the PV arrhythmias were PV tachycardia with a mean cycle length 155 ± 43 ms. After 6-month follow-up, there was no difference in AF freedom in patients with PVT and no PVT.

In one study of 25 patients, 3 (12%) patients displayed PVT with exit block in two PVs concurrently, whilst they were in sustained AF[197]. Two patients had PVT with exit block in the LSPV and RSPV concurrently, and the other in the LSPV and LIPV concurrently. In two patients, RF application in the LSPV restored sinus rhythm and there was no further recurrence of AF, despite no RF application to the other PV with PVT. The patient who had PVT in the RSPV and LSPV had two mapping catheters simultaneously inserted into each PV. This showed that the PVT in each PV were not synchronised. RF in the LSPV only restored sinus rhythm, although a non-sustained PVT was inducible with rapid pacing in the RSPV afterwards. Further ablation in the RSPV prevented inducible PVT. The authors hypothesised that PVT in two simultaneous PVs were due to an "insulated connection" between the two PVs, explained by ablation of one PV affecting the other. However, this did not explain why in one patient, two PVs had non-synchronised PVT. Therefore, PVT may have been triggered in both PVs simultaneously, whilst the PVs were not electrically connected. A possible explanation for this interesting phenomenon is stimulation of a GP with neural connection to multiple PVs initiating tachycardia in the PVs simultaneously. It is known that PVs are the most densely innervated anatomical structures in the left atrium of human hearts, which are surrounded by multiple ganglia clusters that are interconnected. The PV-left atrial junction also have muscular discontinuities and abrupt fibre orientation changes that create an ideal substrate for re-entry mechanisms[160].

In a smaller study by Jiang *et al*[199], 12 patients with paroxysmal AF had ongoing PVT after circumferential PVI. GP clusters identified via anatomical landmarks were ablated outside the PVI line, which terminated PVT in 8 patients.

Our study is the first to show that HFS outside the PVs during the local atrial refractory period induce PVT within electrically isolated PVs, reproducibly. In one of our five patients demonstrating this phenomenon, a cluster of GPs in the roof and near the LSPV ostium triggered sustained PVT in the LSPV and LIPV. Unlike the case reported by Tse *et al*[197], the patient was in sinus rhythm during PVT, and the PVT cycle length was the same in both PVs, most likely due to their electrical connection to one another. We did not test the effect of ablation at the HFS site that triggered this phenomenon, as the patient was randomised to PVI.

6.4.5. Atrial Ectopy with High Frequency Stimulation – An Autonomic Effect?

The examples in Figure 6.7 demonstrate synchronised HFS near the ostium of the PVs which triggered PVT with exit block. Our protocol for synchronised HFS was to deliver HFS after a fixed delay of 20ms from each pacing stimulus. The local refractory period at different anatomical areas of the left atrium was not tested prior to HFS. It is known that there is heterogeneity in the effective refractory period (ERP) within the PV and at the PV-left atrial junction, with shorter ERP than the rest of the left atrium[200,201]. All of the HFS sites that triggered PVT with exit block were within approximately 10mm proximity to the adjacent PV, although there was entrance block with normal (lower current amplitude) pacing. It is possible that high voltage pacing followed by HFS near anatomical structures with short ERP captured the PV myocardium, causing PV ectopy. Figure 6.7

shows PV ectopy triggered with a very short coupling interval to the HFS train, which may indicate direct PV capture with high-output pacing. However, an 80ms burst of HFS should continuously capture the PV if this was the case, and with every train of HFS. This should be expected with high-output, rapid pacing *within* the PV especially. However, the PV ectopy was only triggered *after* the 6th HFS train. This was a reproducibly delayed response when re-tested. Furthermore, it was no longer possible to induce PVT with re-stimulation at this site after ablating ET-GP outside the RSPV. The non-ablated RSPV tissue should not be affected by ablating distant sites. Therefore, it may be assumed that PVT induced by stimulation within the RSPV is via a neural communication. The cluster of GPs outside the RSPV were likely the culprit GP or nerves responsible for the PVT.

All our patients demonstrating inducible PVT with exit block had HFS tested sites were along the lines of conventional PVI. This gives further evidence that GPs induce PV arrhythmia. However, in the presence of durable PVI, PVT were not the cause of the patient's recurrent AF, suggesting another PV trigger from a re-connected PV, or a non-PV trigger.

6.4.6. Targeting Non-PV Triggers of AF

In a study by Lin *et al*[195], 181 patients who received ≥3 AF ablations were studied. 13 (8%) patients had all PV isolated. 127 patients were tested with provocative testing for PV and non-PV triggers. 90 (71%) patients had identifiable PV triggers including PV ectopy and tachycardia, and 36 (28%) patients had non-PV triggers mapped. Although we did not test for non-PV triggers in all patients, 23 out of 26 (88.5%) patients had non-PV triggers identified. This is considerably more than that cited in the literature. In the study by Lin *et al*[195], most non-PV triggers from patients who had ≥1 AF ablations were mapped from the right atrium and the coronary sinus. Patients with a smaller number of

previous AF ablations had a smaller number of non-PV triggers (2 previous AF ablations = 17%, 1 previous AF ablation = 11%). Therefore, with increasing number of repeat AF ablations, there were greater number of non-PV triggers, but still the largest trigger was from the PV. In our study, patients had on average 1.3 AF ablations in the past. The left atrium was mapped only for non-PV and PV triggers, and the largest number of non-PV ectopy was in the roof of the left atrium, followed by the left side of the anterior wall including the left atrial appendage.

Despite identifying significantly more non-PV triggers in this study, ablating them in addition to PVI did not prevent AF significantly more than PVI alone. It can be assumed that as all patients received complete PVI, PV triggers were targeted similarly in both groups. If this is the case, targeting non-PV triggers in addition to PV triggers in our study appeared to be more pro-arrhythmic. The mechanism of this is not clear, but it may be due to the increased heterogeneity of scars created throughout the left atrium from patchy cluster ablations of each AF trigger site.

There was greater amount of RF ablation performed in the ADD-GP group compared to the PVI group, though there was no significant difference in the amount of RF ablation in patients who had AF/AT recurrence with those who did not have recurrence, regardless of their randomised ablation protocol. This suggests that the amount of RF ablation does not independently impact outcomes, but the pattern and the anatomical targets for ablation in the ADD-GP protocol was pro-arrhythmic. This outweighed any potential benefit of eliminating non-PV triggers of AF with the ADD-GP ablation.

6.4.7. Study Limitations

Patients recruited to this study was small and imbalanced due to the initial 2:1 randomisation at the start. Currently, the 12-month follow-up is complete for significantly greater number of patients in the ADD-GP group than in the PVI group. When the 12-month follow-up is complete for all patients, the difference in AF freedom between the two groups may change. The effect of general anaesthesia on the threshold for PV and non-PV triggers mapped with HFS is not known. The right atria was not mapped, as this was outside the protocol approved by the ethics committee. The number and type of PVs re-connections were different between patients, which led to non-uniform RF application to achieve PVI. These limitations may have impacted the outcome of this study.

6.5. Conclusion

Non-PV triggers can be successfully mapped using HFS in patients with or without isolated PVs. A more persistent type of AF as estimated by the total number of electrical cardioversions required during the procedure was an independent predictor of AF recurrence following ablation. The anatomical location of ablation is important, regardless of the quantity of ablation. Results of this feasibility study need further investigation and a more rigorous design will make more valid comparison of outcomes.

7.THE ACUTE AND LONG-TERM IMPACT OF GANGLIONATED PLEXUS ABLATION

7.1. Introduction

During the clinical studies exploring the role of ganglionated (GP) ablation in patients with and without pulmonary vein isolation (PVI), interesting phenomena related to ablation of GPs and re-inducibility of AF post-GP ablation were observed. These phenomena and their relationship with long-term success of AF ablation were evaluated. In addition, we report patients returning for repeat HFS mapping after initial GP ablation. These phenomena and observations give important insight into the role of GP as upstream triggers of AF.

7.2. Methods

100 patients with paroxysmal AF with or without previous PVI were included in the analysis. All had detailed global left atrial high frequency stimulation (HFS) mapping for GPs using the methods described in Chapter 2. When patients triggered sustained AF that for longer than 2 minutes, the culprit GP was ablated first, followed by GPs identified prior to this event. Ablation was stopped when AF terminated to sinus rhythm (SR) or if there were no further GP left to ablate.

Responses to ablation during AF was categorised into: 1) termination to SR, 2) organisation to atrial tachycardia (AT), 3) significant AF cycle length (CL) prolongation. Significant CL prolongation was defined as ≥30ms prolongation of the average 30 AF CL measured immediately after stopping ablation, compared to the average 30 AF CL pre-

ablation. The clearest atrial signal was taken for cycle length measurement before and after ablation.

Patients with and without sustained AF had their 12 month event-free survival estimated using a Kaplan-Meier curve for the primary endpoint (≥30s AF/AT documented recurrence).

If patients remained in sustained AF despite GP ablations and after multiple electrical cardioversions, continuous HFS was performed to identify atrioventricular dissociating GP (AVD-GP). An AVD-GP was defined as >50% average RR prolongation during continuous HFS compared to the average baseline RR interval. After completing HFS mapping, the remaining GP were ablated. All ablated GP were re-tested with HFS thereafter. GP initially identified using synchronised HFS were re-tested with synchronised HFS, and GP initially identified using continuous HFS were re-tested with continuous HFS. Some patients were in SR at the time of re-testing with continuous HFS. We then observed whether AF was re-inducible and sustainable by re-testing with continuous HFS.

Finally, patients referred for repeat AF ablation who previously had HFS mapping were analysed. This included patients who had GP ablation as part of the multi-centre GP ablation study, and those who had HFS mapping but no GP ablation in the ADD-GP study. As most of these patients required full circumferential PVI, HFS mapping was limited to areas that had GPs identified in the last procedure. A comparison was made between the number of GPs identified in previous procedures compared to repeat procedures.

7.3. Results

30/100 (30%) patients displayed different types of phenomena, explored in more detail below.

7.3.1. Acute AF Modification and Long-Term AF/AT Freedom

36 patients having first time GP ablation, who completed 12 months follow-up were studied. 24 (67%) patients triggered sustained AF with ET-GP stimulation and had ET-GP ablation. Some patients triggered multiple episodes of sustained AF with ET-GP stimulation, and others triggered a single episode of sustained AF. Remaining 12 (33%) patients did not trigger sustained AF.

Out of 24 patients with sustained AF, 19 (79%) resulted in acute AF modification including: 14 (58%) with AF termination to SR (Figure 7.1), 5 (21%) with AF organisation to AT (Figure 7.2), and 2 (8%) with significant AF CL slowing (≥30ms). On average, 6 mins 5s ± 7 mins 1s of ablation was performed until successful acute AF modification. This targeted on average 2 ± 2 GP.

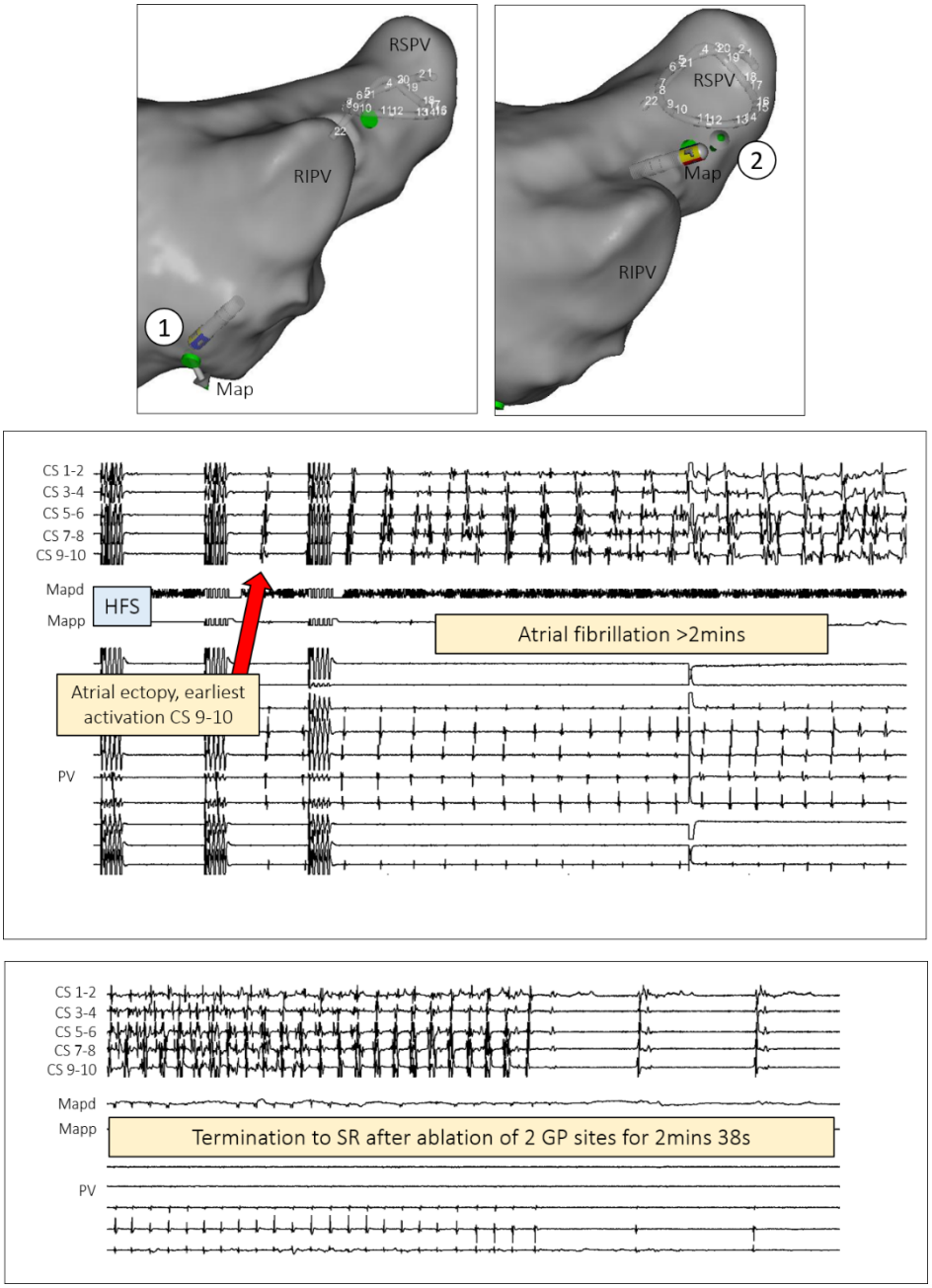

Figure 7.1 Sustained AF termination to sinus rhythm with GP ablation

This patient triggered sustained AF (>2mins) during synchronised HFS of the Map position labelled "1" in the top left-hand panel. This site of stimulation was in the inferior border of the posterior wall. The Lasso PV catheter was positioned in the RSPV at the time. The top trace shows an atrial ectopy with the earliest activation from CS 9-10 triggering after the 10th HFS train (trace starts with the 9th HFS train). This initiated sustained AF. This site was ablated first, for 2mins 20s, then the Map catheter moved to the position in "2" in the top right-hand panel. This was at the ostium of the RSPV in the right carina. Further ablation here for 18s terminated AF to SR. (AF = atrial fibrillation; CS = coronary sinus; GP = ganglionated plexus; RSPV = right superior pulmonary vein; LIPV = left inferior pulmonary vein; Map = mapping catheter RSPV = right superior pulmonary vein; RIPV = right inferior pulmonary vein; SR = sinus rhythm)

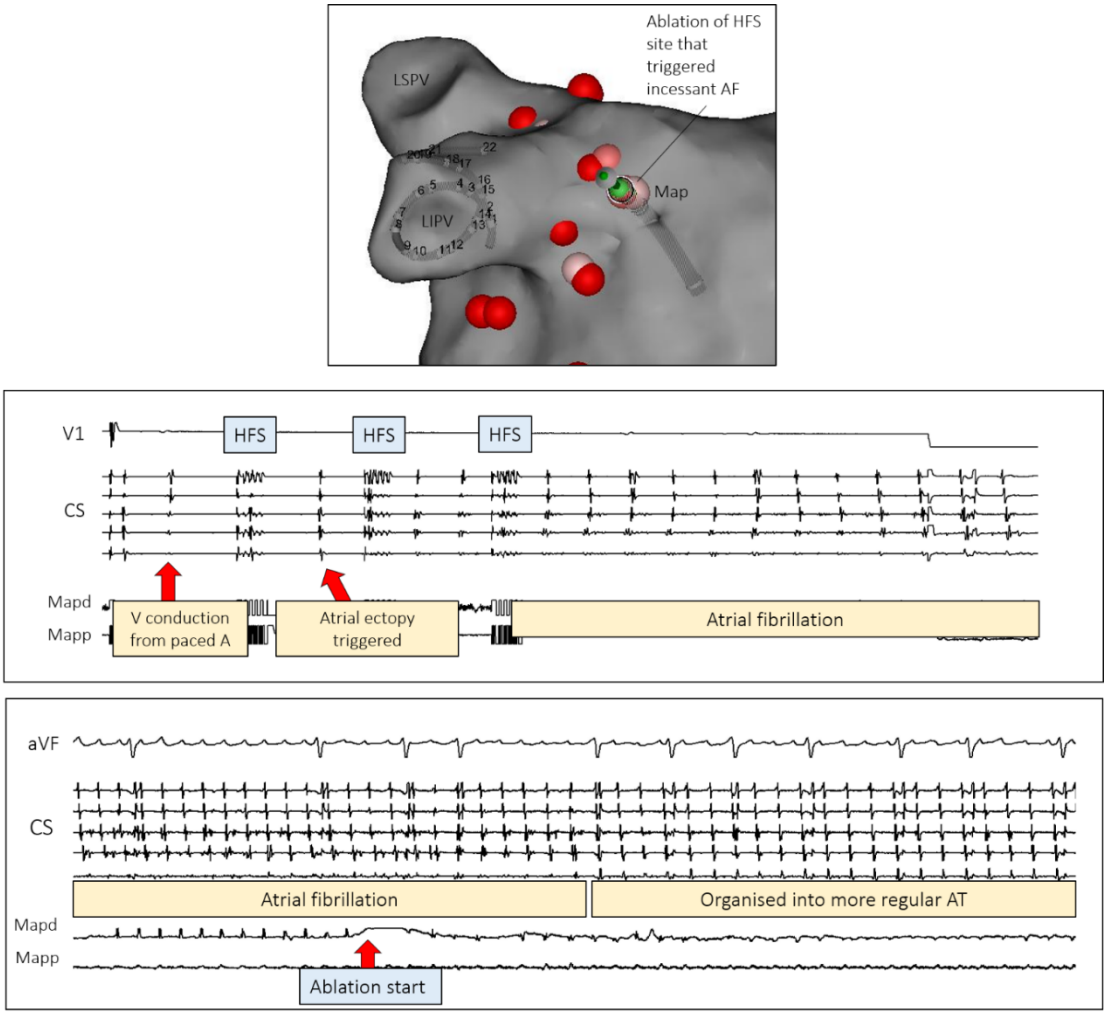

Figure 7.2 Sustained AF organises to AT with GP ablation

The top trace shows an atrial ectopy triggering with the first HFS train. This induced sustained AF. Ablation of this ectopy triggering GP immediately organised AF into a stable, sustained AT with CL 200ms.

(AT = atrial tachycardia; CS = coronary sinus; HFS = high frequency stimulation; Mapd = mapping catheter distal; Mapp = mapping catheter proximal)

There were 1 to 5 sustained AF episodes per patient leading to ET-GP ablation attempts. The rate of acute AF modification per patient ranged from 0% to 100% and all patients completed 12 months follow-up as per the multi-centre ET-GP study protocol. 8 patients (33%) had 100% success with acute AF modification and 5/8 (62.5%) were free from the primary endpoint. 11 patients (46%) had 20-67% success with acute AF modification and 4/11 (36%) were free from the primary endpoint. 5 patients (21%) had no success with

acute AF modification and 2/5 (40%) were free from the primary endpoint. 6/12 (50%) patients who did not have sustained AF were free from the primary endpoint. There was no significant difference in the primary endpoint-free survival between all patient groups (log rank p = 0.75) (Figure 7.3).

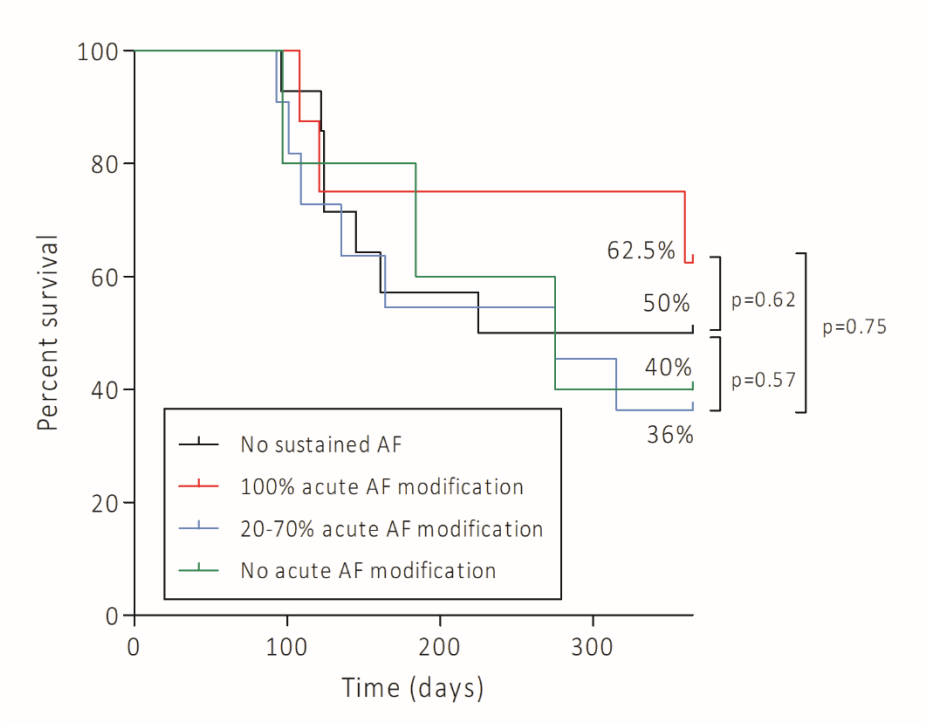

Figure 7.3 AF/AT-free survival stratified by AF modification with ET-GP ablation

The primary endpoint for all groups were not significantly different, at completion of 12-months follow-up.

(AF = atrial fibrillation; AT = atrial tachycardia; ET-GP = ectopy triggering ganglionated plexus)

7.3.2. Suppression of AF After GP Ablation

Some patients had sustained AF throughout the procedure, despite multiple electrical cardioversions. These patients required AVD-GP mapping with continuous HFS. Most patients did not revert to sinus rhythm after ablating all AVD-GP and re-testing with continuous HFS were performed during AF. However, 6 patients were in sinus rhythm after AVD-GP ablation. 2 of these patients had PVI in addition to GP ablation. The

remaining 4 patients only had GP ablation, and the PVs were left electrically connected. These patients underwent re-testing with continuous HFS, which would normally re-induce AF.

The patients had on average 3 ± 3 spontaneous AF episodes, the longest AF episode was 60 ± 11 minutes, and 3 ± 1 electrical cardioversions were performed during their procedures. 3 patients had mixed synchronised and continuous HFS mapping, and the other 3 had purely continuous HFS mapping. This identified 15 ± 6 GPs per patient.

All 6 (100%) patients triggered AF when testing continuous HFS in sinus rhythm at ablated AVD-GP, but AF self-terminated shortly after stopping HFS (Figure 6.2). In total, we performed 30 continuous HFS in SR at ablated AVD-GP sites, and AF was non-sustainable in 27 (90%) of these episodes. The average AF duration after continuous HFS in SR was only 49 ± 69 seconds. After 12-month follow-up with multiple 48hr Holter monitors, 3 patients (50%) reached the primary endpoint, and the remaining 3 patients were free of the primary endpoint.

7.3.3. Single GP Ablation and Long-Term AF Freedom

In one case, a 58yrs old lady with paroxysmal AF, reporting AF episode at least once a month lasting several days at a time. She had hypertension, good left ventricular systolic function and 3.6cm left atrial diameter. She did not take any regular antiarrhythmic medications, but Flecainide on PRN basis. She also had a history of a concealed right-sided septal retrograde pathway that did not induce sustained tachycardia from an electrophysiology study, left unablated. She was referred for AF ablation and underwent HFS mapping for GP ablation.

At the start of the procedure, the patient had frequent spontaneous paroxysms of AF, which then developed into sustained AF. Therefore, the patient was mapped with continuous HFS to identify AVD-GP. The patient was in sustained AF for 51 minutes during continuous HFS mapping, then spontaneously cardioverted to SR. The rest of the left atrium was mapped with synchronised HFS for ET-GP. Overall, 64 HFS sites were tested. This identified 19 GPs (30%), of which 2 were ectopy-triggering GP (ET-GP) and 17 were AVD-GP. Most of the AVD-GP were in the posterior wall, and the two ET-GP were in the LIPV ostium in the posterior wall, and inferior to the left atrial appendage in the left lateral wall. The ET-GP in the LIPV ostium reproducibly induced AF, with the earliest activation within the LIPV (Figure 7.4).

Figure 7.4 Single GP ablation leads to AF termination to sinus rhythm and sinus bradycardia

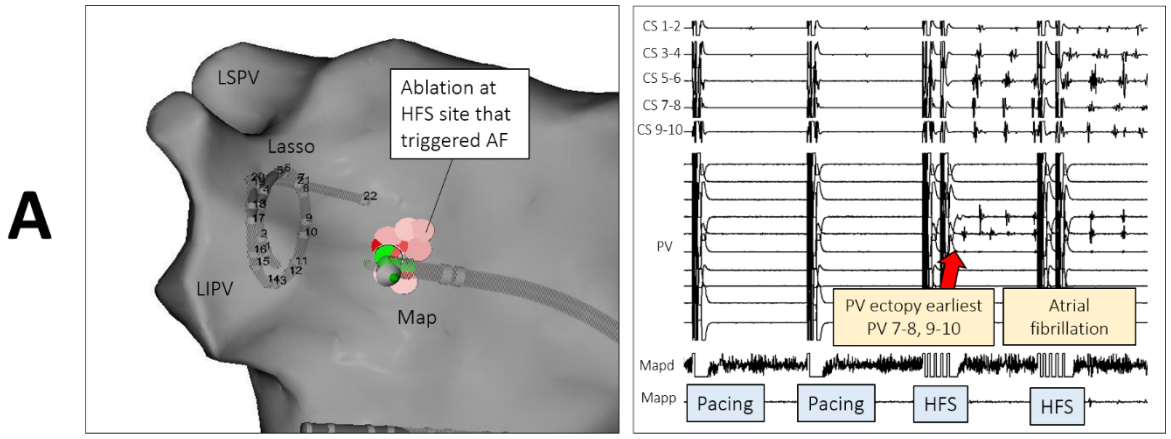

A) Left: Posterior-anterior view of the left atrium showing the anatomical position of the Map catheter which was used to deliver synchronised HFS. It was positioned in the LIPV ostium in the posterior wall. The Lasso PV catheter was positioned in the LIPV at the time of stimulation. Cluster ablation was performed over this GP site.

Right: Trace showing the initiation of PV ectopy in the LIPV leading to AF. The first two artefacts are from pacing the left atrium with high output. With the first train of HFS, PV ectopy is triggered in the LIPV, with the earliest activation signals in PV 7-8 and 9-10. This triggers AF, which self-terminates to SR after 24s.

B

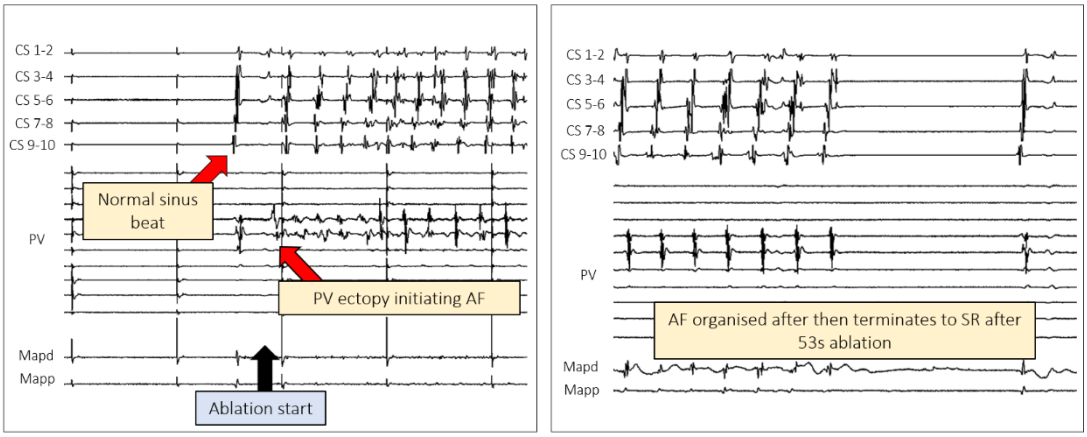

B) Left: Low-output pacing artefact is shown in the beginning of this trace. The patient was in sinus rhythm. Ablation started over the GP site that triggered PV ectopy and AF. This immediately triggered AF.

Right: After ablation of GP site in A) for 53s, AF briefly organised and terminated to SR.

C

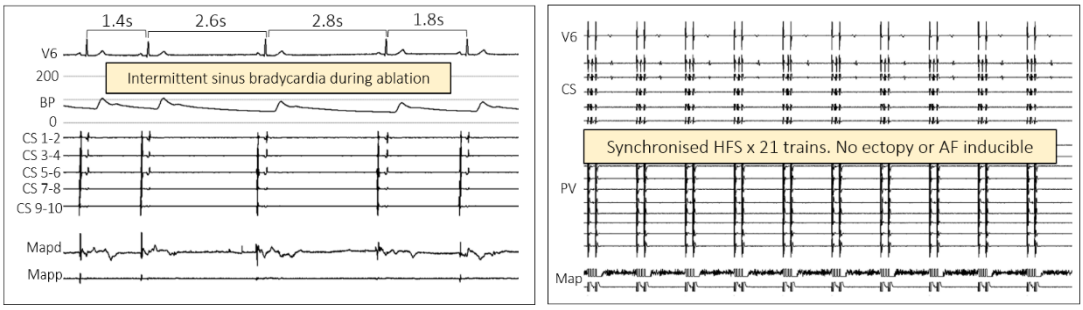

C) Left: The same GP site was continued to be ablated during SR, and intermittent RR prolongation with sinus bradycardia was observed, with pauses of up to 2.8s. Total 197s ablation was delivered at the GP site.

Right: After ablating the GP site in A), synchronised HFS was performed again, up to 21 trains. This did not induce any further PV ectopy or AF. The LIPV remained electrically connected.

(AF = atrial fibrillation; AVD-GP = atrioventricular dissociating GP; CS = coronary sinus; HFS = high frequency stimulation; GP = ganglionated plexus; LAA = left atrial appendage; LIPV = left inferior pulmonary vein; LSPV = left superior pulmonary vein; Map = mapping catheter; PV = pulmonary vein; SR = sinus rhythm)

Other ostial regions of the LIPV were tested with synchronised HFS, but none induced atrial ectopy or AF. The ET-GP that reproducibly triggered LIPV ectopy and AF was ablated. After 53s, AF briefly organised and terminated to SR. Ablation continued, and there was intermittent RR prolongation (>2.5s) with sinus bradycardia. Overall, 197s of

ablation was performed in this discrete ET-GP site, and other GP were left unablated. The ablated ET-GP was re-tested at the end of the procedure with synchronised HFS, which could not trigger PV ectopy or AF. There was also no further spontaneous AF, though this was frequently induced from the start of the procedure. Interestingly, re-testing one of the AVD-GP that were not ablated with continuous HFS during SR resulted in no RR prolongation. Furthermore, AF induced with continuous HFS was not sustainable after stopping HFS. At another unablated AVD-GP site, there was still significant RR prolongation with continuous HFS with AF, but AF self-terminated after 3 minutes. All PVs at the end of the procedure remained electrically connected.

After the procedure, the patient had three 48hr Holter monitors at 74 days, 262 days and 483 days post-GP ablation which did not reveal any AF/AT, but nocturnal sinus bradycardia only. She reported being completely free of AF symptoms since the ablation and has not required a repeat AF ablation for more than 4 years.

7.3.4. Recurrence of GP After Ablation

25 patients with previous HFS mapping for GPs returned for repeat AF ablation. 14 (56%) patients previously had GP ablation without PVI and 11 (44%) patients previously had PVI and HFS mapping for GPs, with or without GP ablation.

There was on average 43.2 ± 28.2% less number of GP at the patients' repeat procedures. 3 patients had no GP recovery. In one patient, large number of GP were previously identified (31 AVD-GP). A 'box' lesion was performed to encircle a large patch of AVD-GP in the right side of the posterior wall (Figure 7.5), and additional RF application at the base of the right inferior PV (RIPV) to re-isolate the vein. Some AVD-GP re-tested outside the box still re-tested positive with continuous HFS. Therefore, further RF touch-up of

these AVD-GP was required. This was despite ablating in the region of the right inferior GP (RIGP) which is known to be the common "gateway" to AVD-GP that regulates AV nodal conduction[173,202]. The patient had AT recurrence after 2 months, and was brought back for AT ablation with HFS mapping after 205 days. A roof line ablation did not terminate the AT. Further mapping and ablation of the AT in the mitral isthmus, which included epicardial ablation in the coronary sinus terminated the AT. Finally, previously identified GP were re-mapped around the left atrium with continuous HFS. There were no identifiable GP.

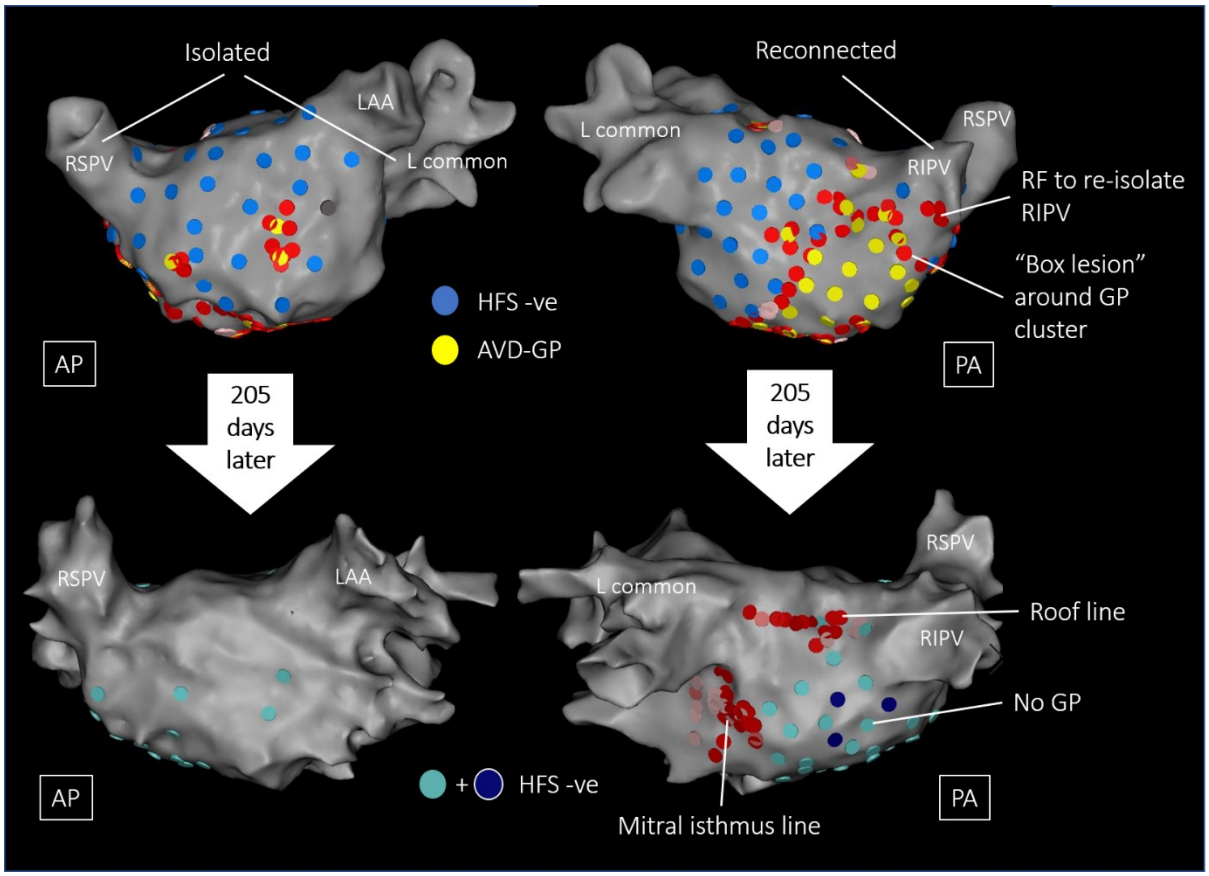

Figure 7.5 No recovery of AVD-GP after 205 days post-GP ablation

This patient had 1 previous PVI procedure and a cavotricuspid line (CTI) ablation 12 years ago for paroxysmal AF and flutter. Only the RIPV was re-connected as shown in the top diagram. The patient induced sustained AF spontaneously, and repeatedly despite several electrical cardioversions. Therefore, we mapped globally around the left atrium with continuous HFS to identify AVD-GP in AF (a positive AVD-GP was defined as >50% average RR prolongation during HFS compared to baseline).

Numerous AVD-GP were identified in a large cluster around the right and inferior border of the posterior wall. A 'box' lesion of ablation was performed around the cluster of GPs in the posterior wall, to minimise the amount of ablation in this region. The cluster of GPs within the box were not ablated. AVD-GP identified in other areas of the left atrium were ablated in clusters (example shown in the anterior wall of AP view). The RIPV was re-isolated afterwards with discrete RF application over the base of the RIPV, as shown in the PA view. All AVD-GP were re-tested with HFS outside the box lesion, as well as a few within the box lesion. Further RF application was applied at the GP that still evoked significant RR prolongation. The patient was cardioverted at the end of the procedure. CTI line remained blocked.

The patient had AT recurrence after 2 months since the above procedure. He had repeat AT ablation after 205 days. He was in AT on the day of the ablation. This was mapped and a roof line was initially performed. This did not terminate AT. Instead, a mitral isthmus line ablation which included epicardial ablation within the coronary sinus terminated AT. We then proceeded to map the left atrium with HFS, where we previously identified AVD-GP. This is shown in the bottom diagram. There was no GP recovery.

(AT = atrial tachycardia; AVD-GP = atrioventricular dissociating ganglionated plexus; CTI = cavotricuspid isthmus line; GP = ganglionated plexus; HFS = high frequency stimulation; L = left; LAA = left atrial appendage; PVI = pulmonary vein isolation; RIPV = right inferior pulmonary vein; RF = radiofrequency; RSPV = right superior pulmonary vein)

In 4 patients, between 3 to 12 GP were identified *in addition* to their original number of GP identified from their 1st procedures (>100% GP recovery). We examined few possible reasons why there were increased number of GPs in these patients.

1) Repeat procedures were on average 361 ± 83 days after the patients' 1st procedures. 15 other patients who had repeat GP mapping had the average 351 ± 150 days elapsed since their 1st procedures was. This was not statistically significant between the two groups (p = 0.65). Also, there was no correlation between the proportion of GPs recovered and the duration of time elapsed since the 1st procedure (Figure 7.6).

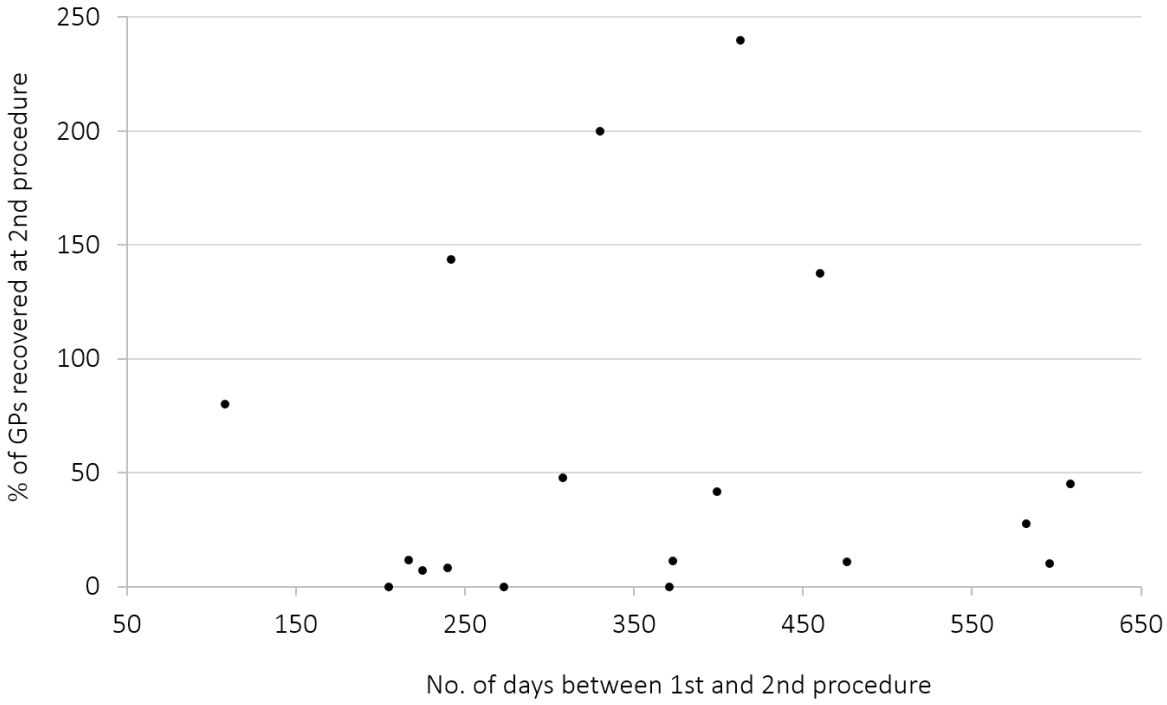

Figure 7.6 The proportion of the number of GPs identified at 2nd procedure to the 1st procedure over time

The *x* axis displays the number of days elapsed between the 1st and 2nd procedures. The *y* axis displays the percentage proportion of the number of GPs identified at the 2nd procedure, to the number of GPs identified at the 1st procedure. There was no correlation between the two variables.

(GP = ganglionated plexus)

2) One of the 4 patients with extra GP recovery had labile blood pressure towards the end of their 1st procedure, and therefore did not have ablated GPs re-tested with HFS for functional confirmation of the absence of further ectopy/AF response. All other patients from the GP ablation studies had additional RF application if ectopy/AF was still inducible with GP stimulation. It is possible that there were GPs that were not completely ablated in this patient, leading to regeneration of nerves.
3) The anatomical sites of GP at repeat procedures were generally in the same sites as those previously ablated, and extended further outwards to neighbouring

regions, indicating new branches of nerves that sprouted outward from ablated sites.

4) The total RF energy delivered was not significantly different from the 4 patients who had additional GPs at their repeat ablations, compared to the 15 others who had reduced number of GPs (22.0 ± 8.3 kWs vs 30.9 ± 15.8 kWs; p = 0.25).

7.4. Discussion

7.4.1. AF Modification with GP Ablation

We demonstrated that in patients with paroxysmal AF, AF and atrial ectopy that leads to AF can be triggered with synchronised HFS, and have localised RF ablation to acutely terminate AF to sinus rhythm, organise to AT, or significantly increase AF CL. This required ablation of 2 AF triggering atrial sites on average. Re-inducing AF with continuous HFS at previously ablated atrial sites did not sustain AF as before.

Continuous HFS is high-output, high-rate atrial pacing that inevitably causes direct myocardial capture and AF when applied during sinus rhythm. In all the patients mapped with continuous HFS, they were significantly likely to initiate susrtained AF with a single atrial ectopy from synchronised HFS, or in some cases, spontaneously with catheter movement. These patients had on average 3 electrical cardioversions due to repeated sustained AF, and sustained AF for more than an hour during continuous HFS mapping. However, after ablating all GPs, re-testing the GPs with continuous HFS during sinus rhythm in six patients did not induce sustained AF in all patients. This suggests electrophysiological modification of their atria which prevents AF inducibility or sustainability post-GP (with or without PVI) ablation.

Experimental studies have shown that AF inducibility is heightened with autonomic stimulation[177], and modification of the autonomic pathway using different methods such as RF ablation, tragus nerve stimulation and botulinum toxin injection suppressed or abolished AF inducibility, via increase in the atrial effective refractory period (AERP) and reducing its dispersion across the atria[137,146,176]. A long-term benefit has also been observed in the clinical setting[139,148]. AF inducibility in these experimental studies were assessed by repeated burst pacing in the atria, which would have been at a lower current output than continuous HFS used in our study. In our studies, we did not measure the changes in the AERP at baseline and after ablation, and therefore cannot make direct comparison with the experimental data. However, the demonstration of AV dissociating effect from neural stimulation of AVD-GP at the start, and absence of this effect after ablation of GPs, in addition to the inability of re-inducing incessant AF with high-rate capture of the atrium suggests an acutely successful neural modification of AF. This did not translate to a long-term AF freedom in half of our patients.

In another 39 patients, sustained AF was triggered with synchronised HFS or spontaneously, during SR. The synchronised HFS protocol delivers HFS within the local atrial refractory period, and therefore avoids direct myocardial capture, and AF. Therefore, AF induced by a correctly delivered synchronised HFS is assumed to be from a neural trigger, via GP stimulation. During sustained AF, we ablated these trigger sites and 48% of incessant AF episodes led to termination of AF to SR, >30s AF CL prolongation, or organisation to AT. Termination to SR was the most common response to GP ablation. This may be from ablating the nerves and GPs, that act as “drivers” that trigger and maintain AF. However, we waited 2 minutes during sustained AF before ablating GPs, and the average time of ablation to AF modification was 6 minutes, which may have been enough time for the patient to spontaneously cardiovert. Therefore, it was not possible

to definitively differentiate the two possible mechanisms of acute AF modification. However, the absence of further atrial ectopy or AF triggered with synchronised HFS after GP ablation suggests acute atrial modification, regardless of its mechanism. Although not statistically significant, the presence of 100% acute modification of AF during GP ablation had more favourable outcomes in preventing AF recurrence, when compared to patients with <70% acute modification of AF or no sustained AF at all. The presence of modifiable neural triggers in patients with 100% acute modification of AF with GP ablation may reflect less advanced atrial disease with more favourable long-term prognosis.

Acute AF modification with GP ablation has also been observed by Yamshiro *et al*[203]. Out of 32 patients, 14 (44%) had paroxysmal AF. The "five major left atrial GPs" were anatomically identified, verified with continuous HFS to observe for significant AV dissociation, then ablated. 8 (27%) patients had AF termination during GP ablation at one or more GP clusters, another 8 during circumferential PVI, and the AF CL within each PV was significantly prolonged after GP ablation, compared to the baseline. There was no long-term follow-up data of these patients.

We observed all of the described GP ablation phenomena to be present in one patient, who had a single ET-GP site ablated, leading to improvement in patient's symptoms and AF freedom. This was achieved without PVI. There was drastic improvement in the patient's acute AF burden during the procedure. The patient demonstrated many short paroxysms of AF prior to ablation, which became more sustained. The source of the sustained AF was repeatedly demonstrable with synchronised HFS at the LIPV ostium in the posterior wall. Localised cluster RF application to this region not only terminated AF to SR, but also demonstrated changes to the sinus node activity during ablation. In addition, AF was not inducible or sustainable thereafter. The AVD-GP remained

unchanged after the single ET-GP ablation by the LIPV ostium. This suggests that the culprit AF trigger of this patient, was identified within the LIPV which had neural connections to the site of ablation. The unablated AVD-GP in the rest of the left atrium were not relevant to this patient's disease. This is evidenced by more than 4 years follow-up after the procedure, where the patient has remained completely asymptomatic.

Acute AF modification and its association with long-term success has been studied more extensively in persistent AF patients, showing mixed results[204–208]. However, there are no such data available in paroxysmal AF patients, and this is the first report with GP ablations.

7.4.2. GP Recovery after Ablation

It is a well-documented phenomenon in both experimental models and humans, that after local injury to peripheral nerves from events such as myocardial infarction, or heart transplantation, denervation extends to viable myocardium beyond the infarcted area, and also regenerate at site of local injury[209–212]. Similarly, RF ablation that damages local nerves lead to regeneration as early as 2 hours after ablation[213]. Heart rate variability, a surrogate marker of the autonomic tone that affects the sinus node has been used in several studies to assess for modulation in the autonomic tone and its effect in preventing AF[100,214,215]. HRV returned to baseline levels mostly at 4 weeks, indicating regeneration of nerves at this point, and longer duration of HRV attenuation was associated with AF freedom. In one experimental study, epicardial GP ablation compared to sham controls led to significant regeneration of nerves at 8 weeks, as evidenced by immunohistochemical staining of parasympathetic and sympathetic nerves. This also led to overall shortening of the AERP and more easily inducible atrial arrhythmia. There was no difference in the inducibility of ventricular arrhythmias[216].

We did not assess for HRV changes, but this is the first study to assess for functional recovery of GPs after GP ablation, that triggers atrial arrhythmia or significant AV dissociation in patients with paroxysmal AF. Interestingly, there were four patients who had increased number of GPs since their index procedures. There was no definite procedural or patient characteristic that influenced this to occur, and the number of patients were too small to derive a meaningful conclusion.

As our cluster ablation lesions for GPs were patchily spread across different regions in the left atrium, it is possible that reinnervation at these discrete and localised regions promoted heterogeneity in the AERP across the atria to cause macro-reentry tachycardias and AF.

7.4.3. Conclusion

Synchronised HFS in the left atrium identifies GPs that can trigger and sustain AF in patients with paroxysmal AF. Localised ablations of these selectively mapped AF trigger sites lead to modification of AF, including termination to SR, slowing of AF CL, organisation to AT, and suppressing AF sustainability. It may be possible to employ this technique to identify AF drivers in persistent AF patients, and observe similar effects.

Ablated GPs recover within 12 months, sometimes more than there were present before GP ablation. Further investigation is required to assess what ablation parameters and patient characteristics lead to more durable GP ablation, promote hyperinnervation, and correlate these to long-term outcomes.

8. THE INTRINSIC CARDIAC NERVES AND ATRIAL ARRHYTHMIA IN LANGENDORFF-PERFUSED PORCINE HEARTS

8.1. Introduction

We have shown that high frequency stimulation (HFS) delivered within the local atrial refractory period of left atrial sites of patients with atrial fibrillation (AF) can trigger atrial ectopy and arrhythmia (Chapter 5). Stimulation of postganglionic nerves at the local stimulation site presumably communicate retrogradely with multiple epicardial ganglia that are interconnected with each other. Ganglia and postganglionic nerves contain both sympathetic and parasympathetic nerves, and their stimulation lead to surge of acetylcholine and catecholamine release which shortens the atrial effective refractory period (AERP) and promote AF[68,174,175]. Our data suggests that ablation of local endocardial sites that triggered atrial ectopy and arrhythmia, without direct ablation of the epicardial GP lead to similar success of AF freedom as conventional pulmonary vein isolation.

Previously, atrial arrhythmia was triggered by intrinsic cardiac nerve stimulation that is independent of the extrinsic cardiac autonomic nervous system in an isolated Langendorff-perfused heart model[217]. In this study, we used this model to stimulate intrinsic cardiac nerves with HFS, and correlate functional response from HFS (ectopy/arrhythmia triggering or no response) to the underlying topography of nerves at the local site of stimulation.

8.2. Methods

All animal tissues were taken under the Home Office license held by the Royal Veterinary College, London, with the approval of their local Animal Welfare and Ethics Body.

8.2.1. Langendorff Apparatus Set-Up

A custom-built Langendorff apparatus was used for whole porcine heart preparation (Figure 8.1). The apparatus consisted of a 5 litre solution reservoir, an oxygen supply to oxygenate the physiological solution, a heating coil for the solution to remain at optimum temperature, a bubble trap to remove air pockets from the system, and a high flow pump to circulate solution around the system at a constant rate (Cole Parmer, UK). The solution chambers were connected to an aortic cannula, where the physiological solution was retrogradely perfused into the coronary arteries and thereby maintaining the metabolic, electrical and contractile activity of the porcine hearts. The perfusate exited the coronary circulation into the right atrium and expelled from the heart. The physiological solution used as substitute for blood was oxygenated Tyrode's solution (10^{-3} mol/l: NaCl, 130; KCl, 4.05; MgCl2, 1.0; NaHCO3, 20; NaH2PO4, 1.0; glucose, 5.5 and CaCl2, 1.35; pH = 7.4). This solution was heated to 42°C.

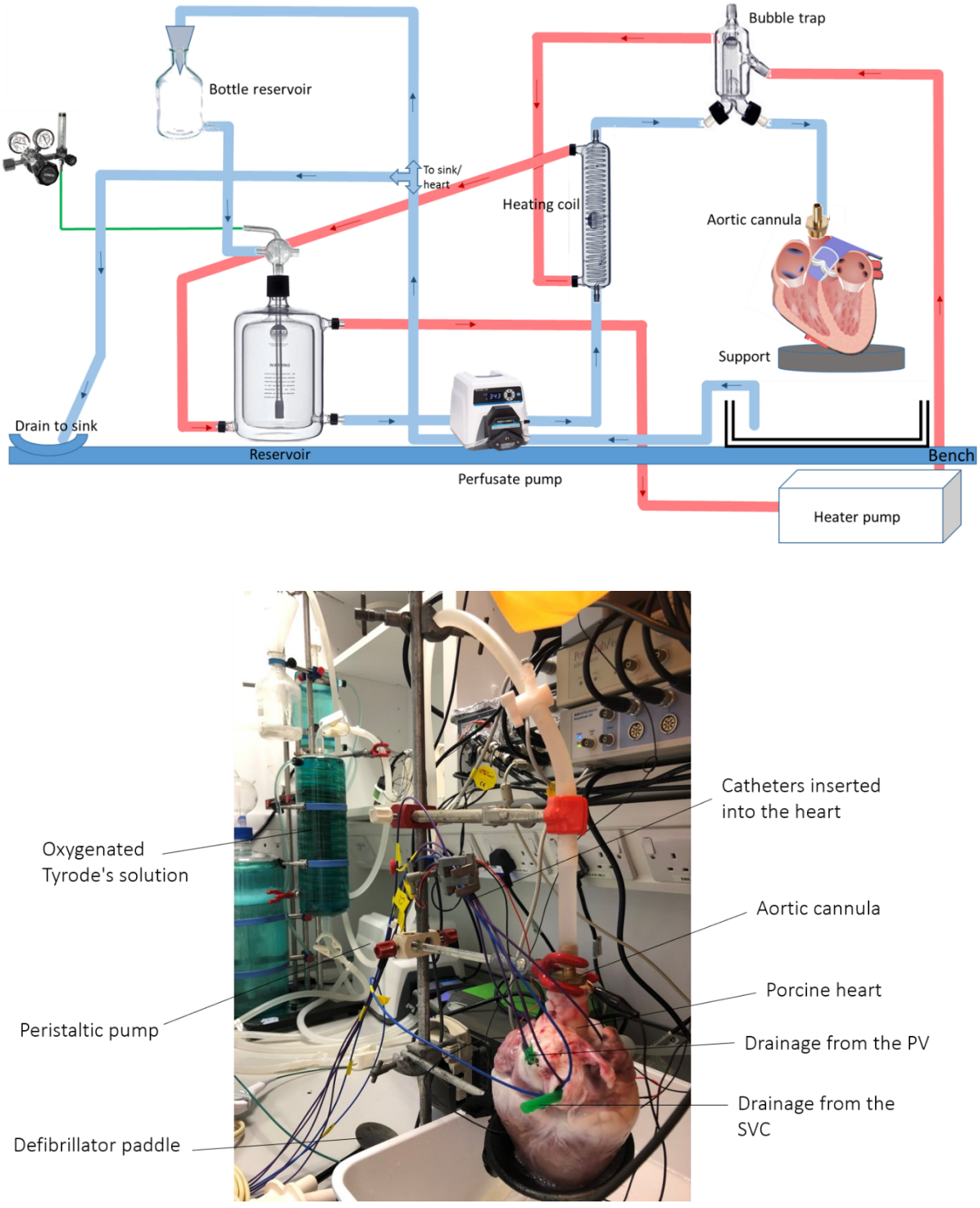

Figure 8.1 Schematic diagram and photograph of Langendorff apparatus set-up for porcine hearts

(PV = pulmonary vein; SVC = superior vena cava)

8.2.2. Whole Heart Preparation

Explanted porcine hearts from anaesthetised pigs were immediately submerged in a cardioplegia solution for up to 90 minutes. Any non-cardiac tissue were carefully excised away, leaving as much fat intact as possible. Aorta was cut down to leave approximately 2cm for cannulation and attachment to the Langendorff apparatus. After securing the cannulation, the hearts were retrograde perfused with oxygenated Tyrode's solution. The flow-rate of the Langendorff pump was set to 75ml/15s. Surface ECG electrodes were attached to the hearts and recorded on LabChart (AD-Instruments, Oxford, UK). Pacing electrodes were also inserted into the hearts and connected up to MicroPace (CA, US). The hearts were stabilised for minimum 20 minutes before beginning experimentation. Reversal of ST segment depression on the ECG usually indicated adequate stabilisation. If the hearts developed ventricular fibrillation, external DC cardioversion was performed to revert to sinus rhythm (SR).

Once the hearts stabilised with their own intrinsic sinus node activity, they were paced at a fixed rate with MicroPace, between 550-700ms, adjusted to an optimal rate that did not provoke atrial or ventricular arrhythmias. A decapolar catheter was inserted into the coronary sinus via the superior vena cava (SVC). Three quadripolar catheters were inserted into the right ventricular (RV) apex, and the left and right atrial appendages. However, depending on the quality of the intracardiac electrogram signals, the catheters were epicardially positioned under the RV/left ventricular apex, or under the atrial appendages. Catheters were fixed into stable positions with clamps. A 3.5mm tip ablation catheter was used to move around the atria to perform HFS. All intracardiac electrograms were recorded at 1000 Hz by an electrophysiology recording system (Bard EP, Lowell,

MA). The ablation catheter was connected to a custom-built neural stimulator (V1.0 and V2.0, Tau-20) for delivering HFS.

8.2.3. Intrinsic Cardiac Nerve Stimulation with HFS

The left and right atria were mapped including the SVC and atrial appendages with synchronised HFS using methods described in Chapter 2. However, HFS was delivered on the epicardial surface of the hearts. Catheter contact with tissue was manually adjusted for equal amount of force to be applied at all test sites. Positive responses to HFS included atrial ectopy, atrial tachycardia or AF, and these sites were re-tested to ensure reproducibility. Ectopy triggering (ET) and non-ectopy triggering (non-ET) intracardiac recordings were labelled on the Bard system, including descriptions of their anatomical locations. Anatomical sites with the corresponding responses to HFS were pinned with labels or photographed for reference. Up to twenty anatomical sites within twenty minutes to an hour time frame were tested, depending on the functional status of the heart.

8.2.4. Immunohistochemistry of HFS Tested Atrial Sites

At the end of the HFS protocol, all labelled HFS tested sites were dissected down in a perpendicular plane to the atrial wall, aiming to include all layers of the atria (fat pad, epicardium, myocardium, endocardium) in each tissue. Each tissue was approximately 1.5 x 1.5 cm in size. Tissues were fixed into Tyrode's solution buffered formalin solution for 24hrs, then transferred to phosphate buffered neutral solution (PBS). The tissues were further cut down to approximately 0.5cm x 0.5cm in size, and automatically processed using increasing concentrations of alcohol. The tissues were cleared in xylene, then embedded in paraffin blocks. Multiple sister sections from each tissue were taken

that were 4-6μm thick. One section from each tissue were stained with Masson's Trichrome, and the remaining sections were used for immunohistochemistry with chicken polyclonal antibody to tyrosine hydroxylase (TH) (Abcam ab76442), and rabbit monoclonal antibody to choline acetyltransferase (CAT) (Abcam ab178850). After washing, secondary antibodies conjugated with fluorescent markers were applied. A goat anti-chicken Alexa-Fluor 568 (Abcam ab175477) for anti-TH primary antibody and donkey anti-rabbit Alexa-Fluor 488 (Abcam ab150073) for anti-CAT primary antibody were used. The anti-TH and anti-CAT primary antibodies were stained in separate sections.

TH antigen retrieval was performed by boiling in citrate buffer (pH 6.0) for 10mins, and for CAT at both pH6 and pH9 in citrate and tris-EDTA buffer respectively. This determined that pH9 tris-EDTA is the superior solution for CAT antigen retrieval. Antigen-blocking was performed for one hour with 5% normal goat and donkey serum in PBS. Antibodies dilutions were then prepared in blocking serum to reduce non-specific binding. Primary antibodies were titrated to ensure optimal dilution (1:250) and allowed to react for 1 hour at room temperature, then washed three times in PBS with 0.1% Triton X-100. Secondary antibodies were used at a dilution of 1:500, and left overnight at 5°C. Following a further three washes in PBS-Triton X, coverslips were added, using a DAPI (4′,6-diamidino-2-phenylindole)-positive mounting agent.

A no-primary PBS solution control was performed for all samples to exclude false positive signals caused by non-specific binding of the secondary antigen to tissue. A rabbit IgG isotype control for monoclonal anti-CAT was performed to exclude non-specific Fc receptor binding or other cellular protein interactions with the primary antibody to tissue. Any non-specific fluorescence identified in the controls and in the reactive samples

were excluded from analysis. An IgG isotype control was not an appropriate test for the anti-TH antibody, due to its polyclonal nature. Instead, we performed no-primary antibody control test for anti-TH antibody.

Positive control tests were performed with a sympathetic nerve trunk and vagus nerves from one of the pigs, known to express TH and CAT respectively. This validated our immunohistochemistry technique.

8.2.5. Image Acquisition and Analysis

Brightfield and fluorescence imaging of the entire tissue area was performed at 10x magnification on a HWF1 – Zeiss AxioObserver microscope controlled by ZEN Pro software (Zeiss). Areas of interest were imaged further at 20x and 40x magnification.

Image analysis was performed using ImageJ (FIJI) software. Tissue anatomy was first examined from brightfield images. Epicardial and nerve area was determined by manual selection of structures, with automated quantification. Colour deconvolution to determine connective tissue and myocardial area was automated, though with manual optimization of colour thresholds, as demonstrated in (Figure 8.2). Empty spaces within the tissue were not included in the total tissue area.

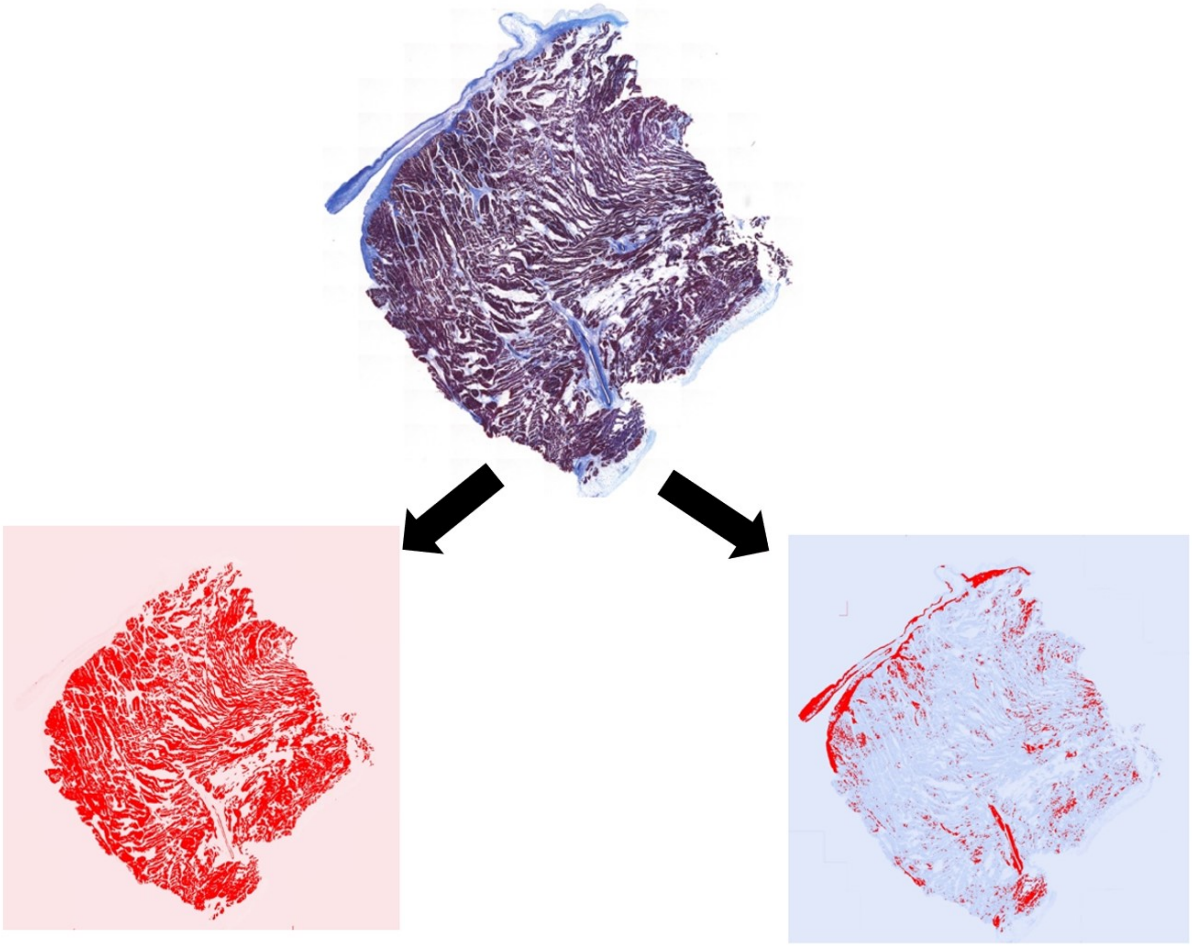

Figure 8.2 Separation of connective tissue and myocardium using an automated process

Using an automated process in ImageJ FIJI, sectioned atrial samples tested with high frequency stimulation (top) had the myocardium (left) and connective tissues (right) separated by colour deconvolution.

Immunofluorescent signals for nerves were determined by eye, and the area of manually selected individual nerve were calculated automatically. The cross-sectional area of nerves was also calculated.

The researcher performing microscopic examinations and nerve quantification was blinded to the tissue's functional response to HFS (ET or non-ET).

8.2.6. Statistical analysis

GraphPad 5 (Prism, San Diego, California) was used for all statistical testing. Normality test was performed using the Shapiro-Wilk test and comparison of means using unpaired t-test or Mann-Whitney test. All continuous variables have been expressed as mean ± standard deviation. The threshold for statistical significance was $p < 0.05$.

8.3. Results

6 porcine hearts were studied and explanted from healthy white female pigs (weight 70-80kg, age 4-5 months old).

The porcine hearts had little visible fat pad on their atria and ventricles (Figure 8.3). All hearts had intact left atrium with visible left and right pulmonary veins.

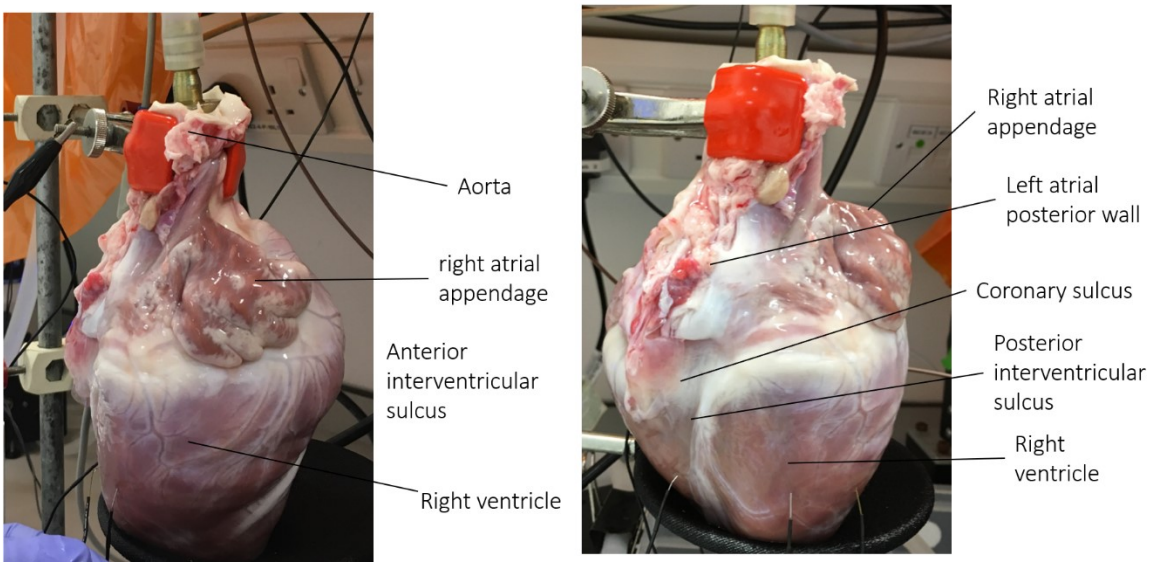

Figure 8.3 Anatomy of a typical whole porcine heart

These are photographs of one of the porcine hearts used for Langendorff perfusion. Porcine hearts and large atrial appendages, with little to no fat lining the atria and ventricles. The porcine hearts had two or three pulmonary veins.

In 4 porcine hearts, 63 atrial sites were tested with HFS, identifying 6 (10%) ectopy-triggering (ET) sites that most commonly triggered single atrial ectopy, less commonly short runs of atrial tachycardia/AF (Figure 8.4). In the remaining 2 pigs, there were no identifiable ET sites with HFS.

Figure 8.4 Reproducibly ectopy-triggering site with synchronised HFS in the ligament of Marshall

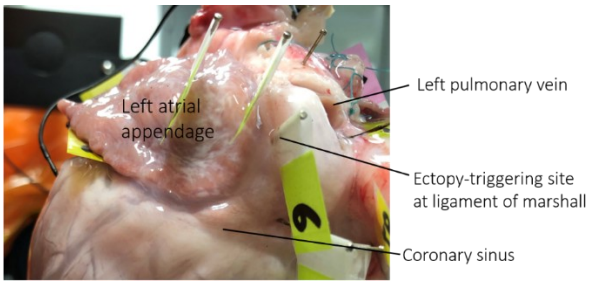

This is a porcine heart triggering atrial ectopy and atrial tachycardia/AF with synchronised HFS. A quadripolar catheter positioned epicardially at the apex of the heart, endocardially in the right atrium, and a decapolar catheter inserted into the CS. An ablation catheter (Mapd) was used to perform HFS.

The photograph above shows the anatomical position of HFS testing (labelled with "6"). This was in the left atrial posterior wall, immediately medial to the base of the left atrial appendage, which was anatomically consistent with ligament of Marshall. The same site was tested four times which induced atrial ectopy and atrial tachycardia/AF in all instances.

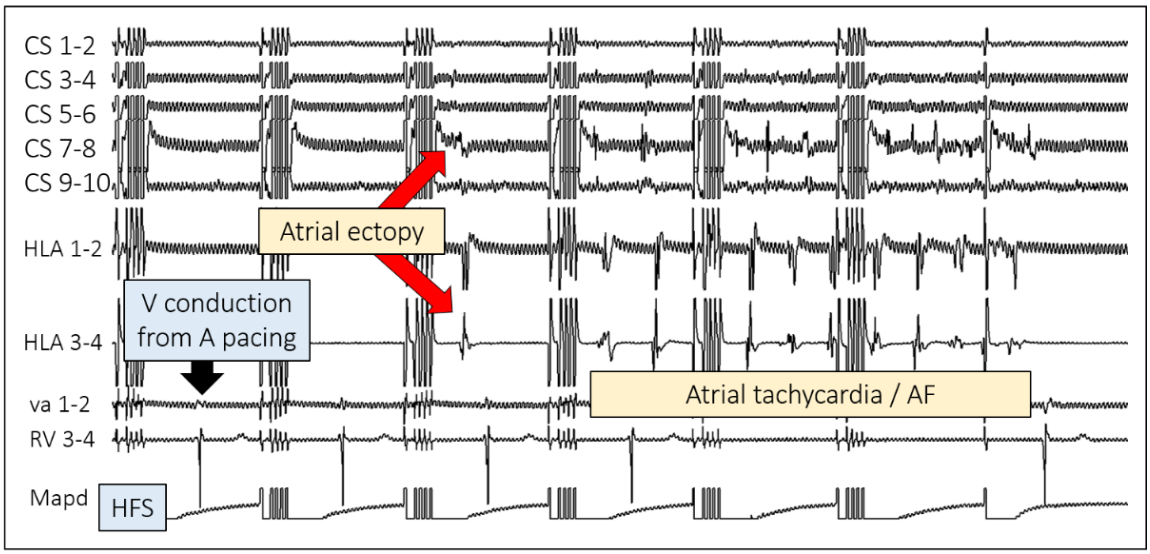

The trace above shows an atrial ectopy that triggered with earliest activation in the CS after the 5th HFS (HFS in this trace starts with the 3rd HFS train) with a coupling interval of 276ms from the pacing stimulus of the HFS train. After the 6th HFS, a short run of atrial tachycardia/AF was triggered with a coupling interval of 244ms from the pacing stimulus of the HFS train with average cycle length 226ms.

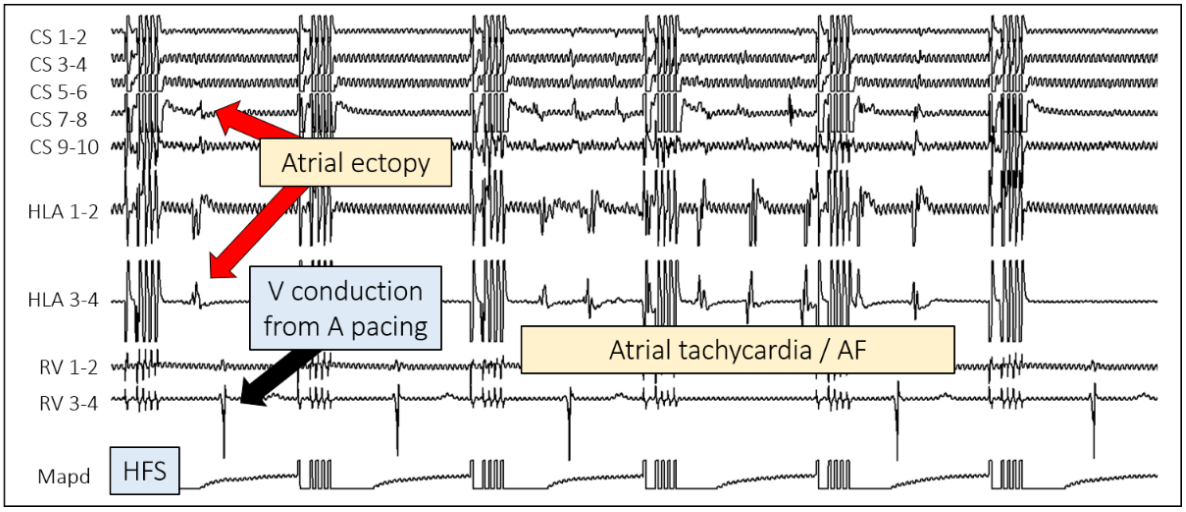

This trace above shows the same anatomical site from the photograph tested with HFS, which triggered atrial ectopy and atrial arrhythmia again. After the 3rd HFS (HFS in this trace starts with the 3rd HFS train), an atrial ectopy was triggered with a coupling interval of 272ms from the pacing stimulus of the HFS train. After the 5th HFS, atrial tachycardia/AF was triggered with the earliest activation from CS 7-8/9-10 with a coupling interval of 284ms from the pacing stimulus of the HFS train. The average cycle length was 220ms.

(AF = atrial fibrillation; CS = coronary sinus; HFS = high frequency stimulation; HRA = high right atrium; Mapd = mapping catheter distal; RV = right ventricle; V = ventricular)

All ET sites and non-ET sites from each porcine heart were dissected and fixed into formalin solution. All 6 ET sites and 6 randomly selected non-ET sites were processed for further histology and immunohistochemistry. 4 ET sites were from the right atrium, and 2 from the left atrium. 2 non-ET sites were from the right atrium, 4 from the left atrium. The anatomical distribution of ET and non-ET sites in the left and right atria was not statistically significant ($p = 0.57$).

8.3.1. Porcine Atrial Tissue Composition

The mean cross-sectional area (CSA) of all tissues (n=12) was 6.6 mm^2 ± 5.4. 9 tissues had similar tissue composition: 59% ± 16 of myocardium, 28.5% ± 6.5 of collagen, and 12.2% ± 9.3 of epicardium. The epicardium contained connective tissue, nerves, vessels and fat. Connective tissue penetrated the myocardium and was often continuous with the epicardium. 3 samples were mostly epicardial fat, 1 of which did not contain any nerves,

and the two others contained 6 and 40 nerves respectively. Excluding these 3 samples, the average proportion of epicardium, myocardium and collagen to the total tissue surface area per sample, was similar in ET and non-ET tissues (Table 8.1).

Table 8.1 Proportion of porcine atrial tissue composition in ET and non-ET sites

Porcine atrial tissue composition	Ectopy triggering (n=6)	Non-ectopy triggering (n=3)	p Value
Epicardium (%)	9 ± 5	18 ± 14.5	0.3
Myocardium (%)	63 ± 12	51 ± 24	0.7
Collagen (%)	28 ± 7	29.5 ± 7	0.9

This table shows the tissue composition of epicardium, myocardium, collagen and nerve in proportion to the total tissue area (%). Values are in mean ± standard deviation. There was no significant difference between ET and non-ET sites.

(ET = ectopy triggering; non-ET = non-ectopy triggering)

Multiple large and small ganglia were identified in the epicardium, surrounded by adipocytes. Smaller nerve bundles were present in the myocardium. These were clearly distinguishable from other tissue structures with the Masson's Trichrome staining (Figure 8.5).

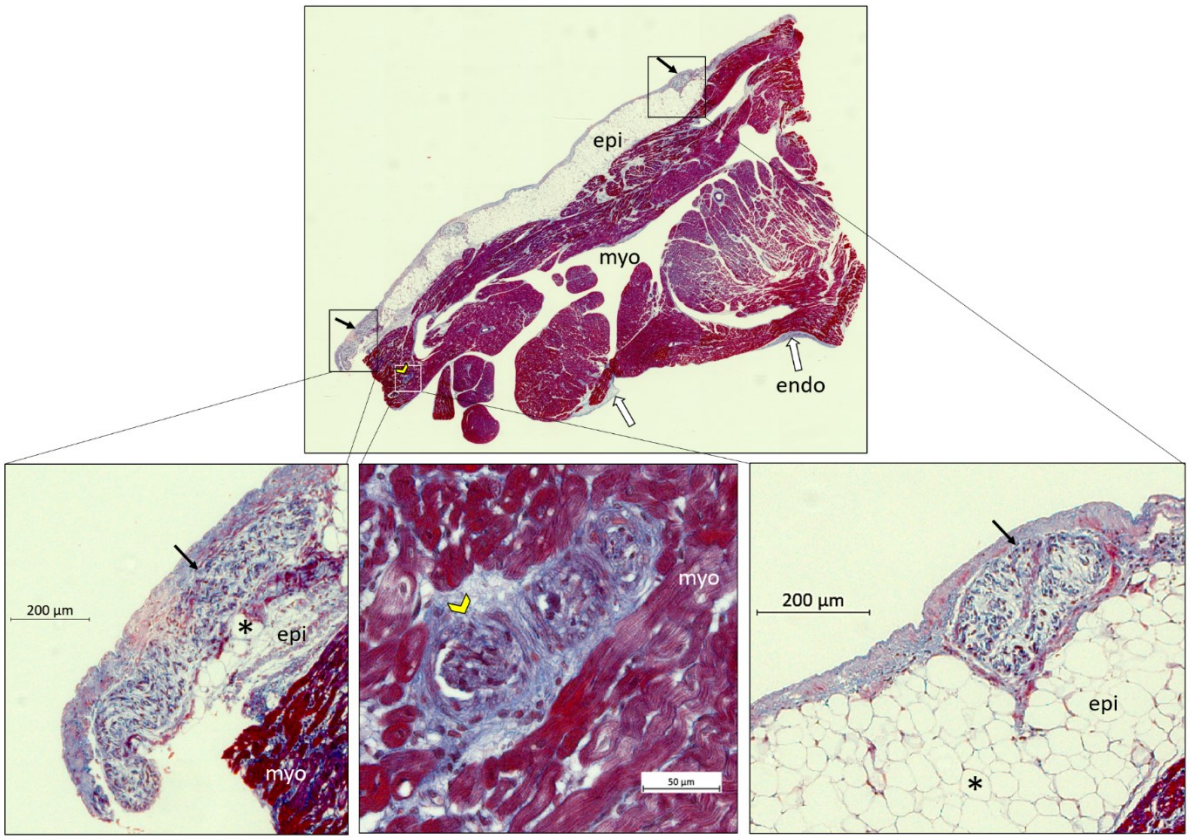

Figure 8.5 Epicardial ganglia and myocardial nerve bundles in an ectopy triggering cross-sectional atrial tissue identified with synchronised HFS

This was a cross-section of a porcine atrial tissue that triggered ectopy with synchronised HFS reproducibly. Anatomically, this site was just posterior to the base of the right atrial appendage. The section was stained with Masson's Trichrome, and the top photograph shows the whole tissue in view.

The Masson's Trichrome stain allowed clear differentiation of nerve tissue from other tissue structures. All nerves (arrows and arrowhead) were stained light to dark purple, always surrounded by dense, light blue connective tissue that represent the epineurium, and multiple nuclei within the ganglia are from schwann cells and fibroblasts. Muscle fibres were stained red, and collagen in the extracellular matrix stained blue. These colours also allowed clear differentiation of the different layers of the atrial wall (epi – epicardium, myo – myocardium, endo (white arrows) – endocardium).

The epicardial layer (epi) was abundant in adipocytes (*). Epicardial ganglia were often the largest nerve tissues in every tissue section (black arrows).

The bottom row shows magnified views of the boxed nerve tissues from the top photograph. The bottom left shows a long-axis view of a large epicardial ganglia (1013 µm x 147 µm), the bottom right shows a short-axis view of a large ganglia (301 µm x 179 µm). In the middle of the bottom row, a short-axis view of small ganglia are shown (195 µm x 101 µm).

(H+E = haematoxylin and eosin stain)

8.3.2. Immunohistochemistry for Phenotyping Nerves

The positive control test for TH and CAT immunoreactivity from a sympathetic trunk and vagus nerves validated our immunohistochemistry methods for detecting both enzymes (Figure 8.6).

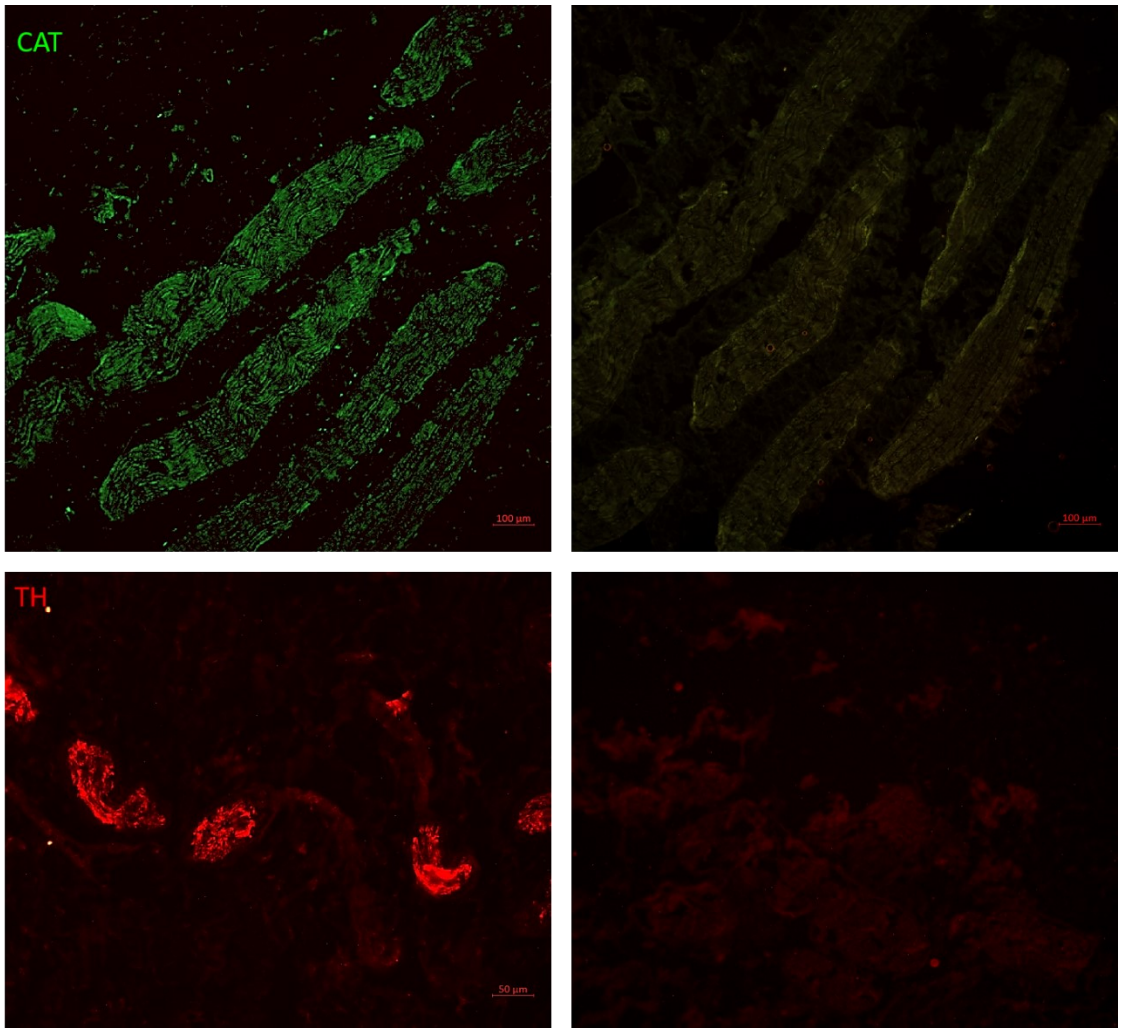

Figure 8.6 Positive controls for tyrosine hydroxylase and choline acetyltransferase detection in porcine nerve tissues

CAT immunostaining was performed on a porcine vagus nerves (top left - green) and TH on porcine sympathetic trunk (bottom left - red) using the same immunohistochemistry technique as we have used in all of our experiments in this study. The nerve structures were strongly immunoreactive to the corresponding enzymes, which validated our immunohistochemistry technique. Photographs on the top right and bottom right are negative controls without any antibodies, absent of any immunofluorescence.

(CAT = choline acetyltransferase; TH = tyrosine hydroxylase)

The total CSA of all tissues examined was 79.5 mm2. 0.8% (0.64 mm2) was nerves, and 45% (0.29 mm2) of the total nerve CSA were immunoreactive to CAT ± TH. This contained 678 nerves, of which 429 (63%) were CAT immunoreactive and 249 (37%) were TH immunoreactive. The average number of CAT and TH immunoreactive nerves per tissue were 36 ± 47 and 21 ± 17, respectively ($p = 0.66$). Although there was no significant difference between the number of TH and CAT immunoreactive nerves, TH immunoreactive nerves were significantly larger than CAT immunoreactive nerves (11.3 mm^2 ± 34.7 vs 2.1 mm^2 ± 5.8; $p<0.0001$). Large TH immunoreactive nerves were often found in the epicardium.

55% of the total CSA of nerves were ganglia and smaller nerve bundles that were non-immunoreactive to TH or CAT. 94% of these non-immunoreactive nerves were in the epicardium.

When comparing density of all nerves that were immunoreactive and non-immunoreactive in the epicardium per mm^2 total tissue area, there was no statistically significant difference between ET and non-ET sites (ET = 2.2 nerves/mm^2 ± 2.5 vs non-ET = 2.6 nerves/mm^2 ± 4.5; $p = 0.31$).

8.3.3. Immunohistochemical Differences in ET and Non-ET Porcine Atrial Tissues

All 6/6 (100%) ET and 5/6 (83%) non-ET sites contained immunoreactive nerves to TH or CAT (Figure 8.7). Small number of nerves were immunoreactive to both enzymes (Figure 8.8).

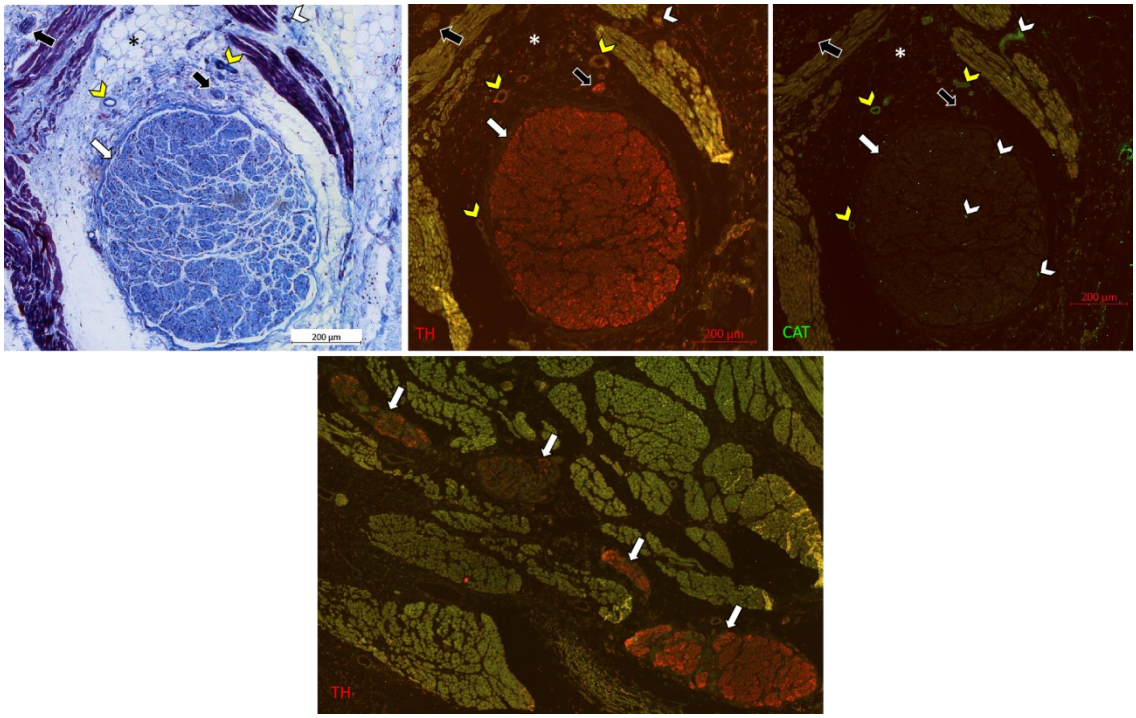

Figure 8.7 A large ganglia that contains mostly adrenergic nerves at a non-ectopy triggering site

This non-ectopy triggering site with synchronised HFS was anatomically located in the inferior border of the left lateral position of the left atrium, near the coronary sinus. The top left photograph shows a cross-section of a large ganglia (white arrow) (695 µm x 590 µm) stained with Masson's Trichrome, with dense and irregular connective tissue surrounding it which are epineurium, and the white-stained perineurium surround each bundle of nerve fibres within the ganglia. Multiple nuclei within the ganglia indicate Schwann cells and fibroblasts. Above the large ganglia, there are several arterioles/venules (yellow arrowheads), differentiated by the smooth muscle cells around them (dark blue) with unstained lumen in the centre. In between the large ganglia and small vessels, there is a small nerve tissue (black arrow), and another in the top left-hand corner (black arrow), and also between the myocardial tissues on the top right-hand corner (white arrowhead). The asterik indicates adipocytes in the epicardium.

The top middle and last photographs show immunoreactivity to TH (red) and CAT (green) respectively. The same ganglia, nerve tissues, and small vessels are labelled as in the top photograph, with immunoreactivity to different antibodies. The large ganglia were mostly TH immunoreactive, there was also some speckled CAT immunoreactivity within the ganglia (white arrowhead).

This indicates that the ganglia were predominantly adrenergic, with very little cholinergic activity. Interestingly, the vessel walls (yellow arrowheads) were immunoreactive to CAT, which may indicate non-neuronal CAT-expressing vascular endothelial cells[218].

The bottom photograph shows other large epicardial ganglia identified in the same non-ectopy triggering tissue, with variable intensity of immunoreactivity to TH, indicating primarily adrenergic ganglia type.

(CAT = choline acetyl transferase; HFS = high frequency stimulation; TH = tyrosine hydroxylase)

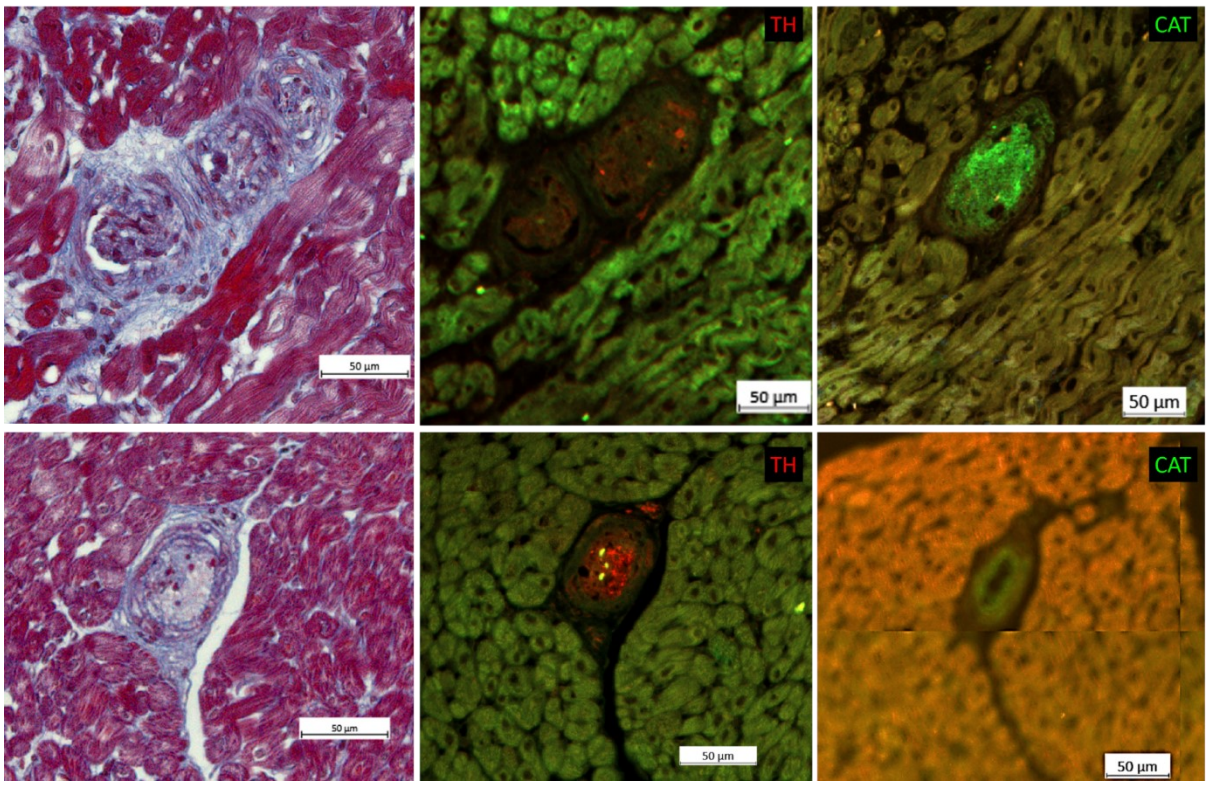

Figure 8.8 Myocardial ganglia immunoreactive to both tyrosine hydroxylase and choline acetyltransferase in an ectopy-triggering site

This atrial tissue was a cross-section taken from a posterior location to the base of the right atrial appendage (same tissue from Figure 8.5). There were multiple small nerve bundles and ganglia like these in the myocardium. The sections were stained as follows from left to right in the following order: Masson's Trichrome, anti-TH antibody (red immunofluorescence), anti-CAT antibody (green immunofluorescence).

The top row ganglia are sister sections that were mostly immunoreactive to CAT than TH. This indicates that these ganglia contain both sympathetic and parasympathetic nerves.

Different ganglia are photographed at the bottom row as sister sections. The CAT-immunoreactivity is confined to a ring shape with a dark lumen in the middle, which correlates anatomically to the thin single layer of epithelial cells in the ganglia stained with Masson's Trichrome. These may be non-neural epithelial cells, which are known to express CAT antibodies[218]. These small ganglia are predominantly adrenergic, with possible non-neural epithelial cells expressing CAT antibodies.

(CAT = choline acetyl transferase; TH = tyrosine hydroxylase)

The nerve density in tissue was defined as the number of nerves per cm^2 of total tissue CSA. There was a significantly greater immunoreactive nerve density in ET compared to non-ET sites (81.2 per cm^2 ± 65.8 vs 34.8 per cm^2 ± 38.5; p = 0.047). There was also greater TH-only nerve density (69.9 per cm^2 ± 54.1 vs 26.1 per cm^2 ± 24.1; p = 0.13) and CAT-only nerve density (92.4 per cm^2 ± 79.4 vs 43.6 per cm^2 ± 49.9; p = 0.24) in ET compared to non-ET sites, trending towards statistical significance (Figure 8.9).

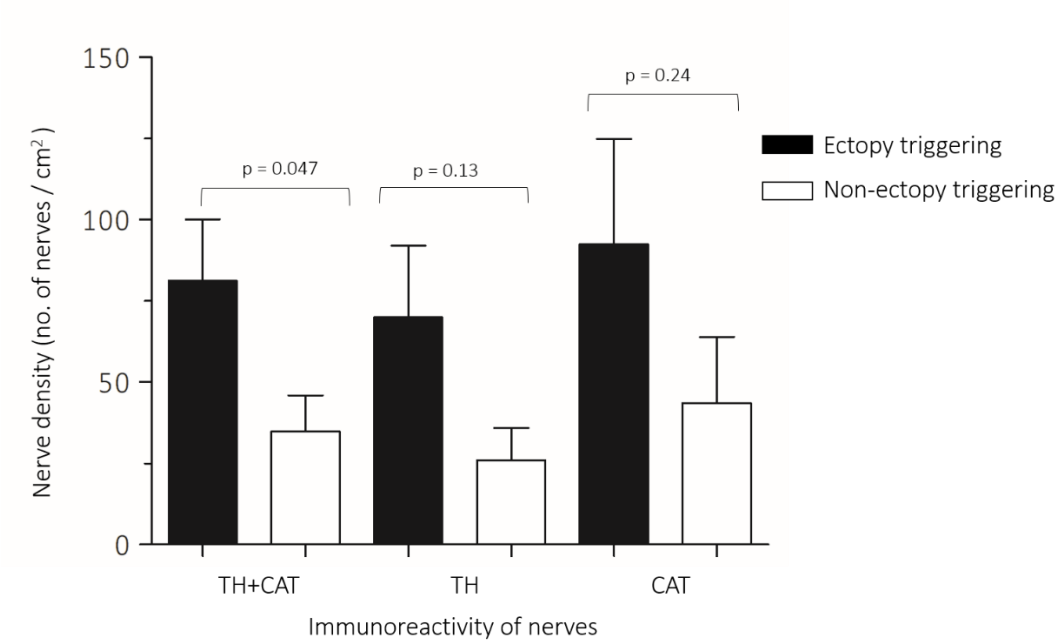

Figure 8.9 Average nerve density in ectopy and non-ectopy triggering tissues

In 4 porcine hearts tested with synchronised HFS, immunohistochemistry was performed on 6 ET sites and 6 non-ET sites, that were immunoreactive to TH and CAT enzymes. Average no. of nerves that were immunoreactive to TH and/or CAT per cm^2 in ET and non-ET tissues were expressed as "nerve density". There was a significantly greater density of immunoreactive nerves in ET compared to non-ET sites (81.2 per cm^2 ± 65.8 vs 34.8 per cm^2 ± 38.5; p = 0.047). There was also greater nerve density in TH only immunoreactivity (69.9 per cm^2 ± 54.1 vs 26.1 per cm^2 ± 24.1; p = 0.13) and CAT only immunoreactivity (92.4 per cm^2 ± 79.4 vs 43.6 per cm^2 ± 49.9; p = 0.24) in ET compared to non-ET sites, trending towards statistical significance.

(CAT = choline acetyl transferase; ET = ectopy triggering; HFS = high frequency stimulation; TH = tyrosine hydroxylase)

ET tissues had significantly smaller CSA of immunoreactive nerves than non-ET tissues (3.0 mm^2 ± 9.3 vs 11.3 mm^2 ± 38.5; p = 0.003). The CSA of TH-only immunoreactive nerves were significantly smaller in ET compared to non-ET tissues (6.0 mm^2 ± 14.6 vs 22.8 mm^2 ± 56.6; p<0.0001), and the CSA of CAT-only immunoreactive nerves were also smaller in ET compared to non-ET tissues, trending towards statistical significance (1.4 mm^2 ± 2.1 vs 3.8 mm^2 ± 10.2; p = 0.06).

The average CSA of TH immunoreactive nerves were significantly larger than CAT immunoreactive nerves, and comparison of ET and non-ET sites demonstrated significantly smaller CSA of TH immunoreactive nerves in ET sites, compared to non-ET sites (6.0 ±14.6 mm^2 vs 22.8 ± 56.6 mm^2; p<0.0001).

The CSA for CAT immunoreactive nerves were also smaller in ET compared to non-ET sites, trending towards statistical significance (1.4 ± 2.1 mm^2 vs 3.8 ± 10.2 mm^2; p = 0.06). Overall, all immunoreactive nerves were smaller in ET sites compared to non-ET sites (3.0 mm^2 ± 9.3 vs 11.3 mm^2 ± 3.9; p = 0.0003).

8.3.4. Non-Neuronal Immunoreactivity to Choline Acetyltransferase

In one ET tissue that contained the ligament of Marshall, non-neuronal immunoreactivity to CAT was abundant within the collagenous extracellular matrix of the myocardium (Figure 8.10), and abundant TH immunoreactive ganglia within the ligament of Marshall.

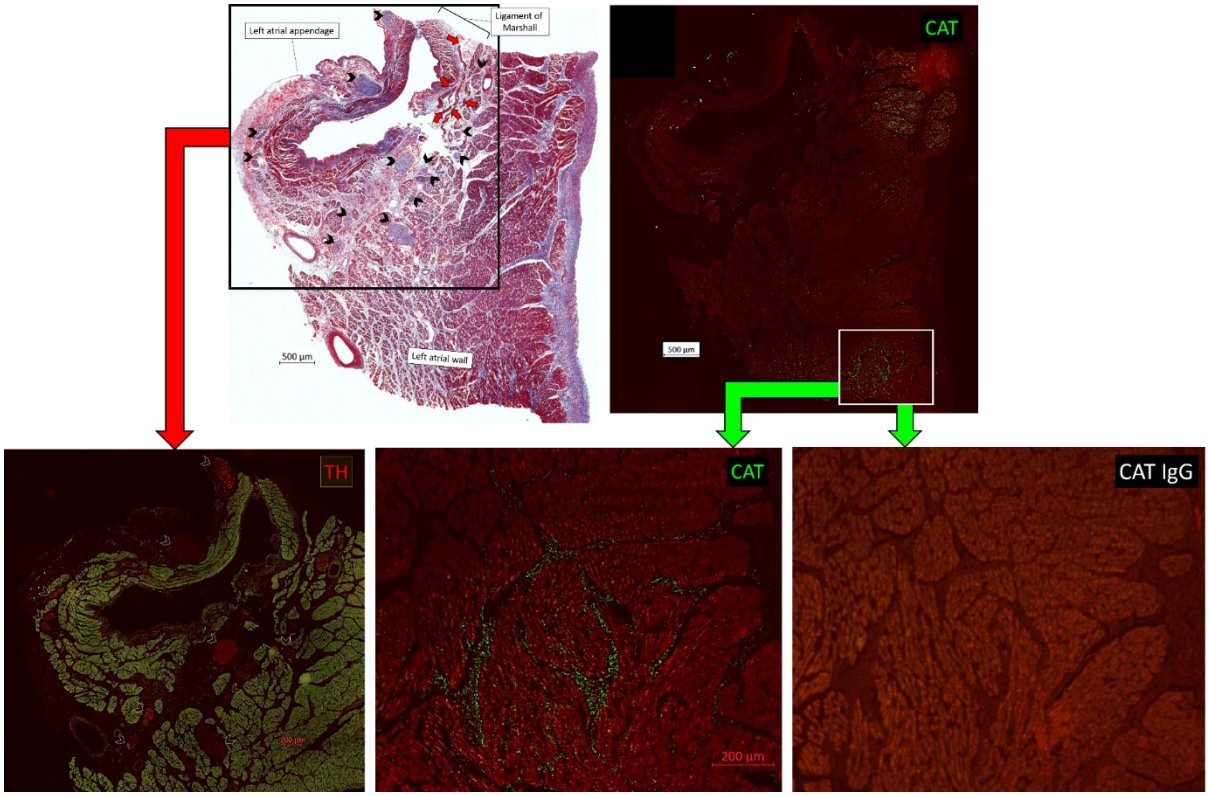

Figure 8.10 Adrenergic ganglia and myocardial non-neuronal cholinergic immunoreactivity in an ectopy-triggering site

This was a cross-sectional section of an ectopy-triggering site with HFS, its anatomical location was at the ligament of Marshall (photograph of its location in Figure 8.4). The top left photograph shows a section stained with Masson's Trichrome. In the large black box, the left atrial appendage tissue is shown. Its epicardium wraps around the surface, containing several large and small ganglia (black arrowheads). The endocardium has the typical folded and irregular appearance of an atrial appendage tissue. The epicardium of the left atrial appendage folds around to meet a fibrofatty tissue, which stretches across the length of the left atrial appendage, containing large ganglia (black arrowheads) and myocardial tracts/Marshall bundles (red arrows). The rest of the left atrial tissue contains myocardium, with dense, collagenous extracellular matrix that runs through the whole tissue (stained dark purple-blue).

The first photograph of the bottom row is a magnified view of the boxed region in the Masson's Trichrome stained tissue. This section was stained with anti-TH antibody, and there were several large and small ganglia with differing immunoreactive intensity (yellow arrowheads). Most ganglia were in the epicardial surface of the left atrial appendage and within the ligament of Marshall. The large ganglia within the ligament of Marshall were mostly absent of CAT immunoreactivity. There were very sparse, small immunoreactivity to TH within the rest of the left atrial myocardium in this tissue.

The top right photograph shows anti-CAT antibody stained sister section, where a lot of dense and speckled CAT immunoreactivity was seen within the collagenous extracellular matrix of the myocardium. A magnified view of one of these regions (white box) is shown in the bottom centre photograph. The bottom right photograph is an IgG isotype control for CAT, which was absent of any immunoreactivity within the myocardium as shown, which excludes non-specific immunoreactivity to the Fc portion of the antibody. This suggests that it is non-neuronal CAT immunoreactivity, which has previously been described in other non-neuronal CAT[219].
(CAT = choline acetyltransferase; HFS = high frequency stimulation; TH = tyrosine hydroxylase)

The tunica media layers of vessels were also strongly immunoreactive to CAT in most tissues (Figure 8.11). These may be non-neuronal cholinergic cells expressing CAT locally[218,220], as the non-specific primary antibody binding was excluded from the IgG isotype control test for anti-CAT.

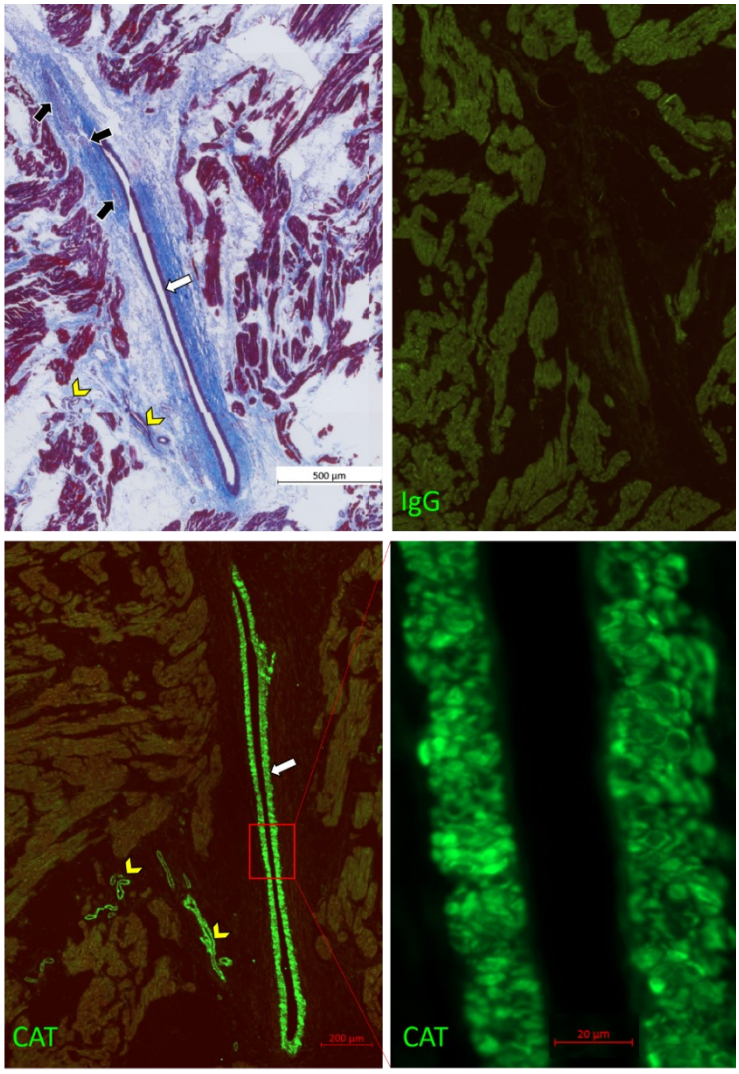

Figure 8.11 CAT immunoreactive venous wall

These photographs were taken from an ectopy-triggering tissue tested with HFS. Anatomically, the tissue was taken from the right atrial posterior wall near the right atrial appendage. The top left shows a Masson's Trichrome stained section, where a large vein is visible with a squashed longitudinal lumen, surrounded by dark purple stained tunica media (white arrow) and collagenous tunica adventitia outside (blue). Smaller venules are marked by yellow arrowheads to the left of the large vein. Superior to the large vein are three discrete ganglia in various sizes (black arrows). In a sister section (not shown), the small ganglia superior the large vein were only immunoreactive to TH.

In the bottom left, a sister section of the tissue was stained for anti-CAT antibodies, where all vessels are immunoreactive (green). A magnified view of the large vein is on the bottom right hand corner, which clearly shows the tunica media layer of the vein; stacked smooth muscle cells with dark nuclei within them. The IgG isotype control for CAT is on the top right hand corner, which shows no immunoreactivity to any of the structures. Control for secondary antibody was also negative. This suggests that these are non-neuronal CAT expressing endothelial cells.

(CAT = choline acetyltransferase; HFS = high frequency stimulation; TH = tyrosine hydroxylase)

There was no statistical difference in the presence of non-neuronal cholinergic activity between ET and non-ET tissues (4 ET tissues vs 2 non-ET tissues; $p = 0.57$).

8.3.5. Non-Immunoreactive Nerves

55% of the total CSA of nerves were ganglia and smaller nerve bundles that were absent of any immunoreactivity to TH or CAT 94% of these non-immunoreactive nerves were in the epicardium.

8.4. Discussion

We performed synchronised HFS to identify ET sites in porcine hearts to understand what underlying immunohistochemical features of local HFS lead to atrial ectopy or atrial arrhythmia, as we observed in our clinical studies. HFS was also performed directly over the epicardial surface of porcine atria, known to contain abundant ganglia, and other atrial structures (e.g. right atrium and atrial appendages) that were difficult to test in the clinical studies.

8.4.1. The Independent Intrinsic Cardiac Autonomic Nervous System

We showed that reproducible atrial ectopy and non-sustained atrial arrhythmia triggered in 4 of 6 decentralised, Langendorff-perfused porcine hearts. Previously, decentralised Langendorff-perfused canine hearts showed that GP stimulation significantly shortened the atrial effective refractory period (AERP) including the pulmonary veins[217]. These findings suggest that the local intrinsic nerve stimulation triggers atrial arrhythmia independently of the external autonomic nervous system influences, and can be more specifically targeted.

8.4.2. The Porcine Atrial Intrinsic Cardiac Autonomic Nervous System

Previous topographical studies of the porcine heart revealed that majority of the GP (91%) were in the atria, the densest collection of ganglia and neurones in the dorsal atrial

surface[221,222]. However, the studies exclusively stained for the epicardial ganglia with acetylcholinesterase and did not quantify nerves within the myocardial or endocardial layers. In this study, majority of large ganglia were in the epicardium, but there were numerous smaller ganglia and nerves within the myocardium. Both TH and CAT were used to quantify adrenergic and cholinergic nerves respectively. This revealed that epicardial ganglia were predominantly adrenergic and significantly larger than cholinergic nerves, and the latter were predominantly found within the myocardium. Preferential adrenergic or cholinergic expression of nerves was also previously reported in the ventricular ganglia of porcine hearts[223], where 70-80% of the ganglia were exclusively CAT immunoreactive.

8.4.3. Ectopy-Triggering Ligament of Marshall with HFS

One of our ET tissues included the ligament of Marshall, which was anatomically identified near the left atrial appendage base of the posterior wall, and histologically characterised by the multiple TH immunoreactive ganglia, surrounded by fibrofatty tissue, with muscular Marshall bundles. There was minimal CAT immunoreactivity within the ganglia themselves. This was consistent with the findings by Rahul *et al*[224] in isolated-perfused canine left atrium after long-term pace induced AF.

We also found dense and diffuse CAT immunoreactivity coursed through the myocardial extracellular matrix that joined the endocardium. Similarly, in another study with normal atria without AF, predominantly CAT-immunoreactive nerves were identified in the ligament of Marshall. This suggests a change in the neural phenotype of ganglia from cholinergic to adrenergic ganglia with increased burden of AF. The diffuse and dense extracellular CAT-immunoreactivity observed in the ET ligament of Marshall in our study

may have been part of the feedback loop to counterbalance the adrenergic response of the TH immunoreactive ganglia to HFS.

8.4.4. Differences in Nerves at Local Site of ET and Non-ET Tissues

The density of epicardial nerves (immunoreactive and non-immunoreactive to CAT or TH) were not significantly different between ET or non-ET tissues. However, the density of TH and CAT immunoreactive nerves across the whole tissue (epicardium, myocardium, endocardium) was significantly greater in ET compared to non-ET tissues. This suggests that atrial ectopy or arrhythmia triggered by HFS is due to high density of adrenergic and cholinergic nerves at the local site of stimulation, or higher density of CAT and TH enzymes are released from similar density of nerve endings. Interestingly, despite adrenergic nerves being significantly larger than cholinergic nerves across all tissues (ET or non-ET), ET tissues contained significantly smaller adrenergic nerves compared to non-ET tissues. Atrial ectopy or arrhythmia triggered with local epicardial HFS may be dependent on the overall density of smaller nerve bundles across whole atrial wall.

8.4.5. Choline Acetyltransferase in Neuronal and Non-Neuronal Structures

ACh serves as the principal neurotransmitter mediating fast synaptic neurotransmission at the preganglionic junction by both the sympathetic and parasympathetic nervous systems. It has also been shown to increase spontaneous ectopic activity and AF inducibility in animal models without electrical stimulation[225,226]. Therefore, we used one of the most reliable markers for cholinergic function - CAT, a biosynthetic enzyme that is responsible for the synthesis of ACh to quantify parasympathetic nerves and their stimulation effect in atrial ectopy induction in porcine hearts. Porcine hearts are known to be abundant in parasympathetic nerves, particularly in the atria. Nerve density was

reported to be the greatest in the endocardium than the epicardium[227] but our study showed that majority of CAT immunoreactive nerves were in the myocardium.

Interestingly, there were non-neural structures within the epicardium and the myocardium including cardiomyocytes, extracellular matrix, tunica media layers of vessel walls that were strongly immunoreactive to CAT. This was consistent across all tissues. These were attributed to non-neuronal cholinergic cells that express CAT for local ACh synthesis[218,220]. Non-neuronal cholinergic system act in an autocrine/paracrine fashion to amplify neuronal cholinergic signalling and thereby protect the heart from sympathetic hyperactivity-induced cardiac remodelling and dysfunction, such as in myocardial infarction and heart failure[223]. It is possible that in our porcine hearts, the non-neuronal cholinergic activity was heightened by progressive heart failure during Langendorff-perfusion, and myocardial ischaemia from explantation.

8.4.6. Tyrosine Hydroxylase in Neuronal Structures

Noradrenaline is the principle neurotransmitter of the sympathetic postganglionic nerve fibres supplying the heart[229]. Adrenergic stimulation modulate Ca^{2+} and action potentials[230,231] that lead to atrial arrhythmias. TH catalyses the initial and rate-limiting step in the biosynthetic pathway of catecholamines including noradrenaline, and adrenaline within the postganglionic nerve terminals[232]. Therefore, TH immunoreactivity is commonly used as a marker of sympathetic innervation. In this study, the density of TH-immunoreactive nerves was greater in ET compared to non-ET tissues, but this was not statistically significant. Most of our TH immunoreactive nerves were in large epicardial ganglia, and in smaller peri-vascular nerve bundles which is consistent with previous findings[156,233–235].

8.4.7. Clinical Implication

In conventional pulmonary vein isolation (PVI) procedures for AF, a good transmural lesion is thought to be an important determinant to achieving durable PVI and long-term AF freedom[116,236]. Previously, in this thesis, we showed that discrete and local endocardial cluster ablation of ET sites lead to similar 12-month AF freedom as PVI (Chapter 5). Sometimes, ablation of ET sites during sustained AF acutely terminated AF to normal sinus rhythm (Chapter 7). In histopathological studies examining ablation lesions from PVI, atrial tissues were replaced by fibrosis, muscles and nerves destroyed in the myocardium[116,237]. In this chapter, we showed that transmural nerve density and cholinergic and adrenergic nerve activities were increased in ET compared to non-ET sites. This suggests that ET response with synchronised HFS is indeed due to local nerve stimulation, and endocardial radiofrequency (RF) energy application at local ET sites destroy nerves that are abundantly located in the myocardium. Indeed, re-testing adequately ablated ET sites abolished further atrial ectopy or arrhythmia with synchronised HFS. Even if epicardial ganglia are not directly destroyed from endocardial ablation, damage to the smaller postganglionic nerves within the myocardium are thought to retrogradely destroy the epicardial ganglia in communication[88], and reducing the overall density of nerves with or without epicardial ganglia destruction is enough to prevent AF.

8.4.8. Study Limitations

There are number of important limitations to this study. Time taken to dissect and fix the tested tissues in formalin varied between samples and hearts. Testing of the first anatomical site to the last had up to an hour elapsed between them. Therefore, although topography of the intrinsic cardiac nerves was preserved, TH and CAT are rate-limiting

biosynthetic enzymes and their activity increases with neuron depolarisation via nerve stimulation[238,239]. Absence of continuous nerve stimulation between testing and fixing tissues may have affected their concentrations, subsequently their immunoreactivity. However, it is not clear how the absence of the extrinsic cardiac nervous system regulates their activity.

Over time, the porcine hearts became progressively more oedematous, and develop heart failure with poor atrial and ventricular contractions. This change in physiology of the failing hearts may have influenced the propensity to trigger atrial arrhythmia with HFS, alter the intrinsic nerve activity, and consequently TH and CAT enzyme levels. However, despite these limitations, there were significant electrophysiological and immunohistochemical differences between ET and non-ET tissues.

In the clinical setting, HFS testing was spaced 6-8mm away from each other, and much more densely mapped; approximately 80 sites tested on average per patient. Due to time limitation, we did not test as densely in this study, and our testing was spread throughout both left and right atria. Therefore, the number of ET sites we identified is likely a significant underestimation.

We cannot exclude the possibility of mechanical irritation with catheter contact triggering atrial ectopy or arrhythmia. However, we re-tested ET sites several times with HFS to show reproducibility. Furthermore, ET sites had significantly increased TH and CAT immunoreactivity than non-ET sites, which suggests that ET response from HFS is due to nerve stimulation.

Results of this study are derived from the 4-6 μm thick cross-section of the atrial wall. Epicardial ganglia are interconnected nerves that form a larger network of ganglionated plexuses (GP) that have influence on distant anatomical structures as well as the local site

of stimulation[170]. Therefore, stimulation of the local ganglia with HFS is likely to communicate with larger number of ganglia and nerves elsewhere in the atria. Our results reflect only the local effects and nerve quantification from epicardial HFS.

Our sample size was small, which likely contributed to some results not reaching statistical significance, despite strong trends.

8.5. Conclusions

Epicardial synchronised HFS, without direct myocardial excitation, stimulate the intrinsic cardiac nerves and reproducibly trigger atrial ectopy and non-sustained atrial arrhythmia in isolated Langendorff-perfused porcine hearts.

The ET response was attributed to significantly increased local density of nerves that were transmurally across all layers of atrial tissue, and the CSA of sympathetic nerves were significantly smaller than in non-ET sites. These local differences may account for the differential functional response to HFS and may apply to the clinical setting.

Further studies with larger numbers are required to validate these novel findings.

9. DEVELOPMENT OF A NOVEL NEURAL STIMULATOR: TAU-20

9.1. Introduction

For the past two decades, Grass stimulators have been used to map and target the cardiac nerves by performing high frequency stimulation (HFS) in mammalian and human hearts. There are no other stimulators capable of delivering stimuli to detect and map the cardiac autonomic nervous system. However, the Grass stimulator has many functional limitations, including its inability to measure tissue impedance, delivering current stimuli with unknown and variable amplitude and temporal profile. The Grass stimulator also uses analogue dials which are prone to inaccuracies when inputting stimuli parameters. Its manual-only operation calls for considerable expertise and experience in autonomic studies. Therefore, we developed a new and improved cardiac stimulator; Tau-20 to address these limitations and with useful additional features (Figure 9.1).

The Tau-20 is an external cardiac stimulator and intracardiac electrogram recorder hybrid instrument featuring up to 24 recording channels and one bipolar stimulation channel; intended to be used for acquiring and delivering signals to cardiac catheters respectively. It is capable of delivering finely controlled output against variable tissue impedance, perform all basic pacing manoeuvres commonly used in clinical electrophysiology studies, and deliver protocolised HFS. It also features a digitalised graphical user interface (GUI) with a QWERTY keyboard for controls which is more intuitive to use compared to the Grass stimulator.

The Grass stimulators are no longer purchasable in Europe and does not comply with the Restriction of the use of certain Hazardous Substances (RoHS). However, the Tau-20 complies with strict safety and isolation regulations (Europe IEC/EN 60601-1 3rd Ed.).

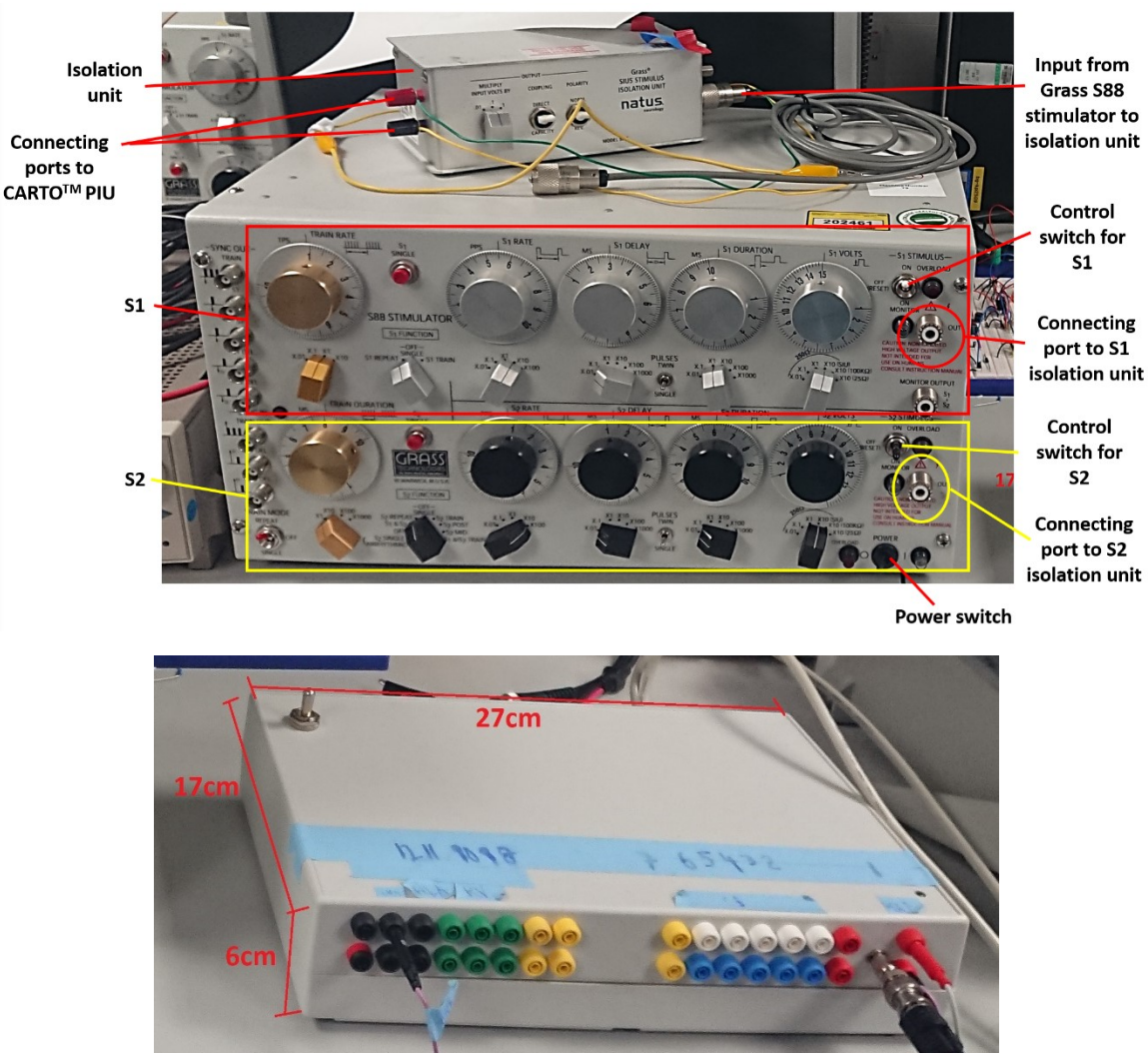

Figure 9.1 The Grass S88 stimulator and the newly developed Tau-20 stimulator

The top instrument is the Grass S88 stimulator with analogue dials and switches to operate two stimuli outputs (S1, top; S2, bottom). The bottom instrument is the newly developed Tau-20 stimulator with in-built 24 channels to directly plug in connectors from catheters for recording and stimulation, and a USB port to plug into the graphical user interface on a laptop for controls to operate the hardware.

9.2. The Tau-20 in Whole Live Pig

The Tau-20's functionality was first tested in isolated pig hearts in Chapter 8, then tested for safety in a whole live pig. A whole pig (approximately 45kg) under general anaesthesia was used to test the Tau-20 The experimental electrophysiology lab was set-up as close as possible to the human clinical lab

Figure 9.2 Experimental electrophysiology lab set-up with whole live pig.

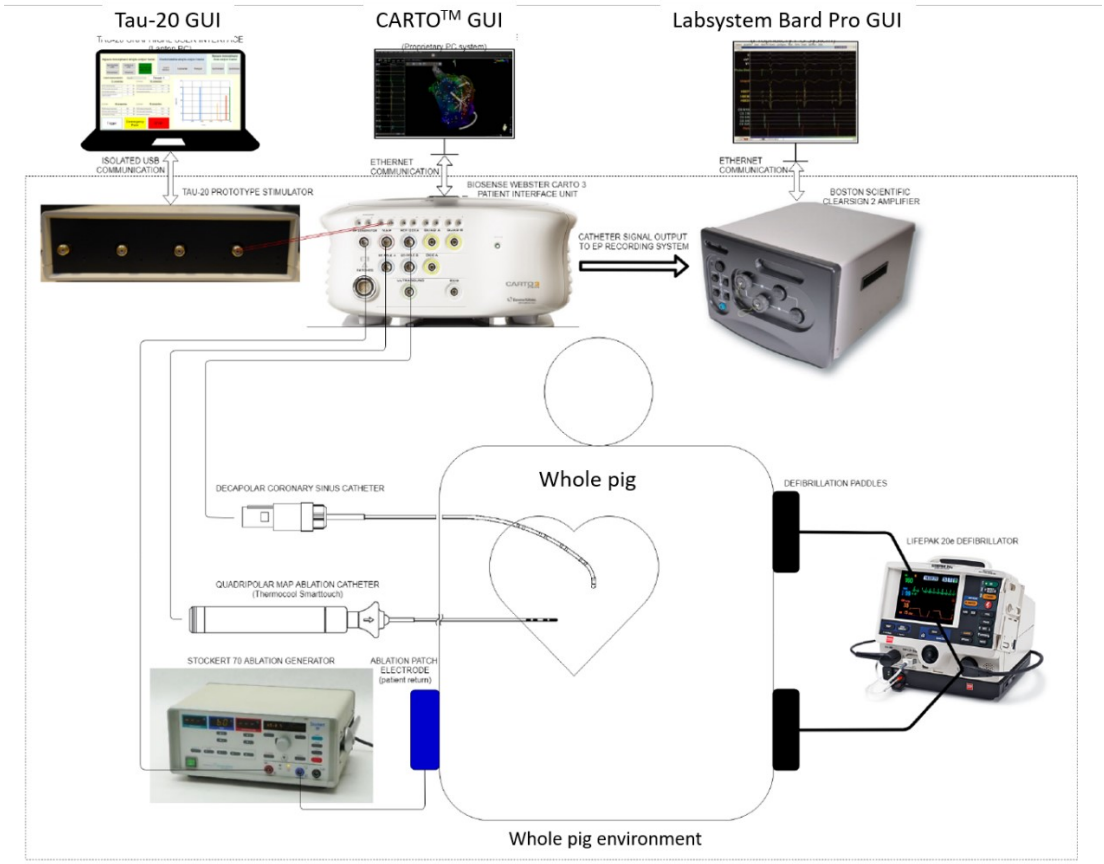

A whole pig under general anaesthesia was used to replicate a real clinical scenario with the same equipment used in patients for Tau-20 testing.

The Tau-20 Graphical User Interface (GUI) was operated on a laptop which was connected directly to the Tau-20 stimulator via a USB port, and the Tau-20 was connected to the CARTO PIU station which communicated with the Bard station. The RF ablation generator was connected to the CARTO PIU station.

The Tau-20 stimulator output was routed to both MAP distal electrodes via the "direct connection pair" of inputs of the CARTO 3™ system, providing, zero-ohm, electrical contact between the stimulator output and catheter electrodes. CS and Map (ablation) catheter signals were acquired using the BARD/Boston Scientific LabSystem Pro EP recorder, also connected through the CARTO™ system. The RF output lead of a Stockert 70 RF generator was connected to the "RF generator" plug on the CARTO PIU, with ablation energy being routed to the MAP1 electrode. A single skin patch electrode was attached for ground of RF signals with three more skin patches placed on the whole pig to enable 3D navigation of both catheters in the atrium using the CARTO 3™ system (Figure 9.2).

Femoral venous access was achieved with a 7Fr and 8Fr sheaths in the right groin. A decapolar catheter was inserted into the coronary sinus and a 3.5mm tip quadripolar ablation catheter was used for mapping of the right atrium, HFS and ablation. CARTO 3™ system was used for 3D anatomic mapping of the right atrium. To reduce the risk of inducing ventricular arrhythmia, mapping and ablation were limited to the right atrium only. At stable positions in the posterior wall of the right atrium, pacing, HFS and ablation were performed. Firstly, a pacing threshold was identified for atrial capture, followed by synchronised and continuous HFS stimulation and drive trains up to two extras (Figure 9.4).

Figure 9.3 Pacing and HFS with Tau-20 in whole pig

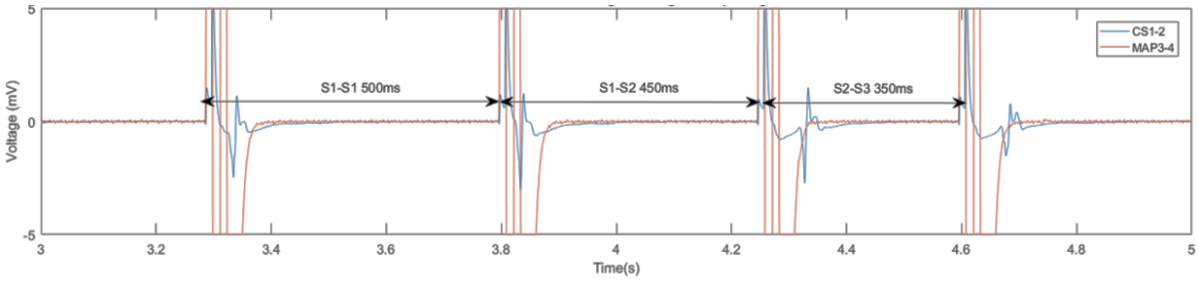

The Tau-20 successfully delivered a drive train up to two extras (S1-S3) at 500ms, 450ms and 350ms. The trace above shows an overlap of the intracardiac recording from CS and MAP.

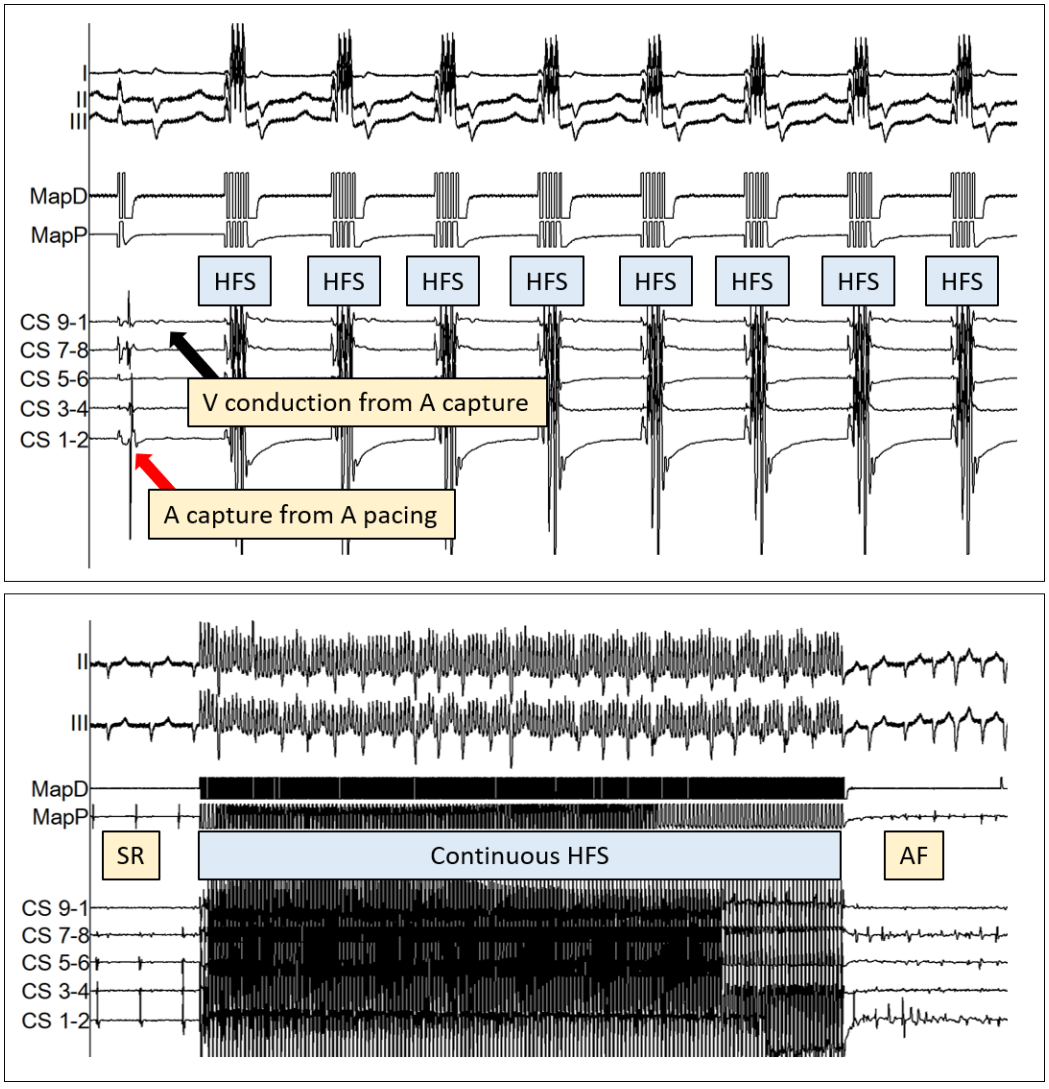

The Tau-20 also successfully performed synchronised HFS (middle) and continuous HFS (bottom). The middle trace shows the first beat that is paced from the right atrium followed by 8 short bursts of HFS without inducing any atrial arrhythmia. The bottom trace shows continuous HFS during sinus rhythm, which initiates AF due to direct myocardial capture. There is no significant AV dissociation and AF is sustained after stopping HFS. (AF = atrial fibrillation; HFS = high frequency stimulation)

Finally, RF ablation was delivered at various power settings for 60 seconds with the stimulator powered on and directly connected to the MAP1 and 2 contacts (Figure 9.4). 360J DC cardioversion was also performed with the Tau-20 connected to the CARTO PIU ports, and pacing protocols repeated thereafter. The stimulator and all other equipment remained fully functional after defibrillation.

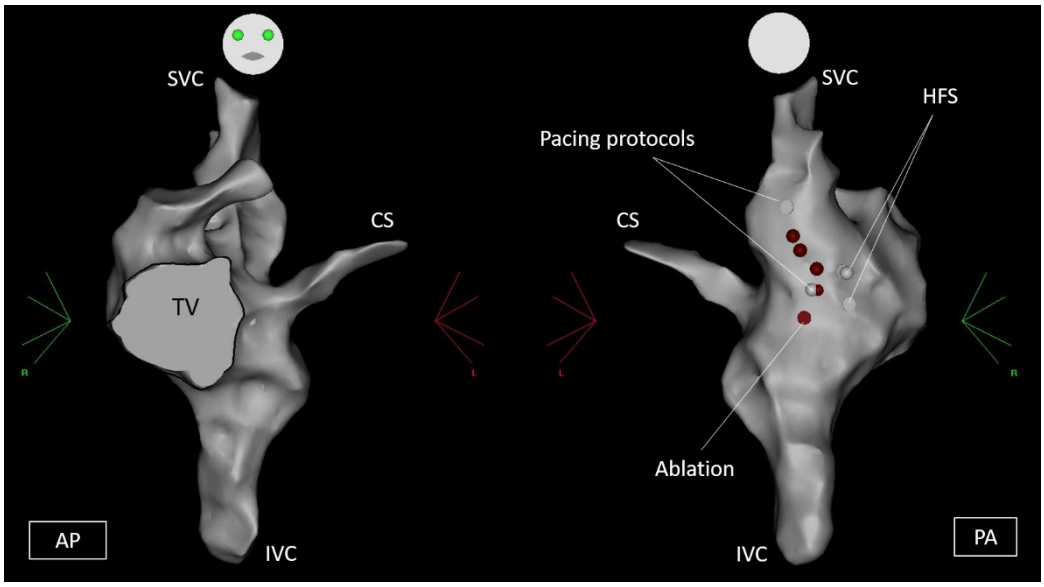

Figure 9.4 3D electroanatomic map of the right atrium in whole pig

HFS and pacing protocols were performed in the posterior right atrium of the whole pig. Red indicates ablation, white indicates pacing or HFS.

(AP = anterior posterior; CS = coronary sinus; HFS = high frequency stimulation; IVC = inferior vena cava; PA = posterior anterior; TV = tricuspid valve; SVC = superior vena cava)

9.3. The Tau-20 in Humans

The animal data with Tau-20 were reviewed independently by an electrophysiologist, who concluded that the stimulator may be tested in the clinical setting with patients. Safety considerations included evaluation of power used with the Grass stimulator, which is up to 0.5W; which is intermediate between the power used for traditional pacing (<0.01W) and that delivered during ablation (up to 60W). To date, clinical studies using

HFS delivered by the Grass stimulator have not shown any evidence of cardiac tissue injury. The Tau-20 has been designed to reproduce the HFS stimulus train that is already being safely delivered in patients using the Grass stimulator, and no tissue injury was observed with direct application of HFS on the surface of the Langendorff perfused whole pig hearts in Chapter 8. In addition, the electrical input into Tau-20 is via an external 12V DC transformer and is therefore isolated from the mains. The maximum output of Tau-20 is 15V (150mA) giving a maximum possible power output of 2.25W. During usual clinical use, the power output will be considerably less than this, and it was assumed that no significant tissue injury will occur at these levels.

Three patients were recruited to test the Tau-20 stimulator. All patients gave written informed consent and the study had ethics approval from the Health Research Authority and the Local Research Ethics Committee. The Tau-20 was used to test basic clinical electrophysiology pacing protocols and HFS. Peri-procedural investigations, equipment and catheters used during the procedures were the same as described in Chapter 2.

The first patient had previous GP ablation and required repeat ET-GP ablation and PVI. At the start of the procedure and before transseptal puncture, the ablation catheter was moved to the high right atrium to perform basic right atrial pacing with the Tau-20 stimulator. This confirmed atrial capture. Pacing amplitude and rate were adjusted using the Tau-20 control software (Figure 9.5).

Pacing GUI

Synchronised HFS GUI

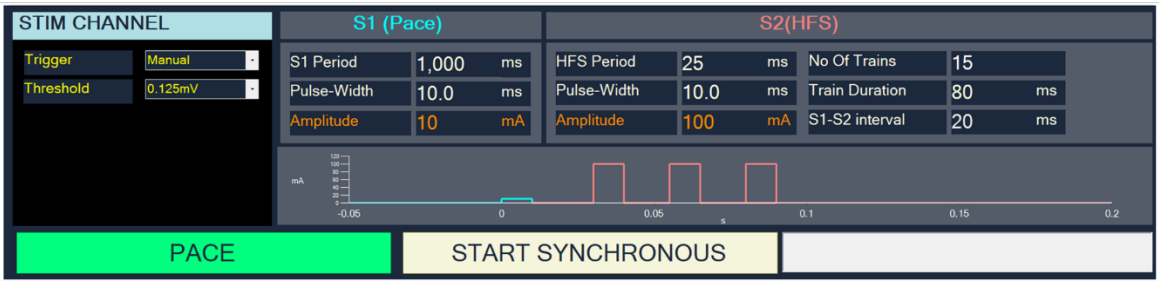

Continuous HFS GUI

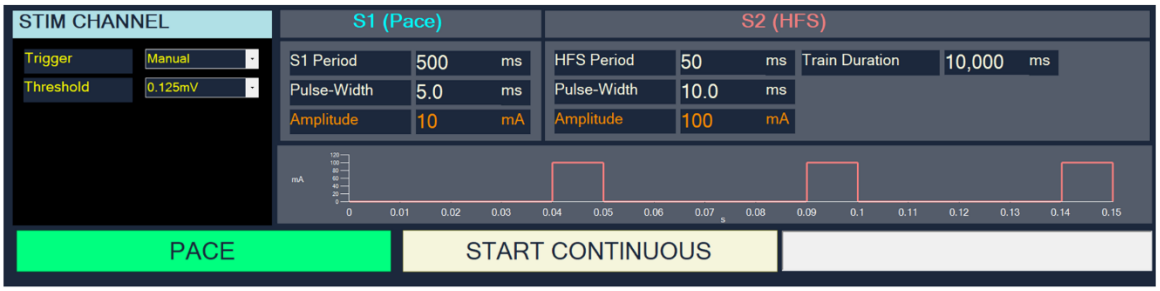

Figure 9.5 Graphical user interface for basic pacing and HFS protocols in Tau-20

The top screenshot shows the whole GUI on a laptop software used for basic pacing protocols, up to three extra-stimuli (S1-S4). Yellow boxes indicate currently activated stimuli. The parameters within boxes can be changed using a keyboard. To activate a protocol, a green box (e.g. “S1-S4 START”) is pressed, then the keyboard space bar held down to pace. Similarly, the bottom two screenshots show synchronised and continuous HFS pre-sets, that are activated and operated the same as the basic pacing protocol.

After transseptal puncture, the patient underwent synchronised HFS mapping protocol as detailed in Chapter 2. The pre-set for synchronised HFS was used on the Tau-20 control software in a laptop. A mouse-click over the "synchronised HFS" button activated the protocol, and the space bar of the keyboard was held down to deliver up to 15 trains of synchronised HFS. The first four beats were paced stimuli to check for ventricular capture, followed by 15 trains of synchronised HFS in total. Letting go of the spacebar immediately stopped pacing and HFS (Figure 9.5).

After completing synchronised HFS mapping, we performed circumferential PVI for all PVs, and confirmed entrance and exit PV block. The Tau-20 was completely disconnected from the CARTO™ PIU during ablations for extra precaution. All remaining ET-GP were ablated and re-tested with HFS to check for no further ectopy or AF.

The first patient had previous ET-GP ablation. 71 sites were tested with synchronised HFS in the left atrium. This identified 40 (56%) ET-GP, where most were located around the PV ostia and mid anterior wall (Figure 9.6).

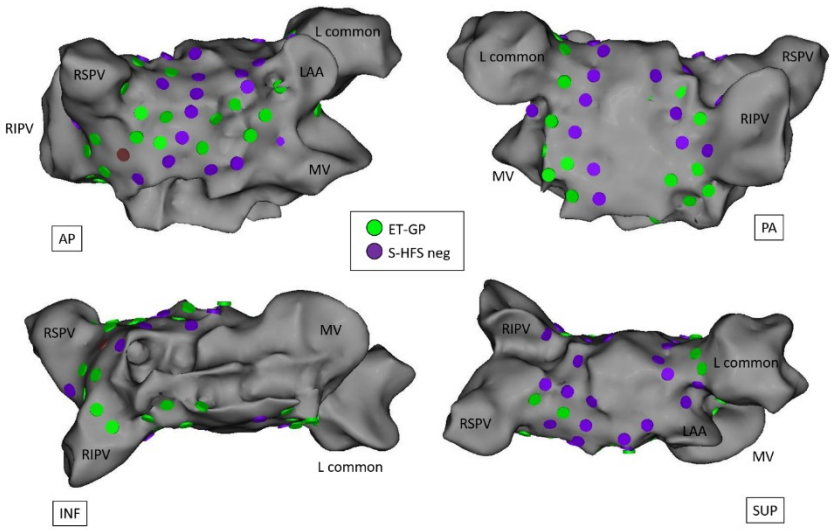

Figure 9.6 ET-GP and negative HFS sites tested with Tau-20 stimulator

This patient had previous GP ablation as part of the multi-centre GP ablation study. We re-tested previously ablated GP sites with Tau-20 stimulator, which identified large number of ET-GP surrounding the pulmonary veins and across the anterior wall. Green dots represent ET-GP and purple dots represent negative HFS sites.

(AP = anterior posterior; ET-GP = ectopy triggering ganglionated plexus; INF = inferior; LAA = left atrial appendage; L common = left common pulmonary vein; MV = mitral valve; PA = posterior anterior; RIPV = right inferior pulmonary vein; RSPV = right superior pulmonary vein)

Stimulation of ET-GP triggered single atrial ectopy, AF/AT, with or without AV block (Figure 9.7). All ET-GP were ablated and re-tested with synchronised HFS using Tau-20. No further atrial ectopy or AF/AT were triggered. The patient developed a minor groin haematoma from vascular punctures but had no other complication.

Figure 9.7 Atrial ectopy with and without AV dissociation with synchronised HFS using Tau-20 stimulator

Testing HFS at two different ET-GP sites in the same patient are shown below. The Mapd signals are absent as HFS is being delivered through this channel via CARTO™.

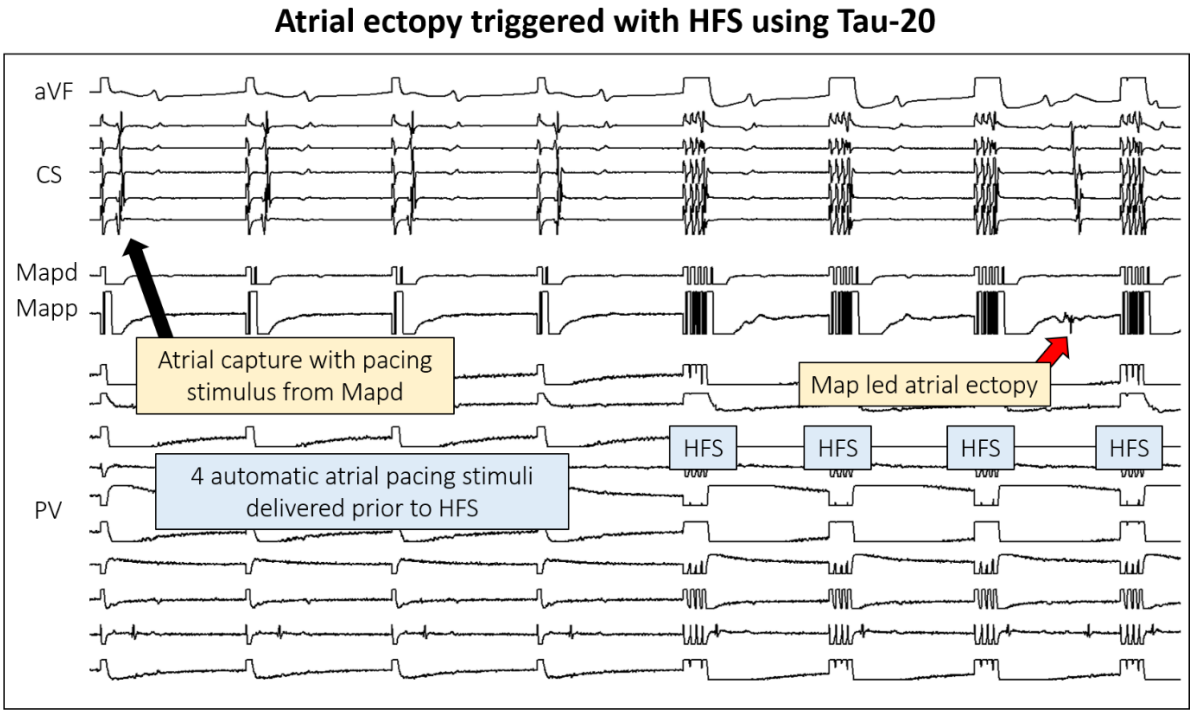

In the trace above, the Map catheter position was in mid anterior left atrial wall, and the Lasso PV catheter was positioned in the left superior pulmonary vein. The first four pacing stimuli were automatically delivered by Tau-20 as part of the synchronised HFS protocol. This confirmed atrial capture and no ventricular capture. After the 3rd train of HFS, an atrial ectopy was triggered, the earliest activation in Mapp. This was a reproducible finding.

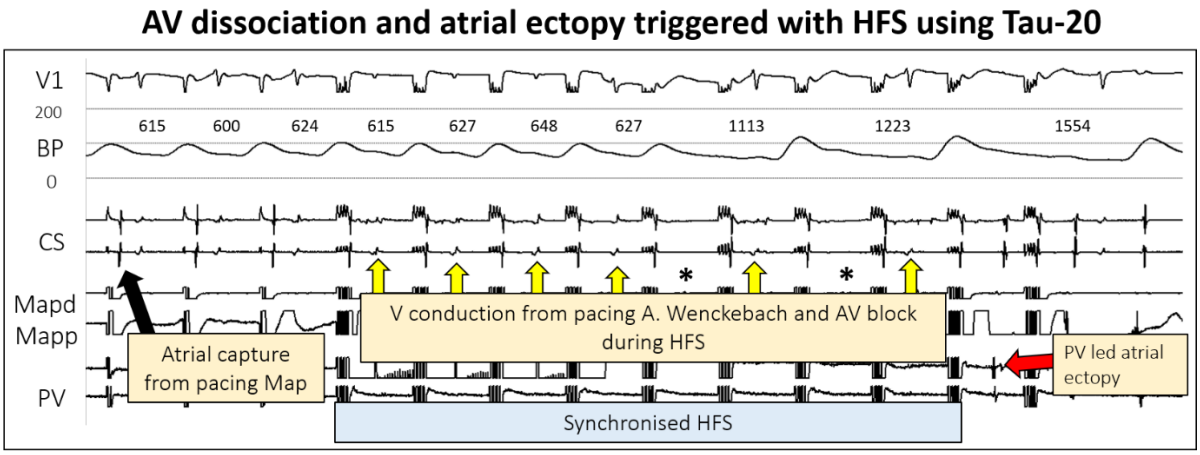

In this trace, the Map catheter position was in lower right border of the left atrial posterior wall. The Lasso was positioned in the right inferior pulmonary vein. During high output pacing from Mapd, there was no Wenckebach. However, with the onset of synchronised HFS, Wenckebach occurred until complete AV block after the 5th train of HFS (*). Yellow arrows indicate ventricular conduction from each pacing stimulus. The numbers above the BP trace are in milliseconds and demonstrate the prolonging RR interval. After the 9th train of HFS, PV led atrial ectopy is triggered. This is an example where the GP site displays both ET and AV dissociating characteristics to neural stimulation.

(AV = atrioventricular; CS = coronary sinus; ET-GP = ectopy triggering ganglionated plexus; HFS = high frequency stimulation; Map = mapping catheter distal; Mapp = mapping catheter proximal; PV = pulmonary vein)

The second patient had redo PVI and cavotricuspid isthmus ablation. At the end of the procedure, the Tau-20 stimulator was used to perform a simple drive train with one extra-stimulus. The ablation catheter (Map) was used to pace in the high right atrium. The atrioventricular nodal effective refractory period (AVNERP) was successfully identified (Figure 9.8). The patient was noted to have pericardial effusion at the end of the procedure, which required pericardiocentesis. This was likely due to challenging double transseptal punctures at the start of the procedure.

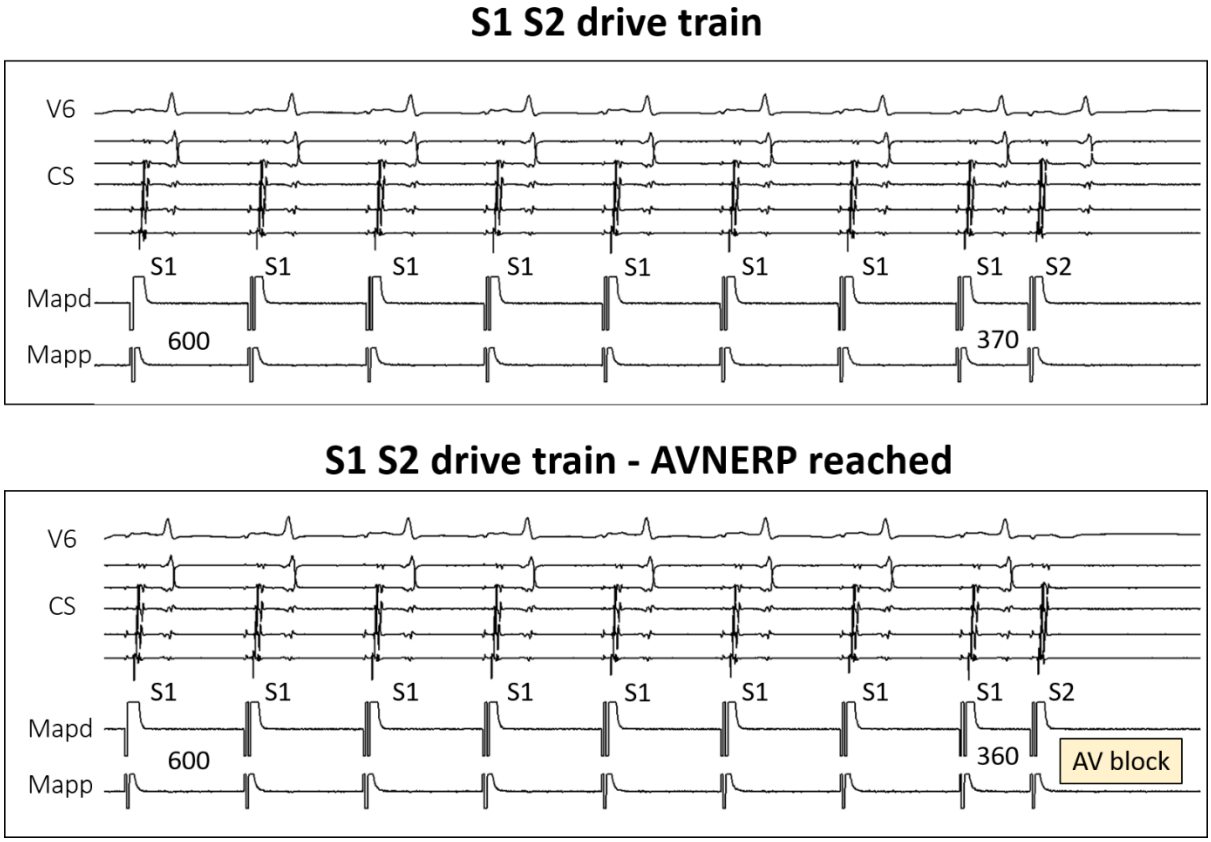

Figure 9.8 Anterograde curve with programmed S1 S2 drive train to AVNERP with Tau-20 stimulator

The Map catheter was positioned in the high right atrium and drive trains up to one extra-stimulus (S1, S2) was performed to identify AVNERP. The top trace shows atrial capture during Mapd pacing at 600ms for 8 trains (S1), followed by an extra-stimulus (S2) after 370ms coupling interval S1.

(AVNERP = atrioventricular nodal effective refractory period; CS = coronary sinus; Mapd = mapping catheter distal; Mapp = mapping catheter proximal)

The third patient was for redo PVI. The Tau-20 stimulator was used to perform single sensed extras by pacing from the coronary sinus (CS 1-2). Burst pacing to AV block was also perfomed from the coronary sinus (CS 1-2), starting from 800ms, decrementing by 10ms with every three stimuli. There was AV block with burst pacing at 570ms (Figure 9.9).

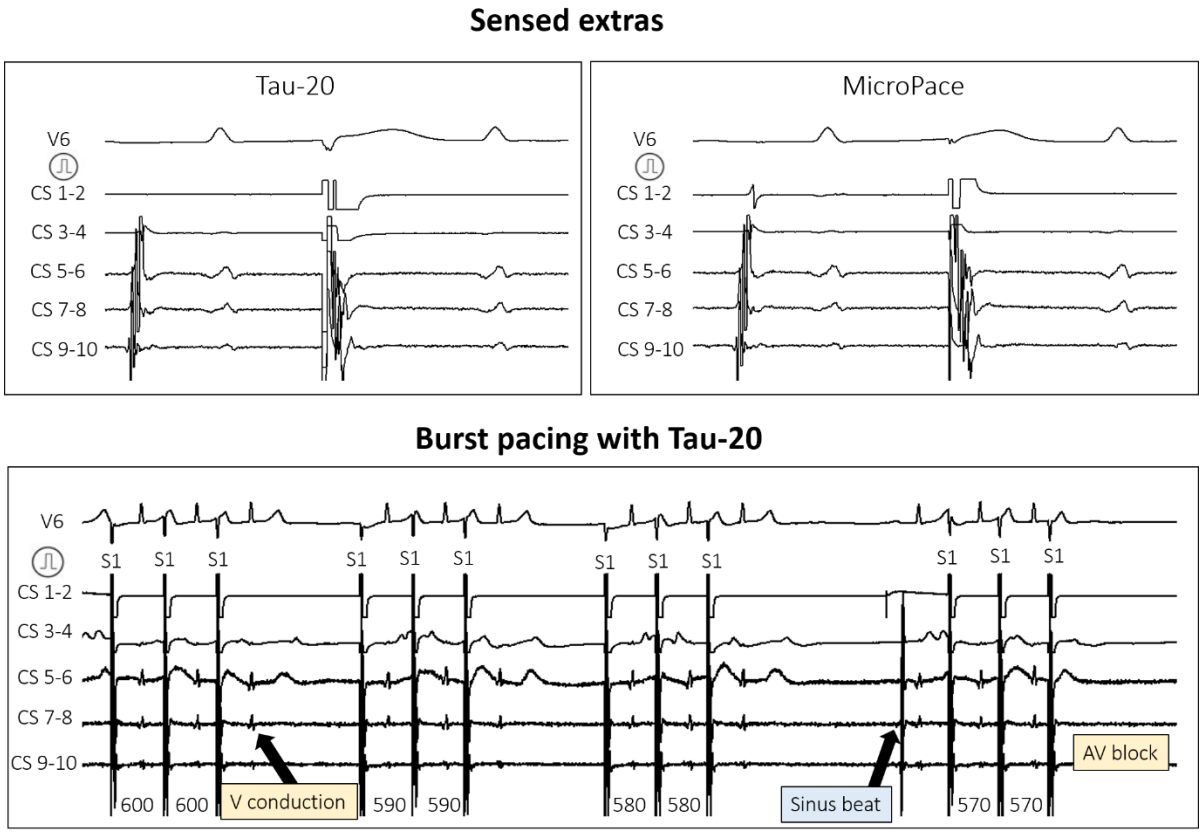

Figure 9.9 Sensed extras and burst pacing with Tau-20 stimulator

Sensed extras were performed successfully from CS 1-2 using Tau-20 stimulator, at 400ms from the sensed CS signals (top left). This was comparable to sensed extras performed with MicroPace (top right). The bottom trace demonstrates burst pacing with Tau20, with automatic 10ms decrement with every 3 stimuli. This was performed at CS 1-2. There was ventricular conduction with every pacing stimuli, until the third stimulus at 570ms, demonstrating AV block (AVNERP).

(AV = atrioventricular; AVNERP = atrioventricular nodal effective refractory period; CS = coronary sinus)

In the same patient, continuous HFS was performed at 4 sites, of which 2 were positive for AVD-GP. The AVD-GP were in the right inferior border of the posterior wall, and in the septum (Figure 9.10). These were in the expected anatomical regions according to the AVD-GP high probability distribution atlas (Chapter 3)[6]. Continuous HFS on the septal AVD-GP caused significant asystole of up to 7.9s from AV dissociation in AF (Figure 9.11).

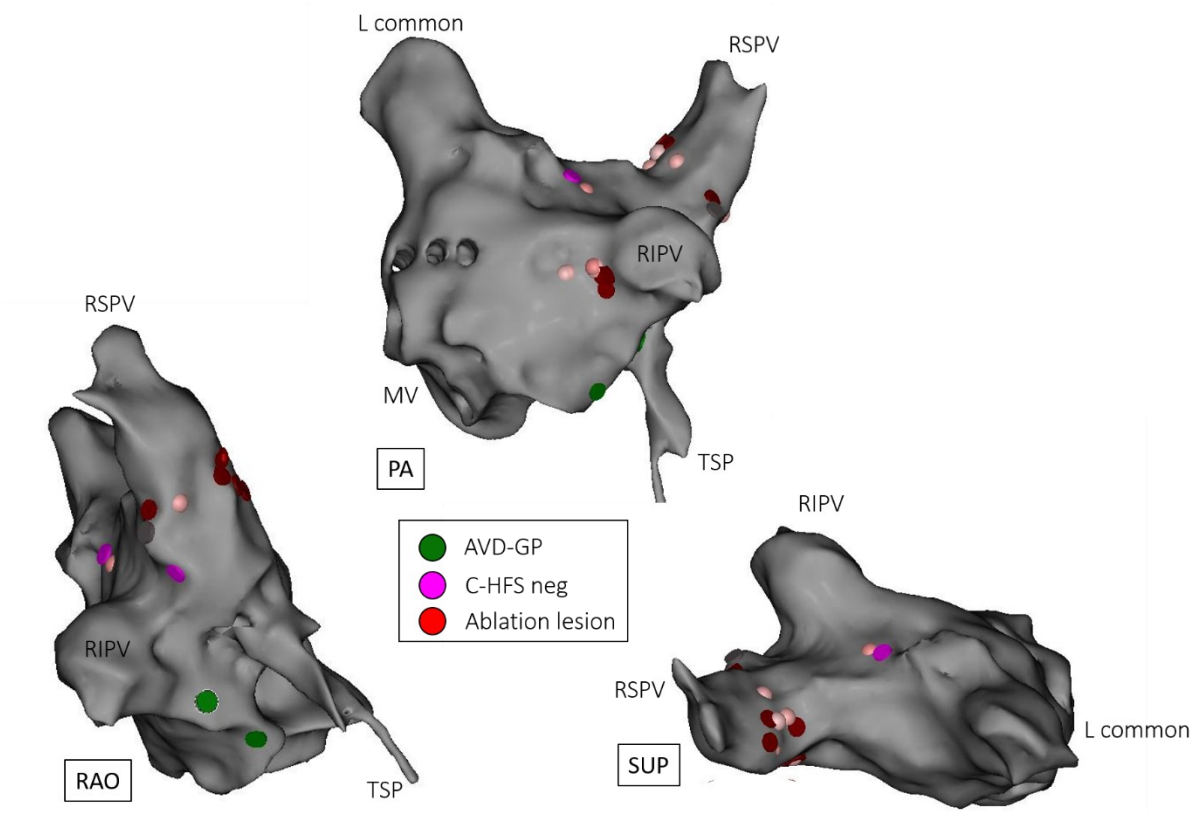

Figure 9.10 Continuous HFS tested sites with Tau-20

This is a patient who had previous PVI, returning with symptomatic AF recurrence. The L common vein was still isolated, and the right sided PVs were reconnected. Three different views of the left atrium are shown, and four sites were tested with continuous HFS using the Tau-20 stimulator. Green dots are AVD-GP, which demonstrated significant AV dissociation with continuous HFS. Pink dots were negative continuous HFS sites. AVD-GP were in the inferior right border of the posterior wall, and in the septum as expected from the AVD-GP probability distribution atlas[6] (Chapter 3). Touch-up radiofrequency ablation was performed to isolate the re-connected PVs.

(AF = atrial fibrillation; AV = atrioventricular; AVD-GP = atrioventricular dissociating ganglionated plexus; C-HFS = continuous high frequency stimulation; L common = left common pulmonary vein; MV = mitral valve; PA = posterior anterior; PVI = pulmonary vein isolation; RAO = right anterior oblique; RIPV = right inferior pulmonary vein; RSPV = right superior pulmonary vein; SUP = superior; TSP = transseptal puncture site)

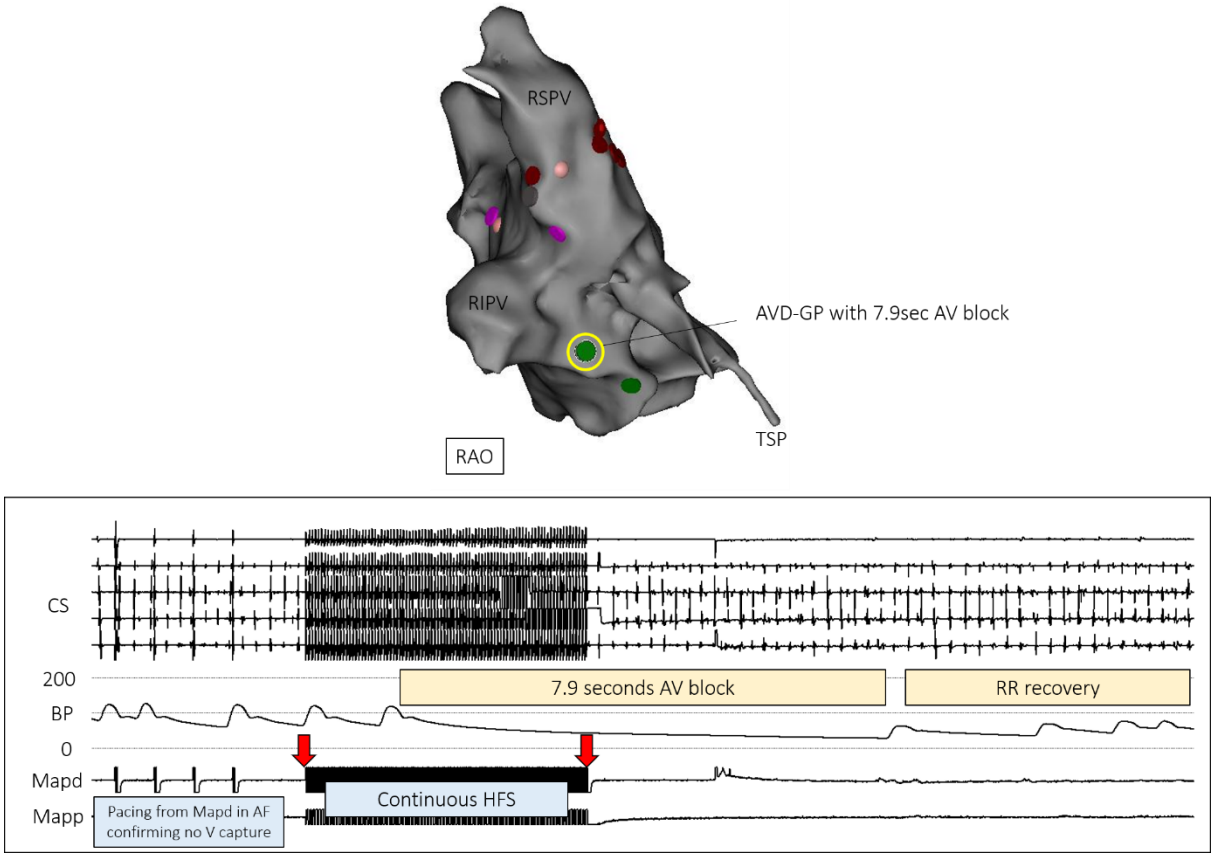

Figure 9.11 Continuous HFS with Tau-20 Stimulator identifying AVD-GP

The top picture shows the left atrium in RAO view. The yellow circled green dot is the site tested with continuous HFS using the Tau-20 stimulator. This was in the septum, posterior to the TSP site. The bottom trace shows pacing during AF with high output (50mA) from the Map catheter. This confirmed no ventricular capture. Within 1.3 seconds of continuous HFS, 7.9 seconds AV block occurred marking this as an AVD-GP. After cessation of HFS, RR interval recovered back to normal and AF continued. Red arrows indicate start and stop of HFS.

(AF = atrial fibrillation; AV = atrioventricular; AVD-GP = atrioventricular dissociating ganglionated plexus; BP = blood pressure; CS = coronary sinus; HFS = high frequency stimulation; Mapd = mapping catheter distal; Mapp = mapping catheter proximal; RAO = right anterior oblique; RIPV = right inferior pulmonary vein; RSPV = right superior pulmonary vein; TSP = transseptal puncture; V = ventricular)

The right sided pulmonary veins were re-isolated with radiofrequency ablation. There was no complication.

9.4. Discussion

The Tau-20's safety and function were validated in the live pig study. Following approvals, we were able to confirm that the Tau-20 can perform standard EP studies similar to Micropace and HFS studies like the Grass S88 stimulator in the clinical setting. In addition, we were capable of switching between continuous and synchronised HFS modes easily using pre-sets saved onto the Tau-20 graphical user interface, without needing to manually adjust the parameters as with the Grass stimulator.

In the human testing, one patient suffered a complication with cardiac tamponade which required pericardiocentesis, but this was most likely due to the difficult, double transseptal puncture at the beginning of the procedure when the patient's blood pressure had dipped. The Tau-20 pacing manoeuvres were tested towards the end of the case without complications.

Future plans for improving the Tau-20 include: 1) direct comparison with the Grass S88 in performing HFS protocol in the clinical setting, 2) building a separate keypad that will enable easier navigation and control, 3) improving noise attenuation during HFS to visualise intracardiac electrogram signals, 4) automatic recognition of relevant intracardiac electrogram signals such as atria ectopy triggered with HFS and interpretation of positive and negative HFS sites.

9.5. Conclusion

The Tau-20 is the first stimulator to be developed that is capable of performing HFS and basic electrophysiology pacing manoeuvres with accurate delivery of pre-defined parameters safely in the clinical setting. With further validation, software and hardware

improvements, we hope to replace the Grass S88 stimulator with the Tau-20 for performing future autonomic procedures. Its improved functional capacity will enable easier navigation through HFS mapping and GP ablation procedures for all users, perform sensitive and accurate detection of subtle intracardiac electrogram features to automatically identify “positive” and “negative” GP sites.

10. CONCLUSIONS

Pulmonary vein isolation (PVI) is currently the gold-standard treatment for paroxysmal atrial fibrillation (AF). However, its first time success rate of 52-54%[114] at 12 months remain unchanged despite continuous improvements in mapping and ablation techniques over the past two decades. AF freedom with PV reconnection and AF recurrence with complete PVI suggests additional mechanism of AF that is incompletely explained by the simple PVI theory.

The autonomic nervous system has been implicated in the pathophysiology of AF since the mid-19th century which has later translated into therapeutic targets for treatment of AF. The intricate and complex network of nerves sit abundantly throughout the atria of human hearts, where there are substantial anatomical variations between individuals, creating a challenge in navigating this network and knowing what and how to target for AF. A simplified view and approach to this complex network of nerves was quickly adopted as "anatomical ganglionated plexus (GP) ablation" which targeted 4-5 common dense regions of nerves known to be present in human hearts. Approximation of these anatomical sites without functional confirmation of their specific autonomic properties is subjective and potentially harmful to patients, as shown in the AFACT study with high rates of complications[127].

In this thesis, we challenged this approach to targeting the complex autonomic nervous system in patients, by utilising high frequency stimulation (HFS) technique to globally map the left atrium of patients with AF. This identified two distinct functional and anatomical types of GP in the human left atrium: atrioventricular dissociating GP (AVD-GP), and ectopy triggering GP (ET-GP). Whilst the AVD-GP predominantly occupied the

infero-posterior wall, floor and septum of the left atrium, ET-GP predominantly occupied the roof, mid anterior wall and PV ostia except for the posterior portion of the right inferior pulmonary vein. Stimulation of the ET-GP triggered single to multiple atrial ectopy including PV and non-PV origins, which led to atrial arrhythmias. It was evident that the conventional PVI targeted most ET-GP inadvertently, which may contribute to the success of PVI.

We then sought to evaluate the effects of targeting specific ET-GP without PVI in patients with paroxysmal AF, and compare with conventional PVI by radiofrequency ablation, in a prospective randomised, controlled, study (GANGLIA-AF). The 12 month follow-up is ongoing, but the results so far suggest no statistically significant difference in the primary outcomes (>30s AF/AT) or in major complications between the two arms, and ET-GP required significantly less amount of average ablation than PVI to achieve this effect.

In view of the promising therapeutic effects of ET-GP ablation alone without PVI, we explored the effects of ET-GP ablation as an adjunctive therapy to PVI in redo AF ablation patients and compared with redo PVI alone. It was safe and feasible to ablate ET-GP in addition to PVI. ET-GP and AVD-GP were also identifiable in small number of patients with complete PVI, and targeting them led to freedom from AF/AT. However, limitations of this study such as the heterogeneity of patient demographics, imbalanced patient numbers in the intervention arms need to be improved in order to make a more valid comparison between the adjunctive technique and PVI.

These two clinical studies allowed interesting observations of acute and long-term GP ablation effects. GP recovered over time, which correlated with recurrence of AF. In some patients, ET-GP ablation led to acute modification of sustained AF (termination to sinus rhythm, organisation into atrial tachycardia, >30s AF cycle slowing) and AVD-GP ablation

led to acute non-sustainability of AF. In these small number of patients studied, there was no statistically significant improvement in ablation outcomes.

Anatomically identified GP are known to be abundant in parasympathetic and sympathetic nerves. We quantified parasympathetic and sympathetic nerves in functionally identified ectopy triggering (ET) sites with synchronised HFS, and compared these with non-ET sites in Langendorff-perfused whole porcine hearts. This confirmed both sympathetic and parasympathetic nerves to be present in ET and non-ET sites, however there was statistically significant increased nerve density at ET sites compared to non-ET sites. These findings suggest similar composition of nerves in the human atrial ET-GP which also produced atrial ectopy and arrhythmia with synchronised HFS, and provide histological evidence for the differences in the functional response with HFS as well.

Finally, we developed a new and improved high frequency stimulator (Tau-20), to overcome the many limitations of the old Grass S88 stimulator. We successfully tested the Tau-20 in live pigs followed by humans in the clinical setting without any safety issues. Testing included basic pacing protocols as part of 4 wire EP studies, synchronised HFS and continuous HFS.

This thesis explored the histological, anatomical and functional characteristics of ET-GP, and compared these to the AVD-GP. We demonstrated that it was safe and feasible to globally map and ablate GP to prevent atrial arrhythmias. In addition, ET-GP ablation targets specific AF triggers that provides individualised patient treatment. Our work provides evidence that ET-GP are upstream triggers of AF, and the newly developed stimulator can facilitate a more accurate and effective HFS mapping for future work.

10.1. Future Projects

Data from this thesis provides the foundation for further exploration of the mechanistic role of the intrinsic cardiac autonomic nervous system in AF.

10.1.1.Predictors of Successful GP Ablation

After the 12 month follow-up is complete on all study patients from this thesis, factors that contributed to success and failure of GP ablation will be explored, such as specific patient demographics, number and distribution of ET-GP, density of HFS mapping and ablation parameters. Further collation of repeat HFS mapping data in patients for redo AF ablation will also clarify the above. This analysis will be key to improving GP ablation technique and potentially outcomes.

10.1.2.ET-GP Intracardiac Electrogram Features

Previously, AVD-GP sites were shown to have unique intracardiac electrogram features that distinguished them as nerve-dense sites. These were primarily evaluated using spectral analysis[240,241]. It is not known what unique intracardiac electrogram features are present specifically at ET-GP sites. If there are unique features, it may be possible to automate mapping for ET-GP without needing to use HFS, and it may also be possible to predict ET-GP sites without any mapping. The aims with an automated process are to rid of subjectivity with signal analysis during HFS mapping, avoid recurrent electrical DC cardioversions to maintain sinus rhythm, create high density map to cover all areas of the left atrium, and overall provide easier and quicker ET-GP mapping technique. First, to analyse large amount of intracardiac electrograms in the most efficient way possible, we will be exporting CARTO™ 3D electroanatomic maps of the left atrium from all GP cases,

including the co-ordinates of every HFS points “tagged” onto the geometry. Each tagged HFS point will also have an intracardiac electrogram recording from the HFS catheter (ablation catheter), which will be fed into an automated algorithm to pick up common features that mark it as ET-GP or negative HFS site. With a machine learning technique, these features will then be used to identify and predict ET-GP sites. One of the initial challenges to this project will be obtaining clear intracardiac electrogram signals retrospectively, that are not obstructed by HFS artefact and excludes far-field signals.

10.1.3.ET-GP ablation in addition to PVI in AF (pilot study).

Most ET-GP are anatomically distributed near PV ostia and roof, which are inadvertently targeted by the conventional wide circumferential antral ablation. Majority of ET-GP trigger PV ectopy and arrhythmia. Preliminary results of the GANGLIA-AF trial showed that PVI similarly prevented AF as specific ET-GP ablation. Experience from the ADD-GP study in redo AF ablation patients suggests that non-PV and PV ET-GP are present even after complete PVI. Therefore, we propose a prospective pilot study that assesses PVI in addition to ET-GP ablation in patients with paroxysmal AF, and compare with PVI alone as control. PVI prevents PV ectopy or arrhythmia conducting into the atria, which will also ablate upstream AF triggers by non-specifically targeting ET-GP around the PV ostia. After PVI, additional ET-GP will be mapped with HFS, which will reveal any PV ET-GP that were not initially targeted by PVI, in addition to non-PV ET-GP. This will theoretically provide a “double barrier” for AF treatment. We anticipate shorter duration of HFS mapping after PVI, as there will be more negative HFS sites and greater chance of maintaining sinus rhythm when using HFS after complete PVI. We also propose the same protocol persistent AF patients, who have more variable success with PVI than paroxysmal AF. The effect of ET-GP ablation in persistent AF is currently unknown.

10.1.4.The Tau-20 Stimulator

The Tau-20's HFS functionality has been successfully tested in humans in the clinical setting. The aim is to improve the functionality and operability of the stimulator further, to replace the old Grass S88 stimulator for all future autonomic ablation cases. Improvements currently under development include incorporating a separate keypad for more intuitive HFS operability, as well as building a more stable graphic user interface to navigate easily. We also plan to incorporate full intracardiac electrogram recording system to the stimulator, with an in-built custom filter that can amplify small intracardiac electrogram signals buried within the noise artefact of HFS to be visualised.

These further works will optimise the accuracy and efficiency of mapping for relevant GP in AF. Determining the factors that contribute to success and failure of GP ablation, including the patient demographics that are most likely to benefit from GP ablation are key to improving GP ablation outcomes. This may provide a new paradigm for our approaches to AF, that is more patient-specific, safe and feasible for wider clinical use.

11. REFERENCES

1. Wolowacz SE, Samuel M, Brennan VK, Jasso-Mosqueda JG, Gelder IC Van. The cost of illness of atrial fibrillation: A systematic review of the recent literature. *Europace* 2011;**13**:1375–1385.

2. Stewart S, Murphy NF, Murphy N, Walker A, McGuire A, McMurray JJ V. Cost of an emerging epidemic: an economic analysis of atrial fibrillation in the UK. *Heart* 2004;**90**:286–292.

3. Kim MH, Johnston SS, Chu BC, Dalal MR, Schulman KL. Estimation of total incremental health care costs in patients with atrial fibrillation in the united states. *Circ Cardiovasc Qual Outcomes* 2011;**4**:313–320.

4. Kuck KH, Fürnkranz A, Chun KRJ, Metzner A, Ouyang F, Schlüter M, Elvan A, Lim HW, Kueffer FJ, Arentz T, Albenque JP, Tondo C, Kühne M, Sticherling C, Brugada J. Cryoballoon or radiofrequency ablation for symptomatic paroxysmal atrial fibrillation: Reintervention, rehospitalization, and quality-of-life outcomes in the FIRE and ICE trial. *Eur Heart J* 2016;**37**:2858–2865.

5. Armour JA, Murphy DA, Yuan BX, Macdonald S, Hopkins DA. Gross and microscopic anatomy of the human intrinsic cardiac nervous system. *Anat Rec* 1997;**247**:289–298.

6. Kim MY, Sikkel MB, Hunter RJ, Haywood GA, Tomlinson DR, Tayebjee MH, Ali RL, Cantwell CD, Gonna H, Sandler BC, Lim E, Furniss G, Panagopoulos D, Begg G, Dhillon G, Hill NJ, O'Neill J, Francis DP, Lim PB, Peters NS, Linton NWF, Kanagaratnam P. A novel approach to mapping the atrial ganglionated plexus network by generating a distribution probability atlas. *J Cardiovasc Electrophysiol* 2018;**29**:1624–1634.

7. Katritsis D, Giazitzoglou E, Sougiannis D, Goumas N, Paxinos G, Camm AJ. Anatomic Approach for Ganglionic Plexi Ablation in Patients With Paroxysmal Atrial Fibrillation. *Am J Cardiol* 2008;**102**:330–334.

8. Katritsis DG, Pokushalov E, Romanov A, Giazitzoglou E, Siontis GCM, Po SS, Camm AJ, Ioannidis JPA. Autonomic denervation added to pulmonary vein isolation for paroxysmal atrial fibrillation: a randomized clinical trial. *J Am Coll Cardiol* 2013;**62**:2318–2325.

9. Driessen AHG, Berger WR, Krul SPJ, Berg NWE van den, Neefs J, Piersma FR, Chan Pin Yin DRPP, Jong JSSG de, Boven WP van, Groot JR de. Ganglion Plexus Ablation in Advanced Atrial Fibrillation. *J Am Coll Cardiol* 2016;**68**:1155–1165.

10. Kapa S, Callans DJ. Looking beyond the ablation shore, treating atrial fibrillation from afar: Integrating anatomic, physiologic, neurologic, and cardiovascular principles into novel therapies. *J Am Coll Cardiol* Elsevier Inc; 2015;**65**:876–878.

11. Lip GYH, Beevers DG. ABC of Atrial Fibrillation: HISTORY, EPIDEMIOLOGY, AND IMPORTANCE OF ATRIAL FIBRILLATION. *Bmj* 1995;**311**:1361.

12. McMichael J. History of atrial fibrillation 1628-1819 Harvey - de Senac - Laennec.

Heart 1982;**48**:193–197.

13. Lower R. Tractatus de corde. *Eary Sci Oxford* 1669;**9**.

14. Senac J de. Traite de la structure du Coeur, de son Action et de ses Maladies. *Paris, J Vincent* 1749;**1**.

15. McMichael J. Sir James Mackenzie and atrial fibrillation--a new perspective. *J R Coll Gen Pract* 1981;**31**:402–406.

16. Waller AD. A Demonstration on Man of Electromotive Changes accompanying the Heart's Beat. *J Physiol* 1887;**8**:229–234.

17. Lewis T. Auricular fibrillation: a common clinical condition. *BMJ* 1909;**2**:1528.

18. Lewis T. Evidences of auricular fibrillation. *BMJ* 1912;**3**:173–193.

19. Marey E. Physiologie médicale de la circulation du sang: basée sur l'étude graphique. *Arch Gesamte Physiol* 1863;

20. Hering H. Das elektrocaardiogramm des irregularis perpetuus. *Dtsch Arch klin Med* 1908;**94**:205–208.

21. Calkins H, Hindricks G, Cappato R, Kim YH, Saad EB, Aguinaga L, Akar JG, Badhwar V, Brugada J, Camm J, Chen PS, Chen SA, Chung MK, Nielsen JC, Curtis AB, Davies DW, Day JD, d'Avila A, Groot NMS (Natasja. de, Biase L Di, Duytschaever M, Edgerton JR, Ellenbogen KA, Ellinor PT, Ernst S, Fenelon G, Gerstenfeld EP, Haines DE, Haissaguerre M, Helm RH, et al. 2017 HRS/EHRA/ECAS/APHRS/SOLAECE expert consensus statement on catheter and surgical ablation of atrial fibrillation. *Hear Rhythm* Elsevier Ltd; 2017;**14**:e275–e444.

22. Haïssaguerre M, Jaïs P, Shah DC, Takahashi A, Hocini M, Quiniou G, Garrigue S, Mouroux A Le, Métayer P Le, Clémenty J. Spontaneous Initiation of Atrial Fibrillation by Ectopic Beats Originating in the Pulmonary Veins. *N Engl J Med* 1998;**339**:659–666.

23. Wijffels MCEF, Kirchhof CJHJ, Dorland R, Allessie MA. Atrial Fibrillation Begets Atrial Fibrillation. *Circulation* 1995;**92**:1954–1968.

24. Morillo CA, Klein GJ, Jones DL, Guiraudon CM. Chronic Rapid Atrial Pacing. *Circulation* 1995;**91**:1588–1595.

25. Garrey WE. Auricular Fibrillation. *Physiol Rev* 1924;**4**:215–250.

26. Moe GK, Rheinboldt WC, Abildskov J. A computer model of atrial fibrillation. *Am Heart J* 1964;**67**:200–220.

27. Chen J. Dynamics of wavelets and their role in atrial fibrillation in the isolated sheep heart. *Cardiovasc Res* 2000;**48**:220–232.

28. Groot N de, Does L van der, Yaksh A, Lanters E, Teuwen C, Knops P, Woestijne P van de, Bekkers J, Kik C, Bogers A, Allessie M. Direct Proof of Endo-Epicardial Asynchrony of the Atrial Wall During Atrial Fibrillation in Humans. *Circ Arrhythmia Electrophysiol* 2016;**9**.

29. Reumann M, Bohnert J, Osswald B, Hagl S, Doessel O. Multiple wavelets, rotors,

and snakes in atrial fibrillation—a computer simulation study. *J Electrocardiol* 2007;**40**:328–334.

30. Nishida K, Nattel S. Atrial fibrillation compendium: Historical context and detailed translational perspective on an important clinical problem. *Circ Res* 2014;**114**:1447–1452.

31. Chen SA, Hsieh MH, Tai CT, Tsai CF, Prakash VS, Yu WC, Hsu TL, Ding YA, Chang MS. Initiation of atrial fibrillation by ectopic beats originating from the pulmonary veins: Electrophysiological characteristics, pharmacological responses, and effects of radiofrequency ablation. *Circulation* 1999;**100**:1879–1886.

32. Jaïs P, Hocini M, Macle L, Choi KJ, Deisenhofer I, Weerasooriya R, Shah DC, Garrigue S, Raybaud F, Scavee C, Metayer P Le, Clémenty J, Haïssaguerre M. Distinctive electrophysiological properties of pulmonary veins in patients with atrial fibrillation. *Circulation* 2002;**106**:2479–2485.

33. Spach MS, Barr RC, Jewett PH. Spread of excitation from the atrium into thoracic veins in human beings and dogs. *Am J Cardiol* 1972;**30**:844–854.

34. Paes de Almeida O, Bohm CM, Paula Carvalho M de, Paes de Carvalho A. The cardiac muscle in the pulmonary vein of the rat: a morphological and electrophysiological study. *J Morphol* 1975;**145**:409–433.

35. Yamane T, Shah DC, Jaïs P, Hocini M, Peng JT, Deisenhofer I, Clémenty J, Haïssaguerre M. Dilatation as a marker of pulmonary veins initiating atrial fibrillation. *J Interv Card Electrophysiol* 2002;**6**:245–249.

36. Guerra PG, Thibault B, Dubuc M, Talajic M, Roy D, Crépeau J, Nattel S, Tardif J-C. Identification of atrial tissue in pulmonary veins using intravascular ultrasound. *J Am Soc Echocardiogr* 2003;**16**:982–987.

37. Perez-Lugones A, McMahon JT, Ratliff NB, Saliba WI, Schweikert RA, Marrouche NF, Saad EB, Navia JL, McCarthy PM, Tchou P, Gillinov AM, Natale A. Evidence of specialized conduction cells in human pulmonary veins of patients with atrial fibrillation. *J Cardiovasc Electrophysiol* 2003;**14**:803–809.

38. Masani F. Node-like cells in the myocardial layer of the pulmonary vein of rats: an ultrastructural study. *J Anat* 1986;**145**:133–142.

39. Gherghiceanu M, Hinescu ME, Andrei F, Mandache E, Macarie CE, Faussone-Pellegrini M-S, Popescu LM. Interstitial Cajal-like cells (ICLC) in myocardial sleeves of human pulmonary veins. *J Cell Mol Med* **12**:1777–1781.

40. Anderson RH, Ho SY. 'Specialized' conducting cells in the pulmonary veins. *J Cardiovasc Electrophysiol* 2004;**15**:121; author reply 121-3.

41. Chen S-A, Yeh H-I. Specialized conduction cells in human pulmonary veins: fact and controversy. *J Cardiovasc Electrophysiol* 2003;**14**:810–811.

42. Verheule S, Wilson EE, Arora R, Engle SK, Scott LR, Olgin JE. Tissue structure and connexin expression of canine pulmonary veins. *Cardiovasc Res* 2002;**55**:727–738.

43. Hocini M, Ho SY, Kawara T, Linnenbank AC, Potse M, Shah D, Jaïs P, Janse MJ,

Haïssaguerre M, Se Bakker JMT. Electrical conduction in canine pulmonary veins: Electrophysiological and anatomic correlation. *Circulation* 2002;**105**:2442–2448.

44. Bakker JMT De, Ho SY, Hocini M. Basic and clinical electrophysiology of pulmonary vein ectopy. *Cardiovasc Res* 2002;**54**:287–294.

45. Wilders R, Wagner MB, Golod DA, Kumar R, Wang YG, Goolsby WN, Joyner RW, Jongsma HJ. Effects of anisotropy on the development of cardiac arrhythmias associated with focal activity. *Pflugers Arch* 2000;**441**:301–312.

46. Gong Y, Xie F, Stein KM, Garfinkel A, Culianu CA, Lerman BB, Christini DJ. Mechanism Underlying Initiation of Paroxysmal Atrial Flutter/Atrial Fibrillation by Ectopic Foci. *Circulation* 2007;**115**:2094–2102.

47. Cheung DW. Electrical activity of the pulmonary vein and its interaction with the right atrium in the guinea-pig. *J Physiol* 1981;**314**:445–456.

48. Yue L, Feng J, Gaspo R, Li GR, Wang Z, Nattel S. Ionic remodeling underlying action potential changes in a canine model of atrial fibrillation. *Circ Res* 1997;**81**:512–525.

49. Ehrlich JR, Cha T-J, Zhang L, Chartier D, Melnyk P, Hohnloser SH, Nattel S. Cellular electrophysiology of canine pulmonary vein cardiomyocytes: action potential and ionic current properties. *J Physiol* 2003;**551**:801–813.

50. ALLESSIE MA, BONKE FIM, SCHOPMAN FJG. Circus Movement in Rabbit Atrial Muscle as a Mechanism of Tachycardia. *Circ Res* 1973;**33**:54–62.

51. Allessie MA, Bonke FI, Schopman FJ. Circus movement in rabbit atrial muscle as a mechanism of tachycardia. III. The 'leading circle' concept: a new model of circus movement in cardiac tissue without the involvement of an anatomical obstacle. *Circ Res* 1977;**41**:9–18.

52. WIENER N, ROSENBLUETH A. The mathematical formulation of the problem of conduction of impulses in a network of connected excitable elements, specifically in cardiac muscle. *Arch Inst Cardiol Mex* 1946;**16**:205–265.

53. WINFREE AT. Vortex Action Potentials in Normal Ventricular Muscle. *Ann N Y Acad Sci* 1990;**591**:190–207.

54. Winfree AT. Varieties of spiral wave behavior: An experimentalist's approach to the theory of excitable media. *Chaos An Interdiscip J Nonlinear Sci* 1991;**1**:303–334.

55. Rensma PL, Allessie MA, Lammers WJ, Bonke FI, Schalij MJ. Length of excitation wave and susceptibility to reentrant atrial arrhythmias in normal conscious dogs. *Circ Res* 1988;**62**:395–410.

56. Vaquero M, Calvo D, Jalife J. Cardiac fibrillation: from ion channels to rotors in the human heart. *Hear Rhythm* 2008;**5**:872–879.

57. Jalife J. Déjà vu in the theories of atrial fibrillation dynamics. *Cardiovasc Res* 2011;**89**:766–775.

58. Pandit S V., Jalife J. Rotors and the dynamics of cardiac fibrillation. *Circ Res* 2013;**112**:849–862.

59. Zhao J, Hansen BJ, Csepe TA, Lim P, Wang Y, Williams M, Mohler PJ, Janssen PML, Weiss R, Hummel JD, Fedorov V V. Integration of High-Resolution Optical Mapping and 3-Dimensional Micro-Computed Tomographic Imaging to Resolve the Structural Basis of Atrial Conduction in the Human Heart. *Circ Arrhythmia Electrophysiol* 2015;**8**:1514–1517.

60. MD M. McWILLIAM, M.D., Professor of the Institutes of Medicine. 1850;**ix**.

61. Winterberg. No Title. *Zeitschr für exper Path u Ther* 1907;636.

62. Kronecker H, Spallitta F. No Title. *Arch Internat de Physiol* **2**:223.

63. Robinson C, Draper G. STUDIES WITH THE ELECTROCARDIOGRAPH ON THE ACTION OF THE VAGUS NERVE ON THE HUMAN HEART: II. THE EFFECTS OF VAGUS STIMULATION ON THE HEARTS OF CHILDREN WITH CHRONIC VALVULAR DISEASE. *J Exp Med* 1912;**15**:14–48.

64. Armour J, Randall W, Sinha S. Localized myocardial responses to stimulation of small cardiac branches of the vagus. *Am J Physiol Content* 1975;**228**:141–148.

65. Randall WC, Ardell JL, O'Toole MF, Wurster RD. Differential autonomic control of SAN and AVN regions of the canine heart: structure and function. *Prog Clin Biol Res* 1988;**275**:15–31.

66. Coumel P. Clinical approach to paroxysmal atrial fibrillation. *Clin Cardiol* 1990;**13**:209–212.

67. Coumel P. Paroxysmal Atrial Fibrillation: A Disorder of Autonomic Tone? *Eur Heart J* 1994;**15**:9–16.

68. Patterson E, Po SS, Scherlag BJ, Lazzara R. Triggered firing in pulmonary veins initiated by in vitro autonomic nerve stimulation. *Hear Rhythm* 2005;**2**:624–631.

69. Chen YJ, Chen SA, Tai CT, Wen ZC, Feng AN, Ding YA, Chang MS. Role of atrial electrophysiology and autonomic nervous system in patients with supraventricular tachycardia and paroxysmal atrial fibrillation. *J Am Coll Cardiol* Elsevier Masson SAS; 1998;**32**:732–738.

70. AMORY DW, WEST TC. Chronotropic response following direct electrical stimulation of the isolated sinoatrial node: a pharmacologic evaluation. *J Pharmacol Exp Ther* 1962;**137**:14–23.

71. Szabo B, Kovacs T, Lazzara R. Role of calcium loading in early afterdepolarizations generated by Cs+ in canine and guinea pig Purkinje fibers. *J Cardiovasc Electrophysiol* 1995;**6**:796–812.

72. SZABO B, SWEIDAN R, RAJAGOPALAN C V., LAZZARA R. Role of Na + :Ca 2+ Exchange Current in Cs + -Induced Early Afterdepolarizations in Purkinje Fibers. *J Cardiovasc Electrophysiol* 1994;**5**:933–944.

73. Shi H, Yang B, Xu D, Wang H, Wang Z. Electrophysiological characterization of cardiac muscarinic acetylcholine receptors: different subtypes mediate different potassium currents. *Cell Physiol Biochem* 2003;**13**:59–74.

74. Schauerte P, Scherlag BJ, Patterson E, Scherlag MA, Matsudaria K, Nakagawa H, Lazzara R, Jackman WM. Focal atrial fibrillation: experimental evidence for a

pathophysiologic role of the autonomic nervous system. *J Cardiovasc Electrophysiol* 2001;**12**:592–599.

75. Scarpa A. Tabulae Neurologicae ad Illustrandam historiam cardiacorum nervorum etc. Ticini. 1794;

76. King TS, Coakley JB. The intrinsic nerve cells of the cardiac atria of mammals and man. *J Anat* 1958;**92**:353-.

77. Remak R. Neurologische Erlauterungen. *Arch Anat Physiol* 1844;463–472.

78. Lee R. On the Ganglia and Nerves of the Heart. *Edinburgh Med Surg J* 1849;**72**:318–321.

79. Kolliker A. Handbuch der Gewebelehre des Menschens. 1865;

80. Cloetta. Über die Nerven des Herzens. *Verh phys Med Ges Wurzb* 1853;**3**.

81. Pauza DH, Skripka V, Pauziene N, Stropus R. Morphology, distribution, and variability of the epicardiac neural ganglionated subplexuses in the human heart. *Anat Rec* 2000;**259**:353–382.

82. Singh S, Johnson PI, Lee RE, Orfei E, Lonchyna VA, Sullivan HJ, Montoya A, Tran H, Wehrmacher WH, Wurster RD. Topography of cardiac ganglia in the adult human heart. *J Thorac Cardiovasc Surg* 1996;**112**:943–953.

83. Gardner E, O'Rahilly R. The nerve supply and conducting system of the human heart at the end of the embryonic period proper. *J Anat* 1976;**121**:571–587.

84. Orts Llorca F, Domenech Mateu JM, Puerta Fonolla J. Innervation of the sinu-atrial node and neighbouring regions in two human embryos. *J Anat* 1979;**128**:365–375.

85. Pauza DH, Skripka V, Pauziene N, Stropus R. Anatomical study of the neural ganglionated plexus in the canine right atrium: Implications for selective denervation and electrophysiology of the sinoatrial node in dog. *Anat Rec* 1999;**255**:271–294.

86. VINCENZI FF, WEST TC. RELEASE OF AUTONOMIC MEDIATORS IN CARDIAC TISSUE BY DIRECT SUBTHRESHOLD ELECTRICAL STIMULATION. *J Pharmacol Exp Ther* 1963;**141**:185–194.

87. LIM PB, MALCOLME-LAWES LC, STUBER T, WRIGHT I, FRANCIS DP, DAVIES DW, PETERS NS, KANAGARATNAM P. Intrinsic Cardiac Autonomic Stimulation Induces Pulmonary Vein Ectopy and Triggers Atrial Fibrillation in Humans. *J Cardiovasc Electrophysiol* 2011;**22**:638–646.

88. Po SS, Nakagawa H, Jackman WM. Localization of left atrial ganglionated plexi in patients with atrial fibrillation: Techniques and technology. *J Cardiovasc Electrophysiol* 2009;**20**:1186–1189.

89. Parker MA, Tung R, Challapalli S, Kadish AH, Goldberger JJ. Relationship of heart rate variability to parasympathetic effect. *Circulation* 2012;**103**:1977–1983.

90. Kleiger RE, Bigger JT, Bosner MS, Chung MK, Cook JR, Rolnitzky LM, Steinman R, Fleiss JL. Stability over time of variables measuring heart rate variability in

normal subjects. *Am J Cardiol* 1991;**68**:626–630.

91. Pagani M, Lombardi F, Guzzetti S, Rimoldi O, Furlan R, Pizzinelli P, Sandrone G, Malfatto G, Dell'Orto S, Piccaluga E. Power spectral analysis of heart rate and arterial pressure variabilities as a marker of sympatho-vagal interaction in man and conscious dog. *Circ Res* 1986;**59**:178–193.

92. Ryan SM, Goldberger AL, Pincus SM, Mietus J, Lipsitz LA. Gender- and age-related differences in heart rate dynamics: are women more complex than men? *J Am Coll Cardiol* 1994;**24**:1700–1707.

93. Moak JP, Goldstein DS, Eldadah BA, Saleem A, Holmes C, Pechnik S, Sharabi Y. Supine low-frequency power of heart rate variability reflects baroreflex function, not cardiac sympathetic innervation. *Hear Rhythm* 2007;**4**:1523–1529.

94. Perini R, Orizio C, Baselli G, Cerutti S, Veicsteinas A. The influence of exercise intensity on the power spectrum of heart rate variability. *Eur J Appl Physiol Occup Physiol* 1990;**61**:143–148.

95. Tulppo MP, Kiviniemi AM, Hautala AJ, Kallio M, Seppänen T, Tiinanen S, Mäkikallio TH, Huikuri H V. Sympatho-vagal interaction in the recovery phase of exercise. *Clin Physiol Funct Imaging* 2011;**31**:272–281.

96. Koh J, Brown TE, Beightol LA, Ha CY, Eckberg DL. Human autonomic rhythms: vagal cardiac mechanisms in tetraplegic subjects. *J Physiol* 1994;**474**:483–495.

97. Agarwal SK, Norby FL, Whitsel EA, Soliman EZ, Chen LY, Loehr LR, Fuster V, Heiss G, Coresh J, Alonso A. Cardiac Autonomic Dysfunction and Incidence of Atrial Fibrillation in a Large Population-Based Cohort. *J Am Coll Cardiol* 2017;**69**:291–299.

98. Kang KW, Kim TH, Park J, Uhm JS, Joung B, Hwang C, Lee MH, Pak HN. Long-term changes in heart rate variability after radiofrequency catheter ablation for atrial fibrillation: 1-year follow-up study with irrigation tip catheter. *J Cardiovasc Electrophysiol* 2014;**25**:693–700.

99. Seaborn GEJ, Todd K, Michael KA, Baranchuk A, Abdollah H, Simpson CS, Akl SG, Redfearn DP. Heart rate variability and procedural outcome in catheter ablation for atrial fibrillation. *Ann Noninvasive Electrocardiol* 2014;**19**:23–33.

100. Pappone C, Santinelli V, Manguso F, Vicedomini G, Gugliotta F, Augello G, Mazzone P, Tortoriello V, Landoni G, Zangrillo A, Lang C, Tomita T, Mesas C, Mastella E, Alfieri O. Pulmonary Vein Denervation Enhances Long-Term Benefit after Circumferential Ablation for Paroxysmal Atrial Fibrillation. *Circulation* 2004;**109**:327–334.

101. Mori H, Kato R, Ikeda Y, Goto K, Tanaka S, Asano S, Shiki Y, Nagase T, Iwanaga S, Nishimura S, Muramatsu T, Matsumoto K. Analysis of the heart rate variability during cryoballoon ablation of atrial fibrillation. *EP Eur* 2018;**20**:1259–1267.

102. Suwalski G, Suwalski P. Successful surgical ablation of atrial fibrillation does not disturb long-term sinus rhythm variability. *Interact Cardiovasc Thorac Surg* 2018;**27**:520–524.

103. Pokushalov E, Kozlov B, Romanov A, Strelnikov A, Bayramova S, Sergeevichev D,

Bogachev-Prokophiev A, Zheleznev S, Shipulin V, Lomivorotov V V., Karaskov A, Po SS, Steinberg JS. Long-Term Suppression of Atrial Fibrillation by Botulinum Toxin Injection into Epicardial Fat Pads in Patients Undergoing Cardiac Surgery: One-Year Follow-Up of a Randomized Pilot Study. *Circ Arrhythmia Electrophysiol* 2015;**8**:1334–1341.

104. Calò L, Rebecchi M, Sciarra L, Luca L De, Fagagnini A, Zuccaro LM, Pitrone P, Dottori S, Porfirio M, Ruvo E De, Lioy E. Catheter ablation of right atrial ganglionated plexi in patients with vagal paroxysmal atrial fibrillation. *Circ Arrhythmia Electrophysiol* 2012;**5**:22–31.

105. Pokushalov E, Romanov A, Shugayev P, Artyomenko S, Shirokova N, Turov A, Katritsis DG. Selective ganglionated plexi ablation for paroxysmal atrial fibrillation. *Hear Rhythm* Elsevier Inc.; 2009;**6**:1257–1264.

106. Donadio V, Nolano M, Provitera V, Stancanelli A, Lullo F, Liguori R, Santoro L. Skin sympathetic adrenergic innervation: an immunofluorescence confocal study. *Ann Neurol* 2006;**59**:376–381.

107. Chan Y-H, Tsai W-C, Shen C, Han S, Chen LS, Lin S-F, Chen P-S. Subcutaneous nerve activity is more accurate than heart rate variability in estimating cardiac sympathetic tone in ambulatory dogs with myocardial infarction. *Hear Rhythm* 2015;**12**:1619–1627.

108. Kusayama T, Wan J, Doytchinova A, Wong J, Kabir RA, Mitscher G, Straka S, Shen C, Everett TH, Chen P-S. Skin sympathetic nerve activity and the temporal clustering of cardiac arrhythmias. *JCI Insight* 2019;**4**:1–15.

109. Chen SA, Hsieh MH, Tai CT, Tsai CF, Prakash VS, Yu WC, Hsu TL, Ding YA, Chang MS. Initiation of atrial fibrillation by ectopic beats originating from the pulmonary veins: Electrophysiological characteristics, pharmacological responses, and effects of radiofrequency ablation. *Circulation* 1999;**100**:1879–1886.

110. Oral H, Scharf C, Chugh A, Hall B, Cheung P, Good E, Veerareddy S, Pelosi F, Morady F. Catheter Ablation for Paroxysmal Atrial Fibrillation: Segmental Pulmonary Vein Ostial Ablation Versus Left Atrial Ablation. *Circulation* 2003;**108**:2355–2360.

111. Jaïs P, Weerasooriya R, Shah DC, Hocini M, Macle L, Choi KJ, Scavee C, Haïssaguerre M, Clémenty J. Ablation therapy for atrial fibrillation (AF): Past, present and future. *Cardiovasc Res* 2002;**54**:337–346.

112. Marrouche NF, Dresing T, Cole C, Bash D, Saad E, Balaban K, Pavia S V, Schweikert R, Saliba W, Abdul-Karim A, Pisano E, Fanelli R, Tchou P, Natale A. Circular mapping and ablation of the pulmonary vein for treatment of atrial fibrillation: impact of different catheter technologies. *J Am Coll Cardiol* 2002;**40**:464–474.

113. Stabile G, Bertaglia E, Senatore G, Simone A De, Zoppo F, Donnici G, Turco P, Pascotto P, Fazzari M, Vitale DF. Catheter ablation treatment in patients with drug-refractory atrial fibrillation: A prospective, multi-centre, randomized, controlled study (Catheter Ablation for the Cure of Atrial Fibrillation Study). *Eur Heart J* 2006;**27**:216–221.

114. Andrade JG, Champagne J, Dubuc M, Deyell MW, Verma A, Macle L, Leong-Sit P,

Novak P, Badra-Verdu M, Sapp J, Mangat I, Khoo C, Steinberg C, Bennett MT, Tang ASL, Khairy P, Parkash R, Guerra P, Dyrda K, Rivard L, Racine N, Sterns L, Leather R, Seifer C, Jolly U, Raymond J-M, Roux J-F, Nault I, Sarrazin J-F, Ramanathan K, et al. Cryoballoon or Radiofrequency Ablation for Atrial Fibrillation Assessed by Continuous Monitoring. *Circulation* 2019;**140**:1779–1788.

115. Ouyang F, Antz M, Ernst S, Hachiya H, Mavrakis H, Deger FT, Schaumann A, Chun J, Falk P, Hennig D, Liu X, Bänsch D, Kuck KH. Recovered pulmonary vein conductiona as a dominant factor for recurrent atrial tachyarrhythmias after complete circular isolation of the pulmonary veins: Lessons from double lasso technique. *Circulation* 2005;**111**:127–135.

116. Kowalski M, Grimes MM, Perez FJ, Kenigsberg DN, Koneru J, Kasirajan V, Wood MA, Ellenbogen KA. Histopathologic characterization of chronic radiofrequency ablation lesions for pulmonary vein isolation. *J Am Coll Cardiol* Elsevier Inc.; 2012;**59**:930–938.

117. Jiang RH, Po SS, Tung R, Liu Q, Sheng X, Zhang ZW, Sun YX, Yu L, Zhang P, Fu GS, Jiang CY. Incidence of pulmonary vein conduction recovery in patients without clinical recurrence after ablation of paroxysmal atrial fibrillation: Mechanistic implications. *Hear Rhythm* 2014;**11**:969–976.

118. Pratola C, Baldo E, Notarstefano P, Toselli T, Ferrari R. Radiofrequency Ablation of Atrial Fibrillation: Is the Persistence of All Intraprocedural Targets Necessary for Long-Term Maintenance of Sinus Rhythm? *Circulation* 2008;**117**:136–143.

119. Nery PB, Belliveau D, Nair GM, Bernick J, Redpath CJ, Szczotka A, Sadek MM, Green MS, Wells G, Birnie DH. Relationship Between Pulmonary Vein Reconnection and Atrial Fibrillation Recurrence: A Systematic Review and Meta-Analysis. *JACC Clin Electrophysiol* 2016;**2**:474–483.

120. Kuck K-H, Hoffmann BA, Ernst S, Wegscheider K, Treszl A, Metzner A, Eckardt L, Lewalter T, Breithardt G, Willems S. Impact of Complete Versus Incomplete Circumferential Lines Around the Pulmonary Veins During Catheter Ablation of Paroxysmal Atrial Fibrillation. *Circ Arrhythmia Electrophysiol* 2016;**9**:1–10.

121. Dukkipati SR, Neuzil P, Kautzner J, Petru J, Wichterle D, Skoda J, Cihak R, Peichl P, Russo A Dello, Pelargonio G, Tondo C, Natale A, Reddy VY. The durability of pulmonary vein isolation using the visually guided laser balloon catheter: Multicenter results of pulmonary vein remapping studies. *Hear Rhythm* 2012;**9**:919–925.

122. Dixit S, Marchlinski FE, Lin D, Callans DJ, Bala R, Riley MP, Garcia FC, Hutchinson MD, Ratcliffe SJ, Cooper JM, Verdino RJ, Patel V V., Zado ES, Cash NR, Killian T, Tomson TT, Gerstenfeld EP. Randomized ablation strategies for the treatment of persistent atrial fibrillation RASTA study. *Circ Arrhythmia Electrophysiol* 2012;**5**:287–294.

123. Biase L Di, Burkhardt JD, Mohanty P, Sanchez J, Mohanty S, Horton R, Gallinghouse GJ, Bailey SM, Zagrodzky JD, Santangeli P, Hao S, Hongo R, Beheiry S, Themistoclakis S, Bonso A, Rossillo A, Corrado A, Raviele A, Al-Ahmad A, Wang P, Cummings JE, Schweikert RA, Pelargonio G, Russo A Dello, Casella M, Santarelli P, Lewis WR, Natale A. Left atrial appendage: An underrecognized trigger site of

atrial fibrillation. *Circulation* 2010;**122**:109–118.

124. Hsu LF, Jaïs P, Keane D, Wharton JM, Deisenhofer I, Hocini M, Shah DC, Sanders P, Scavée C, Weerasooriya R, Clémenty J, Haïssaguerre M. Atrial Fibrillation Originating from Persistent Left Superior Vena Cava. *Circulation* 2004;**109**:828–832.

125. Brachmann J, Hummel J, Wilber D, Sarver A, Rapkin J, Shpun S, Szili-Torok T. Late Breaking Clinical Trials Session I: PROSPECTIVE RANDOMIZED COMPARISON OF ROTOR ABLATION VS CONVENTIONAL ABLATION FOR TREATMENT OF PERSISTENT ATRIAL FIBRILLATION - THE REAFFIRM TRIAL. *Hear Rhythm* 2019;963–965.

126. Parameswaran R, Voskoboinik A, Gorelik A, Lee G, Kistler PM, Sanders P, Kalman JM. Clinical impact of rotor ablation in atrial fibrillation: A systematic review. *Europace* 2018;**20**:1099–1106.

127. Driessen AHG, Berger WR, Krul SPJ, Berg NWE van den, Neefs J, Piersma FR, Chan Pin Yin DRPP, Jong JSSG de, Boven WJP van, Groot JR de. Ganglion Plexus Ablation in Advanced Atrial Fibrillation: The AFACT Study. *J Am Coll Cardiol* 2016;**68**:1155–1165.

128. Scanavacca M, Pisani CF, Hachul D, Lara S, Hardy C, Darrieux F, Trombetta I, Negrão CE, Sosa E. Selective atrial vagal denervation guided by evoked vagal reflex to treat patients with paroxysmal atrial fibrillation. *Circulation* 2006;**114**:876–885.

129. Katritsis DG, Pokushalov E, Romanov A, Giazitzoglou E, Siontis GCM, Po SS, Camm AJ, Ioannidis JPA. Autonomic denervation added to pulmonary vein isolation for paroxysmal atrial fibrillation: A randomized clinical trial. *J Am Coll Cardiol* 2013;**62**:2318–2325.

130. Kampaktsis PN, Oikonomou EK, Y. Choi D, Cheung JW. Efficacy of ganglionated plexi ablation in addition to pulmonary vein isolation for paroxysmal versus persistent atrial fibrillation: a meta-analysis of randomized controlled clinical trials. *J Interv Card Electrophysiol* Journal of Interventional Cardiac Electrophysiology; 2017;**50**:253–260.

131. Katritsis DG, Giazitzoglou E, Zografos T, Pokushalov E, Po SS, Camm AJ. Rapid pulmonary vein isolation combined with autonomic ganglia modification: A randomized study. *Hear Rhythm* 2011;**8**:672–678.

132. Pokushalov E, Romanov A, Katritsis DG, Artyomenko S, Shirokova N, Karaskov A, Mittal S, Steinberg JS. Ganglionated plexus ablation vs linear ablation in patients undergoing pulmonary vein isolation for persistent/long-standing persistent atrial fibrillation: A randomized comparison. *Hear Rhythm* Elsevier; 2013;**10**:1280–1286.

133. Ariyarathna N, Kumar S. Role of Ganglionic Plexus Ablation in Treatment of Atrial Fibrillation: a Systematic Review and Meta-Analysis. *J Am Coll Cardiol* Australasian Society of Cardiac and Thoracic Surgeons and The Cardiac Society of Australia and New Zealand; 2017;**69**:496.

134. Barbano RL. Botulinum toxins in clinical practice: Gaps in knowledge. *Neurol Clin*

Pract 2016;**6**:206–208.

135. Tsuboi M, Furukawa Y, Kurogouchi F, Nakajima K, Hirose M, Chiba S. Botulinum Neurotoxin A Blocks Cholinergic Ganglionic Neurotransmission in the Dog Heart. *Jpn J Pharmacol* 2002;**89**:249–254.

136. Rossetto O, Seveso M, Caccin P, Schiavo G, Montecucco C. Tetanus and botulinum neurotoxins: turning bad guys into good by research. *Toxicon* 2001;**39**:27–41.

137. Oh S, Choi EK, Zhang Y, Mazgalev TN. Botulinum toxin injection in epicardial autonomic ganglia temporarily suppresses vagally mediated atrial fibrillation. *Circ Arrhythmia Electrophysiol* 2011;**4**:560–565.

138. Pokushalov E, Kozlov B, Romanov A, Strelnikov A, Bayramova S, Sergeevichev D, Bogachev-Prokophiev A, Zheleznev S, Shipulin V, Salakhutdinov N, Lomivorotov V V., Karaskov A, Po SS, Steinberg JS. Botulinum toxin injection in epicardial fat pads can prevent recurrences of atrial fibrillation after cardiac surgery: Results of a randomized pilot study. *J Am Coll Cardiol* American College of Cardiology Foundation; 2014;**64**:628–629.

139. Romanov A, Pokushalov E, Ponomarev D, Bayramova S, Shabanov V, Losik D, Stenin I, Elesin D, Mikheenko I, Strelnikov A, Sergeevichev D, Kozlov B, Po SS, Steinberg JS. Long-term suppression of atrial fibrillation by botulinum toxin injection into epicardial fat pads in patients undergoing cardiac surgery: Three-year follow-up of a randomized study. *Hear Rhythm* Elsevier Inc.; 2019;**16**:172–177.

140. Lee S, Khrestian A, Waldo AL, Khrestian CM, Markowitz A, Sahadevan J. Effect of Lidocaine Injection of Ganglionated Plexi in a Canine Model and Patients With Persistent and Long-Standing Persistent Atrial Fibrillation. *J Am Heart Assoc* 2019;**8**:e011401.

141. Wong CX, Ganesan AN, Selvanayagam JB. Epicardial fat and atrial fibrillation: Current evidence, potential mechanisms, clinical implications, and future directions. *Eur Heart J* 2017;**38**:1294–1302.

142. Drossos G, Koutsogiannidis CP, Ananiadou O, Kapsas G, Ampatzidou F, Madesis A, Bismpa K, Palladas P, Karagounis L. Pericardial fat is strongly associated with atrial fibrillation after coronary artery bypass graft surgery. *Eur J Cardio-thoracic Surg* 2014;**46**:1014–1020.

143. Nagashima K, Okumura Y, Watanabe I, Nakai T, Ohkubo K, Kofune M, Mano H, Sonoda K, Hiro T, Nikaido M, Hirayama A. Does location of epicardial adipose tissue correspond to endocardial high dominant frequency or complex fractionated atrial electrogram sites during atrial fibrillation? *Circ Arrhythmia Electrophysiol* 2012;**5**:676–683.

144. Polak T, Markulin F, Ehlis A-C, Langer JBM, Ringel TM, Fallgatter AJ. Far field potentials from brain stem after transcutaneous Vagus nerve stimulation: optimization of stimulation and recording parameters. *J Neural Transm* 2009;**116**:1237–1242.

145. Greif R, Laciny S, Mokhtarani M, Doufas AG, Bakhshandeh M, Dorfer L, Sessler DI. Transcutaneous electrical stimulation of an auricular acupuncture point

decreases anesthetic requirement. *Anesthesiology* 2002;**96**:306–312.

146. Yu L, Scherlag BJ, Li S, Fan Y, Dyer J, Male S, Varma V, Sha Y, Stavrakis S, Po SS. Low-level transcutaneous electrical stimulation of the auricular branch of the vagus nerve: A noninvasive approach to treat the initial phase of atrial fibrillation. *Hear Rhythm* Elsevier; 2013;**10**:428–435.

147. Stavrakis S, Humphrey MB, Scherlag BJ, Hu Y, Jackman WM, Nakagawa H, Lockwood D, Lazzara R, Po SS. Low-level transcutaneous electrical vagus nerve stimulation suppresses atrial fibrillation. *J Am Coll Cardiol* 2015;**65**:867–875.

148. Stavros S, Stoner J, Humphrey M, Scherlag B, Jackman W, Po S. Late Breaking Clinical Trials Session I: TRANSCUTANEOUS ELECTRICAL VAGUS NERVE STIMULATION TO SUPPRESS ATRIAL FIBRILLATION (TREAT AF): A RANDOMIZED CLINICAL TRIAL. *Hear Rhythm* 2019;963–965.

149. Nagashima C, Sakaguchi A, Kamisasa A, Kawanuma S. Cardiovascular complications on upper vagal rootlet section for glossopharyngeal neuralgia; case report. *J Neurosurg* 1976;**44**:248–253.

150. Stavrakis S, Nakagawa H, Po SS, Scherlag BJ, Lazzara R, Jackman WM. The role of the autonomic ganglia in atrial fibrillation. *JACC Clin Electrophysiol* 2015;**1**:1–13.

151. Singh RR, Denton KM. Renal denervation a treatment for hypertension and chronic kidney disease. *Hypertension* 2018;**72**:528–536.

152. Scherlag BJ, Nakagawa H, Jackman WM, Yamanashi WS, Patterson E, Po S, Lazzara R. Electrical stimulation to identify neural elements on the heart: their role in atrial fibrillation. *J Interv Card Electrophysiol* 2005;**13 Suppl 1**:37–42.

153. Ali RL, Cantwell CD, Qureshi NA, Roney CH, Lim PB, Sherwin SJ, Siggers JH, Peters NS. Automated fiducial point selection for reducing registration error in the co-localisation of left atrium electroanatomic and imaging data. *Proc Annu Int Conf IEEE Eng Med Biol Soc EMBS* 2015;**2015**-**Novem**:1989–1992.

154. Lim PB, Malcolme-Lawes LC, Stuber T, Kojodjojo P, Wright IJ, Francis DP, Wyn Davies D, Peters NS, Kanagaratnam P. Stimulation of the intrinsic cardiac autonomic nervous system results in a gradient of fibrillatory cycle length shortening across the atria during atrial fibrillation in humans. *J Cardiovasc Electrophysiol* 2011;**22**:1224–1231.

155. Po SS, Li Y, Tang D, Liu H, Geng N, Jackman WM, Scherlag B, Lazzara R, Patterson E. Rapid and stable re-entry within the pulmonary vein as a mechanism initiating paroxysmal atrial fibrillation. *J Am Coll Cardiol* Elsevier Masson SAS; 2005;**45**:1871–1877.

156. Chen PS, Chen LS, Fishbein MC, Lin SF, Nattel S. Role of the autonomic nervous system in atrial fibrillation: Pathophysiology and therapy. *Circ Res* 2014;**114**:1500–1515.

157. Ardell JL, Armour JA. Neurocardiology: Structure-Based function. *Compr Physiol* 2016;**6**:1635–1653.

158. Pauza DH, Skripka V, Pauziene N, Stropus R. Morphology, distribution, and variability of the epicardiac neural ganglionated subplexuses in the human heart.

Anat Rec 2000;**259**:353–382.

159. Chevalier P, Tabib A, Meyronnet D, Chalabreysse L, Restier L, Ludman V, Aliès A, Adeleine P, Thivolet F, Burri H, Loire R, François L, Fanton L. Quantitative study of nerves of the human left atrium. *Hear Rhythm* 2005;**2**:518–522.

160. Tan AY, Li H, Wachsmann-Hogiu S, Chen LS, Chen PS, Fishbein MC. Autonomic Innervation and Segmental Muscular Disconnections at the Human Pulmonary Vein-Atrial Junction. Implications for Catheter Ablation of Atrial-Pulmonary Vein Junction. *J Am Coll Cardiol* 2006;**48**:132–143.

161. Quan KJ, Lee JH, Hare GF Van, Biblo LA, Mackall UA, Carlson MD. Identification and characterization of atrioventricular parasympathetic innervation in humans. *J Cardiovasc Electrophysiol* 2002;**13**:735–739.

162. Quan KJ, Lee JH, Geha AS, Biblo LA, Hare GF Van, Mackall JA, Carlson MD. Characterization of sinoatrial parasympathetic innervation in humans. *J Cardiovasc Electrophysiol* 1999;**10**:1060–1065.

163. Lazzara R, Scherlag BJ, Robinson MJ, Samet P. Selective in situ parasympathetic control of the canine sinoatrial and atrioventricular nodes. *Circ Res* 1973;**32**:393–401.

164. Randall DC, Brown DR, McGuirt a S, Thompson GW, Armour JA, Ardell JL. Interactions within the intrinsic cardiac nervous system contribute to chronotropic regulation. *Am J Physiol Regul Integr Comp Physiol* 2003;**285**:R1066–R1075.

165. Butler CK, Smith FM, Cardinal R, Murphy D a, Hopkins D a, Armour J a. Cardiac responses to electrical stimulation of discrete loci in canine atrial and ventricular ganglionated plexi. *Am J Physiol* 1990;**259**:H1365-73.

166. Takahashi N, Zipes DP. Vagal modulation of adrenergic effects on canine sinus and atrioventricular nodes. *Am J Physiol* 1983;**244**:H775-81.

167. Scherlag BJ, Yamanashi WS, Schauerte P, Scherlag M, Sun YX, Hou Y, Jackman WM, Lazzara R. Endovascular stimulation within the left pulmonary artery to induce slowing of heart rate and paroxysmal atrial fibrillation. *Cardiovasc Res* 2002;**54**:470–475.

168. Lemery R, Birnie D, Tang ASL, Green M, Gollob M. Feasibility study of endocardial mapping of ganglionated plexuses during catheter ablation of atrial fibrillation. *Hear Rhythm* 2006;**3**:387–389.

169. Verma A, Saliba WI, Lakkireddy D, Burkhardt JD, Cummings JE, Wazni OM, Belden WA, Thal S, Schweikert RA, Martin DO, Tchou PJ, Natale A. Vagal responses induced by endocardial left atrial autonomic ganglion stimulation before and after pulmonary vein antrum isolation for atrial fibrillation. *Hear Rhythm* 2007;**4**:1177–1182.

170. Hou Y, Scherlag BJ, Lin J, Zhou J, Song J, Zhang Y, Patterson E, Lazzara R, Jackman WM, Po SS. Interactive atrial neural network: Determining the connections between ganglionated plexi. *Hear Rhythm* 2007;**4**:56–63.

171. Liao K, Yu L, Zhou X, Saren G, Wang S, Wang Z, Huang B, Yang K, Jiang H. Low-

Level Baroreceptor Stimulation Suppresses Atrial Fibrillation by Inhibiting Ganglionated Plexus Activity. *Can J Cardiol* Canadian Cardiovascular Society; 2015;**31**:767–774.

172. Lu Z, Scherlag BJ, Lin J, Yu L, Guo JH, Niu G, Jackman WM, Lazzara R, Jiang H, Po SS. Autonomic mechanism for initiation of rapid firing from atria and pulmonary veins: Evidence by ablation of ganglionated plexi. *Cardiovasc Res* 2009;**84**:245–252.

173. Malcolme-Lawes LC, Lim PB, Wright I, Kojodjojo P, Koa-Wing M, Jamil-Copley S, Dehbi HM, Francis DP, Davies DW, Peters NS, Kanagaratnam P. Characterization of the left atrial neural network and its impact on autonomic modification procedures. *Circ Arrhythmia Electrophysiol* 2013;**6**:632–640.

174. Scherlag BJ, Yamanashi W, Patel U, Lazzara R, Jackman WM. Autonomically induced conversion of pulmonary vein focal firing into atrial fibrillation. *J Am Coll Cardiol* Elsevier Masson SAS; 2005;**45**:1878–1886.

175. Schauerte P, Scherlag BJ, Patterson E, Scherlag MA, Matsudaria K, Nakagawa H, Lazzara R, Jackman WM. Focal atrial fibrillation: Experimental evidence for a pathophysiologic role of the autonomic nervous system. *J Cardiovasc Electrophysiol* 2001;**12**:592–599.

176. Schauerte P, Scherlag BJ, Pitha J, Scherlag MA, Reynolds D, Lazzara R, Jackman WM. Catheter ablation of cardiac autonomic nerves for prevention of vagal atrial fibrillation. *Circulation* 2000;**102**:2774–2780.

177. Zhou J, Scherlag BJ, Edwards J, Jackman WM, Lazzara R, Po SS. Gradients of atrial refractoriness and inducibility of atrial fibrillation due to stimulation of ganglionated plexi. *J Cardiovasc Electrophysiol* 2007;**18**:83–90.

178. Singh S, Johnson PI, Javed A, Gray TS, Lonchyna VA, Wurster RD. Monoamine- and histamine-synthesizing enzymes and neurotransmitters within neurons of adult human cardiac ganglia. *Circulation* 1999;**99**:411–419.

179. Ardell JL, Randall WC. Selective vagal innervation of sinoatrial and atrioventricular nodes in canine heart. *Am J Physiol - Hear Circ Physiol* 1986;**251**:H764–H773.

180. Hsieh MH, Chen SA, Tai CT, Tsai CF, Prakash VS, Yu WC, Liu CC, Ding YA, Chang MS. Double multielectrode mapping catheters facilitate radiofrequency catheter ablation of focal atrial fibrillation originating from pulmonary veins. *J Cardiovasc Electrophysiol* 1999;**10**:136–144.

181. Lau CP, Tse HF, Ayers GM. Defibrillation-guided radiofrequency ablation of atrial fibrillation secondary to an atrial focus. *J Am Coll Cardiol* Elsevier Masson SAS; 1999;**33**:1217–1226.

182. Stavrakis S, Po S. Ganglionated Plexi Ablation: Physiology and Clinical Applications. *Arrhythmia Electrophysiol Rev* 2017;**6**:186.

183. Kim M, Sandler B, Sikkel M et al. TARGETING AUTONOMIC UPSTREAM DRIVERS OF ATRIAL FIBRILLATION TO TREAT PAROXYSMAL ATRIAL FIBRILLATION WITHOUT PULMONARY VEIN ISOLATION. *Hear Rhythm* 2019;**16**:S186.

184. Hanna P, Rajendran PS, Ajijola OA, Vaseghi M, Andrew Armour J, Ardell JL, Shivkumar K. Cardiac neuroanatomy - Imaging nerves to define functional control. *Auton Neurosci Basic Clin* 2017;**207**:48–58.

185. Benjamin EJ, Levy D, Vaziri SM, D'Agostino RB, Belanger AJ, Wolf PA. Independent risk factors for atrial fibrillation in a population-based cohort. The Framingham Heart Study. *JAMA* 1994;**271**:840–844.

186. Verdecchia P, Angeli F, Reboldi G. Hypertension and Atrial Fibrillation. *Circ Res* 2018;**122**:352–368.

187. Verma A, Wazni OM, Marrouche NF, Martin DO, Kilicaslan F, Minor S, Schweikert RA, Saliba W, Cummings J, Burkhardt JD, Bhargava M, Belden WA, Abdul-Karim A, Natale A. Pre-existent left atrial scarring in patients undergoing pulmonary vein antrum isolation: An independent predictor of procedural failure. *J Am Coll Cardiol* Elsevier Masson SAS; 2005;**45**:285–292.

188. Yamaguchi T, Fukui A, Node K. Bipolar voltage mapping for the evaluation of atrial substrate: Can we overcome the challenge of directionality? *J Atr Fibrillation* 2019;**11**:1–13.

189. Yamaguchi T, Tsuchiya T, Nagamoto Y, Miyamoto K, Murotani K, Okishige K, Takahashi N. Long-term results of pulmonary vein antrum isolation in patients with atrial fibrillation: an analysis in regards to substrates and pulmonary vein reconnections. *Europace* 2014;**16**:511–520.

190. Squara F, Frankel DS, Schaller R, Kapa S, Chik WW, Callans DJ, Marchlinski FE, Dixit S. Voltage mapping for delineating inexcitable dense scar in patients undergoing atrial fibrillation ablation: A new end point for enhancing pulmonary vein isolation. *Hear Rhythm* 2014;**11**:1904–1911.

191. Teunissen C, Kassenberg W, Heijden JF van der, Hassink RJ, Driel VJHM van, Zuithoff NPA, Doevendans PA, Loh P. Five-year efficacy of pulmonary vein antrum isolation as a primary ablation strategy for atrial fibrillation: a single-centre cohort study. *Europace* 2016;**18**:1335–1342.

192. FICHTNER S, CZUDNOCHOWSKY U, HESSLING G, REENTS T, ESTNER H, WU J, JILEK C, AMMAR S, KARCH MR, DEISENHOFER I. Very Late Relapse of Atrial Fibrillation after Pulmonary Vein Isolation: Incidence and Results of Repeat Ablation. *Pacing Clin Electrophysiol* 2010;**33**:1258–1263.

193. Biase L Di, Conti S, Mohanty P, Bai R, Sanchez J, Walton D, John A, Santangeli P, Elayi CS, Beheiry S, Gallinghouse GJ, Mohanty S, Horton R, Bailey S, Burkhardt JD, Natale A. General anesthesia reduces the prevalence of pulmonary vein reconnection during repeat ablation when compared with conscious sedation: Results from a randomized study. *Hear Rhythm* 2011;**8**:368–372.

194. Kim TH, Park J, Uhm JS, Joung B, Lee MH, Pak HN. Pulmonary vein reconnection predicts good clinical outcome after second catheter ablation for atrial fibrillation. *Europace* 2017;**19**:961–967.

195. LIN D, SANTANGELI P, ZADO ES, BALA R, HUTCHINSON MD, RILEY MP, FRANKEL DS, GARCIA F, DIXIT S, CALLANS DJ, MARCHLINSKI FE. Electrophysiologic Findings and Long-Term Outcomes in Patients Undergoing Third or More

Catheter Ablation Procedures for Atrial Fibrillation. *J Cardiovasc Electrophysiol* 2015;**26**:371–377.

196. Voort PH van der, Meijer A. Spontaneous and induced pulmonary vein tachycardia after pulmonary vein isolation. *Europace* 2004;**6**:613–616.

197. Tse HF, Lau CP, Kou W, Pelosi F, Oral H, Kim M, Michaud GF, Knight BP, Moscucci M, Strickberger SA, Morady F. Prevalence and significance of exit block during arrhythmias arising in pulmonary veins. *J Cardiovasc Electrophysiol* 2000;**11**:379–386.

198. Ma C, Dong J, Liu X, Long D, Fang D, Hu F, Yu R, Tang R, Hao P, Lu C. Pulmonary vein tachycardia after pulmonary vein isolation in patients with atrial fibrillation. *Chin Med J (Engl)* 2006;**119**:551–556.

199. Jiang RH, Hu GS, Liu Q, Sheng X, Sun YX, Yu L, Zhang P, Zhang ZW, Chen SQ, Ye Y, Zhu J, Fu GS, Jiang CY. Impact of Anatomically Guided Ganglionated Plexus Ablation on Electrical Firing from Isolated Pulmonary Veins. *PACE - Pacing Clin Electrophysiol* 2016;**39**:1351–1358.

200. Kumagai K, Ogawa M, Noguchi H, Yasuda T, Nakashima H, Saku K. Electrophysiologic properties of pulmonary veins assessed using a multielectrode basket catheter. *J Am Coll Cardiol* Elsevier Masson SAS; 2004;**43**:2281–2289.

201. Adragão P, Santos KR, Aguiar C, Neves JP, Abecassis M, Cavaco D, Morgado F, Bernardo R, Bonhorst D, Queiroz e Melo J, Seabra-Gomes R. Atrial fibrillation and effective refractory period of the pulmonary vein ostia. *Rev Port Cardiol* 2002;**21**:1125–1134.

202. Hou Y, Scherlag BJ, Lin J, Zhang Y, Lu Z, Truong K, Patterson E, Lazzara R, Jackman WM, Po SS. Ganglionated Plexi Modulate Extrinsic Cardiac Autonomic Nerve Input. Effects on Sinus Rate, Atrioventricular Conduction, Refractoriness, and Inducibility of Atrial Fibrillation. *J Am Coll Cardiol* 2007;**50**:61–68.

203. Yamashiro K, Takami K, Sakamoto Y, Koyo S. Abstract 17688: Antifibrillatory Effects by Selective Ganglionated Plexi Ablation in Patients With Atrial Fibrillation. *Circulation* 2010;**122**.

204. O'Neill MD, Wright M, Knecht S, Jais P, Hocini M, Takahashi Y, Jonsson A, Sacher F, Matsuo S, Lim KT, Arantes L, Derval N, Lellouche N, Nault I, Bordachar P, Clementy J, Haissaguerre M. Long-term follow-up of persistent atrial fibrillation ablation using termination as a procedural endpoint. *Eur Heart J* 2009;**30**:1105–1112.

205. Vogler J, Willems S, Sultan A, Schreiber D, Lüker J, Servatius H, Schäffer B, Moser J, Hoffmann BA, Steven D. Pulmonary Vein Isolation Versus Defragmentation. *J Am Coll Cardiol* 2015;**66**:2743–2752.

206. Scherr D, Khairy P, Miyazaki S, Aurillac-Lavignolle V, Pascale P, Wilton SB, Ramoul K, Komatsu Y, Roten L, Jadidi A, Linton N, Pedersen M, Daly M, O'Neill M, Knecht S, Weerasooriya R, Rostock T, Manninger M, Cochet H, Shah AJ, Yeim S, Denis A, Derval N, Hocini M, Sacher F, Haissaguerre M, Jais P. Five-Year Outcome of Catheter Ablation of Persistent Atrial Fibrillation Using Termination of Atrial Fibrillation as a Procedural Endpoint. *Circ Arrhythmia Electrophysiol* 2015;**8**:18–

24.

207. Elayi CS, Biase L Di, Barrett C, Ching CK, Aly M al, Lucciola M, Bai R, Horton R, Fahmy TS, Verma A, Khaykin Y, Shah J, Morales G, Hongo R, Hao S, Beheiry S, Arruda M, Schweikert RA, Cummings J, Burkhardt JD, Wang P, Al-Ahmad A, Cauchemez B, Gaita F, Natale A. Atrial fibrillation termination as a procedural endpoint during ablation in long-standing persistent atrial fibrillation. *Hear Rhythm* 2010;**7**:1216–1223.

208. Kochhäuser S, Jiang CY, Betts TR, Chen J, Deisenhofer I, Mantovan R, Macle L, Morillo CA, Haverkamp W, Weerasooriya R, Albenque JP, Nardi S, Menardi E, Novak P, Sanders P, Verma A. Impact of acute atrial fibrillation termination and prolongation of atrial fibrillation cycle length on the outcome of ablation of persistent atrial fibrillation: A substudy of the STAR AF II trial. *Hear Rhythm* Elsevier Inc.; 2017;**14**:476–483.

209. Nori SL, Gaudino M, Alessandrini F, Bronzetti E, Santarelli P. Immunohistochemical evidence for sympathetic denervation and reinnervation after necrotic injury in rat myocardium. *Cell Mol Biol (Noisy-le-grand)* 1995;**41**:799–807.

210. Cao J-M, Fishbein MC, Han JB, Lai WW, Lai AC, Wu T-J, Czer L, Wolf PL, Denton TA, Shintaku IP, Chen P-S, Chen LS. Relationship Between Regional Cardiac Hyperinnervation and Ventricular Arrhythmia. *Circulation* 2000;**101**:1960–1969.

211. Kim DT, Luthringer DJ, Lai AC, Suh G, Czer L, Chen LS, Chen P-S, Fishbein MC. Sympathetic nerve sprouting after orthotopic heart transplantation. *J Hear Lung Transplant* 2004;**23**:1349–1358.

212. Zhou S, Chen LS, Miyauchi Y, Miyauchi M, Kar S, Kangavari S, Fishbein MC, Sharifi B, Chen P-S. Mechanisms of Cardiac Nerve Sprouting After Myocardial Infarction in Dogs. *Circ Res* 2004;**95**:76–83.

213. Okuyama Y, Pak H-N, Miyauchi Y, Liu Y-B, Chou C-C, Hayashi H, Fu KJ, Kerwin WF, Kar S, Hata C, Karagueuzian HS, Fishbein MC, Chen P-S, Chen LS. Nerve sprouting induced by radiofrequency catheter ablation in dogs. *Hear Rhythm* 2004;**1**:712–717.

214. Sakamoto S, Schuessler RB, Lee AM, Aziz A, Lall SC, Damiano RJ. Vagal denervation and reinnervation after ablation of ganglionated plexi. *J Thorac Cardiovasc Surg* 2010;**139**:444–452.

215. Chiou C-W, Zipes DP. Selective Vagal Denervation of the Atria Eliminates Heart Rate Variability and Baroreflex Sensitivity While Preserving Ventricular Innervation. *Circulation* 1998;**98**:360–368.

216. Mao J, Yin X, Zhang Y, Yan Q, Dong J, Ma C, Liu X. Ablation of epicardial ganglionated plexi increases atrial vulnerability to arrhythmias in dogs. *Circ Arrhythmia Electrophysiol* 2014;**7**:711–717.

217. Wang HT, Li ZL, Fan BY, Su FF, Zhao JB, Ren J, Zheng QS. The independent role of the aortic root ganglionated plexi in the initiation of atrial fibrillation: An experimental study. *J Thorac Cardiovasc Surg* 2014;**148**:73–76.

218. Saw EL, Kakinuma Y, Fronius M, Katare R. The non-neuronal cholinergic system in the heart: A comprehensive review. *J Mol Cell Cardiol* 2018;**125**:129–139.

219. Wessler I, Kirkpatrick CJ. Acetylcholine beyond neurons: the non-neuronal cholinergic system in humans. *Br J Pharmacol* 2008;**154**:1558–1571.

220. Kakinuma Y, Akiyama T, Sato T. Cholinoceptive and cholinergic properties of cardiomyocytes involving an amplification mechanism for vagal efferent effects in sparsely innervated ventricular myocardium. *FEBS J* 2009;**276**:5111–5125.

221. Batulevicius D, Skripka V, Pauziene N, Pauza DH. Topography of the porcine epicardiac nerve plexus as revealed by histochemistry for acetylcholinesterase. *Auton Neurosci Basic Clin* 2008;**138**:64–75.

222. Arora RC, Waldmann M, Hopkins DA, Armour JA. Porcine intrinsic cardiac ganglia. *Anat Rec - Part A Discov Mol Cell Evol Biol* 2003;**271**:249–258.

223. Pauziene N, Rysevaite-Kyguoliene K, Alaburda P, Pauza AG, Skukauskaite M, Masaityte A, Laucaityte G, Saburkina I, Inokaitis H, Plisiene J, Pauza DH. Neuroanatomy of the Pig Cardiac Ventricles. A Stereomicroscopic, Confocal and Electron Microscope Study. *Anat Rec* 2017;**300**:1756–1780.

224. Doshi RN, Wu T-J, Yashima M, Kim Y-H, Ong JJC, Cao J-M, Hwang C, Yashar P, Fishbein MC, Karagueuzian HS, Chen P-S. Relation Between Ligament of Marshall and Adrenergic Atrial Tachyarrhythmia. *Circulation* 1999;**100**:876–883.

225. Sharifov OF, Fedorov V V., Beloshapko GG, Glukhov A V., Yushmanova A V., Rosenshtraukh L V. Roles of Adrenergic and Cholinergic Stimulation in Spontaneous Atrial Fibrillation in Dogs. *J Am Coll Cardiol* 2004;**43**:483–490.

226. Greer-Short A, Poelzing S. Temporal response of ectopic activity in guinea pig ventricular myocardium in response to isoproterenol and acetylcholine. *Front Physiol* 2015;**6**.

227. Ulphani JS, Cain JH, Inderyas F, Gordon D, Gikas P V., Shade G, Mayor D, Arora R, Kadish AH, Goldberger JJ. Quantitative analysis of parasympathetic innervation of the porcine heart. *Hear Rhythm* Elsevier Inc.; 2010;**7**:1113–1119.

228. Roy A, Guatimosim S, Prado VF, Gros R, Prado M a M. Cholinergic activity as a new target in diseases of the heart. *Mol Med* 2015;**20**:527–537.

229. Sviglerova J, Kuncova J, Stengl M. Cardiovascular Models: Heart Secondarily Affected by Disease. Anim. Model. Study Hum. Dis. Elsevier; 2013.

230. Bers DM. Cardiac excitation–contraction coupling. *Nature* 2002;**415**:198–205.

231. Winter J, Bishop MJ, Wilder CDE, O'Shea C, Pavlovic D, Shattock MJ. Sympathetic Nervous Regulation of Calcium and Action Potential Alternans in the Intact Heart. *Front Physiol* 2018;**9**.

232. Robertson DW, Biaggioni I, Burnstock G, Low P, Paton JFR. Primer on the Autonomic Nervous System. Prim. Auton. Nerv. Syst. Elsevier; 2012.

233. Bjurholm A, Kreicbergs A, Terenius L, Goldstein M, Schultzberg M. Neuropeptide Y-, tyrosine hydroxylase- and vasoactive intestinal polypeptide-immunoreactive nerves in bone and surrounding tissues. *J Auton Nerv Syst* 1988;**25**:119–125.

234. Afonso-Oramas D, Cruz-Muros I, Castro-HernÃ¡ndez J, Salas-HernÃ¡ndez J, Barroso-Chinea P, GarcÃ-a-HernÃ¡ndez S, Lanciego JL, GonzÃ¡lez-HernÃ¡ndez T. Striatal vessels receive phosphorylated tyrosine hydroxylase-rich innervation from midbrain dopaminergic neurons. *Front Neuroanat* 2014;**8**.

235. Burgi K, Cavalleri MT, Alves AS, Britto LRG, Antunes VR, Michelini LC. Tyrosine hydroxylase immunoreactivity as indicator of sympathetic activity: simultaneous evaluation in different tissues of hypertensive rats. *Am J Physiol Integr Comp Physiol* 2011;**300**:R264–R271.

236. Hirao T, Nitta J, Adachi A, Takahashi Y, Goya M, Hirao K. First confirmation of histologic changes in the human heart after cryoballoon ablation. *Hear Case Reports* 2019;**5**:93–96.

237. Cabrera JA, Pizarro G, Sanchez-Quintana D. Transmural ablation of all the pulmonary veins: is it the Holy Grail for cure of atrial fibrillation? *Eur Heart J* 2010;**31**:2708–2711.

238. Zigmond RE, Chalazonitis A, Joh T. Preganglionic nerve stimulation increases the amount of tyrosine hydroxylase in the rat superior cervical ganglion. *Neurosci Lett* 1980;**20**:61–65.

239. Vijayaraghavan S, Karami A, Aeinehband S, Behbahani H, Grandien A, Nilsson B, Ekdahl KN, Lindblom RPF, Piehl F, Darreh-Shori T. Regulated Extracellular Choline Acetyltransferase Activity- The Plausible Missing Link of the Distant Action of Acetylcholine in the Cholinergic Anti-Inflammatory Pathway. Silman I, ed. *PLoS One* 2013;**8**:e65936.

240. Rivarola EWR, Scanavacca M, Ushizima M, Cestari I, Hardy C, Lara S, Pisani C, Sosa E. Spectral characteristics of atrial electrograms in sinus rhythm correlates with sites of ganglionated plexuses in patients with paroxysmal atrial fibrillation. *Europace* 2011;**13**:1141–1147.

241. Chang HY, Lo LW, Lin YJ, Lee SH, Chiou CW, Chen SA. Relationship between intrinsic cardiac autonomic Ganglionated Plexi and the atrial fibrillation nest. *Circ J* 2014;**78**:922–928.

12. APPENDIX

Larger versions of figures with electrograms are shown in the Appendix.

Figure 3.2 An intracardiac recording of determination of a B-AVD-GP site

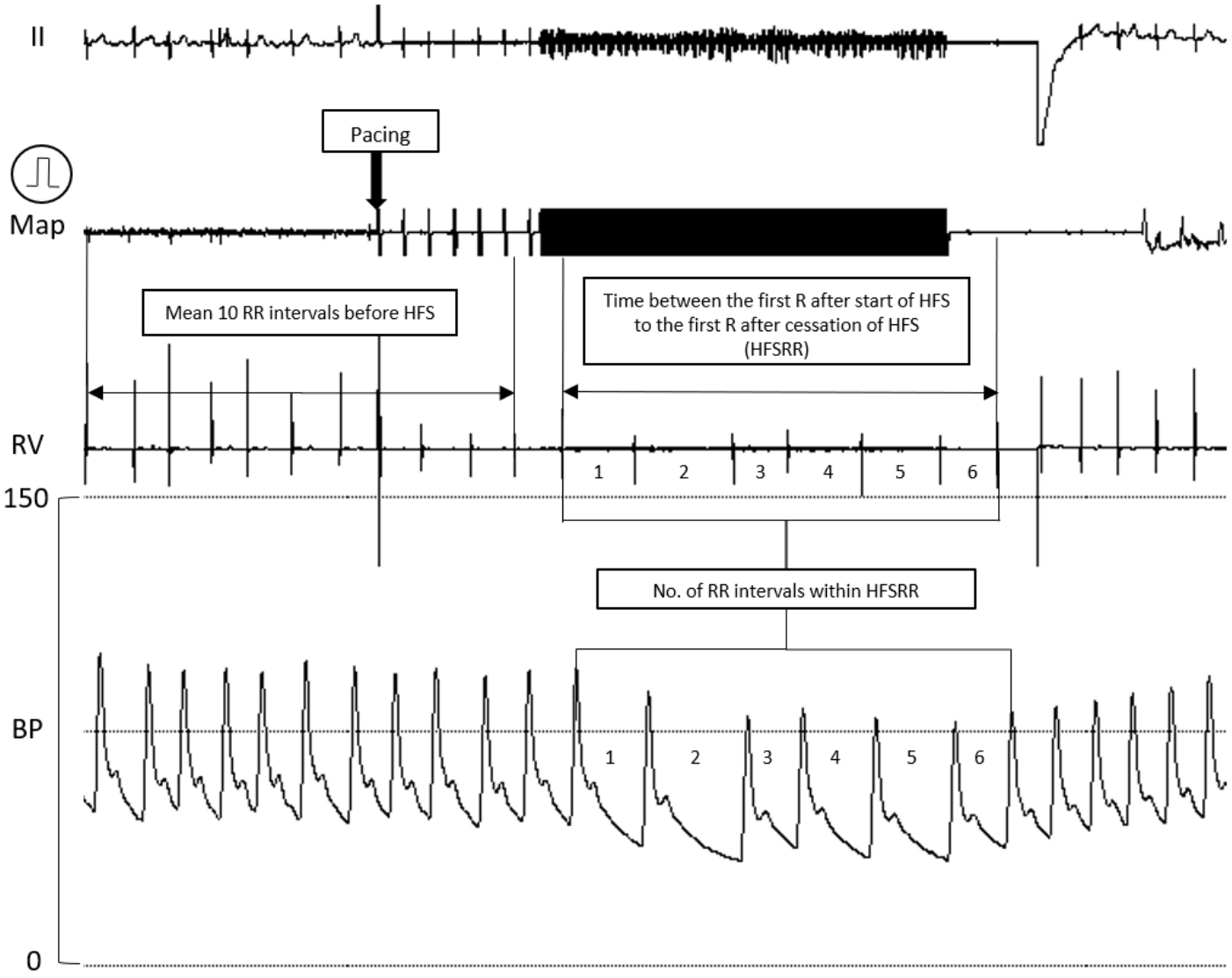

Figure 4.1A. Asystole with synchronised HFS

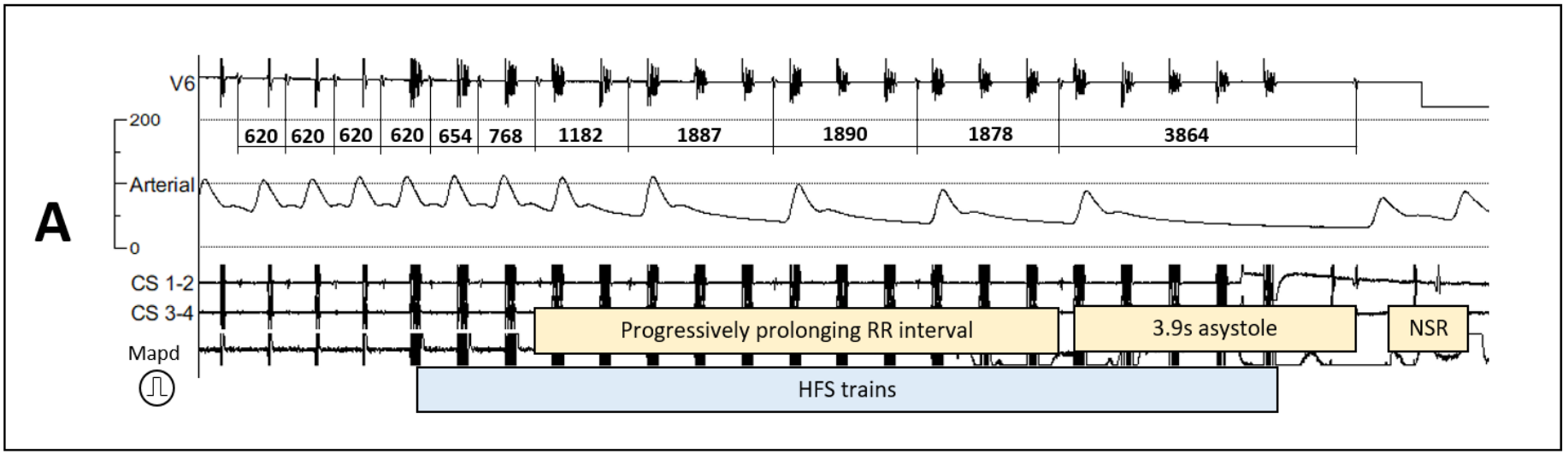

Figure 4.1B. AV block and atrial ectopy with synchronised HFS

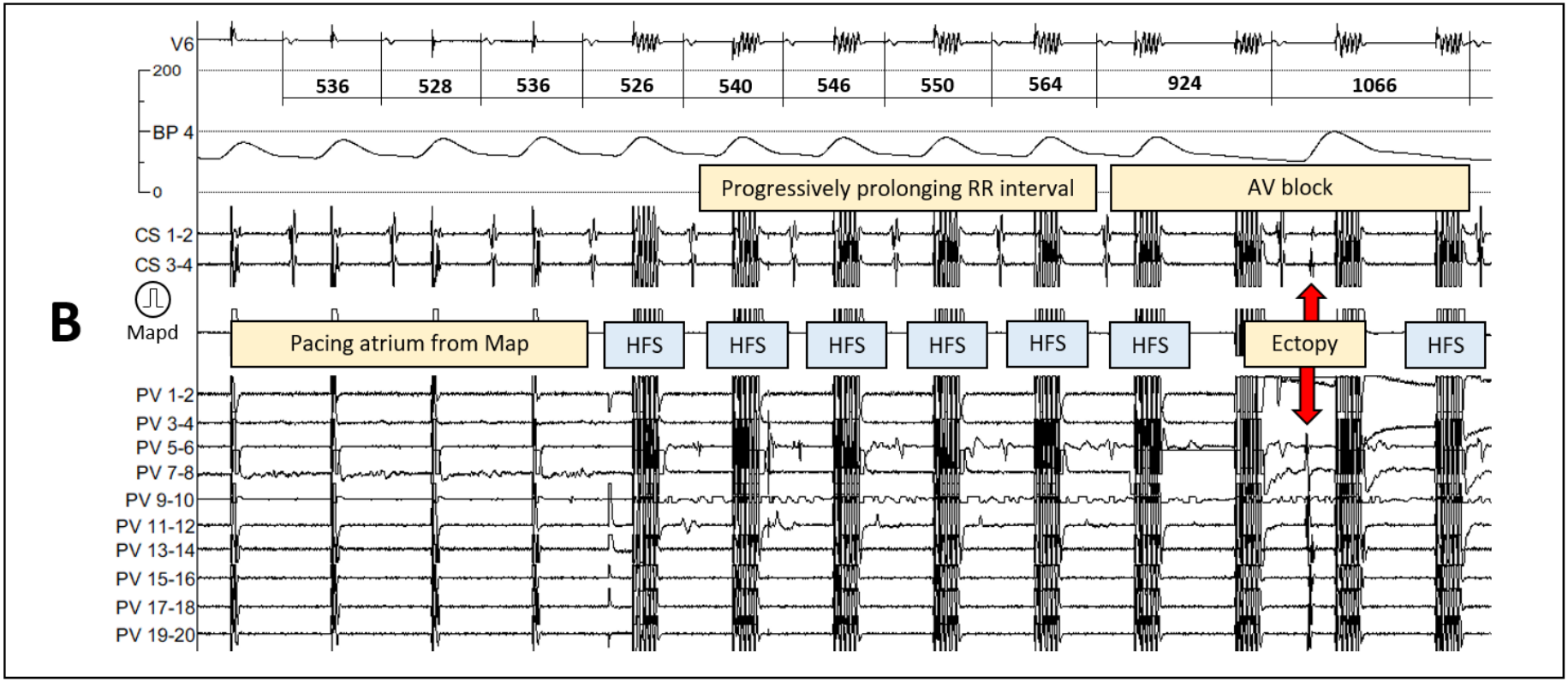

Figure 4.1C. AV block and AF with synchronised HFS

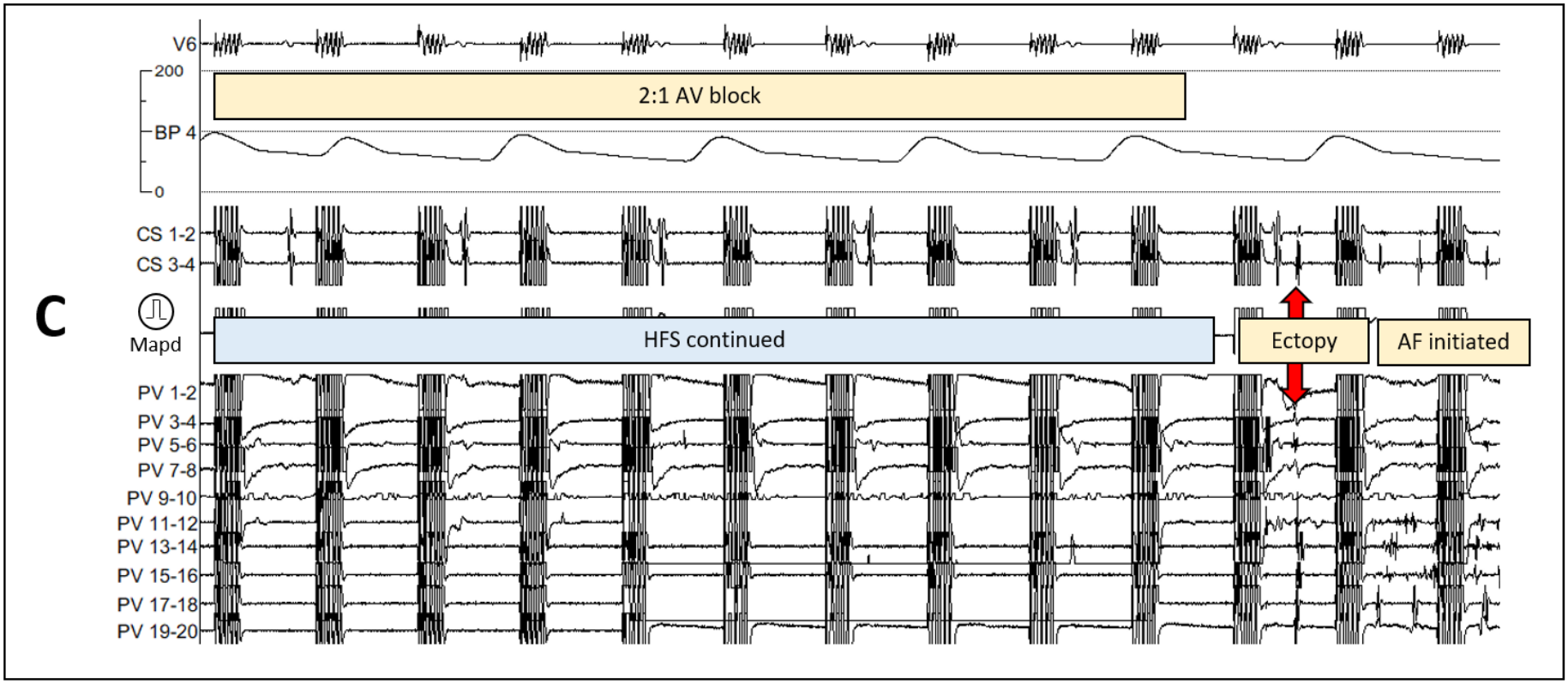

Figure 4.2 Sequential PV ectopy activation with ET-GP stimulation

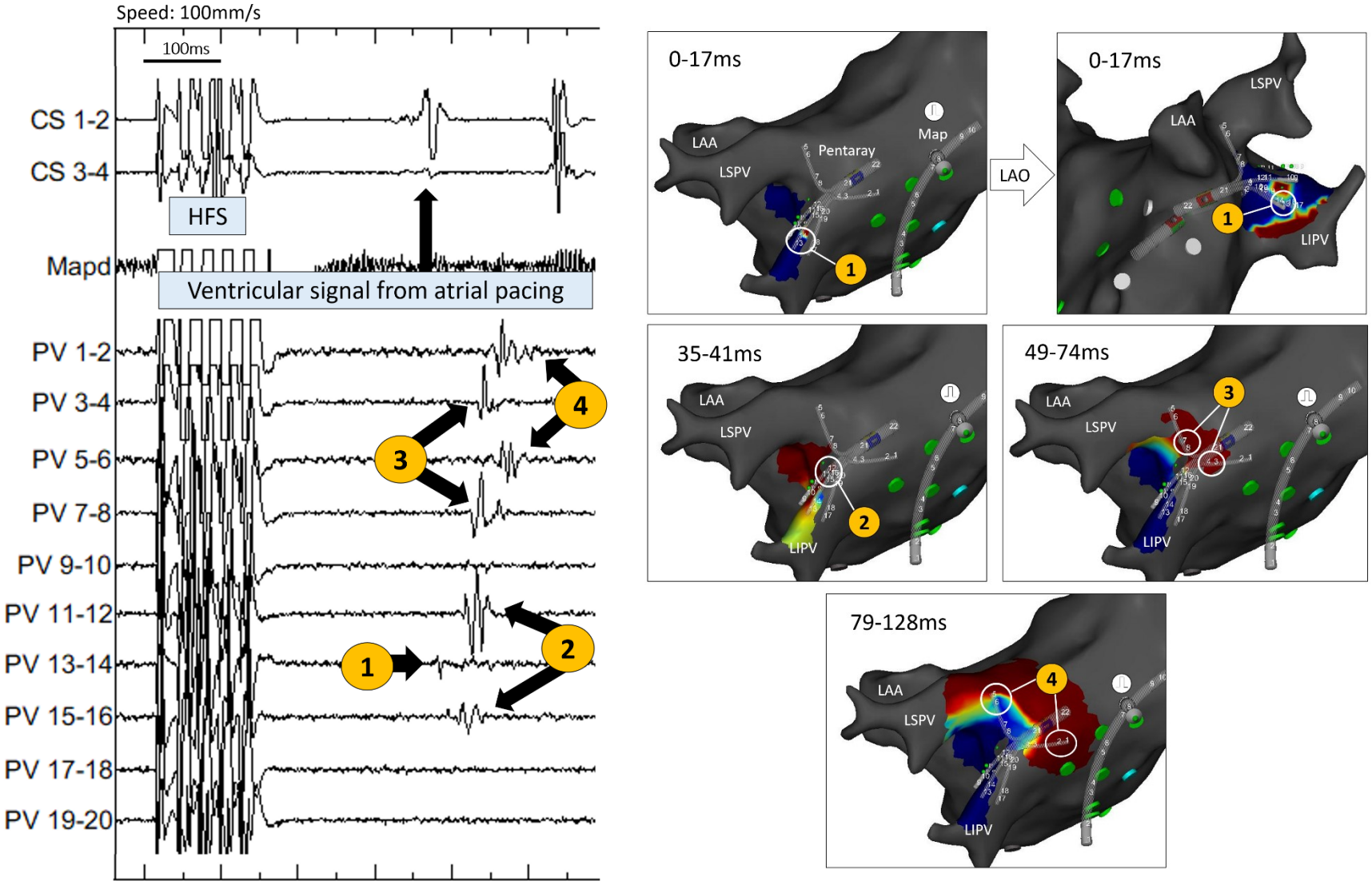

Figure 4.3A. Single ectopy triggered with ET-GP stimulation

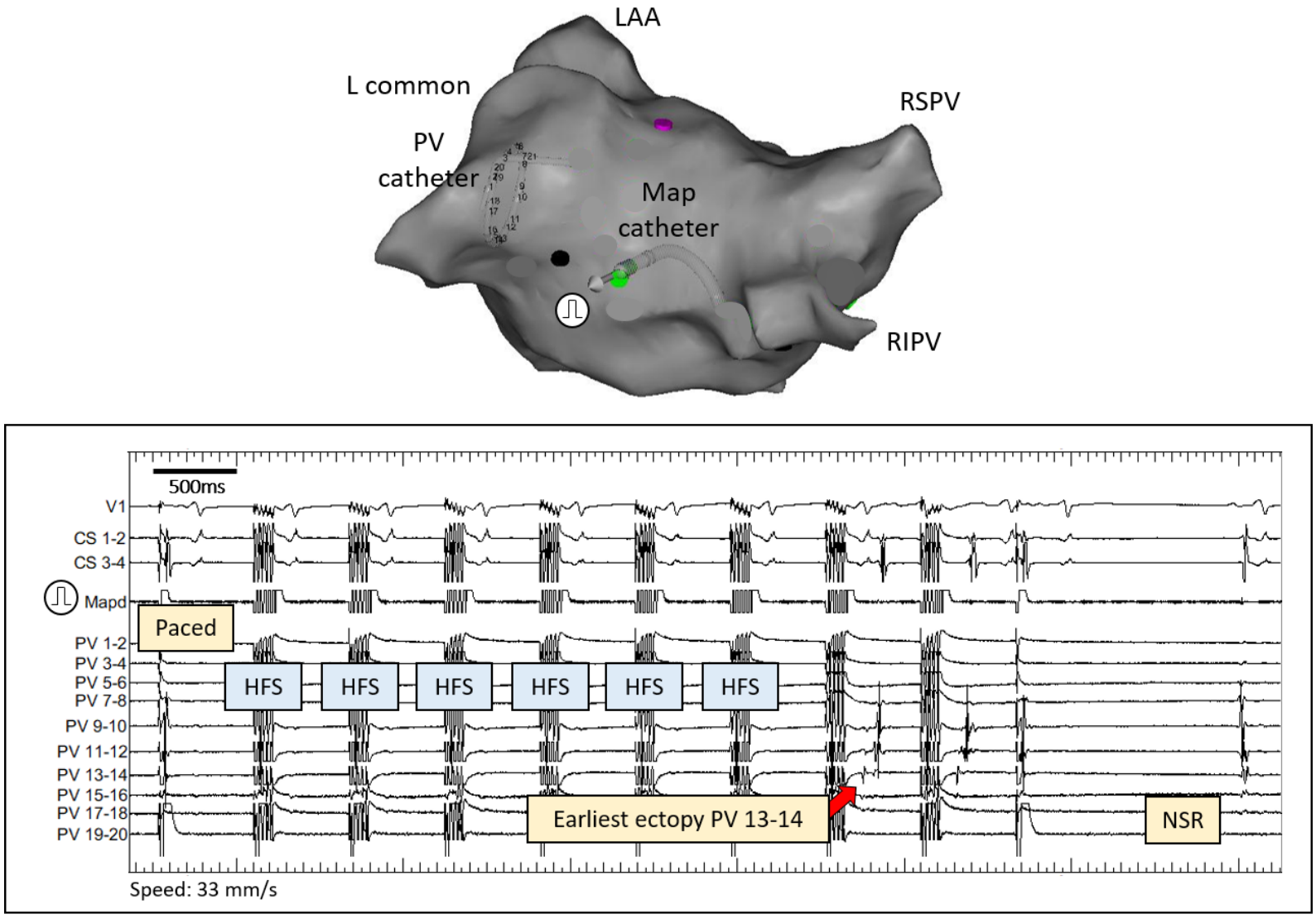

Figure 4.3B. Non-sustained AF triggered with ET-GP stimulation

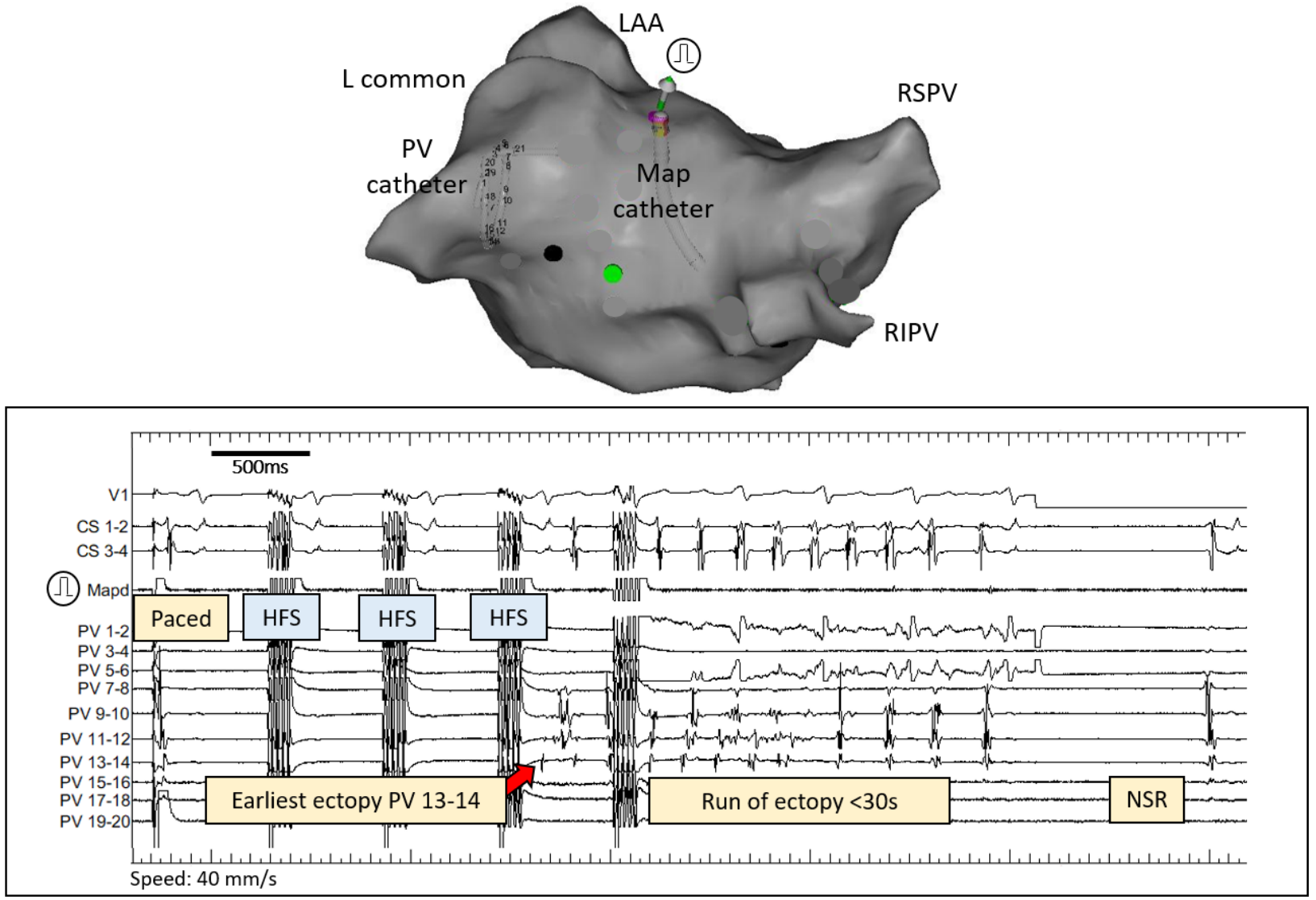

Figure 4.3C. Sustained AF triggered with ET-GP stimulation

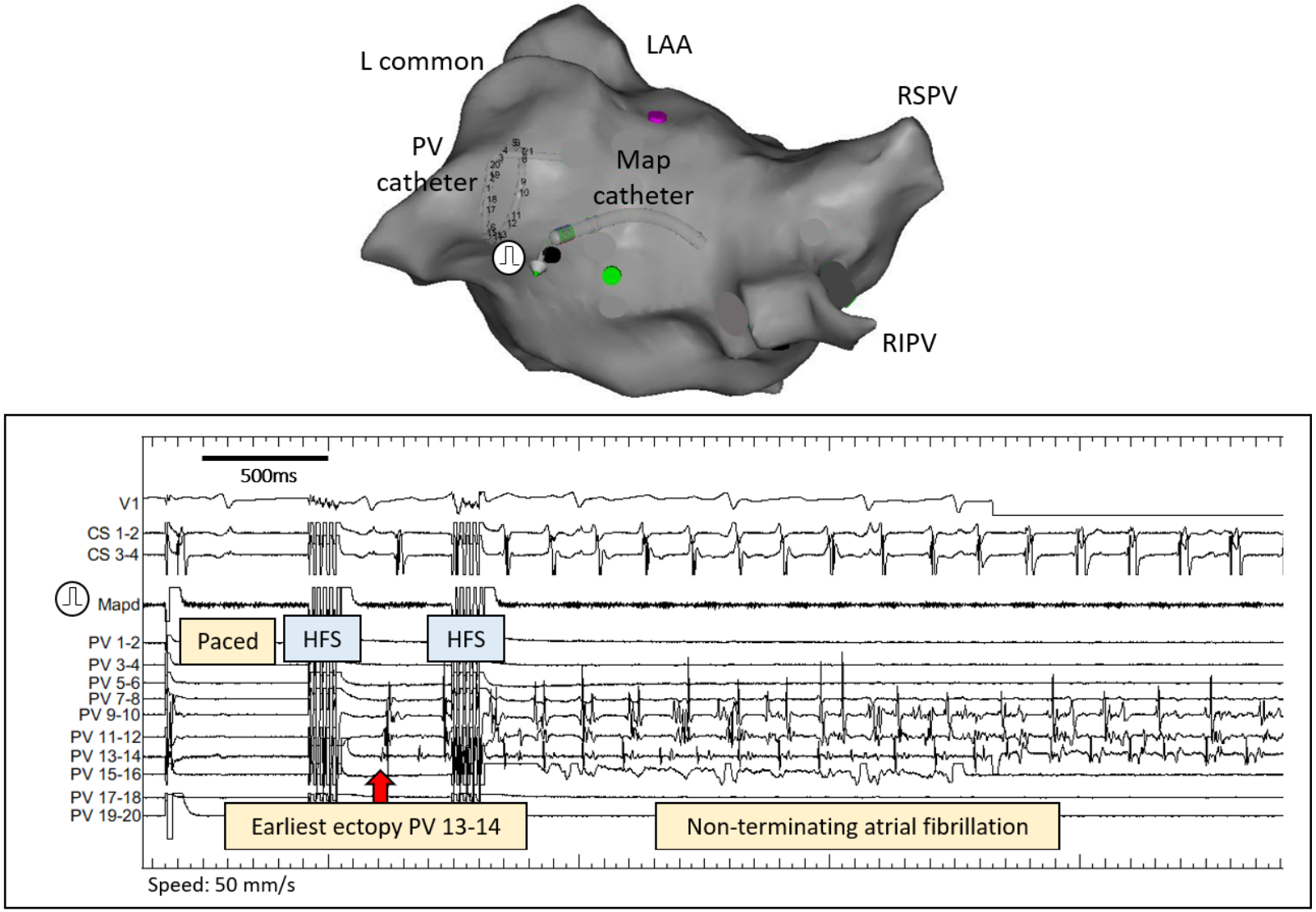

Figure 4.5A PV ectopy with repeat synchronised HFS

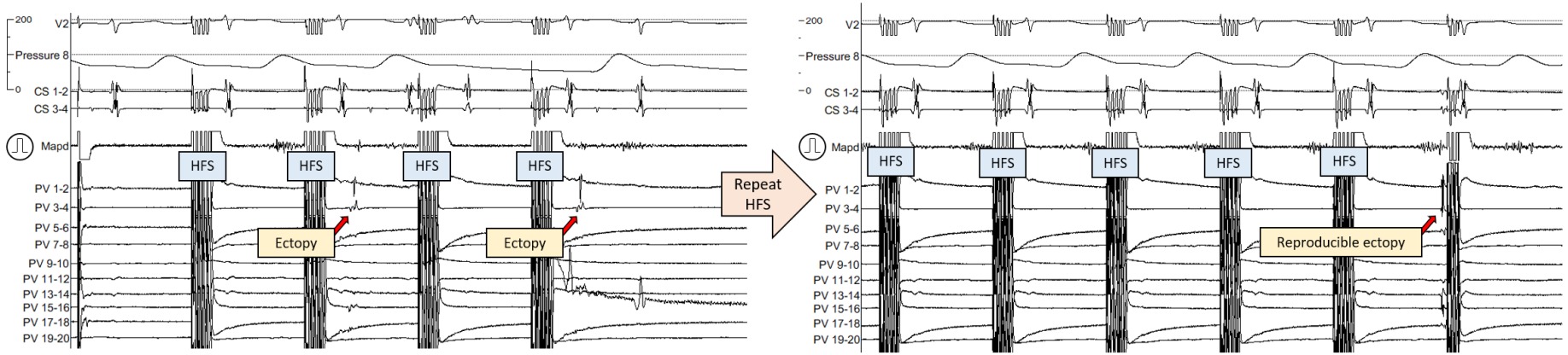

Figure 4.5B AF with repeat synchronised HFS

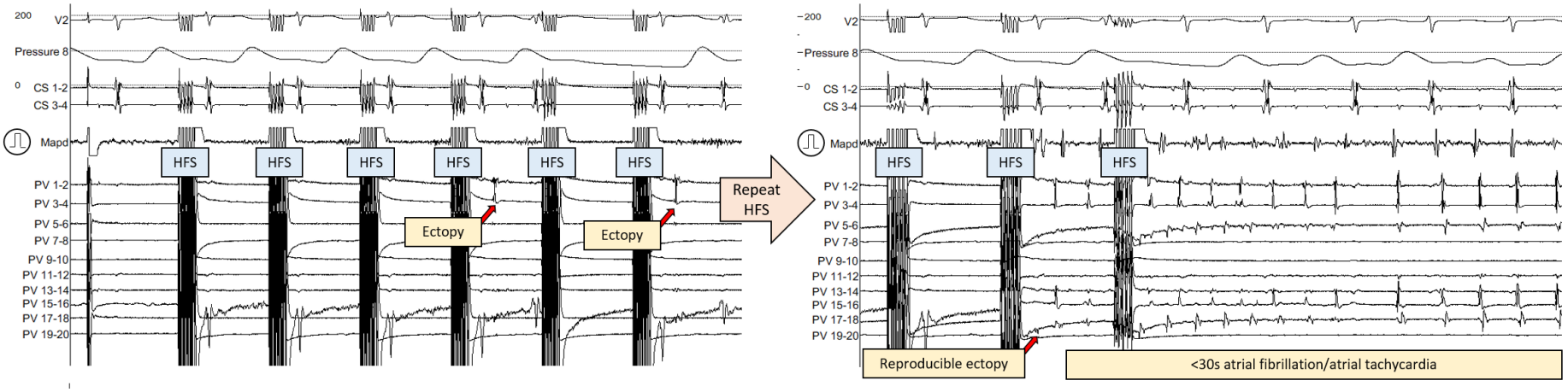

Figure 4.5C. PV ectopy that triggers non-sustained AF with repeat synchronised HFS

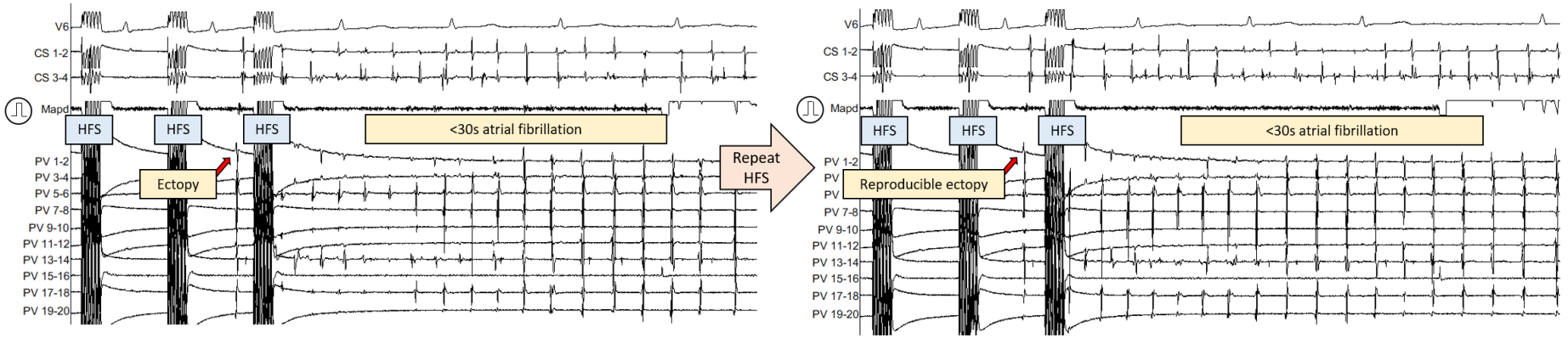

Figure 4.5D. Negative HFS site reproducibility

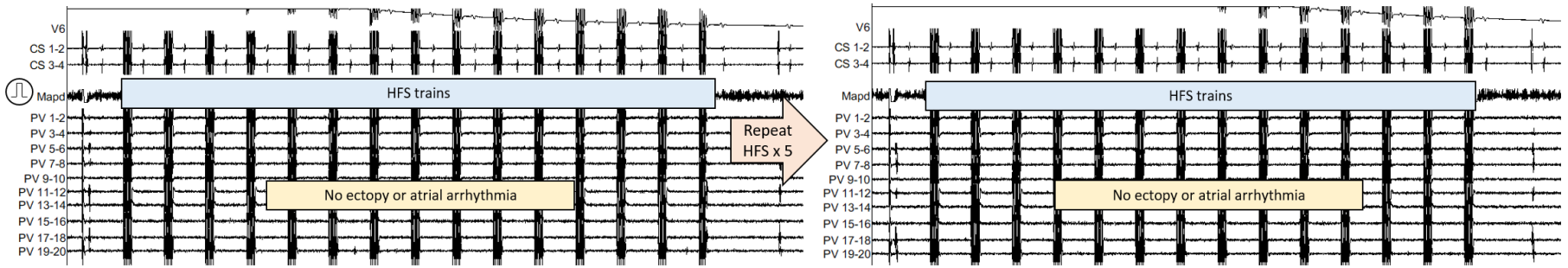

Figure 5.3 Synchronised HFS mapping for ET-GP and its ablation effects

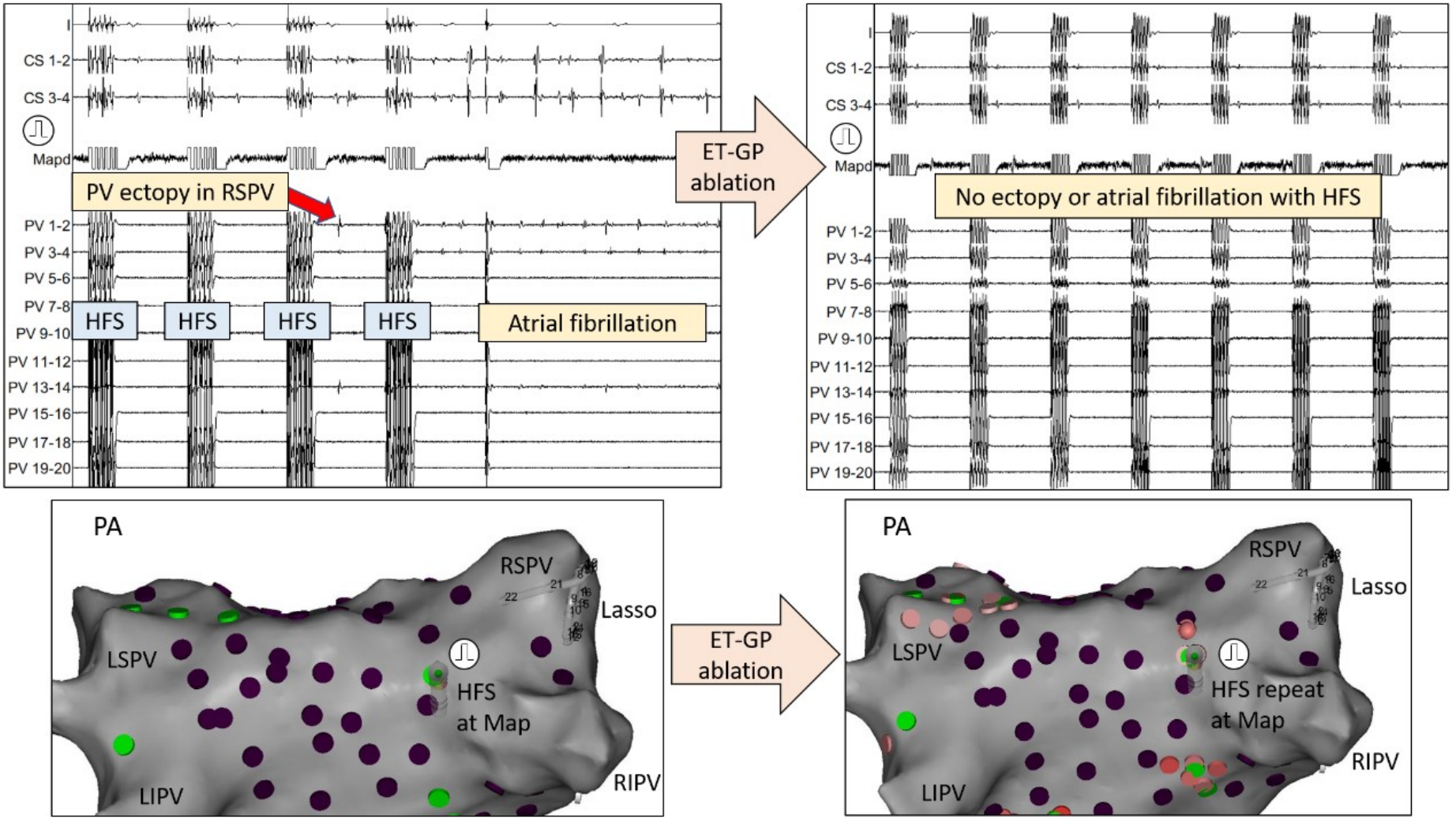

Figure 5.4. Continuous HFS mapping for AVD-GP and its ablation effects

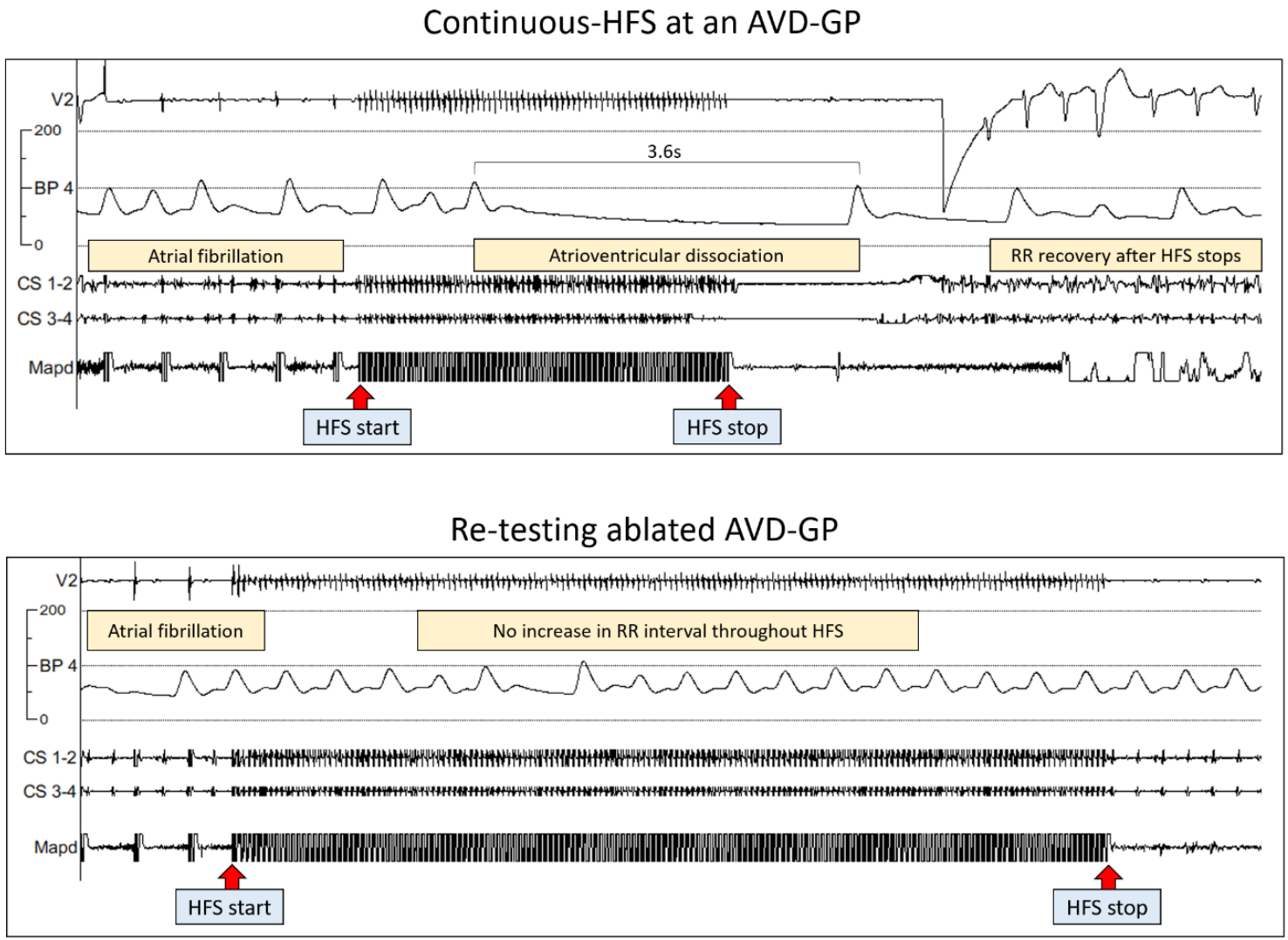

Figure 5.12 Non-inducible AF with rapid atrial pacing after AVD-GP ablation

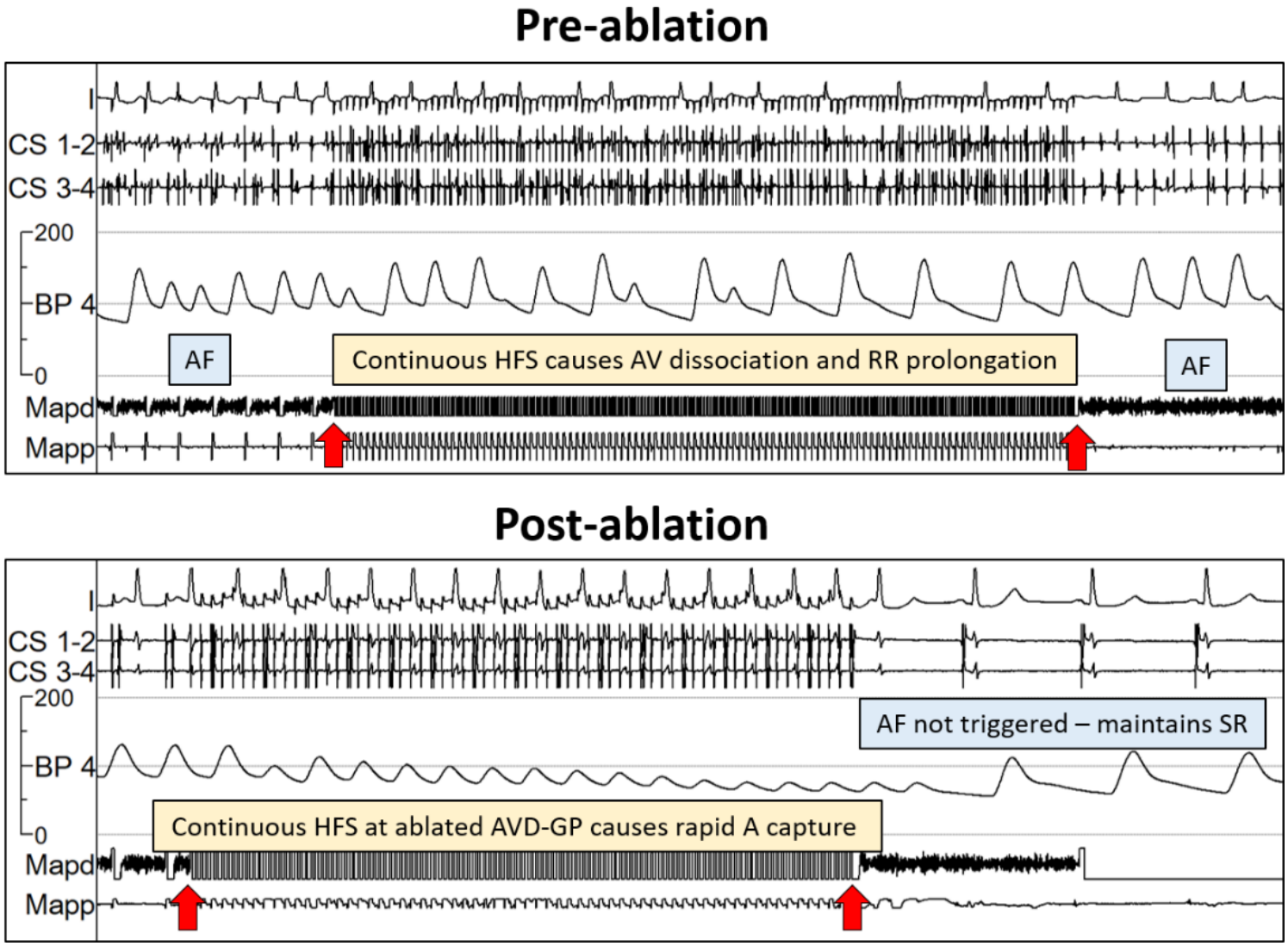

Figure 6.2 Successful AVD-GP ablation leading to acute and long-term freedom from AF

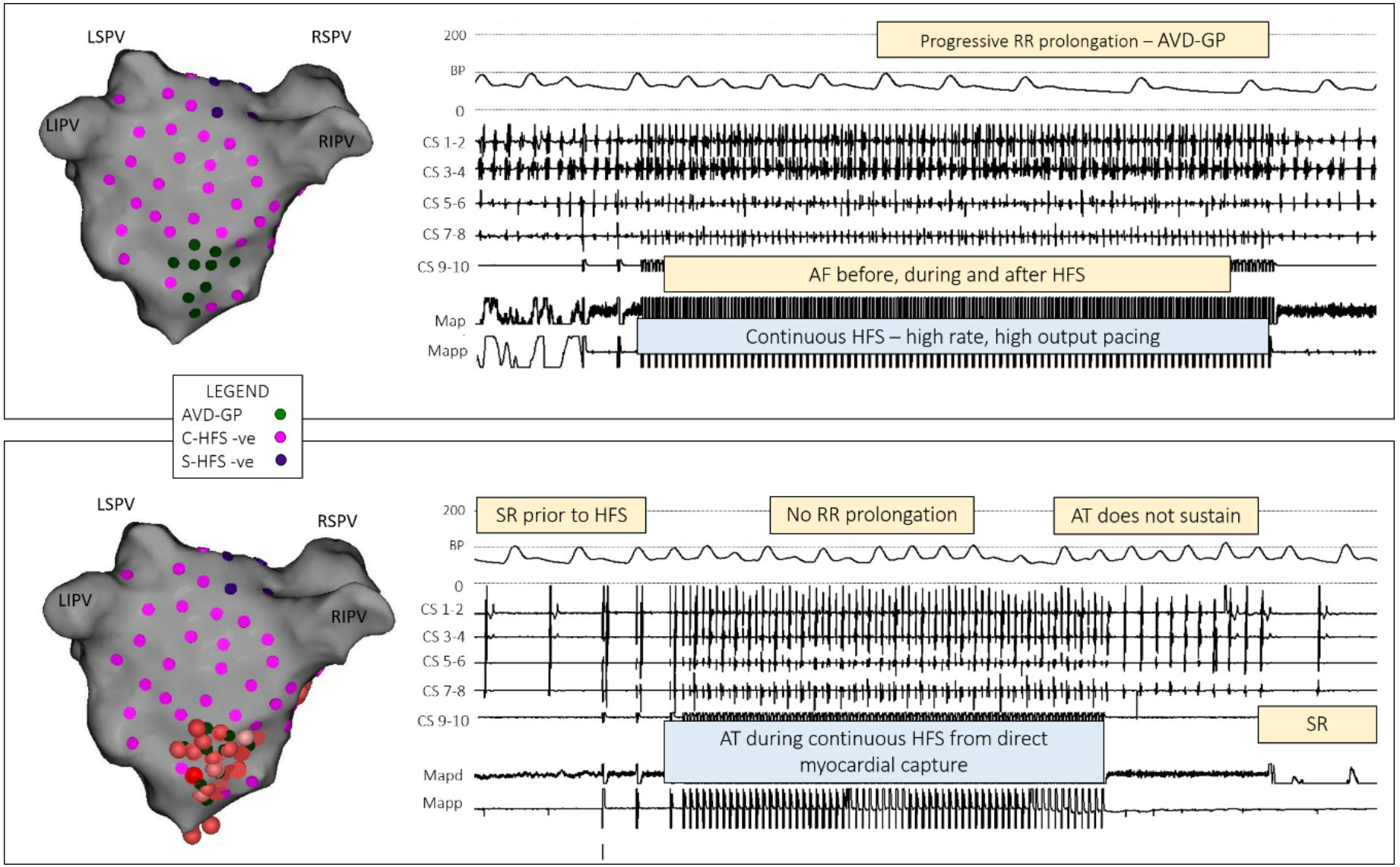

Figure 6.4A. Asystole followed by AF with synchronised HFS

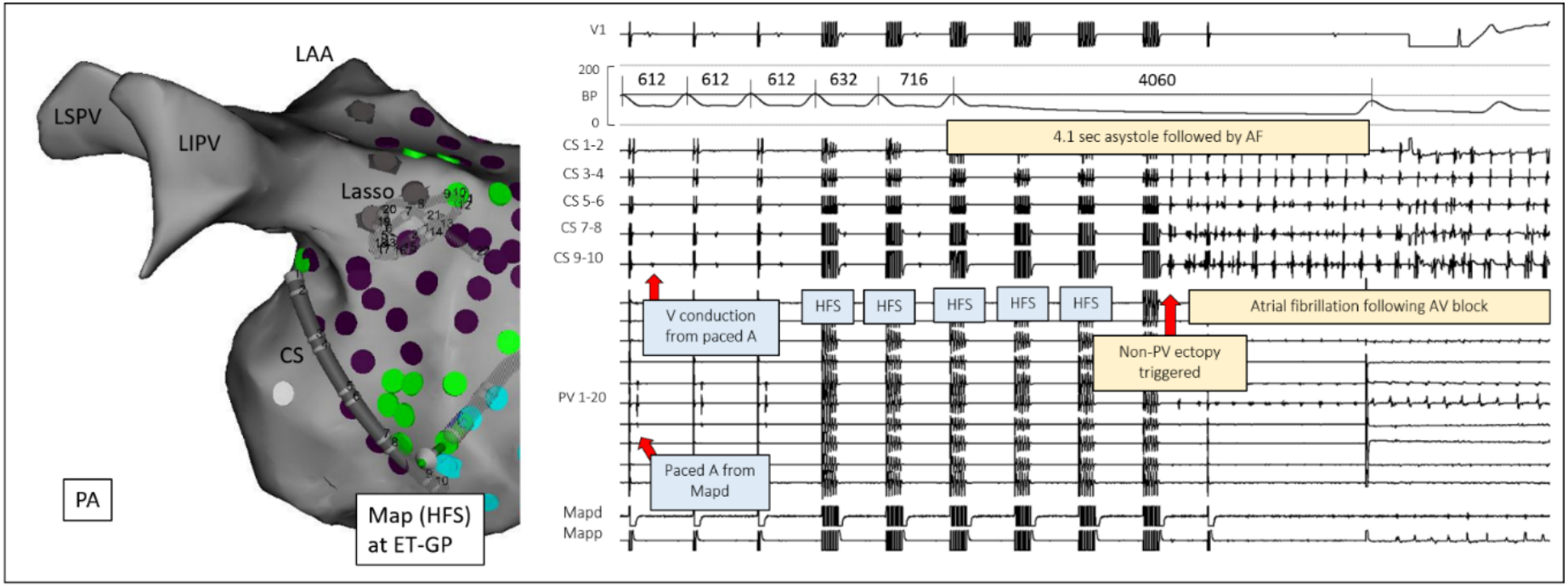

Figure 6.4B Progressive AV block followed by asystole with synchronised HFS

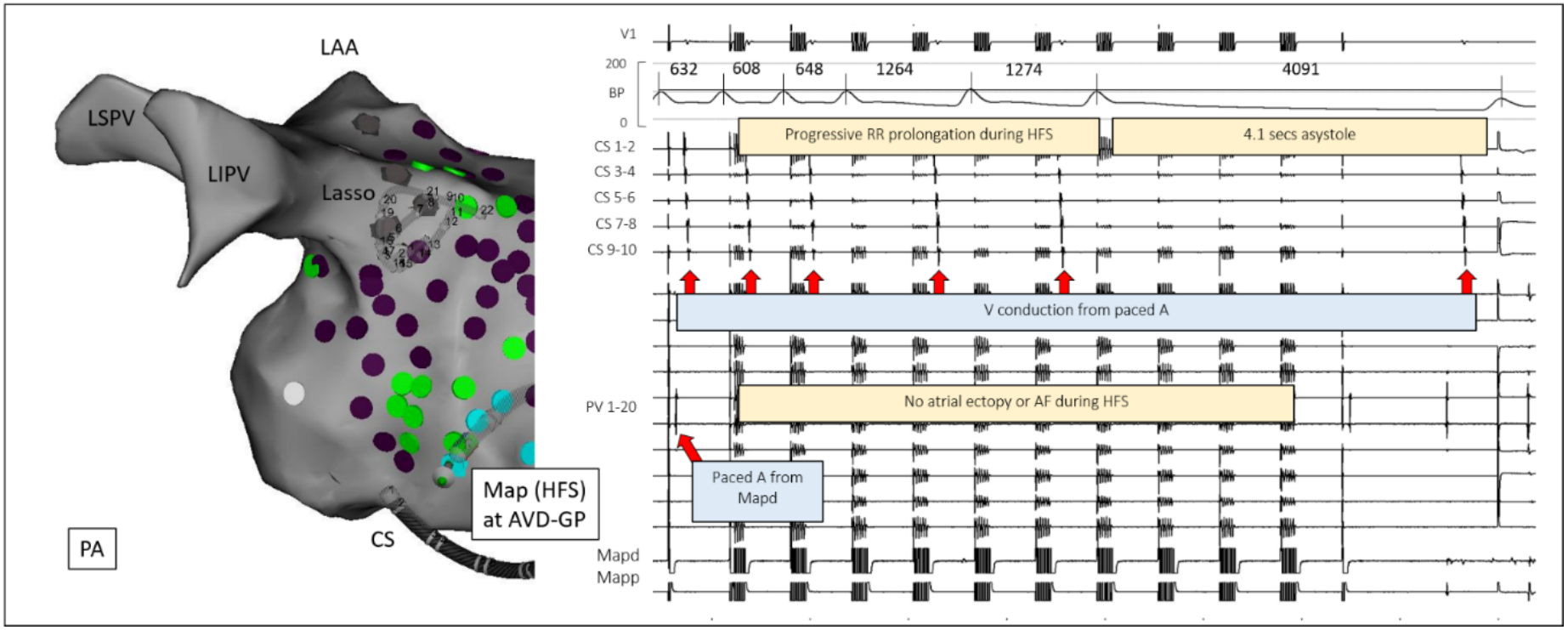

Figure 6.4C Non-PV ectopy without AV block or AF with synchronised HFS

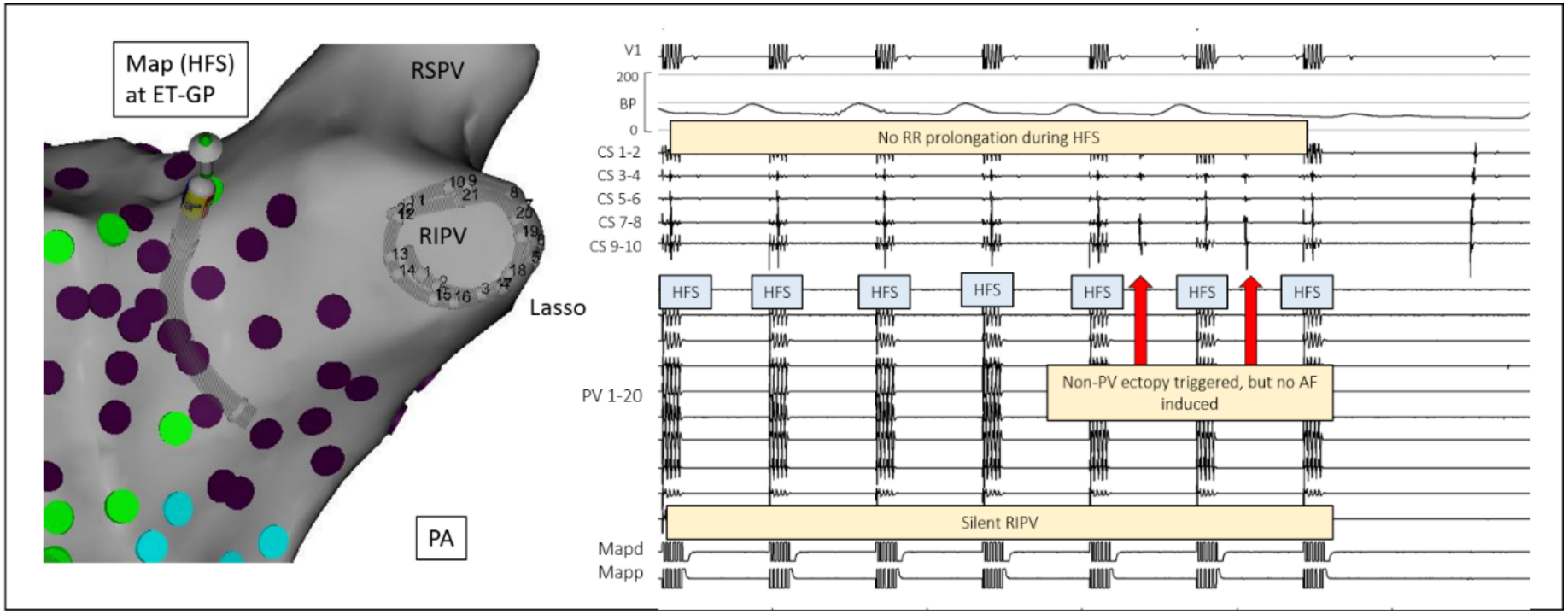

Figure 6.4D Non-PV ectopy and AF without AV block with synchronised HFS

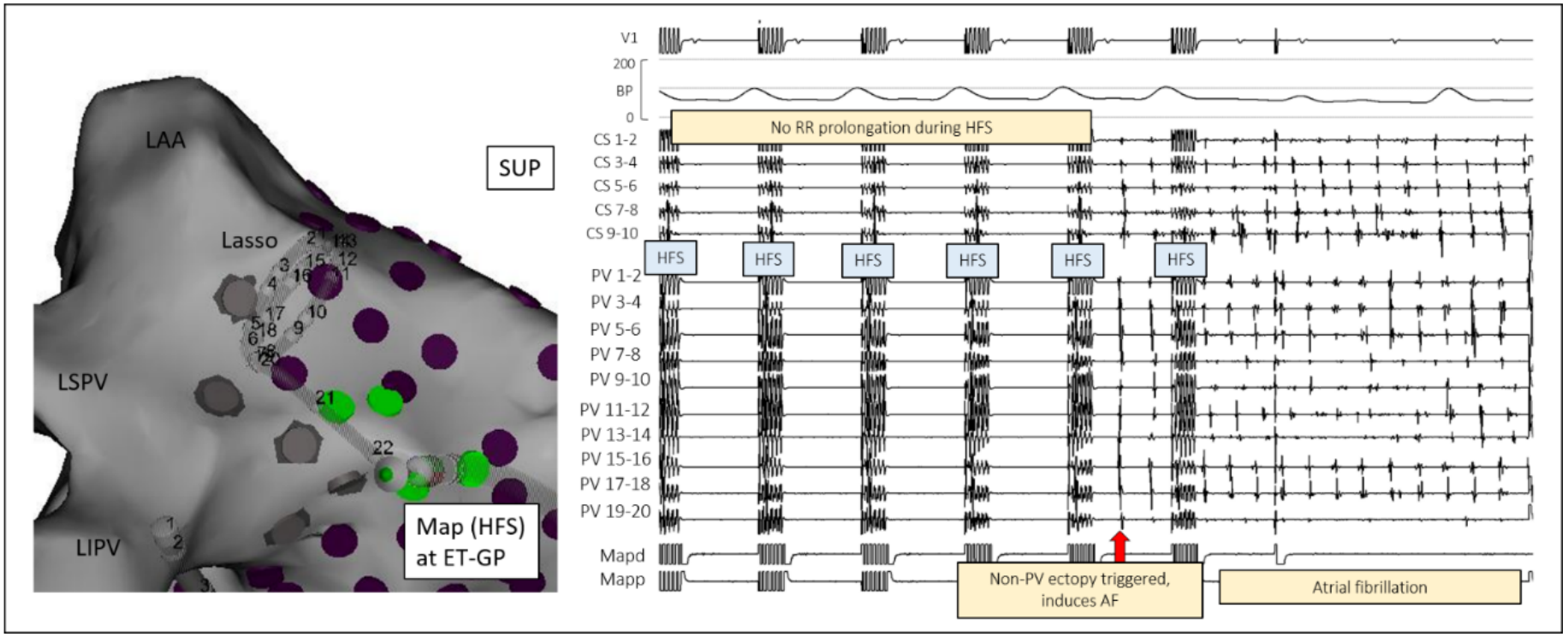

Figure 6.5B. PV ectopy initiating PV tachycardia with exit block at an ET-GP

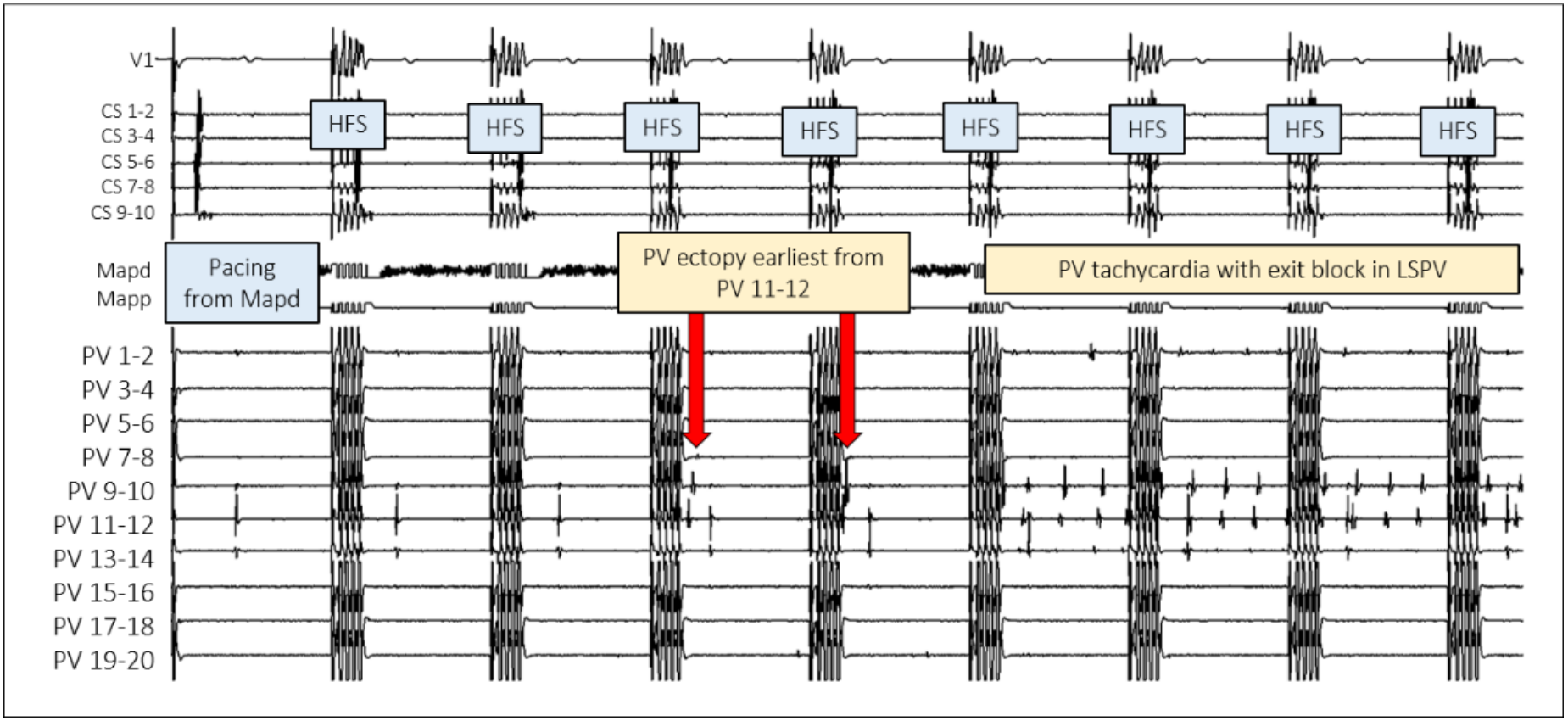

Figure 6.6. The same PV tachycardia in left-sided PVs, right-sided PVs silent

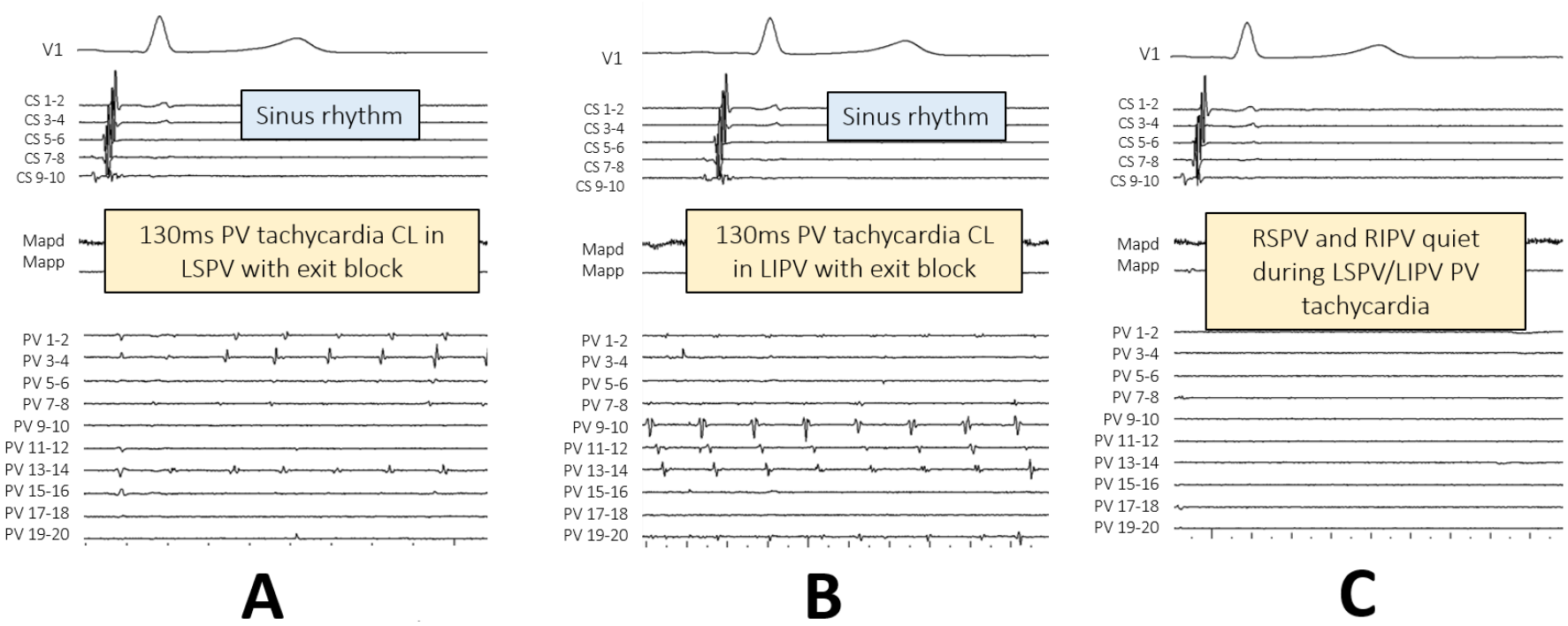

Figure 6.7A. ET-GP stimulation triggering PV tachycardia

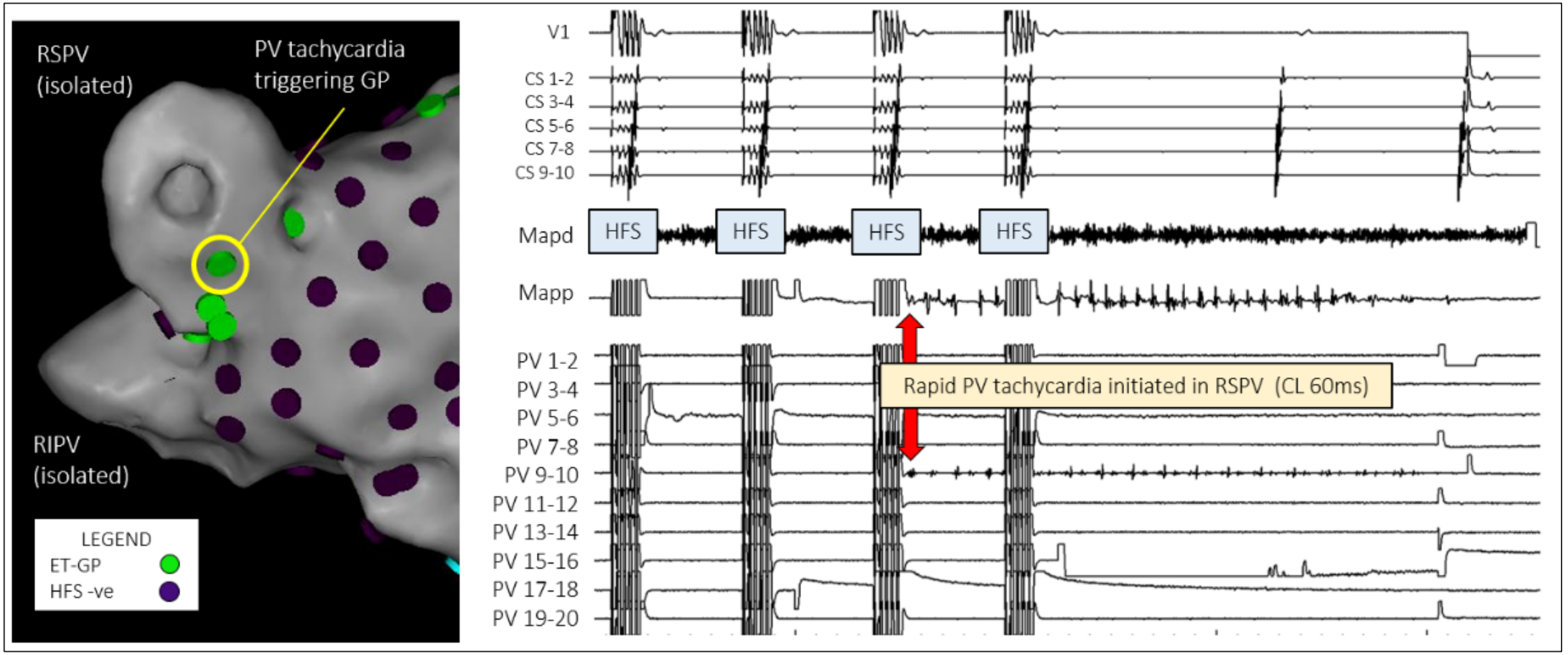

Figure 6.7B. ET-GP ablation abolishes PV tachycardia

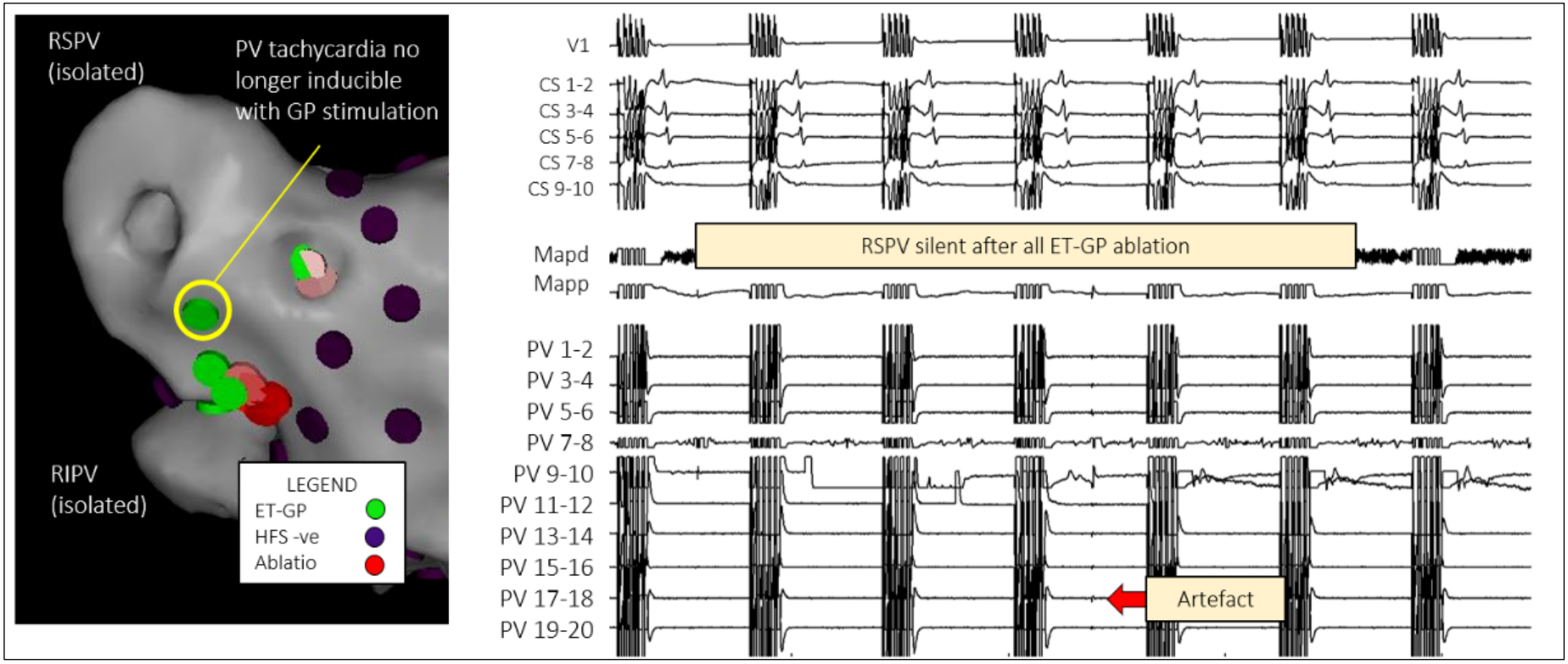

Figure 7.1. Sustained AF termination to sinus rhythm with GP ablation

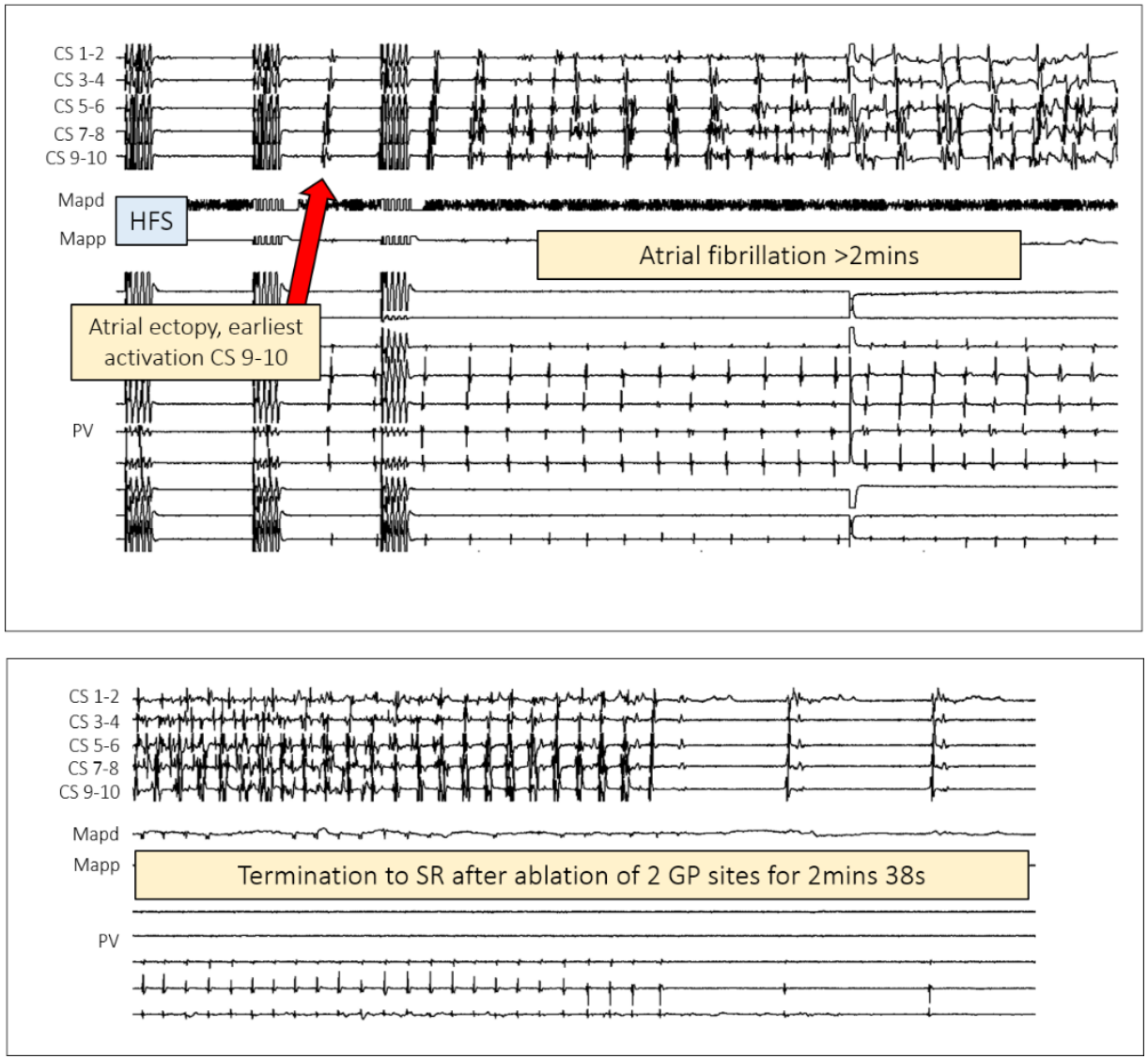

Figure 7.2. Sustained AF organises to AT with GP ablation

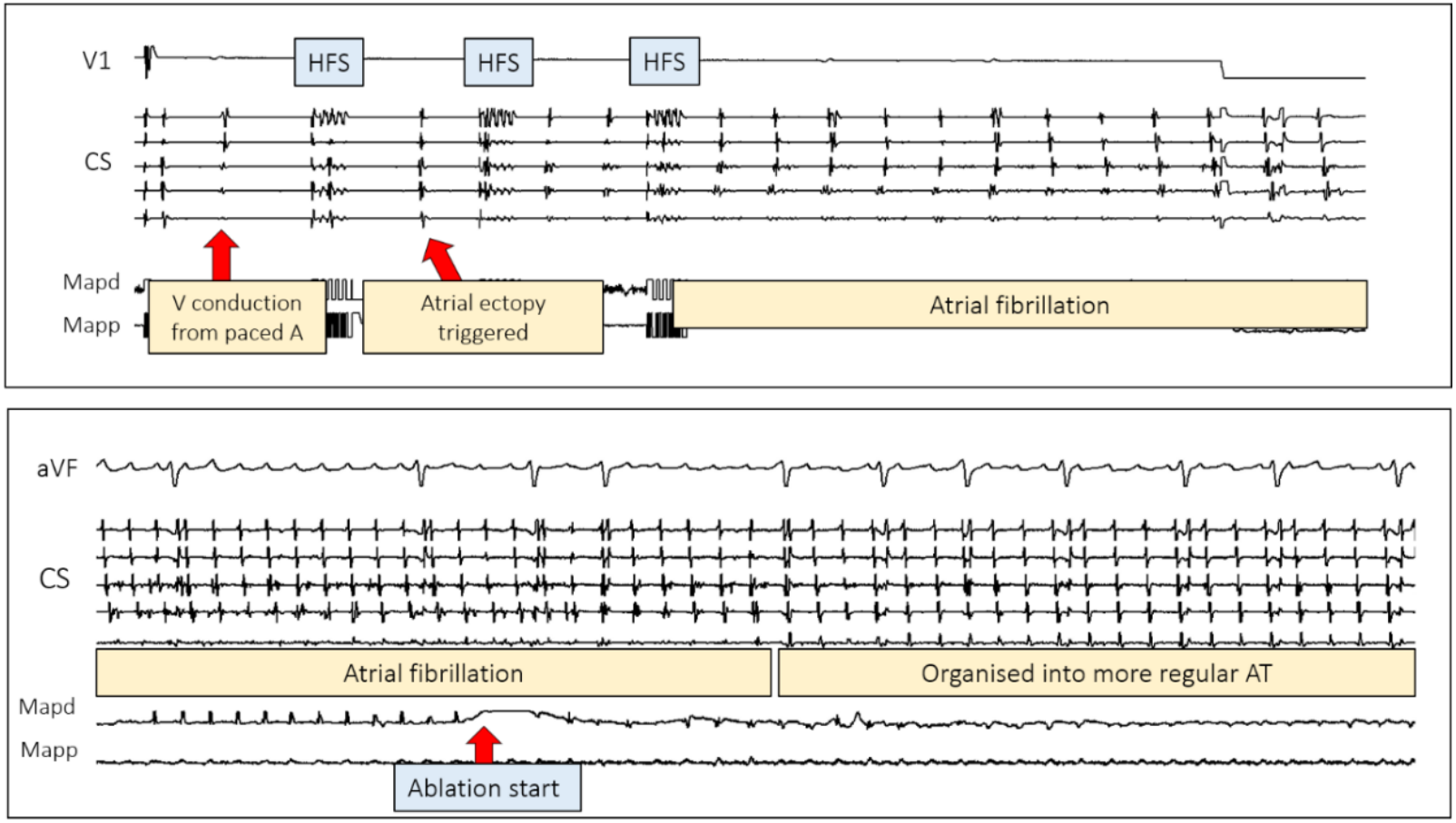

Figure 7.4. Single GP ablation leads to AF termination to sinus rhythm and sinus bradycardia

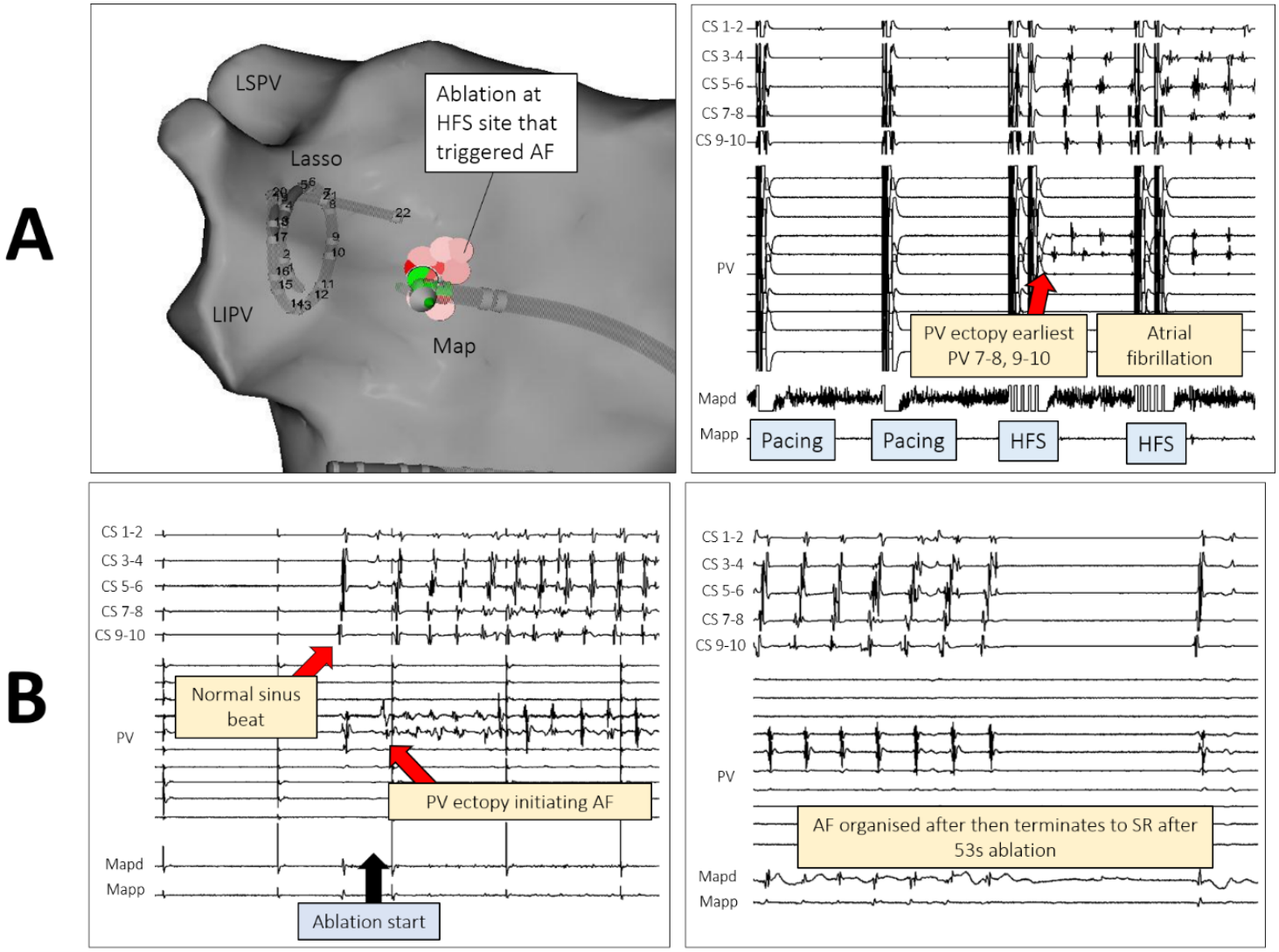

Figure 7.4. Single GP ablation leads to AF termination to sinus rhythm and sinus bradycardia

C

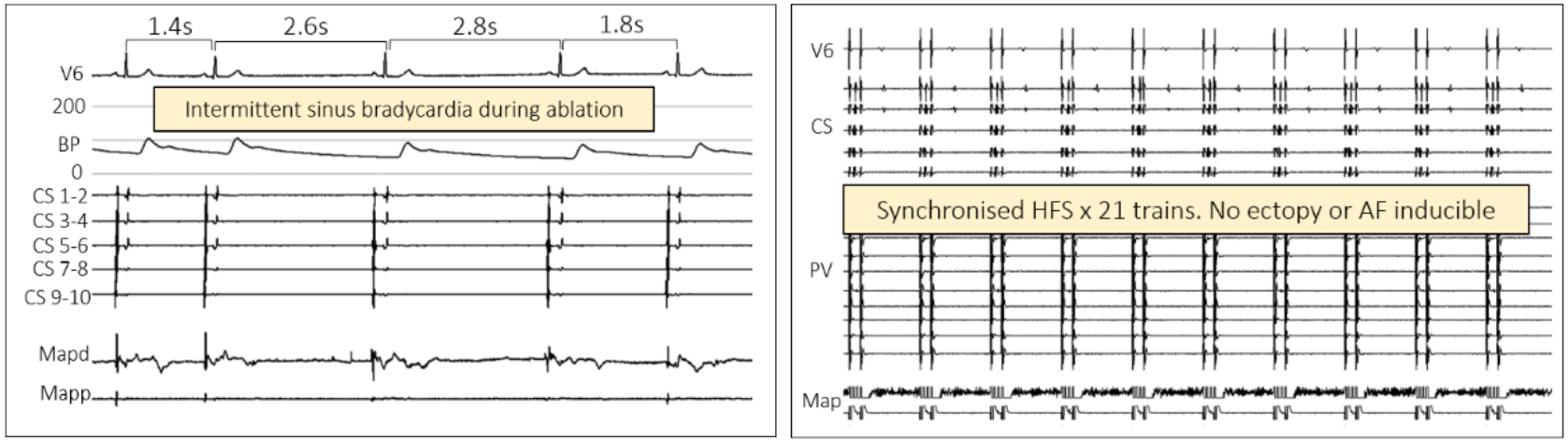

Figure 8.4. Reproducibly ectopy-triggering site with synchronised HFS in the ligament of Marshall

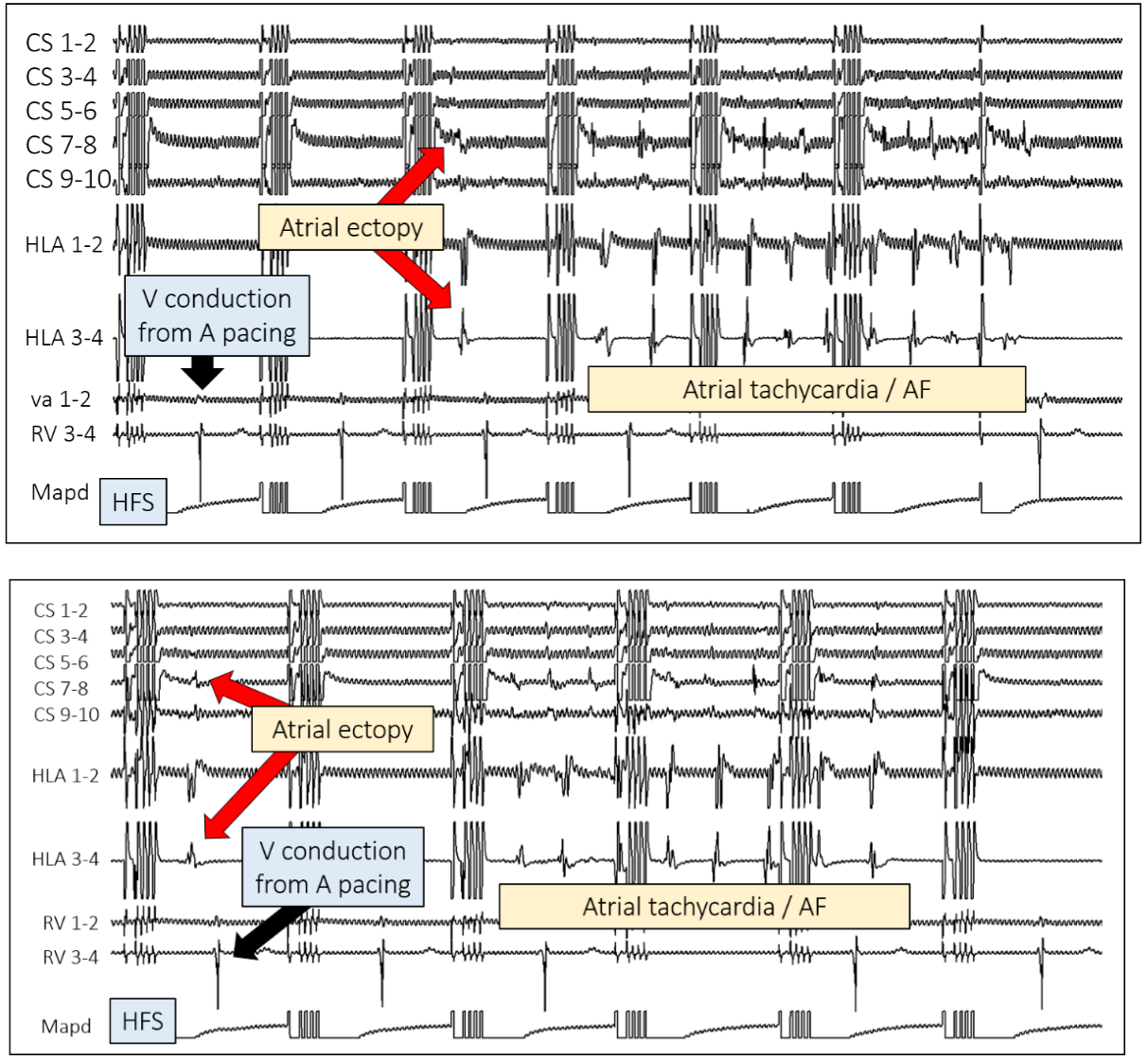

Figure 9.3. Pacing and HFS with Tau-20 in whole pig

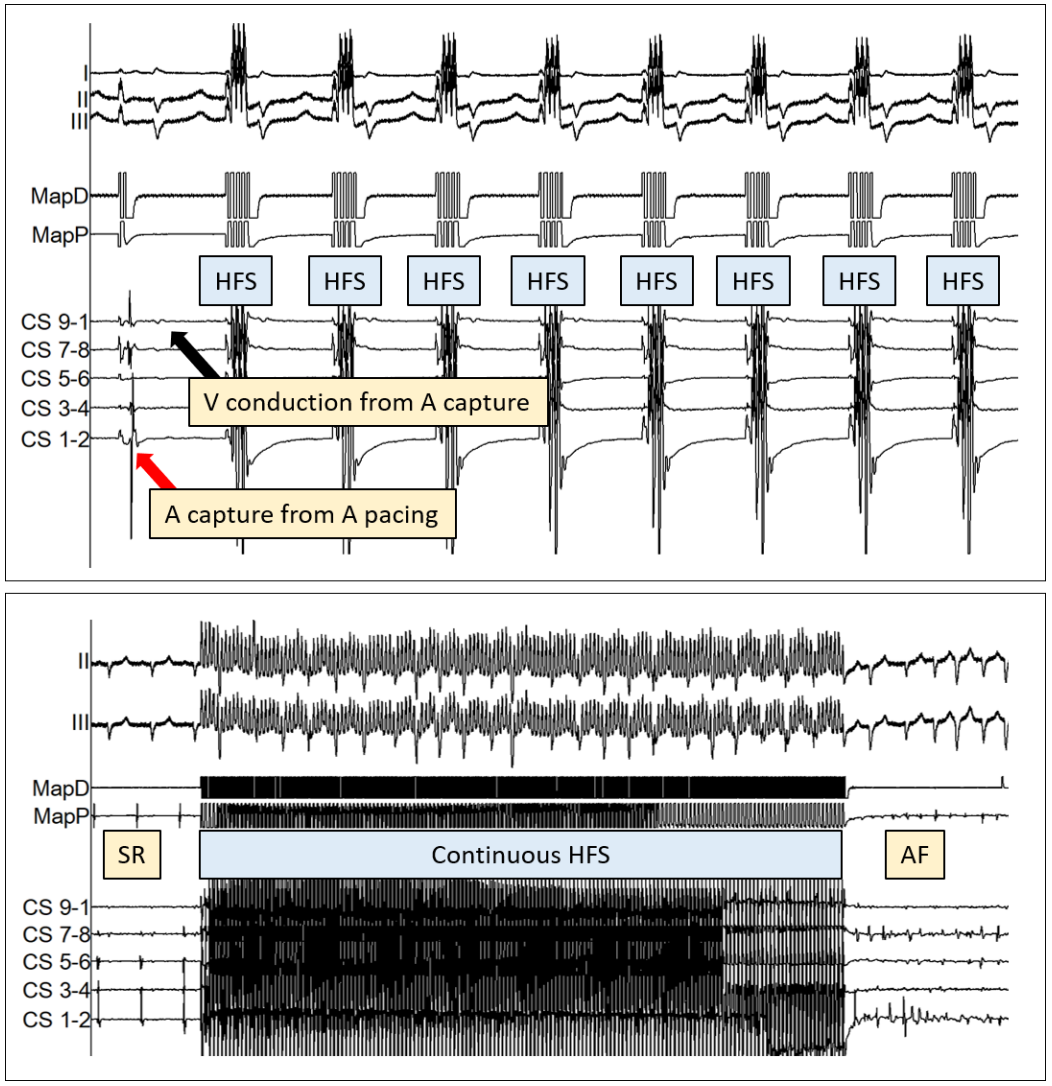

Figure 9.7. Atrial ectopy without AV dissociation with synchronised HFS using Tau-20 stimulator

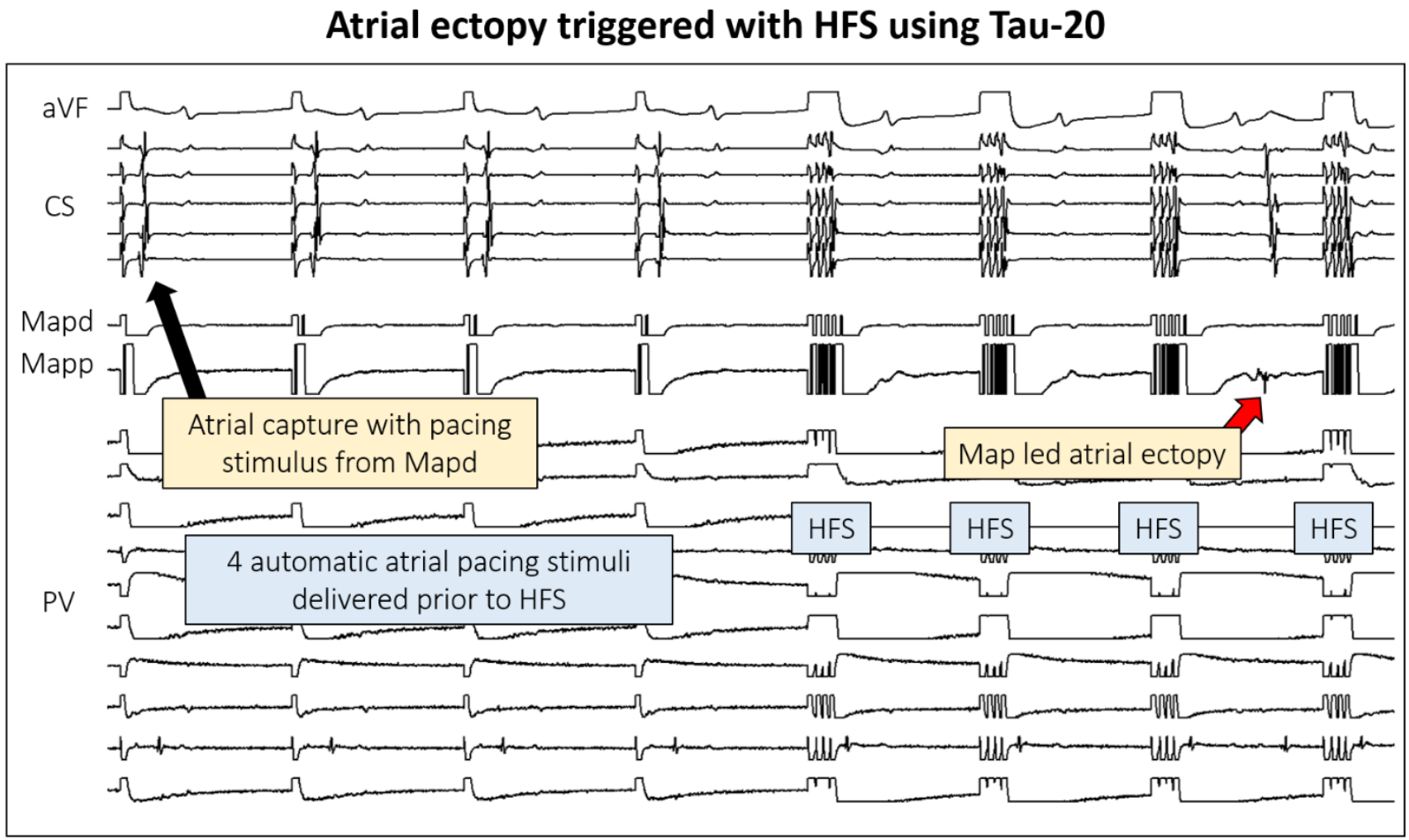

Figure 9.7. Atrial ectopy with AV dissociation with synchronised HFS using Tau-20 stimulator

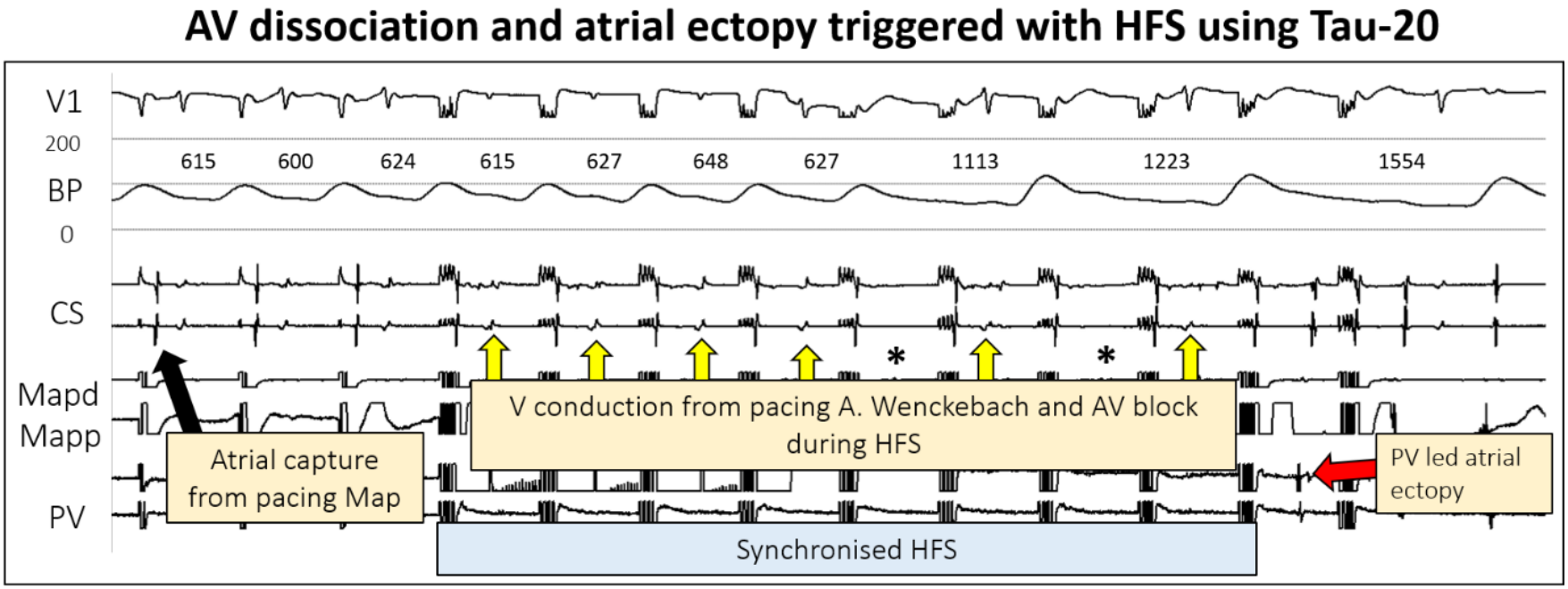

Figure 9.9. Sensed extras and burst pacing with Tau-20 stimulator

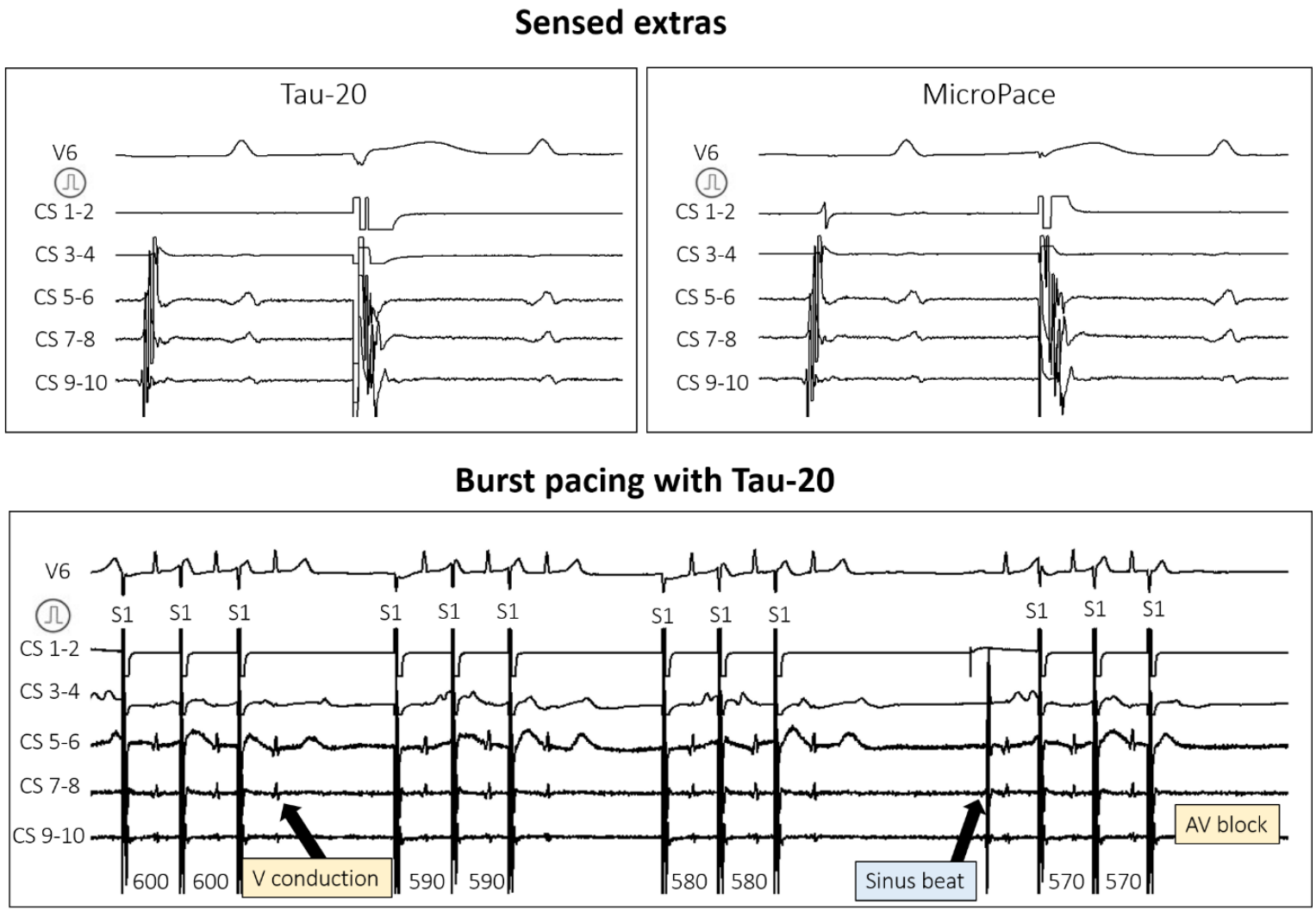

Figure 9.11. Continuous HFS with Tau-20 Stimulator identifying AVD-GP